

On the effects of northern hemisphere cooling on atmospheric circulation patterns in the Eastern Mediterranean: The 8.2 kyr B.P. climatic event at Tenaghi Philippon

Dissertation

zur Erlangung des Doktorgrades
der Naturwissenschaften

vorgelegt beim Fachbereich 11
der Johann Wolfgang Goethe - Universität
in Frankfurt am Main

von

Fabian Schemmel

aus Essen

Frankfurt, 2016

vom Fachbereich 11 der Johann Wolfgang Goethe - Universität als Dissertation
angenommen.

Dekan: Prof. Dr. Peter Lindner

Gutachter: Prof. Dr. Andreas Mulch

Senckenberg Biodiversität und Klima Forschungszentrum (BiK-F)

Frankfurt am Main, Deutschland

und

Goethe Universität Frankfurt am Main, Deutschland

Prof. Dr. Jörg Pross

Senckenberg Biodiversität und Klima Forschungszentrum (BiK-F)

Frankfurt am Main, Deutschland

und

Universität Heidelberg, Deutschland

Datum der Disputation:

Table of contents

List of figures	i
List of tables	iii
Abbreviations	iv
Abstract	1
Chapter 1 - Introduction	3
<i>1.1 Motivation and aim of research</i>	3
<i>1.2 Study site: the classical site of Tenaghi Philippon</i>	10
<i>1.3 Stable isotopes in meteoric waters</i>	11
<i>1.4 Molecular plant fossils as indicators for paleoenvironmental changes</i>	15
<i>1.5 Structure of this PhD thesis</i>	21
<i>1.6 References</i>	23
Chapter 2 - The impact of topography on isotopes in precipitation across the Central Anatolian Plateau	35
<i>2.1 Introduction</i>	36
2.1.1 Why stable isotope paleoaltimetry in Anatolia?	36
2.1.2 Topographic and climatic setting	38
2.1.3 Goal of this study	40
2.1.4 Sampling strategy	40
<i>2.2 Methods</i>	41
<i>2.3 Results and discussion</i>	42
2.3.1 Long-term stability of δD and $\delta^{18}O$ values	43
2.3.2 Spatial distribution of δD and $\delta^{18}O$ values	43
2.3.3 Meteoric water lines	46
2.3.4 Constraining isotopic lapse rates using Average Catchment Elevations	48
<i>2.4 Challenges and perspectives for stable isotope paleoaltimetry</i>	51
2.4.1 The role of winter recharge for δD and $\delta^{18}O$ of near-surface groundwater	52
2.4.2 Topographically driven subsurface groundwater flow	54
<i>2.5 Conclusions</i>	54
<i>2.6 Acknowledgements</i>	55
<i>2.7 References</i>	57

Chapter 3 - Paleohydrological changes in the Eastern Mediterranean region during the early Holocene recorded in plant wax <i>n</i>-alkane $\delta^{13}\text{C}_{\text{TOC}}$ – new data from Tenaghi Philippon, NE Greece	61
3.1 Introduction	62
3.2 Material and methods	64
3.2.1 Study site	64
3.2.2 Lipid extraction, purification, and quantification	66
3.2.3 <i>n</i> -alkane concentration	66
3.2.4 Stable carbon isotope ($\delta^{13}\text{C}_{\text{TOC}}$) measurements	66
3.2.5 Palynology	67
3.3 Results and discussion	67
3.3.1 <i>n</i> -alkane distribution and CPI	67
3.3.2 P_{aq} index	71
3.3.3 ACL values	71
3.3.4 $\delta^{13}\text{C}_{\text{TOC}}$ values	72
3.3.5 Palynological reconstruction	73
3.3.6 Multiproxy reconstructions of early to mid-Holocene paleohydrology	74
3.4 Conclusions	78
3.5 Acknowledgements	78
3.6 References	79
Chapter 4 - Plant wax δD values record changing Eastern Mediterranean atmospheric circulation patterns during the 8.2 kyr B.P. climatic event	84
4.1 Introduction	85
4.1.1 The 8.2 kyr B.P. climatic event	86
4.1.2 Present-day Mediterranean climate	87
4.1.3 Stable isotopes in modern Mediterranean precipitation	88
4.2 Material and methods	89
4.2.1 Study site	89
4.2.2 Lipid extraction, purification, and quantification	90
4.2.3 <i>n</i> -alkane concentration	90
4.2.4 δD measurements	90
4.3 Results	91
4.4 Discussion	93
4.4.1 Environmental influences on $\delta\text{D}_{\text{wax}}$	94

4.4.1.1 Effects of changes in atmospheric circulation patterns and moisture transport on δD_{precip}	94
4.4.1.2 Influences of regional paleoclimatic changes on δD_{wax} variability	95
4.4.1.3 Changes in SST and δD in the moisture source area(s)	97
4.5 Mechanisms	98
4.5.1 The 8.2 kyr B.P. climatic event	98
4.5.1.1 Influence of the Asian summer monsoon	99
4.5.1.2 Hadley circulation	101
4.5.1.3 'Mediterranean Monsoon'	102
4.5.2 Stable isotopes in precipitation prior and after the 8.2 kyr B.P. climatic event	102
4.6 Conclusions	103
4.7 Acknowledgements	104
4.8 References	105
Chapter 5 - Conclusions and outlook	112
5.1 Conclusions	114
5.2 Outlook	114
5.2.1 Tenaghi Philippon: The 8.2 kyr B.P. climatic event...	115
5.2.2 ...and beyond	116
5.2.3 Mediterranean climatic dynamics across the 8.2 kyr B.P. climatic event	116
5.3 References	118
Zusammenfassung	123
Acknowledgements	128
Appendix	130
Curriculum vitae	144
Publication and conference abstracts	146

List of figures

Chapter 1

Fig. 1.1	Map of the drainage route at 8.47 kyr B.P.	4
Fig. 1.2	Map of the Mediterranean region including study sites of this thesis	7
Fig. 1.3	Selection of marine and terrestrial paleoenvironmental reconstructions of the regional responses to northern hemisphere cooling during the 8.2 kyr B.P. climatic event in the greater Aegean region	8
Fig. 1.4	Palynological reconstruction of seasonal temperature and precipitation amounts during the early Holocene from Tenaghi Philippon	9
Fig. 1.5	Map of the classical site of Tenaghi Philippon within the Drama Basin	10
Fig. 1.6	δD and $\delta^{18}\text{O}$ values of globally distributed precipitation	14
Fig. 1.7	Schematic overview of the development of δD and $\delta^{18}\text{O}$ in precipitation forming from an individual air mass during continuous terrestrial rainout	15
Fig. 1.8	Schematic diagram of the hydrogen isotopic relationship between precipitation and leaf wax <i>n</i> -alkanes from terrestrial plants	19
Fig. 1.9	Typical $\delta^{13}\text{C}$ distribution of plants following the C_3 and C_4 photosynthetic pathway	20

Chapter 2

Fig. 2.1	Digital elevation model of the Central Anatolian Plateau showing sample locations as well as selected meteorological stations of the Global Network of Isotopes in Precipitation	37
Fig. 2.2	Distribution of mean annual temperature and mean annual precipitation in Central Anatolia	39
Fig. 2.3	Spatial distribution of δD and $\delta^{18}\text{O}$ over the Central Anatolian Plateau	44
Fig. 2.4	Spatial distribution of deuterium excess (<i>d</i>) values over the Central Anatolian Plateau	45
Fig. 2.5	δD versus $\delta^{18}\text{O}$ of water samples collected on the plateau margins and the plateau interior	47
Fig. 2.6	Meteoric water isotopic regimes over Central Anatolia as derived from the analysis of the Meteoric Water Lines, and compared to the distribution of the mean annual precipitation	48
Fig. 2.7	δD and $\delta^{18}\text{O}$ versus average catchment elevation of water samples collected on the northern and southern plateau margins	50

Fig. 2.8	δD versus $\delta^{18}O$ of water samples collected in a 70-km radius around the GNIP station in Ankara compared to the mean monthly precipitation recorded at this station	53
----------	---	----

Chapter 3

Fig. 3.1	Locations of Tenaghi Philippon and marine core SL152 in the northeastern Mediterranean region	65
Fig. 3.2	<i>n</i> -alkane distributions and stable carbon isotopic composition of total organic carbon of the studied section of core TP-2005	70
Fig. 3.3	Pollen record of the studied section of core TP-2005	74
Fig. 3.4	Comparison of <i>n</i> -alkane distribution, stable carbon isotopic composition of total organic carbon and selected pollen taxa with plant wax-derived stable hydrogen isotopic composition and palynological reconstructions of seasonal temperature and precipitation of the studied section of core TP-2005	76

Chapter 4

Fig. 4.1	Major atmospheric circulation patterns affecting Mediterranean climate dynamics	87
Fig. 4.2	Map of the northeastern Mediterranean region with the locations of Tenaghi Philippon and marine core SL152	89
Fig. 4.3	δD isotopic composition of the long chain <i>n</i> -alkanes <i>n</i> -C ₂₇ , <i>n</i> -C ₂₉ and <i>n</i> -C ₃₁ of core TP-2005	93
Fig. 4.4	Comparison of δD_{wax} of core TP-2005 to local paleoclimatic parameters	96
Fig. 4.5	Comparison of δD_{wax} of core TP-2005 to regional and supraregional paleoclimatic parameters	99
Fig. 4.6	Schematic figures of principal air mass trajectories affecting the Drama Basin before and after and during the isotope events occurring in relation to the 8.2 kyr B.P. climatic event	100

Appendix

Fig. A.1	Spatial distribution of δD and $\delta^{18}O$ from the Aegean coast towards the plateau interior	141
----------	--	-----

List of tables

Chapter 2

Tab. 2.1 Yearly precipitation-weighted mean δD_p and $\delta^{18}O_p$ values of GNIP stations in Central Anatolia 41

Tab. 2.2 Linear correlation coefficients (R^2) between isotopic composition and sampling elevation (SE) as well as average catchment elevation (ACE) for all samples from the windward flanks of the Pontic and Taurus Mountains. 49

Chapter 3

Tab. 3.1 *n*-alkane concentration, *n*-alkane distributions and $\delta^{13}C_{TOC}$ values of the studied interval of core TP-2005. 68

Chapter 4

Tab. 4.1 δD and CPI values of the long chain *n*-alkanes *n*-C₂₇, *n*-C₂₉ and *n*-C₃₁ from the early to mid-Holocene of core TP-2005 92

Appendix

Tab. A.1 geographic coordinates of sample locations (WGS84), elevations, calculated average catchment elevations and stable hydrogen and oxygen isotopic ratios of meteoric water samples in Central Anatolia. 130

Tab. A.2 Isotopic lapse rates in the Pontic and Taurus Mountains based on surface water flows 140

Tab. A.3 Age-depth correlation and sedimentation rates of core TP-2005 for the early to middle Holocene interval studied. 142

Abbreviations

(V)SMOW	(Vienna) Standard Mean Ocean Water
a.s.l.	above sea level
ACE	Average catchment elevation
ACL	Average Chain Length
AMOC	Atlantic Meridional Overturning Circulation
ASTER	Advanced Spaceborne Thermal Emission and Reflection Radiometer
B.P.	before present, (1950)
CAP	Central Anatolian Plateau
CPI	Carbon Preference Index
<i>d</i>	Deuterium excess
ENSO	El Niño-Southern Oscillation
GC	Gas chromatography
GC/MS	Gas chromatography/mass spectrometry
GCM	General circulation model
GDGT	Glycerol dialkyl glycerol tetraether
GIS	Geographic Information System
GISP2	Greenland Ice Sheet Project 2
GMWL	Global Meteoric Water Line
GNIP	Global Network of Isotopes in Precipitation
<i>h</i>	humidity
IAEA	International Atomic Energy Agency
IPCC	Intergovernmental Panel on Climate Change
IRMS	Isotope ratio mass spectrometer
ITCZ	Intertropical Convergence Zone
LMWL	Local Meteoric Water Line
MAP	Mean annual precipitation
MAT	Mean annual temperature
MIS	Marine Isotope Stage
NAO	North Atlantic Oscillation
NAO	North Atlantic Oscillation
P_{aq}	Aquatic Index
PDB	Pee Dee Belemnite
Pont	Pontic Mountains
SD	Standard deviation
SSS	Sea surface salinity
SST	Sea surface temperature
Taur	Taurus Mountains
TIC	Total ion current
TLE	Total lipid extract
TMWL	Turkish Meteoric Water Line
TP	Tenaghi Philippon
TSMS	Turkish State Meteorological Survey
WMO	World Meteorological Organization

Abstract Despite mounting evidence of the anthropogenic influence on the Earth's climate, underlying mechanisms of climate change often remain elusive. The investigation of periods of rapid climate change from geological archives may provide crucial information about magnitude, duration, teleconnections of and regional responses to global and hemispheric scale climate perturbations. Thus, paleoclimate reconstructions may help in mitigating and adapting to the challenges of the coming decades. The '8.2 kyr B.P. climatic event' has previously been proposed as a possible analogue for the future climatic scenario of a reduced Atlantic Meridional Overturning Circulation (AMOC). The catastrophic drainage of the Laurentide meltwater lakes through the Hudson Bay and into the Labrador Sea, that occurred ca. 8.47 kyr B.P., caused the slowdown of the AMOC around 8.2 kyr B.P.. Subsequently, reduced heat transfer towards Europe triggered a substantial decline in (winter) temperature and pronounced changes in atmospheric circulation patterns in many regions of the northern hemisphere, especially the North Atlantic realm and Europe. Among the regions affected by the 8.2 kyr B.P. climatic event, the Eastern Mediterranean region is of particular interest for both past and future climate developments. Traditionally characterized as a region highly sensitive to variations in the climate systems of the high and low latitudes, abrupt climate changes have the potential to strongly alter atmospheric circulation patterns and thus precipitation distribution in the region that may have severe socioeconomical consequences. The analysis of stable hydrogen (δD) and oxygen isotopes ($\delta^{18}\text{O}$) in precipitation is an excellent tool to trace changes in atmospheric circulation. Here, we present a comparative study of δD and $\delta^{18}\text{O}$ in precipitation from the Eastern Mediterranean region both in a present day scenario and during the 8.2 kyr B.P. climatic event. We analyze the influences of topography, air mass trajectory, climate and seasonality among others the stable isotopic compositions of meteoric waters from the Central Anatolian Plateau (CAP), Turkey, in order to create a first-order template which may serve as a reference against which paleoenvironmental proxy data may be more accurately interpreted and tested. Further, we employ a multiproxy approach on the early Holocene peat deposits of the classical site of Tenaghi Philippon (TP), NE Greece, to investigate paleoenvironmental responses to northern hemisphere cooling during the 8.2 kyr B.P. climatic event and aim to determine changes atmospheric circulation from δD of leaf wax *n*-alkanes ($\delta\text{D}_{\text{wax}}$).

Based on δD and $\delta^{18}\text{O}$ data from more than 480 surface water samples from the CAP, we characterize moisture sources affecting the net isotopic budget of precipitation, manifesting in a systematic north-south difference in near-sea level moisture compositions. Rainout, induced by the major orographic barriers of the plateau, the Pontic Mountains to the north and the Taurus Mountains to the south, strongly shape the modern patterns of δD and $\delta^{18}\text{O}$. Stable isotope data from the semi-arid plateau interior provide clear evidence for an evaporitic regime that drastically affects surface water compositions. Strong evaporative

enrichment contrasts rainfall patterns along the plateau margins, in part obfuscating the effects of topography and air mass trajectory.

Consequently, in order to address possible influences of evaporation on δD and $\delta^{18}O$ in paleoprecipitation from TP, we analyze *n*-alkane abundances and distributions along with stable carbon isotope compositions of total organic carbon ($\delta^{13}C_{TOC}$) and palynological data to estimate surface moisture conditions during the early Holocene (ca. 8.7 - 7.5 kyr B.P.) and especially during the 8.2 kyr B.P. climatic event. A period of relatively dry surface conditions from ca. 8.7 to 8.2 kyr B.P., indicated by low values of the 'aquatic index' (P_{aq}) and by elevated Average Chain Length (ACL) values, in concert with elevated $\delta^{13}C_{TOC}$ values, precedes the 8.2 kyr B.P. climatic event. The event itself is characterized by slightly wetter, more humid conditions, as suggested by an increase in P_{aq} values as well as reduced ACL and $\delta^{13}C_{TOC}$ values between ca. 8.2 and 7.9 kyr B.P.. In the upper section of the core, a distinct change in paleohydrology becomes. A steep increase in P_{aq} and a decrease in ACL values as well as variations in $\delta^{13}C_{TOC}$ from 7.9 kyr B.P. onwards imply considerably elevated surface moisture levels, likely caused by the increased activity of the karstic system of the surrounding mountains. Collectively, the biomarker proxies presented here, reveal a concise picture of changing moisture conditions at TP that is consistent with palynological data and provide detailed paleoenvironmental information for the analysis of δD_{wax} as a paleoprecipitation proxy. The long-term decline in δD_{wax} values characterizes the lower section of the core until ca. 8.2 kyr B.P.. The 8.2 kyr B.P. climatic event itself is connected to two distinct positive hydrogen isotope excursions: a minor shift in δD_{wax} around 8.2 kyr B.P. and a major shift in δD_{wax} between ca. 8.1 and 8.0 kyr B.P.. The upper part of the section shows a progressive trend towards higher δD_{wax} values. With no indication of increased evaporitic conditions at TP during the 8.2 kyr B.P. climatic event, as evident in biomarker proxies and pollen data, we link shifts in δD_{wax} to changes in Mediterranean air mass trajectories supplying precipitation to northeastern Greece, with variations in the relative contributions of northerly-derived, D-depleted moisture and southerly-derived, D-enriched moisture. Possible control mechanisms include changes in the influence of the Siberian High and differences in the influence of the African and Asian monsoon circulations on anticyclonic conditions in the Mediterranean region as well as regional inflow of moist air from the Aegean Sea.

Chapter 1

Introduction

1.1 *Motivation and aim of research*

Understanding paleoclimate dynamics requires the investigation of the complex relationship between global and regional responses to internal and external forcing factors on different temporal scales. Over the longer glacial-interglacial timescales, climatic variations are known to be large, both in amplitude as well as in spatial extent (Dansgaard et al., 1993; Kawamura et al., 2007). And while glacial-interglacial climate dynamics strongly correlate with orbital forcing (Hays et al., 1976), external factors alone are not sufficient to explain the observed climate variability. Intervals of periodic warming, labeled 'Dansgaard-Oeschger events' and 'Heinrich events', repeatedly interrupted the last glacial period several times (Bond et al., 1992; Bond and Lotti, 1995). These events have been linked to slowdown of the Atlantic Meridional Overturning Circulation (AMOC), caused by large freshwater discharge into the North Atlantic Ocean (Shackleton et al., 2000; Elliot et al., 2002; McManus et al., 2004). Compared to the large climatic variations of the glacial-interglacial transitions, climatic variations of the current interglacial, the Holocene, generally have been smaller and often spatially incoherent (Wanner et al., 2008). But similar to the previous interglacial, Holocene climate dynamics have been affected by both internal and external forcing factors. A long term global cooling trend, in response to decreasing solar radiation induced by a shift in obliquity (Marcott et al., 2013), is marked by several distinct periods of rapid climate change (Mayewski et al., 2004; Wanner et al., 2011). These periods are mostly characterized by polar cooling, tropical aridity and major atmospheric circulation changes, largely driven by cyclic variations in solar activity, changes in atmospheric greenhouse gas concentrations and volcanic activity (Bond et al., 1997; Bond et al., 2001; Mayewski et al., 2004). Additionally, northern hemisphere deglaciation played a major role in rapid climate changes in the early Holocene (Clark et al., 1999). In general, the presence of ice sheets influences climate because they are large topographic features that create regional anomalies in albedo and radiation balance, thus potentially influencing regional as well as global atmospheric circulation patterns. Also, they represent the largest readily exchangeable freshwater reservoir on Earth, reorganizing continental drainage systems and marine circulations as freshwater fluxes vary during growth and shrink (Clark et al., 1999; Clark et al., 2001). An important component in early Holocene climate dynamics is the Laurentide Ice Sheet on the North American continent (Fig. 1.1).

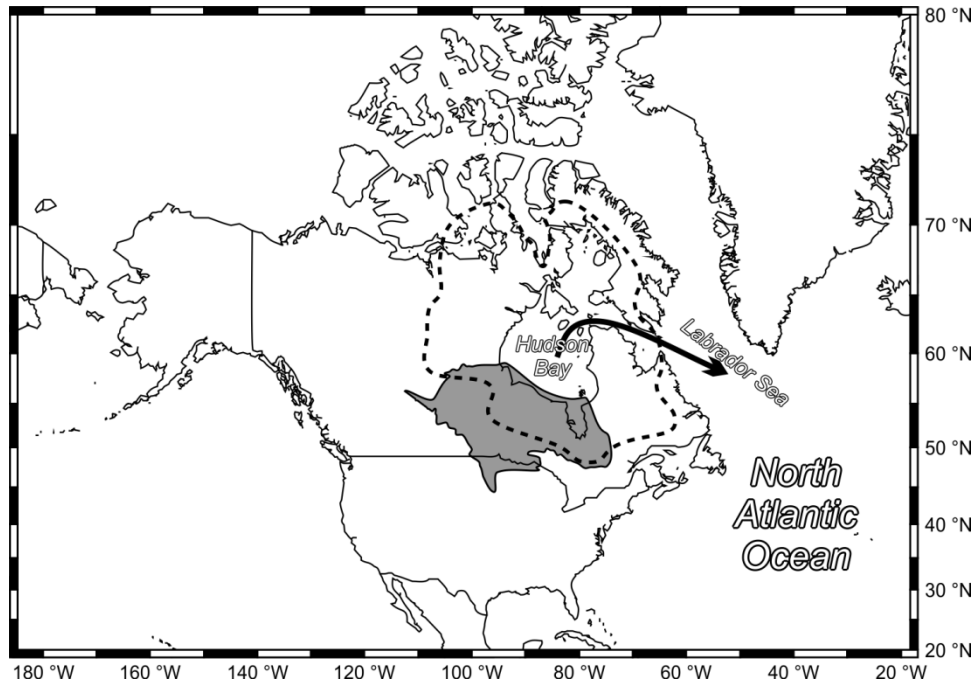


Fig. 1.1 Map of the drainage route at 8.47 kyr B.P.. Area covered by Lake Agassiz and Lake Ojibway is shaded. Dashed line marks the extent of the Laurentide Ice Sheet at ca. 9 ¹⁴C kyr B.P.. Arrow indicates drainage route into the Hudson Bay and through Labrador Strait into the North Atlantic (after Teller et al., 2002).

During the last deglaciation, two proglacial lakes formed on the boundary of the Laurentide Ice Sheet: Lake Agassiz and Lake Ojibway. After merging in the final stages of the retreat of the Laurentide Ice Sheet prior to 8.45 kyr B.P., these two meltwater lakes formed the largest proglacial lake in North America, with an extent of more than 800,000 km² (Leverington et al., 2000; Teller et al., 2004). Over its 5000-year history, Lake Agassiz drained several times through various routes into the Gulf of Mexico, the Arctic Ocean, the North Atlantic Ocean and the Hudson Bay (Teller et al., 2002). The final and largest of these drainage events occurred around 8470 years B.P., subglacially releasing an estimated amount of 100,000 to 200,000 km³ freshwater in less than a year through the Hudson Bay into the Labrador Sea and eventually into the North Atlantic Ocean (Barber et al., 1999; Leverington et al., 2000; Clarke et al., 2004; Teller et al., 2004; Hillaire-Marcel et al., 2007). Upon reaching the region of deep water formation in the North Atlantic, a vital component of the AMOC, the massive amount of freshwater effectively capped surface water and significantly altered deep water circulation between ca. 8.38 and 8.27 kyr B.P. (Ellison et al., 2006; Kleiven et al., 2006). The ensuing slowdown of the AMOC severely reduced heat transfer by North Atlantic Ocean currents towards Europe (Renssen et al., 2001; Bauer et al., 2004; Wiersma and Renssen, 2006), thus causing arguably the strongest deterioration in Holocene climate of the northern hemisphere: the '8.2 kyr B.P. climatic event'.

The 8.2 kyr B.P. climatic event was first described as the largest deviation in nearly all Holocene ice core proxy records from the Greenland Ice Sheet (Alley et al., 1997). While the general pattern of the event - notably pronounced cooling and drying, accompanied with changes in atmospheric circulation - is similar to previous rapid cooling events, like the Younger Dryas, the magnitude of the 8.2 kyr B.P. climatic event is generally estimated to be roughly half compared to the Younger Dryas, albeit of significantly shorter duration (Alley et al., 1997). Based on ice core chronologies from Greenland, the 8.2 kyr B.P. climatic event lasted around 160 years (Thomas et al., 2007). It began around 8.2 kyr B.P. with a period of rapid cooling of ca. 3.3 ± 1.1 °C that lasted ca. 20 years. Several decades of reduced temperatures were then followed by a gradual climatic recovery over a period of ca. 70 years (Kobashi et al., 2007). However, the effects of the 8.2 kyr B.P. climatic event were not limited to Greenland. The slowdown of the AMOC and the resulting reduction in heat transfer towards Europe brought generally cold and dry conditions, especially in winter, to many regions in the northern hemisphere, albeit most strongly pronounced in the North Atlantic realm and in Europe (Alley and Ágústsdóttir, 2005; Morrill et al., 2013). However, model studies and proxy records suggest a (near) global response to the freshwater outburst from the Laurentide meltwater lakes. Changes in large scale atmospheric circulations, like the monsoonal systems (Wang et al., 2005; Cheng et al., 2009; Liu et al., 2013) and the Intertropical Convergence Zone (ITCZ) (Haug et al., 2001), coincide with northern hemisphere cooling around 8.2 kyr B.P.. The notion of a large-scale impact of the 8.2 kyr B.P. climatic event on atmospheric circulation patterns is strengthened by model studies and proxy records implying the simultaneous occurrence of atmospheric circulation changes in Greenland and on hemispheric scale (LeGrande et al., 2006; Thomas et al., 2007). Also, despite the scarcity of proxy records from the tropics and the southern hemisphere (Morrill and Jacobsen, 2005), model studies suggest a contribution of meltwater outbursts from the retreating Laurentide Ice Sheet to early Holocene cold conditions in the southern hemisphere (Renssen et al., 2010). This notwithstanding, identifying regional responses to the effects of northern hemisphere cooling around 8.2 kyr B.P. is challenging as the rapid cooling event is embedded in a period of weak millennial-scale cooling oscillation from ca. 8.5 and 8.0 kyr B.P., previously linked to solar forcing (Bond et al., 1997; Bond et al., 2001; Rohling and Pälike, 2005). Therefore, in order to fully characterize the impact of the 8.2 kyr B.P. climatic event on a regional scale, sufficiently resolved proxy records are required that consider the centennial as well as seasonal nature of the event.

The 8.2 kyr B.P. climatic event provides a relatively solid force-to-impact relationship between the slowdown of the AMOC due to freshwater forcing and hemispheric to global

rapid climatic change. As such, the 8.2 kyr B.P. climatic event has previously been suggested as an 'upper limit' for the possible future scenario of partial or total shutdown of the AMOC due to anthropogenic influences (Alley and Ágústsdóttir, 2005). The Intergovernmental Panel on Climate Change (IPCC) state in their fifth assessment report that it is very likely that the AMOC will weaken over the course of the 21st century between 11 % and 34 % in response to rising CO₂ levels in the atmosphere as well as freshwater influx from the shrinking Greenland Ice Sheet (Collins et al., 2013). As such, climatic variations related to the 8.2 kyr B.P. climatic event provides valuable insight into hemispheric to global climate dynamics as well as potentially serve as an analogue for predicted future climate fluctuations. Among the regions of particular interest in that regard is the Mediterranean Sea region. The Mediterranean Sea and its bordering landmasses are considered highly vulnerable to climate changes (Kovats et al., 2012). Traditionally described as a region with inherently complex climate patterns due to the diverse morphology of the Mediterranean borderlands, the vulnerability to supraregional climate variations stems from the basins transitional location between the climatic systems of the temperate north and the subtropical south (Lionello et al., 2012). Fluctuations in these high and low latitude climate systems, eventually caused by interhemispheric or even global climatic deviations, have the potential to leave a strong imprint on annual as well as seasonal regional climate and hence can cause severe changes in temperature and precipitation distribution. With the high human population in the Mediterranean Sea region, these projected large-scale climatic perturbations present profound socio-ecological challenges that need to be addressed in the coming decades (UNEP/MAP-Plan Bleu, 2009).

The present-day climate of the Mediterranean region is marked by strong geographical and seasonal contrasts (Lionello et al., 2012). The traditional classification describes Mediterranean climate as temperate with a dry, warm or hot summer season (Köppen, 1900). However, other temperate, arid and snow climates are present on the landmasses surrounding the Mediterranean Sea. Despite being linked to the dynamics of the Mediterranean Sea, mesoscale climate of the Mediterranean region is to a large extent forced by synoptic scale climate patterns (Ulbrich et al., 2012). Variations in the North Atlantic Oscillation (NAO) (Dükeloh and Jabobeit, 2003; Xoplaki et al., 2003), the monsoonal circulations (Rodwell and Hoskins, 1996; Ziv et al., 2004) and even the El Niño-Southern Oscillation (ENSO) (Mariotti et al., 2002) contribute to spatial and temporal Mediterranean climate variability. Thus, (paleo)climatic investigation of Mediterranean climate provides an excellent opportunity to investigate teleconnections between regional and hemispheric scale to global climatic patterns. However, the regional responses to large-scale forcing factors in the Mediterranean basin are

complex. The complicated land-sea distribution divides the basin into two larger subbasins, the Western Mediterranean and the Eastern Mediterranean basin, connected through the Strait of Sicily, as well as several smaller subbasins, often bordered by steep coastal mountain ranges, especially in the northern borderlands of the Mediterranean Sea (Fig. 1.2).

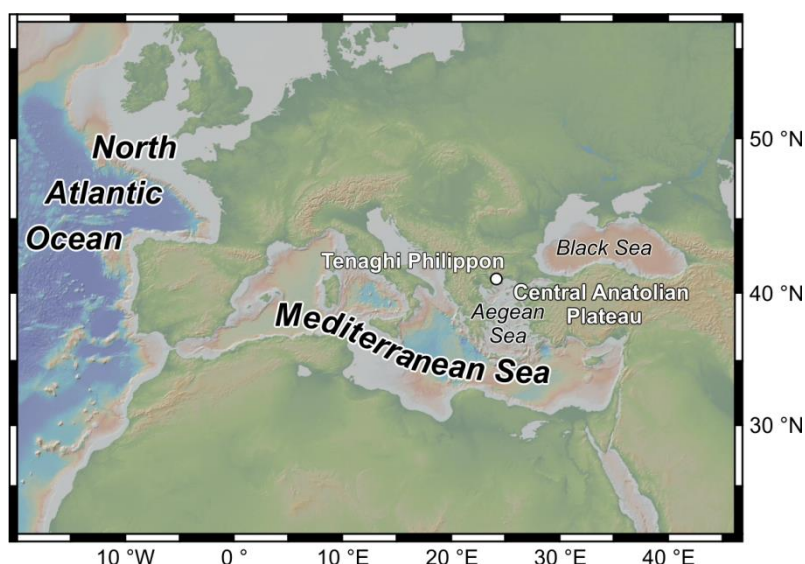


Fig. 1.2 Map the Mediterranean region including study sites of this thesis.

These topographic features produce a distinct spatial heterogeneity in Mediterranean climate, most pronounced in the spatial distribution of precipitation (Lionello et al., 2012; Ulbrich et al., 2012). Regional differences notwithstanding, hydrological conditions in the circum-Mediterranean region have varied substantially throughout the Holocene (Jalut et al., 2009). In the early Holocene (ca. 11.7 to 7 kyr B.P.), over all humid conditions with wetter winters and drier summers compared to the present, prevailed in many regions. Following the decrease in insolation in the mid-Holocene, a transitional phase from ca. 7 to 5 kyr B.P. preceded widespread aridification and successively decreasing seasonality from ca. 5 kyr B.P. to the present. Superimposed on the general hydrological evolution are several phases of short-lived climatic oscillation that have been linked to substantial changes in Neolithic societies (Staubwasser and Weiss, 2006). Especially in the Eastern Mediterranean region, centennial scale dry episodes in the early to mid-Holocene may have reduced agricultural activity and induced migration of human communities in the region (Weiss, 1978; Weninger et al., 2006). Alongside archeological indications, various paleoclimatic records attest to the strong impact of rapid climate change during the 8.2 kyr B.P. climatic event on paleoclimatic and paleoceanographic conditions in the Eastern Mediterranean region, such as the Aegean region. Episodes of pronounced cooling of the Aegean Sea surface have been linked to increases in strength, duration and/or frequency of outbreaks of continental, polar air masses that are typical for regional

winter climate, and imply a stronger influence of the high-latitude Siberian High on the Aegean region at the expense of low-latitude, monsoonally-influenced circulation patterns, otherwise prevalent during the early Holocene (Rohling et al., 2002; Kotthoff et al., 2008a; Marino et al., 2009). This concept is corroborated by multiple marine and terrestrial reconstructions, suggesting pronounced cooling and/or drying related to northern hemisphere cooling around 8.2 kyr B.P. (Fig. 1.3).

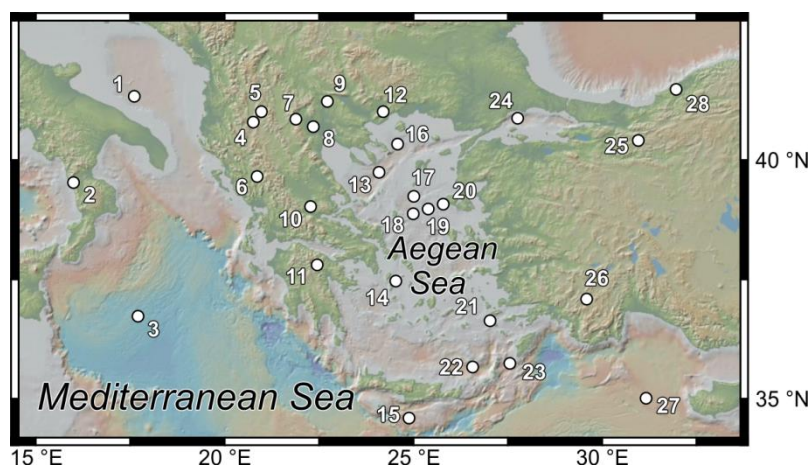


Fig. 1.3 Selection of marine and terrestrial paleoenvironmental reconstructions of the regional responses to northern hemisphere cooling during the 8.2 kyr B.P. climatic event in the greater Aegean region. 1. MD90-917 (Siani et al., 2010; Combourieu Nebout et al., 2013; Siani et al., 2013; Sicre et al., 2013). 2. Lake Trifoglietti (Joannin et al., 2012; Peyron et al., 2013). 3. RL11 (Emeis et al., 2000). 4. Lake Maliq (Bordon et al. 2009). 5. Lake Prespa (Panagiotopoulos et al., 2013). 6. Lake Ionnina (Wilson et al. 2008). 7. Nisi Fen (Lawson et al. 2005). 8. Neo Nikomideia (Ghilardi et al. 2012). 9. Lake Dojran (Francke et al., 2013). 10. Lake Xinias (Digerfeldt et al. 2007). 11. Lake Stymphalia (Heymann et al., 2013). 12. Tenaghi Philippon (Pross et al., 2007; Peyron et al., 2011; this thesis) 13. SL-148 (Ehrmann et al., 2007; Kuhnt et al., 2007; Hamann et al., 2008; Schmiedl et al., 2010). 14. SLA-9 (Casford et al., 2003). 15. HCM2-22 (Kouli et al., 2012). 16. SL-152 (Kotthoff et al., 2008a, b; Dormoy et al., 2009). 17. MNB3 (Gogou et al., 2007; Geraga et al., 2010; Kouli et al., 2012). 18. SL-31 (Schmiedl et al., 2010). 19. SL-21 (Casford et al., 2003; Marino et al., 2009). 20. SL-11 (Casford et al., 2003). 21. NS-14 (Triantaphyllou et al., 2009; Kouli et al., 2012). 22. LC-21 (Rohling et al., 2002; Casford et al., 2003; Marino et al. 2009). 23. SL-123 (Ehrmann et al., 2007; Kuhnt et al., 2007; Schmiedl et al., 2010). 24. KL71 (Sperling et al., 2003). 25. Lake Sünnet (Oçakoğlu et al., 2013). 26. Gölhisar Gölü (Eastwood et al., 2006). 27. LC-31 (Schmiedl et al., 2010). 28. Sufolar cave (Fleitmann et al., 2009, Gökturk et al., 2011).

However, while most paleoclimatic studies from the Aegean region link observed climatic deteriorations to increased outbreaks of the Siberian High, thus supporting the notion of the 8.2 kyr B.P. climatic event being biased towards winter climate (Alley and Ágústsdóttir, 2005, Rohling and Pälike, 2005), changes in atmospheric circulation in spring and summer are less well constrained. Present day precipitation seasonality in the Eastern Mediterranean region is reinforced by strong anticyclonic activity over the Mediterranean Sea (Lionello et al., 2006). Yet, palynological reconstructions of seasonally resolved temperature and precipitation values imply a reduction in seasonality in the Aegean region during the 8.2 kyr B.P. climatic event (Fig. 1.4; Pross et al., 2009; Peyron et al., 2011).

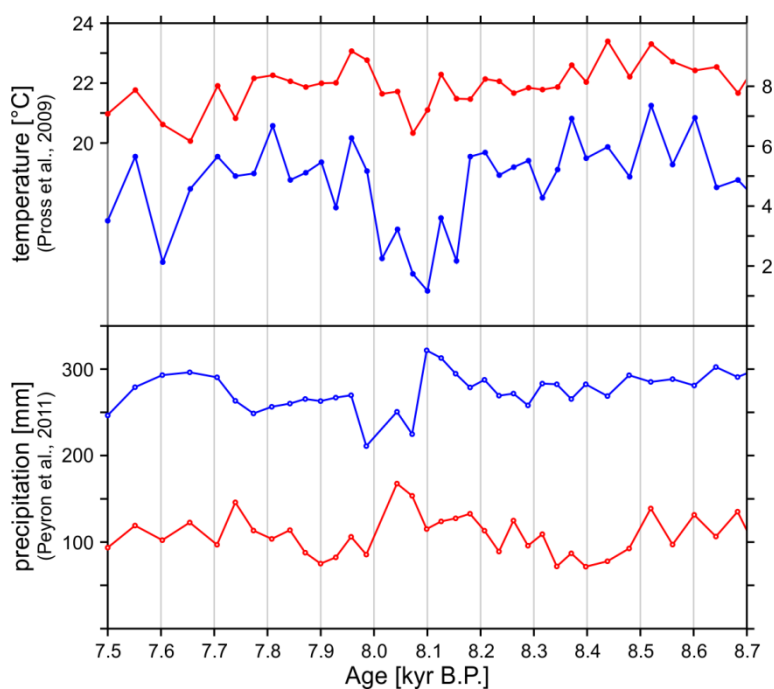


Fig. 1.4 Palynological reconstruction of seasonal temperature and precipitation amounts during the early Holocene from Tenaghi Philippon (Pross et al., 2009; Peyron et al., 2011).

While temperature seasonality changes can well be explained with an increase in outbreaks of polar, continental air, thus supporting the winter bias of the 8.2 kyr B.P. climatic event (Pross et al., 2009), shifts in precipitation seasonality, with decreasing amount of winter precipitation and increasing amount of summer precipitation, suggest pronounced changes in atmospheric circulation beyond the influence of the Siberian High. Thus, raising the question:

How does northern hemisphere cooling during the 8.2 kyr B.P. climatic event affect spring and summer atmospheric circulation patterns in the Aegean region?

The investigation of stable isotopes in precipitation is an excellent tool for tracing atmospheric circulation changes. Stable hydrogen isotopic compositions of leaf wax *n*-alkanes derived from vascular terrestrial plants reflect the isotopic composition of source water during plant growth which in turn is modulated by hydrological processes. A brief overview of the relevant mechanism affecting stable isotopic compositions of both precipitation and leaf wax *n*-alkanes will be presented in sections 1.3 and 1.4 respectively. The classical site of Tenaghi Philippon in northeastern Greece provides the unique opportunity to reconstruct paleoclimatic dynamics in the Aegean region across the early Holocene, and thus regional responses to northern hemisphere cooling of the 8.2 kyr B.P. climatic event.

1.2 Study site: the classical site of Tenaghi Philippon

The classical site of Tenaghi Philippon (TP) is located in the Philippi peatland in the southeastern part of the Drama Basin, northeastern Greece (Fig. 1.5). Formed as a result of post-orogenic extension beginning in the early to middle Miocene, the Drama Basin is largest graben structure in northeastern Greece and the Balkanides (Pross et al., 2015). Characterized as a low-elevation, intramontain basin typical for the region, the Drama Basin is bordered by the Phalakron Range (2232 m.a.s.l.) to the north, the Menikion (1266 m.a.s.l.) and Pangaeon (1956 m.a.s.l.) ranges to the west and south, the Lekanis Mountains (1150 m.a.s.l.) to the east and separated from the Aegean Sea by the Symvolon Range (477 m.a.s.l.) to the southeast.

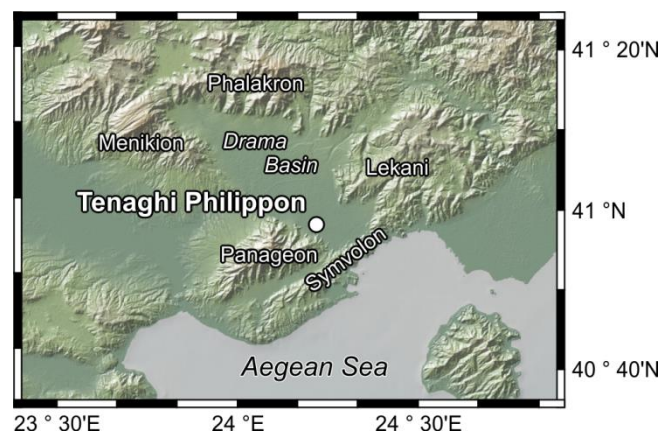


Fig. 1.5 Map of the classical site of Tenaghi Philippon within the Drama Basin.

During the subsidence in the Miocene and the Pliocene, a continuous succession of terrestrial, fluvial and lacustrine sediments was deposited in the basin. Steady sedimentation of terrestrial material led to the formation of a topogenic fen since the early Pleistocene. Interrupted by several lacustrine episodes, telmatic conditions prevailed across the basin since the middle Pleistocene until being artificially drained in the 1930s and 1940s (Christanis, 1983; Pross et al., 2015). Hydrological conditions in the basin are controlled by variations in surface runoff from the Phalakron Range to the north of the basin along with inflow from the karstic systems of the Pangaeon and Lekanis ranges on the southwestern and eastern edges of the basin (Christanis, 1983; Kalaitzidis and Christanis, 2003). The sedimentary sequence of the Philippi peatland consists mainly of fen peat and lignite as well as marls and calcareous clay. Coarse-grained alluvial sediments are present along the basin margins (Pross et al., 2015). The vegetation in the Philippi peatland has been significantly altered by human activity. Original vegetation consisted primarily of Cyperaceae, mostly *Carex* sp. and *Cladium mariscus*, along with *Nymphaea alba*, *Polygonum amphibium*, *Phragmites communis*, *Iris pseudacorus*, *Typha angustifolia* and *Schoneplectus tabernaemontani*. Wetland trees

comprised *Alnus* sp., *Populus* sp., *Betula pendula* and *Salix* sp. (Wijmstra, 1969; Pross et al., 2015).

Since the 1960s, the site of TP has been subject of extensive palynological studies (see review by Pross et al., 2015). The first scientific drilling campaign was conducted in 1963 (TF-2; Wijmstra, 1969; Wijmstra and Smit, 1976; Van der Wiel and Wijmstra, 1987a), followed by a second campaign in 1976/77 (TF-3; Wijmstra and Groenhart, 1983; Van der Wiel and Wijmstra, 1987b; Mommersteeg et al., 1995). Spanning ca. 1.35 Ma, the spliced pollen record of TF-2 and TF-3 has been recognized as one of the most prominent terrestrial climate records in Europe (Tzedakis et al., 2006). In 2005, a new coring campaign was initiated to retrieve the upper 60 m of this archive (Pross et al., 2007). This new core, TP-2005 (40° 58.40' N, 24° 13.42' E, 40 m.a.s.l.) covers the interval from the Holocene to Marine Isotope Stage (MIS) 9c, comprising ca. 312 ka (Fletcher et al., 2013). TP-2005 has since yielded new pollen data from the Holocene (Pross et al., 2009; Peyron et al., 2011), MIS 2-4 (Müller et al., 2011), MIS 5 (Milner et al., 2012, 2013) and MIS 7e-9c (Fletcher et al., 2013). The chronology of TP-2005 is mainly based radiocarbon dates and, especially for the Holocene section, is supported by correlation with the palynological record from marine core SL 152 from the NE Aegean Sea (Fig. 1.3; Kotthoff et al., 2008a, b), due to a pronounced hard-water effect (Pross et al., 2009).

The paleoecological and paleoclimatological insights gained from extensive palynological research as well as the abundance of organic material in the peat sequence, along with the core's intriguing location in the northern borderlands of the Aegean Sea make TP an excellent choice for the stable isotopic approach of reconstructing paleoprecipitation across the Holocene with focus on the regional impact of the 8.2 kyr B.P. climatic event.

1.3 *Stable isotopes in meteoric waters*

Over the past decades, the investigation of stable isotopes from environmental sources allowed insight into various naturally-occurring biotic and abiotic processes (e.g., Clark and Fritz, 1997). The essential principle of stable isotope geochemistry is the knowledge of mass differences among atoms of a given element and the observation of fractionation processes that shift the ratio of light versus heavy isotopes in environmental reservoirs. Hydrogen and oxygen in water molecules comprise the light isotopes Hydrogen-1 (^1H) and Oxygen-16 (^{16}O) and the heavy isotopes Hydrogen-2 or "Deuterium" (D) and Oxygen-18 (^{18}O). Due to the considerably higher abundance of the

light isotopes, 99.98 % for ^1H compared to 0.015 % for D and 99.762 % for ^{16}O in contrast to 0.204 % for ^{18}O , the majority of water molecules in meteoric waters are considered "light water" ($^1\text{H}_2^{16}\text{O}$) whereas the heavy isotopologues of water ($^1\text{H}^{16}\text{O}$ and $^1\text{H}_2^{18}\text{O}$) are usually much less abundant. However, the proportion of "light" and "heavy" water molecules and thus the ratio of light versus heavy isotopes can differ significantly between waters from different reservoirs. Variations in the ratios of D/ ^1H and $^{18}\text{O}/^{16}\text{O}$ in meteoric waters are strongly controlled by meteorological processes that fractionate the two isotopes in a rather predictable way (Craig, 1961). Since fractionation processes impart only slight differences on the absolute ratios of D/ ^1H and $^{18}\text{O}/^{16}\text{O}$, isotope ratios are commonly expressed as δ -values, measured in permil (‰) differences from a known reference. Thus, variations in hydrogen isotopes are given as

$$\delta\text{D}_{\text{sample}} = \left(\frac{(\text{D}/\text{H})_{\text{sample}}}{(\text{D}/\text{H})_{\text{reference}}} - 1 \right) \cdot 1000 \text{‰ VSMOW}$$

and for oxygen isotopes as

$$\delta^{18}\text{O}_{\text{sample}} = \left(\frac{(^{18}\text{O}/^{16}\text{O})_{\text{sample}}}{(^{18}\text{O}/^{16}\text{O})_{\text{reference}}} - 1 \right) \cdot 1000 \text{‰ VSMOW}$$

where the reference used is Vienna Standard Mean Ocean Water (VSMOW).

Isotopic fractionation occurs in any thermodynamic reaction due to different rates of reaction of different isotopes and results in disproportionate concentration of one isotope over the other on one side of the reaction (Urey, 1947). Fractionation in meteoric waters is predominantly associated with phase changes between the liquid and the vapor phase through the hydrological cycle. Evaporation (liquid-vapor transition) and condensation (vapor-liquid transition) fractionate hydrogen and oxygen isotopes amongst the respective reservoirs, albeit following different fraction reactions (Dansgaard, 1964).

The evolution of meteoric waters begins with primary evaporation of ocean water and subsequent integration of the evaporate water vapor into an air mass. Due to the lower vapor pressure of the heavy isotopologues of water, the rate of the evaporation reaction is faster for $^1\text{H}_2^{16}\text{O}$ than for $^1\text{H}^{16}\text{O}$ and $^1\text{H}_2^{18}\text{O}$. Thus, the light isotopologues evaporate preferentially, enriching the vapor phase in ^1H and ^{16}O while the liquid phase gets enriched in D and ^{18}O . Consequently, evaporation produces water vapor with higher δD and $\delta^{18}\text{O}$ values compared to the source water. The degree of isotopic fractionation between the liquid phase and the vapor phase during evaporation is primarily the result of nonequilibrium or *kinetic* isotope effects, affected by sea surface temperature (SST), wind shear, sea surface salinity (SSS) and, most importantly, humidity. Under high

humidity conditions (h close to 100 %), isotopic equilibrium persists whereby D and ^{18}O can exchange freely between the liquid phase and the vapor phase. Decreasing levels of humidity limit water-vapor exchange, making evaporation an increasingly nonequilibrium process. At low humidity, evaporative enrichment follows Rayleigh-type fractionation, leading to progressively higher δD and $\delta^{18}\text{O}$ values in both the residual water as well as the derived water vapor (Gonfiantini, 1986). However, the isotopic composition of atmospheric water vapor is not only the result of kinetic evaporation from the ocean (primary evaporation) but a rather complex mechanism of mixing between water vapor from primary evaporation, water recycling (secondary evaporation) as well as condensation and the eventual formation of precipitation (Craig and Gordon, 1965).

The basic requirement for the formation of precipitation is the formation of clouds (e.g., Clark and Fritz, 1997). As a vapor mass cools, either by adiabatic expansion during ascend or by radiative heat loss, water vapor begins to condensate once the dew point is passed in order to maintain thermodynamic equilibrium. A cloud forms from the vapor mass in which water vapor and water droplets coexist as a mixture at 100 % humidity. Isotopic equilibrium conditions persist between the liquid phase and the vapor phase and water-vapor exchange occurs largely unhindered. Equilibrium fractions preferentially partitions D and ^{18}O into the water droplets while enriching the vapor phase in the ^1H and ^{16}O . As the cloud follows a trajectory away from the water source and continues to cool, eventually it loses water in the form of precipitation. Removal of the isotopically heavy water droplets from the cloud depletes the remaining vapor mass in D and ^{18}O . As rain out progresses and D and ^{18}O preferentially continues to partition into the droplets under equilibrium fractionation conditions, increasingly enriches the vapor mass in ^1H and ^{16}O according to Rayleigh-type distillation. Thus, the first precipitation to form from a vapor mass shows comparably high δD and $\delta^{18}\text{O}$ values and, as rainout continues and δD and $\delta^{18}\text{O}$ of the residual vapor phase decreases, so will δD and $\delta^{18}\text{O}$ of the derived precipitation. δD and $\delta^{18}\text{O}$ values of meteoric waters correlate strongly, primarily due to the temperature dependence of the condensation process (Craig, 1961). On a global scale, δD and $\delta^{18}\text{O}$ values of precipitation fall along the Global Meteoric Water Line (GMWL) that follows the equation

$$\delta\text{D} = 8.13 \delta^{18}\text{O} + 10.8.$$

The difference in absolute values between δD and $\delta^{18}\text{O}$ in meteoric waters is caused by differences in vapor pressure between $^1\text{H}^1\text{D}^{16}\text{O}$ and $^1\text{H}_2^{18}\text{O}$ during condensation under equilibrium conditions that imparts a roughly 8 times greater enrichment of D in the liquid phase compared to ^{18}O .

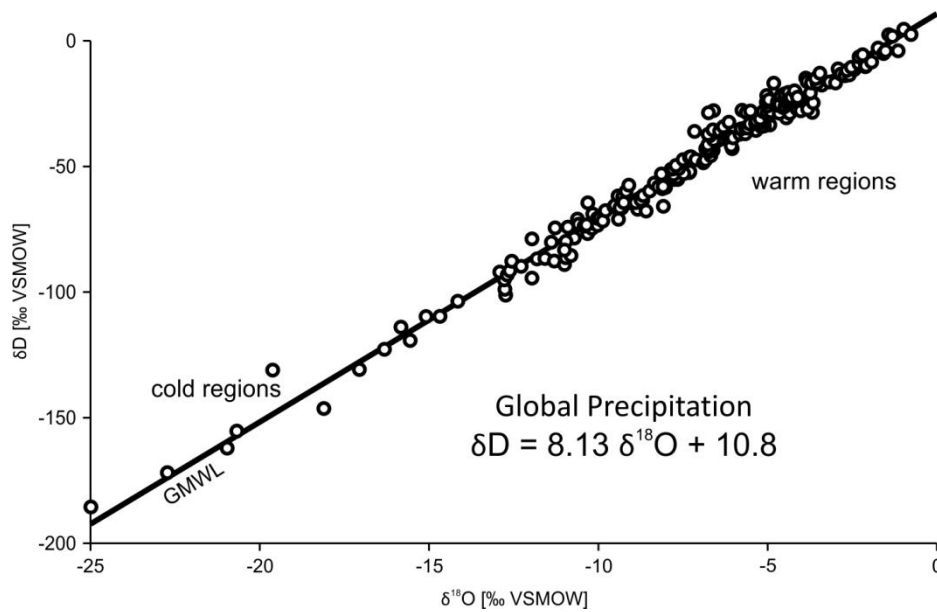


Fig. 1.6 δD and $\delta^{18}O$ values of globally distributed precipitation (after Rozanski et al., 1993).

Globally, high δD and $\delta^{18}O$ values in precipitation are associated with warm regions while low δD and $\delta^{18}O$ values have been linked cold regions (Fig. 1.6; Rozanski et al., 1993). This '*latitude effect*' can be observed on a global scale as a gradient between the tropical region and the Polar Regions (e.g., Clark and Fritz, 1997). Considerably higher δD and $\delta^{18}O$ values occur in tropical (mean annual) precipitation compared to polar (mean annual) precipitation due to temperature differences and further enhanced by the Polar Regions being situated at the end of large scale atmospheric Rayleigh-type rainout processes. Deviations from the general latitudinal trends occur over the continents where the stable isotopic composition of precipitation evolves more rapidly due to topographic effects and temperature changes that characterize continental climates (e.g., Clark and Fritz, 1997). As a vapor mass follows a trajectory away from the source region across a continent and is subjected to Rayleigh-type distillation during continuous rainout, precipitation will be progressively depleted in the heavy isotopes ('*continentality effect*') (Fig. 1.7). Additionally, continental precipitation is subjected to stronger seasonal differences, lacking the mediating marine influence on temperature, resulting in lower δD and $\delta^{18}O$ values during the cold season and higher δD and $\delta^{18}O$ values during the warm season. Also, topography strongly influences the isotopic composition of precipitation (e.g., Clark and Fritz, 1997). Adiabatic ascend of vapor masses on the windward side of mountain ranges drives rainout. Thus, at higher elevations with lower average temperatures, precipitation will be isotopically depleted ('*altitude effect*') (Fig. 1.7). The degree of depletion is given as the isotopic lapse rate, the decrease in δD and $\delta^{18}O$ per change in elevation, thus separating the evolution of isotopes in precipitation on the

windward side of a mountain range from the development of δD and $\delta^{18}O$ on the leeward side (Fig. 1.7). Also, the actual amount of precipitation can potentially affect δD and $\delta^{18}O$ values. The 'amount effect' describes kinetic fractionation between rain drops during light rainfall events falling through an exceedingly arid air mass, leading to evaporative enrichment of D and ^{18}O in the liquid phase (Dansgaard, 1964).

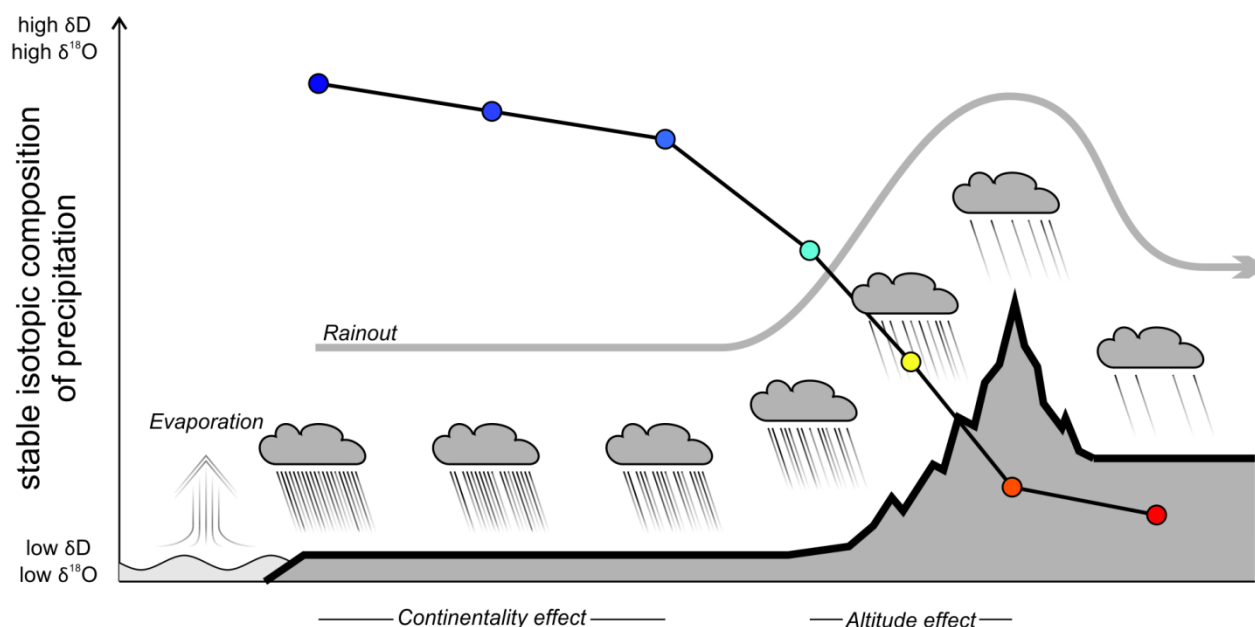


Fig. 1.7 Schematic overview of the development of δD and $\delta^{18}O$ in precipitation forming from an individual air mass during continuous terrestrial rainout.

Collectively, the effects of continentality, topography and precipitation amounts along with possible seasonal and local temperature differences strongly affect δD and $\delta^{18}O$ values of precipitation on a regional scale and are reflected in the Local Meteoric Waterline (LMWL) of an individual vapor mass. The LMWL of a given vapor mass and thus of the derived meteoric waters may deviate strongly from the GMWL, depending on the conditions of the vapor source region, vapor mass trajectory, mixing with other vapor masses, temperature changes and interactions with regional topography and allows the characterization of distinct vapor masses.

1.4 Molecular plant fossils as indicators for paleoenvironmental changes

Ever since their first emergence in the Ordovician (Wellmann et al., 2003), terrestrial plants had to develop mechanisms to adapt to a hostile environment. The appearance of plant cuticles and the stomatal apparatus in early cormophytes during the Late Silurian and Early Devonian has been widely recognized to be an important aspect among the physiological adaptations of the basal precursors of modern terrestrial plants to a relatively dry atmosphere (Raven, 1977, 2001; Edwards et al., 1996). While plant cuticle

and the stomatal apparatus are essential in maintaining the plant's water balance between uptake from the roots and transpiration from the leaves, both serve numerous important ecological functions. The stomatal apparatus is crucial for controlling the gas flux in and out of the leaf by opening or closing the stomata on the lower epidermis. Closing of the stomata limits gas exchange between the leaf and the environment, thereby preventing the loss of water vapor and reducing the risk of desiccation while limiting the uptake of CO₂ required for photosynthesis. The cuticle is a protective layer of polymeric hydrocarbons and soluble waxes, covering the outer surface of epidermis cells of vascular plants. Coated by a film of epicuticular waxes that often form a visible layer on the leaf's surface, the cuticle serves a variety of functions, from protection against water vapor loss, controlling gas exchange, water and particle repellence, protection from mechanical damage of the plant tissue, attenuation of photosynthetically active and UV light to interaction with microorganisms and insects among others (Riederer, 2006 and references therein). The epicuticular wax layer typically consist of a mixture of homologue series of *n*-alkanes, primary *n*-alcohols, *n*-aldehydes, esters and fatty acids that form microcrystalline and/or amorphous structures on the plant cuticle (e.g., Jetter et al., 2006). The mechanism of wax deposition on the leaf surface is poorly understood but it is assumed that the compounds are being synthesized within the leaf before being transported across the cuticle by various proteins and rapidly deposited during leaf flush (Jeffree, 2006; Kunst et al., 2006; Shepard and Griffiths, 2006). Among the molecular constituents of the epicuticular wax layer, *n*-alkanes are likely the most widely used in (paleo)environmental and (paleo)ecological research (see reviews by Eglinton and Eglinton, 2008; Castañeda and Schouten, 2011; Sachse et al., 2012). Typically, leaf wax *n*-alkanes are present as a homologue series with chain lengths of 20 to almost 40 carbon atoms with the odd-numbered chain lengths usually in much higher abundance. The predominance of odd- over even-numbered carbon chain lengths is the result of the polyketide biosynthetic pathway that forms odd-numbered *n*-alkanes by loss of a single carbon atom from the even-numbered precursor *n*-alkanoic acid (e.g., Eglinton and Eglinton, 2008; Sachse et al., 2012). The actual chain length distribution of *n*-alkanes varies widely between different plant groups with one or two homologues usually occurring predominantly over several others. Short chain length *n*-alkanes (*n*-C₁₇ to *n*-C₂₁) dominate in aquatic algae (Giger et al., 1980; Cranwell et al., 1987) whereas mid-chain homologues (*n*-C₂₃ to *n*-C₂₅) often maximize in submerged aquatic plants (Ficken et al., 2000). Long-chain *n*-alkanes (*n*-C₂₇ and above) are the main components of the epicuticular leaf waxes of vascular terrestrial plants (Eglinton and Hamilton, 1963, 1967). Leaf wax *n*-alkanes of vascular terrestrial plants accumulate rapidly in the epicuticular wax layer during leaf maturation in spring and early summer and preserve their

characteristic distribution patterns throughout the remainder of the growth season (Tipple et al., 2013). The significance of leaf wax *n*-alkanes for (paleo)environmental and (paleo)ecological research is due to their recalcitrant nature, making them excellent biomarkers. As part of the epicuticular wax layer, *n*-alkanes are transported into the environment in and on leaf fragments or by wind abrasion from the leaf surface and can be transported over long distances by wind and water (Gagosian et al., 1987; Conte and Weber, 2002; Schefuß et al., 2003; Rommerskirchen et al., 2003). Lacking any functional groups, the covalently bound carbon and hydrogen atoms make *n*-alkane molecules difficult to break without high energy input, radical attacks or specific enzymatic activity, making them remarkably stable and capable of persisting over geological timescales (e.g., Sessions et al., 2004). Incorporated into the sedimentary record, leaf wax *n*-alkanes largely retain their molecular structure and distribution patterns as well as carbon and hydrogen stable isotopic composition. Thus, due to their recalcitrant nature, *n*-alkanes are excellent biomarkers for the investigation of past environmental conditions (e.g., Eglinton and Eglinton, 2008; Castañeda and Schouten, 2011; Sachse et al., 2012). In order to further characterize a given distribution of sedimentary *n*-alkanes in terms of preservation and ecological changes over time, several methods have been developed. Among the most widely used in paleoenvironmental and paleoecological research are the Carbon Preference Index (CPI), the average chain length (ACL) and the aquatic index (P_{aq}). CPI is the measure of the relative abundances of the odd-numbered over the even-numbered carbon chain lengths (Bray and Evans, 1961). Typically, the vast majority of (modern) terrestrial plants have a strong odd-over-even predominance and thus $CPI \gg 1$ (Bush and McInerney, 2013). Once deposited, the high odd-over-even predominance of leaf wax *n*-alkanes is altered by diagenetic processes. Due to the loss of odd-numbered carbon chain length *n*-alkanes during expulsion of hydrocarbons and random cleavage of other compounds, producing *n*-alkanes without odd-over-even predominance, CPI values successively decrease and eventually approach unity (e.g., Killips and Killips, 2005). Therefore, high CPI values in sedimentary samples suggest little to no diagenetic alteration and high fidelity of the *n*-alkane signal to the original plant sources. ACL is the weighted average of mid- and long chain *n*-alkanes in a given sample. Apart from the quantification of *n*-alkane input to the sediment, changes in ACL have been linked to changes in paleoclimatic conditions. The observations that the microcrystalline structure as well as the chemical composition of the epicuticular wax layer is dependent on environmental parameters (Koch and Ensikat, 2008; Shepard and Griffiths, 2008), along with the knowledge of increasing melting points of *n*-alkanes with increasing chain lengths, gave rise to the hypothesis that terrestrial plants tend to synthesize longer chain length

n-alkanes in warmer/more arid/more irradiated environments (Peltzer and Gargosian, 1989; Rommerskirchen et al., 2003; Vogts et al., 2012; Bush and McInerney, 2013), though possibly not in all ecosystems (Diefendorf et al., 2011). Additional paleoecological information is provided by the P_{aq} index. As mentioned above, contributions of submerged aquatic and vascular terrestrial plants to the sediment can be readily identified by their respective characteristic *n*-alkane chain length distributions. P_{aq} is the ratio of the abundance of mid-chain length *n*-alkanes over the sum of mid- and long chain length *n*-alkanes (Ficken et al., 2000). Increasing P_{aq} values indicate an increase in the relative contribution of aquatic plant material and a corresponding decrease in the relative contribution of terrestrial input to the sediment, allowing estimations of past climatic and hydrological conditions. In addition to the (paleo)environmental and (paleo)ecological information that can be inferred from *n*-alkane abundances and distributions, the recalcitrant nature of *n*-alkanes also permits the investigation of the stable isotopic compositions of hydrogen carbon (δD) and carbon ($\delta^{13}C$).

Water is the main hydrogen source for all photosynthesizing organisms and their biosynthetic products. The stable hydrogen isotopic composition of the biosynthetic water pool strongly influences δD values of all organic molecules produced by plants. The water used for biosynthesis may vary largely for different plants but equals precipitation in most cases (see review by Sachse et al., 2012). Many aquatic organisms take up water from precipitation fed rivers, lakes and bogs, while most terrestrial plants depend on soil moisture as their primary water source. The biosynthesis of leaf wax *n*-alkanes occurs during the time of leaf formation in spring and early summer (Sachse et al., 2010; Tipple et al., 2013). After leaf maturation, δD of leaf wax *n*-alkanes remains largely stable over the remainder of the growth season, unless being subjected to strong environmental stress like wind abrasion and turnover of surface waxes (Chikaraishi et al., 2004; Sachse et al., 2009). However, while being largely determined by the stable isotopic composition of precipitation, δD of leaf wax *n*-alkanes usually is strongly offset from δD in precipitation.

The net or apparent fractionation between precipitation and leaf wax *n*-alkanes is the result of local hydrological processes as well as isotopic fractionation during biosynthesis (Fig. 1.8). As mentioned in chapter 1.3, the stable isotopic composition of precipitation is strongly dependent on environmental processes. Conditions in the source region, temperature, air mass trajectory, mixing, interactions with topography and seasonality among others collectively determine δD (and $\delta^{18}O$) of rainfall and in turn soil moisture.

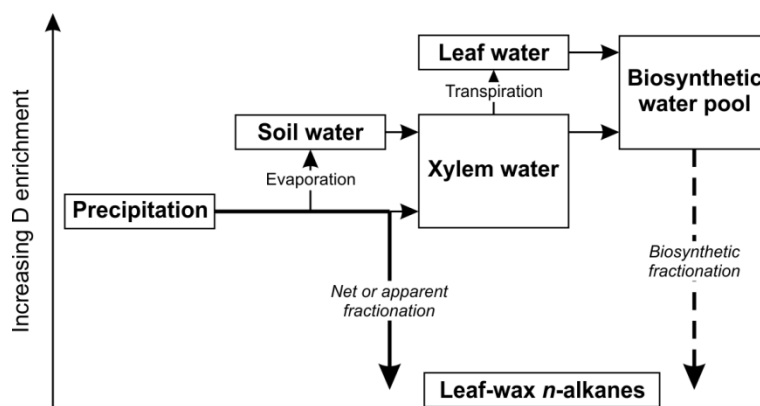


Fig. 1.8 Schematic diagram of the hydrogen-isotopic relationship between precipitation and leaf wax *n*-alkanes from terrestrial plants (after Sachse et al., 2012).

However, as soil moisture is subjected to environmental influences, evaporation in the upper soil horizons may enrich soil moisture in D compared to precipitation as light isotopologues preferentially evaporate (Fig. 1.8). Also, while there is no fractionation during the uptake via the roots and the transport through the plant's xylem, evaporative enrichment by means of transpiration from the leaves can potentially impact δD of leaf water (e.g., Sachse et al., 2012). Hence, the biosynthetic water pool may be enriched in D compared to precipitation solely based on the influence of evotranspiration on soil water and leaf water. However, the large offset in δD between precipitation and leaf wax *n*-alkanes is the result of biosynthetic processes (Fig. 1.8). The hydrogen transfer reactions during the biosynthesis of *n*-alkanes produce substantial isotopic fractionation between the biosynthetic water pool and the hydrocarbon molecules (see review by Sachse et al., 2012). Biosynthetic fractionation factors are assumed to be rather constant for a given species, attaining values of ca. -160 ‰, albeit with significant differences between species (Sessions et al., 1999; Kahmen et al., 2013a, b). Thus, the apparent fractionation between precipitation and leaf wax *n*-alkane incorporates the effects of soil water evaporation, leaf water transpiration and biosynthetic fractionation and is important for the interpretation of sedimentary leaf wax *n*-alkanes as a paleoenvironmental proxy. Comparing the apparent fractionation factors of various modern plant species from different ecosystems implies that evaporation and transpiration exerts stronger control on leaf wax *n*-alkane δD under dry/arid conditions, resulting in lower apparent fractionation between precipitation and leaf wax *n*-alkanes (Smith and Freeman, 2006; Feakins and Sessions, 2010). Additionally, strong differences in apparent fractionation among modern plant life-forms have been observed (Sachse et al., 2012). Apparent fractionation between δD of precipitation and δD of *n*-C₂₉ averages at -99 ‰ ± 32 ‰ in shrubs, whereas trees (mean = -121 ‰ ± 22 ‰) and forbs (mean = -128 ‰ ± 30 ‰) show a larger apparent fractionation. The largest apparent fractionation values however occur in grasses (C₃ graminoids: mean = -149 ‰ ± 29 ‰;

C₄ graminoids: mean = -132 ‰ ± 25 ‰). While smaller values for shrubs compared to trees and forbs have been explained with climatological differences by means of evotranspirational isotopic enrichment, the larger values of grasses might be related to physiological and/or biosynthetic differences (Sachse et al., 2012; Kahmen et al., 2013a, b). These observations are significant for paleoenvironmental applications of sedimentary leaf wax *n*-alkane δD, especially where large vegetation changes are known to occur (i.e., from palynological investigations) since profound shifts in prevailing vegetation may potentially over- or underestimate variations in the isotopic composition of paleoprecipitation.

In addition, the stable carbon isotopic composition of plant material in the sedimentary record may provide important paleoenvironmental information. Primarily dependent on the isotopic composition of atmospheric CO₂, δ¹³C of *n*-alkanes and plant material in general is largely influenced by the applied photosynthetic pathway. Photosynthetic processes discriminate against the heavier ¹³C isotope, resulting in lower δ¹³C values of plant material compared to the atmospheric CO₂ (O'Leary, 1988). Differences in carbon fixation and CO₂ diffusion between the C₃ and the C₄ photosynthetic pathways produce characteristic δ¹³C ranges for the respective C₃ and C₄ plants, with C₃ plants generally being more depleted in ¹³C than C₄ plants (Fig. 1.9).

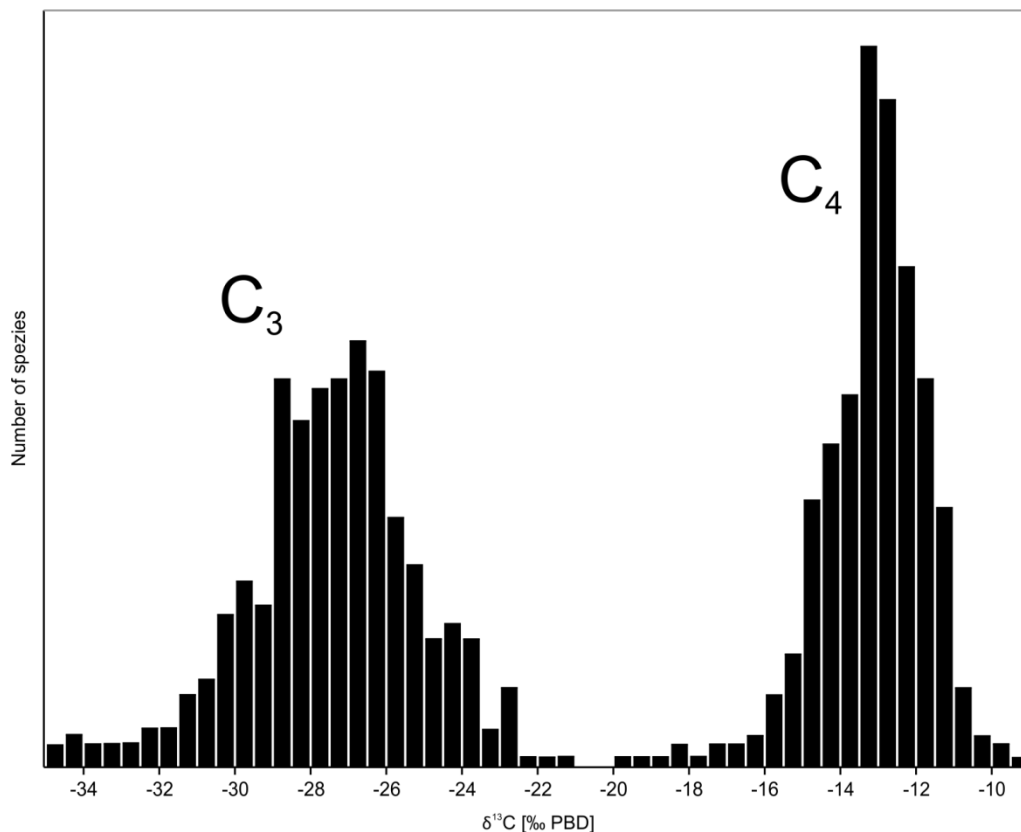


Fig. 1.9 Typical δ¹³C distribution of plants following the C₃ and C₄ photosynthetic pathway (after O'Leary, 1988).

Thus, large scale shifts in sedimentary $\delta^{13}\text{C}$ values of plant material could indicate profound changes in predominant vegetation and therefore in paleoclimatic conditions. Additionally, variations in $\delta^{13}\text{C}$ of plant material may reflect the adaptation of vascular plants to climatic changes over time. Vascular plants may respond to increases in atmospheric CO_2 concentrations and/or decreases in humidity by reducing their stomatal conductance, thus reducing gas exchange between the leaves and the atmosphere in order to maintain their CO_2 as well as water balance (Cowan and Farquhar, 1977; Farquhar et al., 1989; Marshall et al., 2008). Reduced stomatal conductance limits the loss of water vapor from the leaf and decreases diffusion of atmospheric CO_2 into the leaf, while photosynthetic demand for CO_2 is still high. In turn, CO_2 within the leaves and ultimately of all photosynthates produced will be progressively depleted in ^{13}C . Thus, $\delta^{13}\text{C}$ values of plant material in the geological record may preserve important (paleo)ecological information (e.g., Kohn, 2010).

1.5 *Structure of this PhD thesis*

In order to address the question of changing atmospheric circulation patterns in the Aegean region in response to northern hemisphere cooling during the 8.2 kyr B.P. climatic event, this PhD thesis comprises 3 studies of (paleo)environmental reconstructions from the Eastern Mediterranean region.

In Chapter 2, a study entitled 'The impact of topography on isotopes in precipitation across the Central Anatolian Plateau (Turkey)' by Fabian Schemmel, Tamás Mikes, Bora Rojay, and Andreas Mulch is presented. Here, the influences of climate, topography, atmospheric circulation and seasonality, among others, on δD and $\delta^{18}\text{O}$ in meteoric waters are characterized with the purpose of establishing a first-order template of present day stable isotopes in precipitation against which continental paleoclimate proxy data from the Eastern Mediterranean can be interpreted.

In Chapter 3, a study entitled 'Paleohydrological changes in the Eastern Mediterranean region during the early Holocene recorded in plant wax *n*-alkane distributions and $\delta^{13}\text{C}_{\text{TOC}}$ - new data from Tenaghi Philippon, NE Greece' by Fabian Schemmel, Eva M. Niedermeyer, Andreas Koutsodendris, Jörg Pross, Jens Fiebig, and Andreas Mulch is presented. Here, changes in the abundance and distribution of *n*-alkanes is compared with $\delta^{13}\text{C}_{\text{TOC}}$ and available palynological data from TP in order to reconstruct variability in surface moisture conditions at the site during the early Holocene and especially in response to the 8.2 kyr B.P. climatic event. Thus, this study provides essential paleoclimatic information for the characterization of environmental influences on stable

isotopes in precipitation, obtained from geological archives in the Eastern Mediterranean region.

In Chapter 4, a study entitled 'Plant wax δD values record changing Eastern Mediterranean atmospheric circulation patterns during the 8.2 kyr B.P. climatic event' by Fabian Schemmel, Eva M. Niedermeyer, Valérie Schwab, Gerd Gleixner, Jörg Pross, and Andreas Mulch is presented. Here, variations in early Holocene δD values of long-chain *n*-alkanes from TP are being discussed in terms of available paleoecological and paleoclimatic information related to northern hemisphere cooling during the 8.2 kyr B.P. climatic event. Consequently, this study reveals the possibility of atmospheric circulation changes in the Aegean region between ca. 8.1 and 8.0 kyr B.P. and gives insight into the teleconnections between the climate systems of the Eastern Mediterranean region and the high and low latitudes.

Finally, Chapter 5 summarizes the results of this thesis and provides an outlook on paleoclimate research on the 8.2 kyr B.P. climatic event as well as on other periods of orbitally-influenced and rapid climate changes at TP and beyond.

1.6 References

- Alley, R. B., and Ágústsdóttir, A. M., 2005, The 8k event: cause and consequences of a major Holocene abrupt climate change: *Quaternary Science Reviews*, v. 24, no. 10–11, p. 1123–1149, doi: 10.1016/j.quascirev.2004.12.004.
- Alley, R. B., Mayewski, P. A., Sowers, T., Stuiver, M., Taylor, K. C., and Clark, P. U., 1997, Holocene climatic instability: A prominent, widespread event 8200 yr ago: *Geology*, v. 25, no. 6, p. 483–486, doi: 10.1130/0091-7613(1997)025<0483.
- Barber, D. C., Dyke, A., Hillaire-Marcel, C., Jennings, A. E., Andrews, J. T., Kerwin, M. W., Bilodeau, G., McNeely, R., Southon, J., Morehead, M. D., and Gagnon, J.-M., 1999, Forcing of the cold event of 8,200 years ago by catastrophic drainage of Laurentide lakes: *Nature*, v. 400, no. July, p. 344–348.
- Bauer, E., Ganopolski, A., and Montoya, M., 2004, Simulation of the cold climate event 8200 years ago by meltwater outburst from Lake Agassiz: *Paleoceanography*, v. 19, no. 3, p. 1–13, doi: 10.1029/2004PA001030.
- Bond, G. C., and Lotti, R., 1995, Iceberg discharges into the North Atlantic on millennial time scales during the last glaciation: *Science*, v. 267, no. 5200, p. 1005–1010, doi: 10.1126/science.267.5200.1005.
- Bond, G., Heinrich, H., Broecker, W., Labeyrie, L., McManus, J., Andrews, J., Huon, S., Jantschik, R., Clasen, S., Simet, C., Tedesco, K., Klas, M., Bonani, G., and Ivy, S., 1992, Evidence for massive discharges of icebergs into the North Atlantic Ocean during the last glacial period: *Nature*, v. 360, p. 245 - 249.
- Bond, G., Showers, W., Cheseby, M., Lotti, R., Almasi, P., DeMenocal, P., Priore, P., Cullen, H., Hajdas, I., and Bonani, G., 1997, A Pervasive Millennial-Scale Cycle in North Atlantic Holocene and Glacial Climates: *Science*, v. 278, no. 5341, p. 1257–1266, doi: 10.1126/science.278.5341.1257.
- Bond, G., Kromer, B., Beer, J., Muscheler, R., Evans, M. N., Showers, W., Hoffmann, S., Lotti-Bond, R., Hajdas, I., and Bonani, G., 2001, Persistent solar influence on North Atlantic climate during the Holocene: *Science*, v. 294, no. 5549, p. 2130–6, doi: 10.1126/science.1065680.
- Bordon, A., Peyron, O., Lézine, A.-M., Brewer, S., and Fouache, E., 2009, Pollen-inferred Late-Glacial and Holocene climate in southern Balkans (Lake Maliq): *Quaternary International*, v. 200, no. 1–2, p. 19–30, doi: 10.1016/j.quaint.2008.05.014.
- Bray, E., and Evans, E., 1961, Distribution of *n*-paraffins as a clue to recognition of source beds: *Geochimica et Cosmochimica Acta*, v. 22, no. 1, p. 2–15, doi: 10.1016/0016-7037(61)90069-2.
- Bush, R. T., and McInerney, F. A., 2013, Leaf wax *n*-alkane distributions in and across modern plants: Implications for paleoecology and chemotaxonomy: *Geochimica et Cosmochimica Acta*, v. 117, p. 161–179, doi: 10.1016/j.gca.2013.04.016.
- Casford, J. S., Rohling, E., Abu-Zied, R., Fontanier, C., Jorissen, F., Leng, M., Schmiedl, G., and Thomson, J., 2003, A dynamic concept for eastern Mediterranean circulation and oxygenation during sapropel formation: *Palaeogeography, Palaeoclimatology, Palaeoecology*, v. 190, p. 103–119, doi: 10.1016/S0031-0182(02)00601-6.
- Castañeda, I. S., and Schouten, S., 2011, A review of molecular organic proxies for examining modern and ancient lacustrine environments: *Quaternary Science Reviews*, v. 30, no. 21–22, p. 2851–2891, doi: 10.1016/j.quascirev.2011.07.009.

- Cheng, H., Fleitmann, D., Edwards, R. L., Wang, X., Cruz, F. W., Auler, A. S., Mangini, A., Wang, Y., Kong, X., Burns, S. J., and Matter, A., 2009, Timing and structure of the 8.2 kyr B.P. event inferred from ^{18}O records of stalagmites from China, Oman, and Brazil: *Geology*, v. 37, no. 11, p. 1007–1010, doi: 10.1130/G30126A.1.
- Chikaraishi, Y., Naraoka, H., and Poulson, S. R., 2004, Hydrogen and carbon isotopic fractionations of lipid biosynthesis among terrestrial (C_3 , C_4 and CAM) and aquatic plants: *Phytochemistry*, v. 65, no. 10, p. 1369–81, doi: 10.1016/j.phytochem.2004.03.036.
- Christanis, K., 1983, Genese und Fazies der Torf-Lagerstätte von Philippi (Griechisch-Mazedonien) als Beispiel der Entstehung einer Braunkohle-Lagerstätte vom stark telmatischen Typ: Technische Universität Carolo-Wilhelmina zu Braunschweig, 1-180 p.
- Clark, I., and Fritz, P., 1997, *Environmental Isotopes in Hydrogeology*, CRC Press.
- Clark, P. U., Marshall, S. J., Clarke, G. K. C., Hostetler, S. W., Licciardi, J. M., and Teller, J. T., 2001, Freshwater Forcing of Abrupt Climate Change During the Last Glaciation: *Science*, v. 293, no. 5528, p. 283–287, doi: 10.1126/science.1062517.
- Clarke, G. K. C., Leverington, D. W., Teller, J. T., and Dyke, A. S., 2004, Paleohydraulics of the last outburst flood from glacial Lake Agassiz and the 8200BP cold event: *Quaternary Science Reviews*, v. 23, no. 3–4, p. 389–407, doi: 10.1016/j.quascirev.2003.06.004.
- Collins, M., Knutti, R., Arblaster, J., Dufresne, J.-L., Fichet, T., Friedlingstein, P., Gao, X., Gutowski, W. J., Johns, T., Krinner, G., Shongwe, M., Tebaldi, C., Weaver, A. J., and Wehner, M., 2013, Long-term Climate Change: Projections, Commitments and Irreversibility, *in* Stocker, T.F., Qin, D., Plattner, G.-K., Tignor, M., Allen, S. K., Boschung, J., Nauels, A., Xia, Y., Bex, V., and Midgley, P. M. (Eds.), *Climate Change 2013: The Physical Science Basis. Contribution of Working Group I to the Fifth Assessment Report of the Intergovernmental Panel on Climate Change*, Cambridge University Press, Cambridge, United Kingdom and New York, NY, USA.
- Combourieu-Nebout, N., Peyron, O., Bout-Roumazeilles, V., Goring, S., Dormoy, I., Joannin, S., Sadori, L., Siani, G., and Magny, M., 2013, Holocene vegetation and climate changes in the central Mediterranean inferred from a high-resolution marine pollen record (Adriatic Sea): *Climate of the Past*, v. 9, no. 5, p. 2023–2042, doi: 10.5194/cp-9-2023-2013.
- Conte, M. H., and Weber, J. C., 2002, Long-range atmospheric transport of terrestrial biomarkers to the western North Atlantic: *Global Biogeochemical Cycles*, v. 16, no. 4, p. 89-1-89–17, doi: 10.1029/2002GB001922.
- Cowan, I. R., and Farquhar, G. D., 1977, Stomatal function in relation to leaf metabolism and environment: *Symposia of the Society for Experimental Biology*, v. 31, p. 471505.
- Craig, H., and Gordon, L., 1965, Deuterium and oxygen-18 variation in the ocean and the marine atmosphere, *in* Tongiorgi, E. (Ed.), *Stable Isotopes in Oceanographic Studies and Paleotemperatures*, Spoleto, 1965: 9-130.
- Craig, H., 1961, Isotopic Variations in Meteoric Waters: *Science*, v. 133, no. 3465, p. 1702–3, doi: 10.1126/science.133.3465.1702.
- Cranwell, P. A., Eglinton, G., and Robinson, N., 1987, Lipids of aquatic organisms as potential contributors to lacustrine sediments—II: *Organic Geochemistry*, v. 11, no. 6, p. 513–527, doi: 10.1016/0146-6380(87)90007-6.
- Dansgaard, W., Johnsen, S. J., Clausen, H. B., Dahl-Jensen, D., Gundestrup, N. S., Hammer, C. U., Hvidberg, C. S., Steffensen, J. P., Sveinbjörnsdóttir, A. E., Jouzel, J., and Bond, G., 1993, Evidence for general instability of past climate from a 250-kyr ice-core record: *Nature*, v. 364, p. 218–220.

- Dansgaard, W., 1964, Stable isotopes in precipitation: *Tellus*, v. 16, no. 4, p. 436–468, doi: 10.3402/tellusa.v16i4.8993.
- Diefendorf, A. F., Freeman, K. H., Wing, S. L., and Graham, H. V., 2011, Production of *n*-alkyl lipids in living plants and implications for the geologic past: *Geochimica et Cosmochimica Acta*, v. 75, no. 23, p. 7472–7485, doi: 10.1016/j.gca.2011.09.028.
- Digerfeldt, G., Sandgren, P., and Olsson, S., 2007, Reconstruction of Holocene lake-level changes in Lake Xinias, central Greece: *The Holocene*, v. 17, no. 3, p. 361–367, doi: 10.1177/0959683607076449.
- Dormoy, I., Peyron, O., Combourieu Nebout, N., Goring, S., Kotthoff, U., Magny, M., and Pross, J., 2009, Terrestrial climate variability and seasonality changes in the Mediterranean region between 15 000 and 4000 years BP deduced from marine pollen records: *Climate of the Past*, v. 5, no. 4, p. 615–632, doi: 10.5194/cp-5-615-2009.
- Dünkeloh, A., and Jacobeit, J., 2003, Circulation dynamics of Mediterranean precipitation variability 1948–98: *International Journal of Climatology*, v. 23, no. 15, p. 1843–1866, doi: 10.1002/joc.973.
- Eastwood, W. J., Leng, M. J., Roberts, N., and Davis, B., 2006, Holocene climate change in the eastern Mediterranean region: a comparison of stable isotope and pollen data from Lake Gölhisar, southwest Turkey: *Journal of Quaternary Science*, v. 22, no. 4, p. 327–341, doi: 10.1002/jqs.1062.
- Edwards, D., Abbott, G. D., and Raven, J. A., 1996, Cuticles of early land plants: a palaeoecophysiological evaluation, in Kerstiens, G. (Ed.), *Plant Cuticles: An Integrated Functional Approach*, BIOS Scientific Publishers, Oxford, pp. 1–32.
- Eglinton, T. I., and Eglinton, G., 2008, Molecular proxies for paleoclimatology: *Earth and Planetary Science Letters*, v. 275, no. 1–2, p. 1–16, doi: 10.1016/j.epsl.2008.07.012.
- Eglinton G., and Hamilton R. J., 1963, The distribution of alkanes, in Swain, T. (Ed.), *Chemical Plant Taxonomy*, Academic Press, London.
- Eglinton, G., and Hamilton, R. J., 1967, Leaf Epicuticular Waxes: *Science*, v. 156, no. 780, p. 1322–35.
- Ehrmann, W., Schmiedl, G., Hamann, Y., Kuhnt, T., Hemleben, C., and Siebel, W., 2007, Clay minerals in late glacial and Holocene sediments of the northern and southern Aegean Sea: *Palaeogeography, Palaeoclimatology, Palaeoecology*, v. 249, no. 1–2, p. 36–57, doi: 10.1016/j.palaeo.2007.01.004.
- Elliot, M., Labeyrie, L., and Duplessy, J. C., 2002, Changes in North Atlantic deep-water formation associated with the Dansgaard-Oeschger temperature oscillations (60–10 ka): *Quaternary Science Reviews* 21, 1153–1165.
- Ellison, C. R. W., Chapman, M. R., and Hall, I. R., 2006, Surface and deep ocean interactions during the cold climate event 8200 years ago: *Science*, v. 312, no. 5782, p. 1929–32, doi: 10.1126/science.1127213.
- Emeis, K.-C., Struck, U., Schulz, H.-M., Rosenberg, R., Bernasconi, S., Erlenkeuser, H., Sakamoto, T., and Martinez-Ruiz, F., 2000, Temperature and salinity variations of Mediterranean Sea surface waters over the last 16,000 years from records of planktonic stable oxygen isotopes and alkenone unsaturation ratios: *Palaeogeography, Palaeoclimatology, Palaeoecology*, v. 158, p. 259–280.
- Farquhar, G. D., Ehleringer, J. R., and Hubick, K. T., 1989, Carbon Isotope Discrimination and Photosynthesis: *Annual Review of Plant Physiology and Plant Molecular Biology*, v. 40, p. 503–537.
- Feakins, S. J., and Sessions, A. L., 2010, Controls on the D/H ratios of plant leaf waxes in an arid ecosystem: *Geochimica et Cosmochimica Acta*, v. 74, no. 7, p. 2128–2141, doi: 10.1016/j.gca.2010.01.016.

- Ficken, K. J., Li, B., Swain, D. L., and Eglinton, G., 2000, An *n*-alkane proxy for the sedimentary input of submerged/floating freshwater aquatic macrophytes: *Organic Geochemistry*, v. 31.
- Fleitmann, D., Cheng, H., Badertscher, S., Edwards, R. L., Mudelsee, M., Göktürk, O. M., Fankhauser, A., Pickering, R., Raible, C. C., Matter, A., Kramers, J., and Tüysüz, O., 2009, Timing and climatic impact of Greenland interstadials recorded in stalagmites from northern Turkey: *Geophysical Research Letters*, v. 36, no. 19, p. L19707, doi: 10.1029/2009GL040050.
- Fletcher, W. J., Müller, U. C., Koutsodendris, A., Christanis, K., and Pross, J., 2013, A centennial-scale record of vegetation and climate variability from 312 to 240 ka (Marine Isotope Stages 9c–a, 8 and 7e) from Tenaghi Philippon, NE Greece: *Quaternary Science Reviews*, v. 78, p. 108–125, doi: 10.1016/j.quascirev.2013.08.005.
- Francke, A., Wagner, B., Leng, M. J., and Rethemeyer, J., 2013, A Late Glacial to Holocene record of environmental change from Lake Dojran (Macedonia, Greece): *Climate of the Past*, v. 9, no. 1, p. 481–498, doi: 10.5194/cp-9-481-2013.
- Gagosian, R. B., Peltzer, E. T., and Merrill, J. T., 1987, Long-range transport of terrestrially derived lipids in aerosols from the south Pacific: *Nature*, v. 325, no. 26, p. 800–803.
- Geraga, M., Ioakim, C., Lykousis, V., Tsaila-Monopolis, S., and Mylona, G., 2010, The high-resolution palaeoclimatic and palaeoceanographic history of the last 24,000 years in the central Aegean Sea, Greece: *Palaeogeography, Palaeoclimatology, Palaeoecology*, v. 287, no. 1–4, p. 101–115, doi: 10.1016/j.palaeo.2010.01.023.
- Ghilardi, M., Psomiadis, D., Cordier, S., Delanghe-Sabatier, D., Demory, F., Hamidi, F., Paraschou, T., Dotsika, E., and Fouache, E., 2012, The impact of rapid early- to mid-Holocene palaeoenvironmental changes on Neolithic settlement at Nea Nikomideia, Thessaloniki Plain, Greece: *Quaternary International*, v. 266, p. 47–61, doi: 10.1016/j.quaint.2010.12.016.
- Giger, W., Schaffner, C., and Wakeham, S. G., 1980, Aliphatic and olefinic hydrocarbons in recent sediments of Greifensee, Switzerland: *Geochimica et Cosmochimica Acta* 44, p. 119–129.
- Gogou, A., Bouloubassi, I., Lykousis, V., Arnaboldi, M., Gaitani, P., and Meyers, P. A., 2007, Organic geochemical evidence of Late Glacial–Holocene climate instability in the North Aegean Sea: *Palaeogeography, Palaeoclimatology, Palaeoecology*, v. 256, no. 1–2, p. 1–20, doi: 10.1016/j.palaeo.2007.08.002.
- Gonfiantini, R., 1986. Environmental isotopes in lake studies, *in* Fritz, P. and Fontes, J.-Ch. (Eds.) *Handbook of Environmental Isotope Geochemistry*, Vol. 2, *The Terrestrial Environment*, B. Elsevier, Amsterdam, The Netherlands:113–168.
- Göktürk, O. M., Fleitmann, D., Badertscher, S., Cheng, H., Edwards, R. L., Leuenberger, M., Fankhauser, A., Tüysüz, O., and Kramers, J., 2011, Climate on the southern Black Sea coast during the Holocene: implications from the Sofular Cave record: *Quaternary Science Reviews*, v. 30, no. 19–20, p. 2433–2445, doi: 10.1016/j.quascirev.2011.05.007.
- Hamann, Y., Ehrmann, W., Schmiedl, G., Krüger, S., Stuut, J.-B., and Kuhnt, T., 2008, Sedimentation processes in the Eastern Mediterranean Sea during the Late Glacial and Holocene revealed by end-member modelling of the terrigenous fraction in marine sediments: *Marine Geology*, v. 248, no. 1–2, p. 97–114, doi: 10.1016/j.margeo.2007.10.009.
- Haug, G. H., Hughen, K. A., Sigman, D. M., Peterson, L. C., and Röhl, U., 2001, Southward migration of the intertropical convergence zone through the Holocene: *Science*, v. 293, no. 5533, p. 1304–8, doi: 10.1126/science.1059725.

- Hays, J. D., Imbrie, J., and Shackleton, N. J. J., 1976, Variations in the Earth's Orbit: Pacemaker of the Ice Ages: *Science*, v. 194, no. 4270, p. 1121–1132, doi: 10.1126/science.194.4270.1121.
- Heymann, C., Nelle, O., Dörfler, W., Zagana, H., Nowaczyk, N., Xue, J., and Unkel, I., 2013, Late Glacial to mid-Holocene palaeoclimate development of Southern Greece inferred from the sediment sequence of Lake Stymphalia (NE-Peloponnese): *Quaternary International*, v. 302, p. 42–60, doi: 10.1016/j.quaint.2013.02.014.
- Hillaire-Marcel, C., de Vernal, A., and Piper, D. J. W., 2007, Lake Agassiz Final drainage event in the northwest North Atlantic: *Geophysical Research Letters*, v. 34, no. 15, doi: 10.1029/2007GL030396.
- Jalut, G., Dedoubat, J. J., Fontugne, M., and Otto, T., 2009, Holocene circum-Mediterranean vegetation changes: Climate forcing and human impact: *Quaternary International*, v. 200, no. 1–2, p. 4–18, doi: 10.1016/j.quaint.2008.03.012.
- Jeffree, C. E., 2006, The fine structure of the plant cuticle, *in* Riederer, M., and Müller, C. (Eds.), *Biology of the Plant Cuticle*, Blackwell Publishing, Oxford.
- Jetter R., Kunst L., and Samuels A. L., 2006, Composition of plant cuticular waxes, *in* Riederer, M., and Müller, C. (Eds.), *Biology of the Plant Cuticle*, Blackwell Publishing, Oxford.
- Joannin, S., Brugiapaglia, E., de Beaulieu, J.-L., Bernardo, L., Magny, M., Peyron, O., Goring, S., and Vannièrè, B., 2012, Pollen-based reconstruction of Holocene vegetation and climate in southern Italy: the case of Lago Trifoglietti: *Climate of the Past*, v. 8, no. 6, p. 1973–1996, doi: 10.5194/cp-8-1973-2012.
- Kahmen, A., Schefuß, E., and Sachse, D., 2013a, Leaf water deuterium enrichment shapes leaf wax *n*-alkane δD values of angiosperm plants I: Experimental evidence and mechanistic insights: *Geochimica et Cosmochimica Acta*, v. 111, p. 39–49, doi: 10.1016/j.gca.2012.09.003.
- Kahmen, A., Hoffmann, B., Schefuß, E., Arndt, S. K., Cernusak, L. A., West, J. B., and Sachse, D., 2013b, Leaf water deuterium enrichment shapes leaf wax *n*-alkane δD values of angiosperm plants II: Observational evidence and global implications: *Geochimica et Cosmochimica Acta*, v. 111, p. 50–63, doi: 10.1016/j.gca.2012.09.004.
- Kalaitzidis, S., and Christanis, K., 2003, Scanning electron microscope studies of the Philippi peat (NE Greece): initial aspects: *International Journal of Coal Geology*, v. 54, no. 1–2, p. 69–77, doi: 10.1016/S0166-5162(03)00020-X.
- Kawamura, K., Parrenin, F., Lisiecki, L., Uemura R., Vimeux, F., Severinghaus, J. P., Hutterli, M. A., Nakazawa, T., Aoki, S., Jouzel, J., Raymo, M. E., Matsumoto, K., Nakata, H., Motoyama, H., Fujita, S., Goto-Azuma, K., Fujii, Y., and Watanabe, O., 2007, Northern Hemisphere forcing of climatic cycles in Antarctica over the past 360,000 years: *Nature*, v. 448, p. 912–916, doi:10.1038/nature06015.
- Killops, S., and Killops, V., 2005, *Introduction to Organic Geochemistry*, Blackwell Publishing, Malden, MA.
- Kleiven, H. (Kikki) F., Kissel, C., Laj, C., Ninnemann, U.S., Richter, T.O., and Cortijo, E., 2008, Reduced North Atlantic deep water coeval with the glacial Lake Agassiz freshwater outburst: *Science*, v. 319, no. 5859, p. 60–4, doi: 10.1126/science.1148924.
- Kobashi, T., Severinghaus, J. P., Brook, E. J., Barnola, J.-M., and Grachev, A. M., 2007, Precise timing and characterization of abrupt climate change 8200 years ago from air trapped in polar ice: *Quaternary Science Reviews*, v. 26, no. 9–10, p. 1212–1222, doi: 10.1016/j.quascirev.2007.01.009.
- Koch, K., and Ensikat, H. J., 2008, The hydrophobic coatings of plant surfaces: Epicuticular wax crystals and their morphologies, crystallinity and molecular self-assembly: *Micron*, v. 39, no. 7, p. 759–772, doi: 10.1016/j.micron.2007.11.010.

- Kohn, M. J., 2010, Carbon isotope compositions of terrestrial C₃ plants as indicators of (paleo)ecology and (paleo)climate: *Proceedings of the National Academy of Sciences of the United States of America*, v. 107, no. 46, p. 19691–5, doi: 10.1073/pnas.1004933107.
- Köppen, W., 1900, Versuch einer Klassifikation der Klimate, vorzugsweise nach ihren Beziehungen zur Pflanzenwelt: *Geogr. Z.* 6, 593–611. 657–679.
- Kotthoff, U., Pross, J., Müller, U. C., Peyron, O., Schmiedl, G., Schulz, H., and Bordon, A., 2008a, Climate dynamics in the borderlands of the Aegean Sea during formation of sapropel S1 deduced from a marine pollen record: *Quaternary Science Reviews*, v. 27, no. 7–8, p. 832–845, doi: 10.1016/j.quascirev.2007.12.001.
- Kotthoff, U., Müller, U. C., Pross, J., Schmiedl, G., Lawson, I. T., Van De Schootbrugge, B., and Schulz, H., 2008b, Lateglacial and Holocene vegetation dynamics in the Aegean region: an integrated view based on pollen data from marine and terrestrial archives: *The Holocene*, v. 18, no. 7, p. 1019–1032, doi: 10.1177/0959683608095573.
- Kouli, K., Gogou, A., Bouloubassi, I., Triantaphyllou, M. V., Ioakim, C., Katsouras, G., Roussakis, G., and Lykousis, V., 2012, Late postglacial paleoenvironmental change in the northeastern Mediterranean region: Combined palynological and molecular biomarker evidence: *Quaternary International*, v. 261, p. 118–127, doi: 10.1016/j.quaint.2011.10.036.
- Kovats, R. S., Valentini, R., Bouwer, L. M., Georgopoulou, E., Jacob, D., Martin, E., Rounsevell, M., and Soussana, J.-F., 2014, Europe, *in* Barros, V. R., Field, C. B., Dokken, D. J., Mastrandrea, M. D., Mach, K. J., Bilir, T. E., Chatterjee, M., Ebi, K. L., Estrada, Y. O., Genova, R. C., Girma, B., Kissel, E. S., Levy, A. N., MacCracken, S., Mastrandrea, P. R., and White, L. L. (Eds.), *Climate Change 2014: Impacts, Adaptation, and Vulnerability. Part B: Regional Aspects. Contribution of Working Group II to the Fifth Assessment Report of the Intergovernmental Panel on Climate Change*, Cambridge University Press, Cambridge, United Kingdom and New York, NY, USA, pp. 1267–1326.
- Kuhnt, T., Schmiedl, G., Ehrmann, W., Hamann, Y., and Hemleben, C., 2007, Deep-sea ecosystem variability of the Aegean Sea during the past 22 kyr as revealed by Benthic Foraminifera: *Marine Micropaleontology*, v. 64, no. 3–4, p. 141–162, doi: 10.1016/j.marmicro.2007.04.003.
- Kunst, L., Jetter, R., and Samuels, A. L., 2006, Biosynthesis and transport of plant cuticular waxes, *in* Riederer, M., and Müller, C. (Eds.), *Biology of the Plant Cuticle*, Blackwell Publishing, Oxford.
- Lawson, I. T., Al-Omari, S., Tzedakis, P. C., Bryant, C. L., and Christanis, K., 2005, Lateglacial and Holocene vegetation history at Nisi Fen and the Boras mountains, northern Greece: *The Holocene*, v. 15, no. 6, p. 873–887, doi: 10.1191/0959683605hl860ra.
- LeGrande, A. N., Schmidt, G. A., Shindell, D. T., Field, C. V., Miller, R. L., Koch, D. M., Faluvegi, G., and Hoffmann, G., 2006, Consistent simulations of multiple proxy responses to an abrupt climate change event: *Proceedings of the National Academy of Sciences*, v. 103, no. 27, p. 837–842.
- Leverington, D. W., Mann, J. D., and Teller, J. T., 2000, Changes in the Bathymetry and Volume of Glacial Lake Agassiz between 11,000 and 9300 14C yr B.P.: *Quaternary Research*, v. 54, p. 174–181, doi: 10.1006/qres.2001.2311.
- Lionello, P., Boscolo, R., Alpert, P., Artale, V., Li, L., Luterbacher, J., May, W., Trigo, R., Tsimplis, M., Ulbrich, U., and Xoplaki, E., 2006, The Mediterranean Climate: An Overview of the Main Characteristics and Issues, *in* Lionello, P., Malanotte-Rizzoli, P., and Boscolo, R. (Eds.), *Mediterranean Climate Variability*, Elsevier B.V., Amsterdam, p. 1–26.
- Lionello, P., Abrantes, F., Congedi, L., Dulac, F., Gacic, M., Gomis, D., Clare, G., Hoff, H., Kutiel, H., Luterbacher, J., Planton, S., Reale, M., Schröder, K., Struglia, M. V., Toreti, A., Tsimplis, M., Ulbrich, U., and Xoplaki, E., 2012, Mediterranean Climate - Background Information, *in* Lionello, P. (Ed.), *The Climate of the Mediterranean Region*, Elsevier B. V., Amsterdam, p. 1-56.

- Liu, Y.-H., Henderson, G. M., Hu, C.-Y., Mason, A. J., Charnley, N., Johnson, K. R., and Xie, S.-C., 2013, Links between the East Asian monsoon and North Atlantic climate during the 8,200 year event: *Nature Geoscience*, v. 6, no. 2, p. 117–120, doi: 10.1038/ngeo1708.
- Marcott, S. A., Shakun, J. D., Clark, P. U., and Mix, A. C., 2013, A Reconstruction of Regional and Global Temperature for the Past 11,300 Years: *Science*, v. 339, no. 6124, p. 1198–1201, doi: 10.1126/science.1228026.
- Marino, G., Rohling, E. J., Sangiorgi, F., Hayes, A., Casford, J. L., Lotter, A. F., Kucera, M., and Brinkhuis, H., 2009, Early and middle Holocene in the Aegean Sea: interplay between high and low latitude climate variability: *Quaternary Science Reviews*, v. 28, no. 27–28, p. 3246–3262, doi: 10.1016/j.quascirev.2009.08.011.
- Mariotti, A., Struglia, M. V., Zeng, N., and Lau, K.-M., 2002, The Hydrological Cycle in the Mediterranean Region and Implications for the Water Budget of the Mediterranean Sea: *Journal of Climate*, v. 15, p. 1674–1690, doi: 10.1175/1520-0442(2002)015<1674:THCITM>2.0.CO;2.
- Marshall, J. D., Brooks, J. R., and Lajtha, K., 2008, Sources of variation in the stable isotopic composition of plants, in Michener, R. and Lajtha, K. (Eds.), *Stable Isotopes in Ecology and Environmental Science*, Wiley-Blackwell, p. 22–60.
- Mayewski, P. A., Rohling, E. E., Curt Stager, J., Karlén, W., Maasch, K. A., David Meeker, L., Meyerson, E. A., Gasse, F., van Kreveld, S., Holmgren, K., Lee-Thorp, J., Rosqvist, G., Rack, F., Staubwasser, M., et al., 2004, Holocene climate variability: *Quaternary Research*, v. 62, no. 3, p. 243–255, doi: 10.1016/j.yqres.2004.07.001.
- McManus, J. F., Francois, R., Gherardi, J.-M., Keigwin, L. D., and Brown-Leger, S., 2004, Collapse and rapid resumption of Atlantic meridional circulation linked to deglacial climate changes: *Nature*, v. 428, p. 834–837.
- Milner, A. M., Collier, R. E. L., Roucoux, K. H., Muller, U. C., Pross, J., Kalaitzidis, S., Christanis, K., and Tzedakis, P. C., 2012, Enhanced seasonality of precipitation in the Mediterranean during the early part of the Last Interglacial: *Geology*, v. 40, no. 10, p. 919–922, doi: 10.1130/G33204.1.
- Milner, A. M., Müller, U. C., Roucoux, K. H., Collier, R. E. L., Pross, J., Kalaitzidis, S., Christanis, K., and Tzedakis, P. C., 2013, Environmental variability during the Last Interglacial: a new high-resolution pollen record from Tenaghi Philippon, Greece: *Journal of Quaternary Science*, v. 28, no. 2, p. 113–117, doi: 10.1002/jqs.2617.
- Mommersteeg, H. J. P. M., Loutre, M. F., Young, R., Wijmstra, T. A., and Hooghiemstra, H., 1995, Orbital forced frequencies in the 975,000 year pollen record from Tenaghi Philippon (Greece): *Climate Dynamics*, v. 11, p. 4–24.
- Morrill, C., and Jacobsen, R., M., 2005, How widespread were climate anomalies 8200 years ago? *Geophysical Research Letters*, v. 32, no. 19, p. 1–4, doi: 10.1029/2005GL023536.
- Morrill, C., Anderson, D. M., Bauer, B. A., Buckner, R., Gille, E. P., Gross, W. S., Hartman, M., and Shah, A., 2013, Proxy benchmarks for intercomparison of 8.2 ka simulations: *Climate of the Past*, v. 9, no. 1, p. 423–432, doi: 10.5194/cp-9-423-2013.
- Müller, U. C., Pross, J., Tzedakis, P. C., Gamble, C., Kotthoff, U., Schmiedl, G., Wulf, S., and Christanis, K., 2011, The role of climate in the spread of modern humans into Europe: *Quaternary Science Reviews*, v. 30, p. 16040–16045, doi: 10.1016/j.quascirev.2010.11.016.
- O’Leary, M. H., 1988, Carbon Isotopes Photosynthesis - Fractionation techniques may reveal new aspects of carbon dynamics in plants: *BioScience*, v. 38, no. 5, p. 328–336.

- Oçakoğlu, F., Kır, O., Yılmaz, İ. Ö., Açıkalın, S., Erayık, C., Tunoğlu, C., and Leroy, S. A. G., 2013, Early to Mid-Holocene Lake level and temperature records from the terraces of Lake Sünnet in NW Turkey: *Palaeogeography, Palaeoclimatology, Palaeoecology*, v. 369, p. 175–184, doi: 10.1016/j.palaeo.2012.10.017.
- Panagiotopoulos, K., Aufgebauer, A., Schäbitz, F., and Wagner, B., 2013, Vegetation and climate history of the Lake Prespa region since the Lateglacial: *Quaternary International*, v. 293, p. 157–169, doi: 10.1016/j.quaint.2012.05.048.
- Peltzer, E. T., and Gagosian, R. B., 1989, Organic geochemistry of aerosols over the Pacific Ocean, *in* *Chemical Oceanography 10. SEAREX: the Sea/Air Exchange Program*. Academic Press, New York, pp. 281–338.
- Peyron, O., Goring, S., Dormoy, I., Kotthoff, U., Pross, J., de Beaulieu, J.-L., Drescher-Schneider, R., Vanniere, B., and Magny, M., 2011, Holocene seasonality changes in the central Mediterranean region reconstructed from the pollen sequences of Lake Accesa (Italy) and Tenaghi Philippon (Greece): *The Holocene*, v. 21, no. 1, p. 131–146, doi: 10.1177/0959683610384162.
- Peyron, O., Magny, M., Goring, S., Joannin, S., de Beaulieu, J.-L., Brugiapaglia, E., Sadori, L., Garfi, G., Kouli, K., Ioakim, C., and Combourieu-Nebout, N., 2013, Contrasting patterns of climatic changes during the Holocene across the Italian Peninsula reconstructed from pollen data: *Climate of the Past*, v. 9, no. 3, p. 1233–1252, doi: 10.5194/cp-9-1233-2013.
- Pross, J., Tzedakis, P., Schmiedl, G., Christanis, K., Hooghiemstra, H., Müller, U. C., Kotthoff, U., Kalaitzidis, S., and Milner, A., 2007, Tenaghi Philippon (Greece) Revisited: Drilling a Continuous Lower-Latitude Terrestrial Climate archive of the Last 250,000 Years: *Scientific Drilling*, v. 5, p. 44–46, doi: 10.2204/iodp.sd.5.06.2007.
- Pross, J., Kotthoff, U., Müller, U. C., Peyron, O., Dormoy, I., Schmiedl, G., Kalaitzidis, S., and Smith, A.M., 2009, Massive perturbation in terrestrial ecosystems of the Eastern Mediterranean region associated with the 8.2 kyr B.P. climatic event: *Geology*, v. 37, no. 10, p. 887–890, doi: 10.1130/G25739A.1.
- Pross, J., Koutsodendris, A., Christanis, K., Fischer, T., Fletcher, W. J., Hardiman, M., Kalaitzidis, S., Knipping, M., Kotthoff, U., Milner, A. M., Müller, U. C., Schmiedl, G., Siavalas, G., Tzedakis, P.C., et al., 2015, The 1.35-Ma-long terrestrial climate archive of Tenaghi Philippon, northeastern Greece: Evolution, exploration, and perspectives for future research: *Newsletters on Stratigraphy*, v. 48, no. 3, p. 253–276, doi: 10.1127/nos/2015/0063.
- Raven, J. A., 1977, The evolution of vascular land plants in relation to supracellular transport processes, *Advances in Botanical Research*, 5, 153–219.
- Raven, J.A., 2002, Selection pressures on stomatal evolution, *New Phytologist*, 153, 371–386.
- Renssen, H., Goosse, H., Fichefet, T., and Campin, J.-M., 2001, The 8.2 kyr BP event simulated by a global atmosphere-sea-ice-ocean model: *Geophysical Research Letters*, v. 28, no. 8, p. 1567–1570.
- Renssen, H., Goosse, H., Crosta, X., and Roche, D. M., 2010, Early holocene laurentide ice sheet deglaciation causes cooling in the high-latitude southern hemisphere through oceanic teleconnection: *Paleoceanography*, v. 25, no. 3, p. 1–15, doi: 10.1029/2009PA001854.
- Riederer, M., 2006, Introduction: biology of the plant cuticle, *in* Riederer, M., and Müller, C. (Eds.), *Biology of the Plant Cuticle*, Blackwell Publishing, Oxford.
- Rodwell, M. J., and Hoskins, B. J., 1996, Monsoons and the dynamics of deserts: *Quarterly Journal of the Royal Meteorological Society*, no. 122, p. 1385–1404.

- Rohling, E. J., and Pälike, H., 2005, Centennial-scale climate cooling with a sudden cold event around 8,200 years ago: *Nature*, v. 434, no. 7036, p. 975–979.
- Rohling, E. J., Mayewski, P. A., Abu-Zied, R. H., Casford, J. S. L., and Hayes, A., 2002, Holocene atmosphere-ocean interactions: records from Greenland and the Aegean Sea: *Climate Dynamics*, v. 18, no. 7, p. 587–593, doi: 10.1007/s00382-001-0194-8.
- Rommerskirchen, F., Eglinton, G., Dupont, L., Güntner, U., Wenzel, C., and Rullkötter, J., 2003, A north to south transect of Holocene southeast Atlantic continental margin sediments: Relationship between aerosol transport and compound-specific $\delta^{13}\text{C}$ land plant biomarker and pollen records: *Geochemistry Geophysics Geosystems*, v. 4, no. 12, p. 1–29.
- Rozanski, K., Araguás-Araguás, L., and Gonfiantini, R., 1993, Isotopic Patterns in Modern Global Precipitation, in Swart, P.K., Lohmann, K.C., McKenzie, J., and Savin, S. (Eds.), *Climate Change in Continental Isotopic Records*, American Geophysical Union, p. 1–36.
- Sachse, D., Kahmen, A., and Gleixner, G., 2009, Significant seasonal variation in the hydrogen isotopic composition of leaf-wax lipids for two deciduous tree ecosystems (*Fagus sylvatica* and *Acer pseudoplatanus*): *Organic Geochemistry*, v. 40, no. 6, p. 732–742, doi: 10.1016/j.orggeochem.2009.02.008.
- Sachse, D., Gleixner, G., Wilkes, H., and Kahmen, A., 2010, Leaf wax *n*-alkane δD values of field-grown barley reflect leaf water δD values at the time of leaf formation: *Geochimica et Cosmochimica Acta*, v. 74, no. 23, p. 6741–6750, doi: 10.1016/j.gca.2010.08.033.
- Sachse, D., Billault, I., Bowen, G. J., Chikaraishi, Y., Dawson, T. E., Feakins, S. J., Freeman, K. H., Magill, C. R., McInerney, F. A., van der Meer, M. T. J., Polissar, P., Robins, R. J., Sachs, J. P., Schmidt, H.-L., et al., 2012, Molecular Paleohydrology: Interpreting the Hydrogen-Isotopic Composition of Lipid Biomarkers from Photosynthesizing Organisms: *Annual Review of Earth and Planetary Sciences*, v. 40, no. 1, p. 221–249, doi: 10.1146/annurev-earth-042711-105535.
- Schefuß, E., Rattmeyer, V., Stuut, J.-B. W., Jansen, J. H. F., and Sinninghe Damsté, J. S., 2003, Carbon isotope analyses of *n*-alkanes in dust from the lower atmosphere over the central eastern Atlantic: *Geochimica et Cosmochimica Acta*, v. 67, no. 10, p. 1757–1767, doi: 10.1016/S0016-7037(02)01414-X.
- Schmiedl, G., Kuhnt, T., Ehrmann, W., Emeis, K.-C., Hamann, Y., Kotthoff, U., Dulski, P., and Pross, J., 2010, Climatic forcing of eastern Mediterranean deep-water formation and benthic ecosystems during the past 22000 years: *Quaternary Science Reviews*, v. 29, no. 23–24, p. 3006–3020, doi: 10.1016/j.quascirev.2010.07.002.
- Sessions, A. L., Burgoyne, T. W., Schimmelmann, A., and Hayes, J. M., 1999, Fractionation of hydrogen isotopes in lipid biosynthesis: *Organic Geochemistry*, v. 30, no. 9, p. 1193–1200, doi: 10.1016/S0146-6380(99)00094-7.
- Sessions, A. L., Sylva, S. P., Summons, R. E., and Hayes, J. M., 2004, Isotopic exchange of carbon-bound hydrogen over geologic timescales: *Geochimica et Cosmochimica Acta*, v. 68, no. 7, p. 1545–1559, doi: 10.1016/j.gca.2003.06.004.
- Shackleton, N. J., Hall, M. A., and Vincent, E., 2000, Phase relationships between millennial-scale events 64,000 to 24,000 years ago: *Paleoceanography* 15: 565-569.
- Shepherd, T., and Griffiths, D. W., 2006, The effects of stress on plant cuticular waxes: *The New phytologist*, v. 171, no. 3, p. 469–99, doi: 10.1111/j.1469-8137.2006.01826.x.
- Siani, G., Paterne, M., and Colin, C., 2010, Late glacial to Holocene planktic foraminifera bioevents and climatic record in the South Adriatic Sea: *Journal of Quaternary Science*, v. 25, no. 5, p. 808–821, doi: 10.1002/jqs.1360.

- Siani, G., Magny, M., Paterne, M., Debret, M., and Fontugne, M., 2013, Paleohydrology reconstruction and Holocene climate variability in the South Adriatic Sea: *Climate of the Past*, v. 9, no. 1, p. 499–515, doi: 10.5194/cp-9-499-2013.
- Sicre, M.-A., Siani, G., Genty, D., Kallel, N., and Essallami, L., 2013, Seemingly divergent sea surface temperature proxy records in the central Mediterranean during the last deglaciation: *Climate of the Past*, v. 9, no. 3, p. 1375–1383, doi: 10.5194/cp-9-1375-2013.
- Smith, F. A., and Freeman, K. H., 2006, Influence of physiology and climate on δD of leaf wax *n*-alkanes from C₃ and C₄ grasses: *Geochimica et Cosmochimica Acta*, v. 70, no. 5, p. 1172–1187, doi: 10.1016/j.gca.2005.11.006.
- Sperling, M., Schmiedl, G., Hemleben, C., and Emeis, K. C., 2003, Black Sea impact on the formation of eastern Mediterranean sapropel S1? Evidence from the Marmara Sea: *Paleogeography, Paleoclimatology, Paleoecology*, v. 190, p. 9–21.
- Staubwasser, M., and Weiss, H., 2006, Holocene climate and cultural evolution in late prehistoric–early historic West Asia: *Quaternary Research*, v. 66, no. 3, p. 372–387, doi: 10.1016/j.yqres.2006.09.001.
- Teller, J. T., Leverington, D. W., and Mann, J. D., 2002, Freshwater outbursts to the oceans from glacial Lake Agassiz and their role in climate change during the last deglaciation: *Quaternary Science Reviews*, v. 21, no. 8–9, p. 879–887, doi: 10.1016/S0277-3791(01)00145-7.
- Teller, J. T., and Leverington, D. W., 2004, Glacial Lake Agassiz: A 5000 yr history of change and its relationship to the $\delta^{18}O$ record of Greenland: *Geological Society of America Bulletin*, v. 116, no. 5, p. 729, doi: 10.1130/B25316.1.
- Thomas, E. R., Wolff, E. W., Mulvaney, R., Steffensen, J. P., Johnsen, S. J., Arrowsmith, C., White, J. W. C., Vaughn, B., and Popp, T., 2007, The 8.2ka event from Greenland ice cores: *Quaternary Science Reviews*, v. 26, no. 1–2, p. 70–81, doi: 10.1016/j.quascirev.2006.07.017.
- Tipple, B. J., Berke, M. A., Doman, C. E., Khachatryan, S., and Ehleringer, J. R., 2013, Leaf-wax *n*-alkanes record the plant-water environment at leaf flush: *Proceedings of the National Academy of Sciences of the United States of America*, v. 110, no. 7, p. 2659–64, doi: 10.1073/pnas.1213875110.
- Triantaphyllou, M. V., Ziveri, P., Gogou, A., Marino, G., Lykousis, V., Bouloubassi, I., Emeis, K.-C., Kouli, K., Dimiza, M., Rosell-Melé, A., Papanikolaou, M., Katsouras, G., and Nunez, N., 2009, Late Glacial–Holocene climate variability at the south-eastern margin of the Aegean Sea: *Marine Geology*, v. 266, no. 1–4, p. 182–197, doi: 10.1016/j.margeo.2009.08.005.
- Tzedakis, P. C., Hooghiemstra, H., and Pälike, H., 2006, The last 1.35 million years at Tenaghi Philippon: revised chronostratigraphy and long-term vegetation trends: *Quaternary Science Reviews*, v. 25, no. 23–24, p. 3416–3430, doi: 10.1016/j.quascirev.2006.09.002.
- Ulbrich, U., Lionello, P., Belušić, D., Jacobeit, J., Knippertz, P., Kuglitsch, F. G., Leckebusch, G. C., Luterbach, J., Maugeri, M., Maheras, P., Nissen, K. M., Pavan, V., Pinto, J. G., Saarnoi, H., Seubert, S., Toreti, A., Xoplaki, E., and Ziv, B., 2012, Climate of the Mediterranean: Synoptic Patterns, Temperature, Precipitation, Winds, and Their Extremes, *in* Lionello, P. (Ed.), *The Climate of the Mediterranean Region*, Elsevier B. V., Amsterdam, p. 301–346.
- UNEP/MAP-Plan Bleu: State of the Environment and Development in the Mediterranean, UNEP/MAP-Plan Bleu, Athens, 2009, retrieved from www.planbleu.org/sites/default/files/publications/soed2009_en.pdf.
- Urey, H.C., 1947, The thermodynamic properties of isotopic substances: *Journal of Chemical Society*, 1947: 562–581

- Van der Wiel, A. M., Wijmstra, T. A., 1987a, Palynology of the lower part (78–120 m) of the core Tenaghi Philippon II, Middle Pleistocene of Macedonia, Greece: *Review of Palaeobotany and Palynology* 52, 73–88.
- Van der Wiel, A. M., Wijmstra, T. A., 1987b, Palynology of the 112.8–197.8 m interval of the core Tenaghi Philippon III, Middle Pleistocene of Macedonia, Greece: *Review of Palaeobotany and Palynology* 52, 89–117.
- Vogts, A., Schefuß, E., Badewien, T., and Rullkötter, J., 2012, *n*-Alkane parameters from a deep sea sediment transect off southwest Africa reflect continental vegetation and climate conditions: *Organic Geochemistry*, v. 47, p. 109–119, doi: 10.1016/j.orggeochem.2012.03.011.
- Wang, Y., Cheng, H., Edwards, R. L., He, Y., Kong, X., An, Z., Wu, J., Kelly, M. J., Dykoski, C. A., Li, X., 2005. The Holocene Asian monsoon: links to solar changes and North Atlantic climate: *Science*, 308 (no. 5723), 854–857. <http://dx.doi.org/10.1126/science.1106296>.
- Wanner, H., Beer, J., Büttikofer, J., Crowley, T. J., Cubasch, U., Flückiger, J., Goosse, H., Grosjean, M., Joos, F., Kaplan, J. O., Küttel, M., Müller, S. A., Prentice, I. C., Solomina, O., et al., 2008, Mid- to Late Holocene climate change: an overview: *Quaternary Science Reviews*, v. 27, no. 19–20, p. 1791–1828, doi: 10.1016/j.quascirev.2008.06.013.
- Wanner, H., Solomina, O., Grosjean, M., Ritz, S. P., and Jetel, M., 2011, Structure and origin of Holocene cold events: *Quaternary Science Reviews*, v. 30, no. 21–22, p. 3109–3123, doi: 10.1016/j.quascirev.2011.07.010.
- Weiss, H., 1975, Kish, Akkad and Agade: *Journal of the American Oriental Society* 95, 434–453.
- Wellman, C. H., Osterloff, P. L., and Mohiuddin, U., 2003, Fragments of the earliest land plants: *Nature*, v. 425, p. 282–285. doi:10.1038/nature01884.
- Weninger, B., Alram-Stern, E., Bauer, E., Clare, L., Danzeglocke, U., Jöris, O., Kubatzki, L., Rollefson, C., Todorova, H., and van Andel, T., 2006, Climate Forcing due to the 8200 cal BP event observed at Early Neolithic sites in the Eastern Mediterranean: *Quaternary Research* 66, 401–420.
- Wiersma, A. P., Renssen, H., Goosse, H., and Fichet, T., 2006, Evaluation of different freshwater forcing scenarios for the 8.2 ka BP event in a coupled climate model: *Climate Dynamics*, v. 27, no. 7–8, p. 831–849, doi: 10.1007/s00382-006-0166-0.
- Wijmstra, T. A., Groenhardt, M. C., 1983, Record of 700,000 years vegetational history in Eastern Macedonia (Greece): *Revista de la Academia Colombiana de Ciencias Exactas, Físicas y Naturales*, v. 15, p. 87–98.
- Wijmstra, T. A., Smit, A., 1976, Palynology of the middle part (30–78 meters) of a 120 m deep section in northern Greece (Macedonia): *Acta Botanica Neerlandica*, v. 25, p. 297–312.
- Wijmstra, T. A., 1969, Palynology of the first 30 m of a 120 m deep section in northern Greece: *Acta Botanica Neerlandica*, v. 18, p. 511–527.
- Wilson, G. P., Reed, J. M., Lawson, I. T., Frogley, M. R., Preece, R. C., and Tzedakis, P. C., 2008, Diatom response to the Last Glacial-Interglacial Transition in the Ioannina basin, northwest Greece: implications for Mediterranean palaeoclimate reconstruction: *Quaternary Science Reviews*, v. 27, p. 428–440, doi: 10.1016/j.quascirev.2007.10.013.
- Xoplaki, E., González-Rouco, F. J., Luterbacher, J., and Wanner, H., 2003, Mediterranean summer air temperature variability and its connection to the large-scale atmospheric circulation and SSTs: *Climate Dynamics*, v. 20, p. 723–739, doi: 10.1007/s00382-003-0304-x.

Ziv, B., Saaroni, H., and Alpert, P., 2004, The factors governing the summer regime of the eastern Mediterranean: *International Journal of Climatology*, v. 24, no. 14, p. 1859–1871, doi: 10.1002/joc.1113.

Chapter 2

The impact of topography on isotopes in precipitation across the Central Anatolian Plateau (Turkey)

Fabian Schemmel^{1,3}, Tamás Mikes^{1,2}, Bora Rojay⁴ and Andreas Mulch^{1,2,3}

¹ Senckenberg Biodiversity and Climate Research Centre (BiK-F), Frankfurt am Main, Germany

² Goethe University, Institute of Geosciences, Frankfurt am Main, Germany

³ Senckenberg Research Institute and Natural History Museum, Frankfurt am Main, Germany

⁴ Middle East Technical University, Institute of Geological Engineering, Ankara, Turkey

Published in American Journal of Science (2013), 313, p. 61-80, doi: 10.2475/02.2013.01

Abstract Paleoelevation reconstructions of mountain belts and orogenic plateaus based on stable isotope climate and precipitation records benefit greatly from present-day calibrations that relate the fractionation of hydrogen (δD) and oxygen ($\delta^{18}\text{O}$) isotopes in precipitation to orographic rainfall. Here, we establish a first-order template of δD and $\delta^{18}\text{O}$ of modern meteoric waters across the Central Anatolian Plateau (CAP) and its bordering Pontic and Taurus Mountains. We identify key regions in the plateau interior and along the plateau margins that have the potential to reliably record topography-related paleotemperature and paleoprecipitation changes as recovered from stable isotope paleosol, fossil teeth or lipid proxy data. Based on δD and $\delta^{18}\text{O}$ data of more than 480 surface water samples from small catchments and springs, we characterize moisture sources affecting the net isotopic budget of precipitation over the CAP and analyze how orographic rainout and plateau aridity shape modern patterns of δD and $\delta^{18}\text{O}$ in precipitation. The Taurus Mountains bordering the CAP to the south act as a major orographic barrier for transport of predominantly winter moisture and exhibit isotopic lapse rates of approximately -20‰/km for δD and -2.9‰/km for $\delta^{18}\text{O}$ across an elevation range of nearly 3000 m. The Pontic Mountains at the northern margin of the CAP force perennial moisture to ascend and condensate revealing lapse rates of -19‰/km for δD and -2.6‰/km for $\delta^{18}\text{O}$. The difference in the predominant moisture source for the southern and northern margins of the CAP (North African versus Atlantic air masses) is manifested in systematic north–south differences in near-sea level meteoric water compositions of $\Delta(\delta\text{D}_{\text{N-S}}) \approx 20\text{‰}$ and $\Delta(\delta^{18}\text{O}_{\text{N-S}}) \approx 3\text{‰}$ in a swath across the central part of the plateau. Stable isotope data from the semi-arid plateau interior with rainfall as low as 300 to 500 mm/yr and mean summer temperatures attaining 23°C , provide clear evidence for an evaporative regime that drastically affects surface

water and runoff compositions and results in a local meteoric water line for the plateau interior that follows $\delta D = 4.0 \cdot \delta^{18}O - 29.3$. Strongly evaporitic conditions contrast rainfall patterns along the plateau margins including their immediate leeward flanks where δD - and $\delta^{18}O$ -elevation relationships are reliable predictors of modern topography.

2.1 Introduction

2.1.1 Why stable isotope paleoaltimetry in Anatolia?

Reconstructing paleoelevation of major mountain belts and continental plateau regions such as Tibet, the Andes, or western North America plays an important role in relating Earth surface dynamics to the geodynamic processes of the Earth's interior. Stable isotope paleoaltimetry, despite being a relatively young field, has been instrumental in many of such studies (e.g., Chamberlain et al., 1999; Garzzone et al., 2000a, b; Rowley et al., 2001; Horton et al., 2004; Currie et al., 2005; Cyr et al., 2005; Garzzone et al., 2006; Mulch et al., 2006; Rowley and Currie, 2006; Mulch and Chamberlain, 2007; Mulch et al., 2008; Garzzone et al., 2008; Mulch et al., 2010; Quade et al., 2011; Mix et al., 2011; Campani et al., 2012). Stable isotope paleoaltimetry builds on the orographic rainout effect, the thermodynamically controlled systematic decrease of stable hydrogen (δD) and oxygen ($\delta^{18}O$) isotope ratios in precipitation with increasing elevation and hence decreasing condensation temperatures on the windward side of a mountain range. This process is commonly accompanied by the development of an "isotopic rain shadow", a zone of local stable isotopic minima confined to the immediate leeward side, where the isotopic values are mostly controlled by the elevation of the range alone (e.g., Dansgaard, 1964; Ingraham and Taylor, 1991; Blisniuk and Stern, 2005). Recovery of the spatio-temporal changes in the hydrogen and oxygen isotopic composition of authigenic minerals may hence reveal changes in paleoclimate and track the evolution of regional topography (e.g., Quade et al., 2007; Mulch and Chamberlain 2007). However, uncertainties in reconstructing past rainfall-topography relationships can arise with the interplay of certain climatic and/or topographic conditions such as (1) upstream changes in the source area of water vapor, (2) variable air parcel trajectories, (3) mixing of air masses or evaporation of meteoric waters under (semi-)arid climate regimes, or (4) changes in stable isotope in precipitation-elevation relationships ("isotopic lapse rate") over geologic time. These factors can mask δD and $\delta^{18}O$ signals in the geologic record and may lead to over- or underestimation of past changes in climate and topography (e.g., Ehlers and Poulsen, 2009; Galewsky, 2009; Insel et al., 2009; Poulsen et al., 2010, Vachon et al., 2010; Lechler and Niemi, 2011).

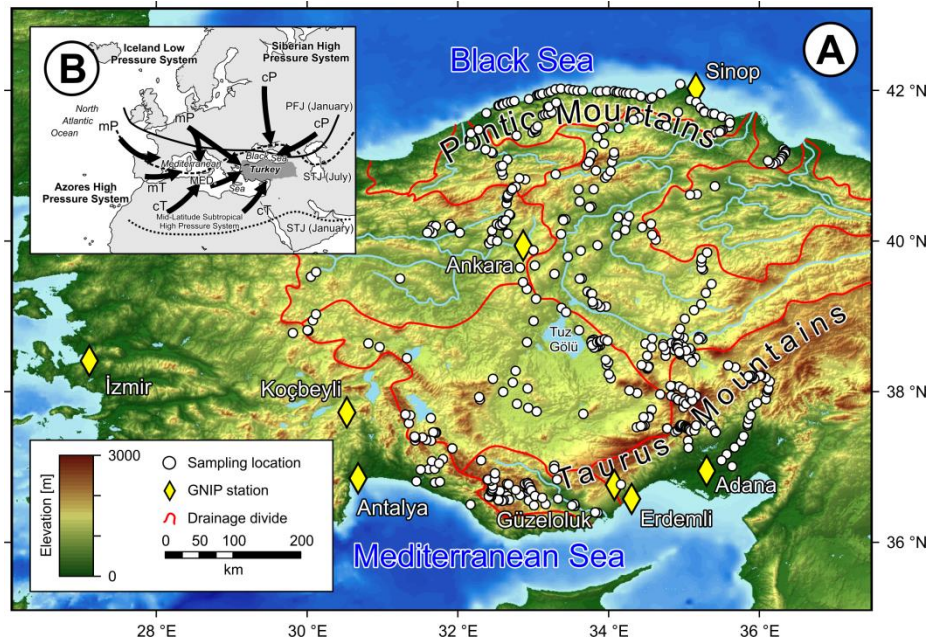


Fig. 2.1 (A): Digital elevation model of the Central Anatolian Plateau showing sample locations as well as selected meteorological stations of the Global Network of Isotopes in Precipitation (GNIP, IAEA/WMO, 2006 – see text for details). (B): Schematic diagram of major air masses affecting Anatolian climate (modified after Sariş et al., 2010). Abbreviations: cT – continental tropical air mass; cP – continental polar air mass; mT – marine tropical air mass; mP – marine polar air mass; MED – Mediterranean air mass; PFJ – Polar Front Jet; STJ - Sub-tropical Jet.

Despite its important role in the Mediterranean geodynamic and climate history little is known about the Neogene elevation history of the Central Anatolian Plateau (CAP). Being the third largest orogenic plateau on Earth, it is situated in the Alpine-Himalayan orogenic belt in the Eastern Mediterranean. The CAP shares many of the characteristics of the large continental plateau regions: aridity and relatively subdued topography in the plateau interior as well as high-elevation plateau-bounding mountain ranges, albeit on an overall smaller scale than for example the Altiplano and Tibet (Fig. 2.1A). Located in a progressively changing stress field between the collision zone of Africa and Arabia with Eurasia in the E and the back-arc extensional province behind the Aegean subduction zone in the W, principal driving mechanisms of elevation gain in the CAP region involve both (1) mantle upwelling due to slab tear of the northward-dipping, downgoing African plate (at the southern plateau margin – Gans et al., 2009; Biryol et al., 2011; Cosentino et al., 2012; Schildgen et al., 2012a, b) and (2) upper crustal shortening (at the northern plateau margin – Yıldırım et al., 2011). The onset of accelerated surface uplift of the plateau margins dates back to about 8 to 7 Ma in the south (Cosentino et al., 2012; Schildgen et al., 2012b) and to the Late Miocene to Early Pliocene in the north (Yıldırım et al., 2011). As suggested by numerical paleotopographic reconstructions and by apatite fission track thermochronology respectively, both margins were to some extent characterized by topographic relief before the onset of the major uplift (Cavazza et al.,

2011; Schildgen et al., 2012b). The youngest marine sediments in the CAP interior are Eocene in age (Lüttig and Steffens, 1975; Görür and Tüysüz, 2001).

The CAP therefore lends itself favorably for reconstructing the coupled geodynamic, climatic, and Earth surface processes that together shaped its modern topography. The topographic history of Central Anatolia over the past 10 Ma plays a key role in understanding the interplay between lithospheric-scale geodynamic processes and Earth surface dynamics, due to the tight links between the Late Neogene-to-recent dynamics of the Mediterranean slab subducting beneath Anatolia, slab break-off, asthenospheric upwelling, continental volcanism, seismicity, brittle tectonics, and surface uplift (Şengör et al., 2005; Biryol et al., 2011; Cosentino et al., 2012; Schildgen et al., 2012a, b). Equally important is the role of Central Anatolian Earth surface dynamics in controlling regional climate patterns and the development of ecosystems in the Eastern Mediterranean; one of the crossroads of hominids between Africa and Eurasia (Görür et al., 1995; Müller et al., 2011).

2.1.2 Topographic and climatic setting

Bordered by two E–W trending mountain ranges roughly 400 km apart, the CAP attains an average elevation of about 1000 m. To the N along the Black Sea coast, the Pontic Mountains reach average elevations of up to 1400 m, while the Taurus Mountains along the Mediterranean coast to the S are characterized by an average elevation of about 2400 m with highest peaks attaining 3756 m (Demirkazık Dağı) (Fig. 2.1A). Atmospheric moisture is transported to Anatolia by two principal air masses that are sourced in the polar and in the tropical regions (Fig. 2.1B). Winter precipitation is connected primarily to the Icelandic Low Pressure System above the N Atlantic and the Mediterranean Depression as well as to anticyclones controlled by the Azores High Pressure System and subordinately to the stable, continental high-pressure systems centered above Siberia. Summer rains are brought by continental tropical air masses sourced in Northern Africa that typically merge en route with Arabian and Middle Eastern systems before reaching the Anatolian region (Türkeş and Erlat, 2005). The modern climate of Anatolia is diverse, with topography exerting a strong control on precipitation and temperature distribution (Fig. 2.2). It is temperate, semi-humid to humid in the coastal regions where the bulk of annual precipitation occurs (Türkeş and Erlat, 2005). The plateau interior in contrast is semi-arid and characterized by hot and dry summers and cold winters. Mean annual temperatures (MAT) in the northern part of the CAP of about

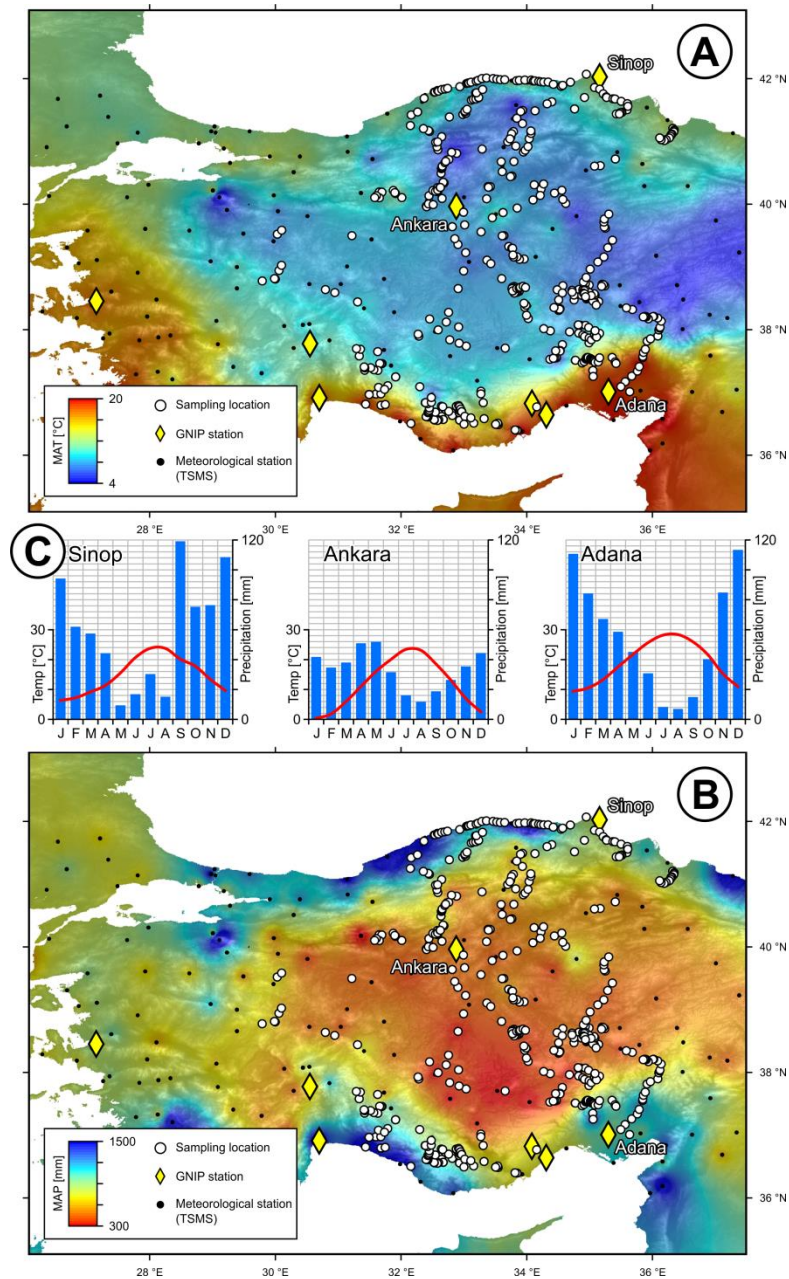


Fig. 2.2 Distribution of (A) mean annual temperature and (B) mean annual precipitation in Central Anatolia. The maps were calculated by inverse distance-weighted interpolation of long-term data recorded by the station network of the Turkish State Meteorological Survey, Ankara (TSMS; data courtesy of M. Demircan). (C) Long-term mean monthly temperature and precipitation trends of the GNIP stations at Sinop, Ankara, and Adana (IAEA/WMO, 2006).

9 °C are slightly lower than in the south (12 °C). The mean temperature of the driest (summer) months is approximately 23 °C (2 °C in the winter months). Mean annual temperatures of up to 20 °C characterize the Mediterranean coast whereas the Black Sea coast is uniformly colder (MAT of about 13 °C). Mean summer (winter) temperatures in the coastal regions close to sea level are 23 °C (7 °C) in the N and 29 °C (9 °C) in the S (Sensoy et al., 2008). Most of the precipitation on the plateau falls between December and May, amounting to 300 to 500 mm/yr, with a slight S-to-N increase. Summer precipitation however is very limited and usually does not balance the water deficit that

emerges during the warm, dry, evaporation-dominated summer months (Sensoy et al., 2008; Ankara in Fig. 2.2C). The coastal mountain fronts receive more than 1000 mm/yr orographic precipitation (Türkeş and Erlat, 2005), largely restricted to the period from October to May with the Pontic Mountains usually being humid over the course of the year.

2.1.3 Goal of this study

Here we present stable hydrogen (δD) and oxygen ($\delta^{18}\text{O}$) isotopic data of modern meteoric waters from the Central Anatolian Plateau in Turkey. We aim (1) to characterize the isotopic composition of moisture transported to Anatolia, and (2) to assess the effects of orographic rainout, the change in isotopic composition of precipitation as a function of elevation (“isotopic lapse rate”) on the windward sides of both the Taurus and the Pontic Mountains. Third, (3) we characterize the oxygen and hydrogen isotopic rain shadows on the leeward sides of the Pontic and Taurus mountain ranges, and (4) identify the effects of evaporation on meteoric water δD and $\delta^{18}\text{O}$ values within the plateau interior. Based on data from more than 480 stream, creek, and near-surface groundwater samples, we establish a robust first-order isotopic template at the scale of the entire CAP and its margins, against which continental paleoclimate proxy data can be interpreted.

2.1.4 Sampling strategy

For surface water sampling, we focused on streams and creeks from small catchments as well as tapped springs (locally referred to as *çeşme*). This approach, besides a large spatial coverage, has distinct advantages over sampling precipitation directly as it provides robust, long-term, yet spatially highly resolved patterns of the isotopic composition of precipitation and near-surface groundwaters by reducing bias (1) from shorter-term, daily to seasonal hydrometeorological variations and (2) from downstream mixing of waters from catchments in markedly different isotopic (climatic and topographic) regimes (Kendall and Coplen, 2001). We tested the robustness of our approach by comparing our data to the precipitation-weighted longer-term (> 1 yr) averages of the monthly δD_p and $\delta^{18}\text{O}_p$ data series recorded at the stations of the Global Network of Isotopes in Precipitation (GNIP) in Turkey (IAEA/WMO, 2006; T. Chavez and S. Terzer, personal communication; Fig. 2.1; Tab. 2.1).

Tab. 2.1 Yearly precipitation-weighted mean δD_p and $\delta^{18}O_p$ values of GNIP stations in Central Anatolia (IAEA/WMO, 2006).

GNIP station	WMO code	elevation (m)	δD_p [SMOW]		$\delta^{18}O_p$ [SMOW]		d [‰]	instrumental records
			‰	n	‰	n		
Ankara	1713000	902	-52.3	415	-7.93	440	11.2	1963 - 2009
Antalya	1730000	49	-24.2	299	-4.57	311	12.3	1970 - 2009
Adana	1735000	73	-22.4	281	-4.34	281	12.3	1978 - 2009
Erdemli	1735201	10	-35.4	17	-5.56	11	9.1	1991 - 1993
Güzeloluk	1735202	1400	-48.4	21	-7.67	33	13.0	1990 - 1993
İzmir	1722000	120	-30.3	14	-5.25	14	11.6	2008 - 2009
Koçbeyli	1702600	1025	-58.4	35	-8.74	35	11.5	1989 - 1993
Sinop	1702600	32	-47.0	18	-7.36	16	11.8	2008 - 2009

2.2 Methods

We sampled a total of 482 natural waters from a wide range of elevations that cover most of the area of the Central Anatolian Plateau as well as the Taurus and Pontic Mountains (Fig. 2.1). Several transects were collected from the coasts to the plateau interior to assess the hydrogen and oxygen isotope fractionation that accompanies orographic rainout. Field campaigns took place during the months of May to October from 2008 to 2011 in order to collect the samples under conditions as close to base flow as possible. The sampling elevations cover a range from 0 to 1911 m, with high-elevation locations well represented in both mountain ranges. The sample set consists of 180 surface water samples from streams and creeks as well as 302 spring water samples. At each sampling site 30 ml of unfiltered water were collected in high-density polyethylene bottles, with as little air volume as possible in the closed bottles. Samples were kept at room temperature and in the dark until return to the laboratory for refrigeration and analysis.

Stable hydrogen and oxygen isotope ratio measurements were made on 1 ml aliquots using an LGR 24d liquid isotope water analyzer at the Institute of Geology (University of Hannover) and at the Institute of Geoscience (Goethe University Frankfurt), using identical data acquisition protocols. δD and $\delta^{18}O$ values were corrected based on internal lab standards which are calibrated against SMOW. The analytical precision is typically better than 0.6 ‰ and 0.2 ‰ (both 2σ) absolute for δD and $\delta^{18}O$, respectively. Absolute stable isotope values of the sample set range from -24 to -96 ‰ for δD and -4.5 to -13.0 ‰ for $\delta^{18}O$. The entire dataset is provided in Tab. A1 in the Appendix.

Sampling perennial streams, creeks, and springs provides an amount-weighted, long-term average of precipitation characteristic for individual catchments. Determining the elevation at which these catchments are recharged by rainfall is, however, not straightforward (Rowley et al., 2001; Currie et al., 2005; Galewsky, 2009; Quade et al.,

2011). Whereas sampling elevations may correlate well with the actual condensation height in small high-elevation catchments significant local relief can lead to an underestimation of the elevation at which the bulk of precipitation occurred and hence obscure isotope–elevation relationships. Therefore, we adopted an approach of deriving catchment sizes and average catchment elevations (ACEs) for each water sample. Since the relief distribution in the catchment is accounted for by these calculated ACEs, they provide a very good estimate for the catchment-wide hypsometric mean precipitation elevation. We did not attempt to derive precipitation-weighted hypsometric mean elevations due to the lack of high-resolution rainfall data for individual mountain catchments. The ACEs of each sampled water flow were calculated using an elevation-weighted flow accumulation model in ESRI® ArcGIS™ 10.0, based on version 1 of the ASTER Global Digital Elevation Model which has a spatial resolution of 1 arc second (approximately 30 m) and is provided by the Earth Remote Sensing Data Analysis Center, Japan.

2.3 *Results and discussion*

Four main features characterize our δD and $\delta^{18}\text{O}$ data (Fig. 2.3): (1) Samples along the coasts generally show the least negative δD and $\delta^{18}\text{O}$ values with those from the Mediterranean Sea coast being notably higher (about 21 ‰ in δD and about 3.1 ‰ in $\delta^{18}\text{O}$) compared to samples from the Black Sea coast. (2) Hydrogen and oxygen isotope ratios change systematically across the Pontic and Taurus Mountains and attain the lowest δD and $\delta^{18}\text{O}$ values on the leeward sides of both mountain ranges. (3) From the leeward plateau margin towards the plateau center δD and $\delta^{18}\text{O}$ both show a trend of increasing δD (about 20 to 25 ‰) and $\delta^{18}\text{O}$ (about 5 to 6 ‰) values paralleled by a general increase in variability. (4) Deuterium excess (d) is generally high in the coastal areas and decreases towards the plateau interior.

The median catchment size upstream of our 180 surface water samples is 69 km², with only a few major rivers draining into the Mediterranean or the Black Sea having catchments up to about 20,000 km² upstream the sampling site (Tab. A.1 in the Appendix). In any of the identified geographic zones as described below, neither the stable isotope ratios nor the deuterium excess values d show any clear dependence on the sizes of the individual catchments.

2.3.1 Long-term stability of δD and $\delta^{18}\text{O}$ values

Our δD and $\delta^{18}\text{O}$ values of local streams, creeks, and springs show good agreement with the small number of long-term instrumental records of GNIP stations within the CAP and at its margins (Fig. 2.3). Matching long-term and surface runoff/spring data demonstrates that most of the surface water flows sampled in this study represent modern, longer-term (multi-year to decadal) average rainfall conditions across Central Anatolia. Second, for most of the sampling sites we do not observe a significant difference in the spatial distribution of δD or $\delta^{18}\text{O}$ values between stream/creek waters and spring waters (Fig. 2.3C and D). The latter observation suggests that at these scales (both temporally and spatially) the majority of the sampled water is representative of local meteoric water. Hence, the sampled springs most likely tap near-surface groundwaters with negligible contribution from deeper, distally derived groundwaters (for a discussion of the effects of distal groundwater sources and residence times see below).

2.3.2 Spatial distribution of δD and $\delta^{18}\text{O}$ values

We observe a strong difference in near-sea level δD and $\delta^{18}\text{O}$ values between the northern and southern coastal regions of the plateau of $\geq 21\text{‰}$ for $\Delta(\delta\text{D})$ Taur–Pont and $\geq 3.1\text{‰}$ for $\Delta(\delta^{18}\text{O})$ Taur–Pont (Fig. 2.3C and D). This difference is also visible in different deuterium excess values, defined as $d = \delta\text{D} - 8 \cdot \delta^{18}\text{O}$ (Craig and Gordon, 1965). d is somewhat higher on the windward flanks of the Taurus Mountains but accompanied by a larger scatter ($d = 18.1 \pm 5.0$) than observed on the northern flanks of the Pontic Mountains ($d = 15.8 \pm 1.9$) (Fig. 2.4). The difference in the initial δD and $\delta^{18}\text{O}$ values, (and possibly in d) most likely results from different air parcel trajectories of advected moisture that eventually controls precipitation patterns of Central Anatolia. Overall, the δD and $\delta^{18}\text{O}$ data are in excellent agreement with available air mass trajectories that indicate multiple moisture sources (Fig. 2.1B; Rindsberger et al., 1983; Gat et al., 2003; Türkeş, 2003; Dirican et al., 2005; Türkeş and Erlat, 2005; Pfahl and Wernli, 2008; Sariş et al., 2010).

With respect to potential stable isotope paleoaltimetry reconstructions, the strong decrease in both δD and $\delta^{18}\text{O}$ values across the Taurus Mountains is one of the most important characteristics of the data presented here (Fig. 2.3). Orographic rainfall produces a decrease in D and ^{18}O that equals about 50 to 60 ‰ for $\Delta(\delta\text{D})$ windward–leeward and about 7 to 8 ‰ for $\Delta(\delta^{18}\text{O})$ windward–leeward in the Taurus Mountains. We

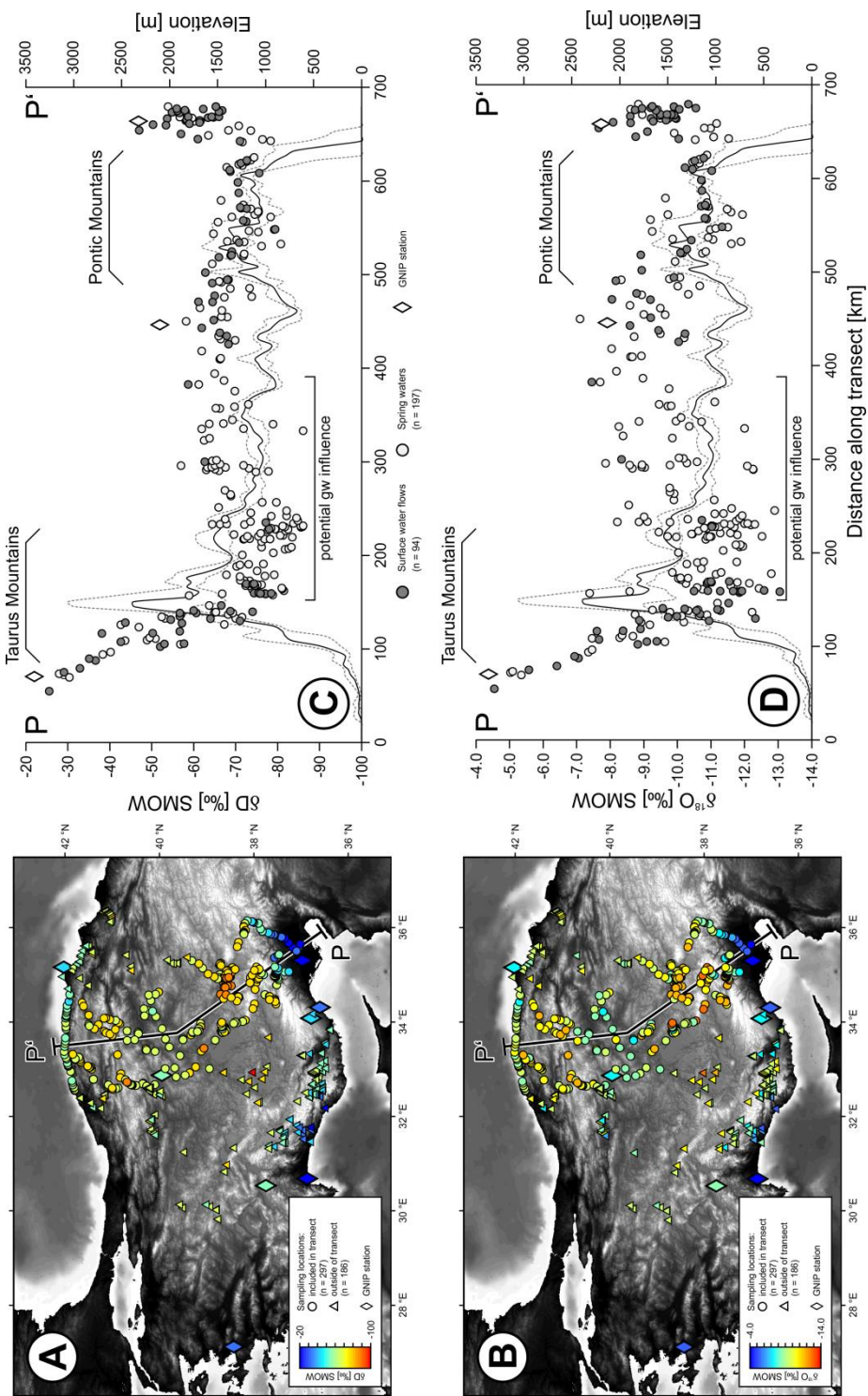


Fig. 2.3 Spatial distribution of (A) δD and (B) $\delta^{18}O$ over the Central Anatolian Plateau. Sampling transects (C) and (D) pass through the Taurus Mountains, the plateau interior, and the Pontic Mountains and include samples within a 70-km-wide swath along the profile along with the long-term δD_p and $\delta^{18}O_p$ values of the GNIIP stations at Adana, Ankara and Sinop (IAEA/WMO, 2006). Elevations (dotted and solid lines) correspond to the $Q_{.25}$, $Q_{.50}$ and $Q_{.75}$ quantiles of the elevation distribution at any point along the swath profile. The GNIIP data from the northernmost station at Sinop are plotted in Fig. 2.3C and D to facilitate comparison. Area of potential groundwater influence constrained by extent of Konya Closed Basin (Fig. 2.4). See text for details of potential distal groundwater influence.

observe a similar decrease yet of smaller magnitude in the Pontic Mountains with $\Delta(\delta D)$ windward–leeward of about 25 ‰ and $\Delta(\delta^{18}O)$ windward–leeward of about 3 ‰. Systematic altitude effects on δD and $\delta^{18}O$ in precipitation are characteristic for many of the world’s major mountain belts (e.g., Dansgaard, 1964; Poage and Chamberlain, 2001; Rowley and Garzione, 2007, Quade et al., 2011). The resulting spatial pattern of low δD and $\delta^{18}O$ values in near-surface groundwater and runoff (“isotopic rain shadow”) on the leeward sides of both mountain ranges does not necessarily correlate with regional changes in rainfall amount (Fig. 2.2 and 2.3). From the immediate lee towards the plateau interior, both δD and $\delta^{18}O$ values show a general increase of about 20 to 25 ‰ and 5 to 6 ‰, respectively. This increase is accompanied by an increasing variability of δD and $\delta^{18}O$ values (Fig. 2.3). We attribute this to the increased aridity within the plateau interior (Fig. 2.2; Sensoy et al., 2008), which promotes secondary (sub-cloud and surface) evaporation of meteoric waters. This conclusion is further supported by the strongly contrasting meteoric water lines of the coastal and plateau regions (see discussion below).

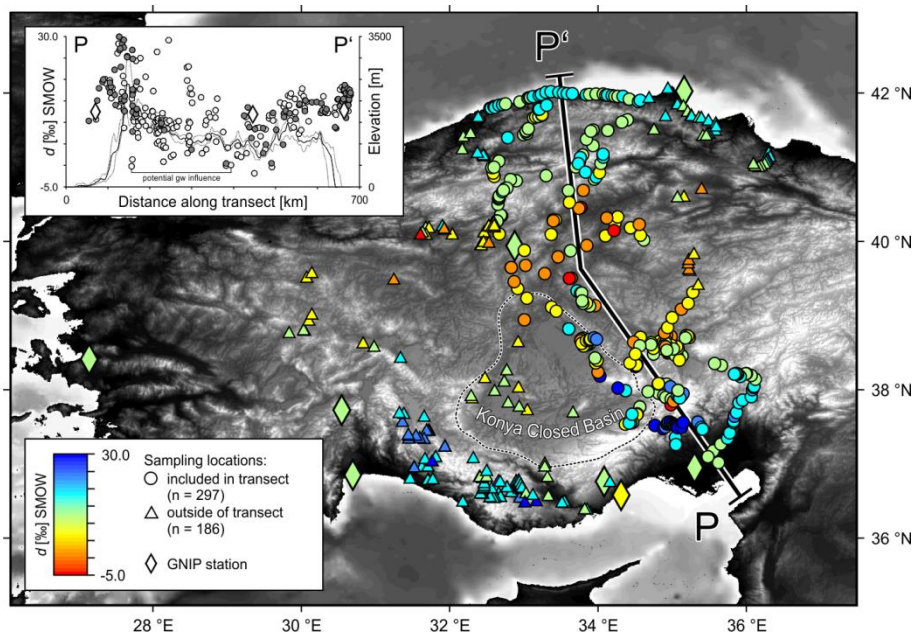


Fig. 2.4 Spatial distribution of deuterium excess (d) values over the Central Anatolian Plateau. The transect shows d of the samples along with the long-term d of the GNIP stations at Adana, Ankara, and Sinop (IAEA/WMO, 2006). Samples included in the calculation are within a 70-km-wide swath along the profile and elevations (solid and dotted lines in the inset) correspond to the $Q_{.25}$, $Q_{.50}$ and $Q_{.75}$ quantiles of the elevation distribution at any point along the swath profile. Location of the Konya Closed Basin is taken from Bayari et al. (2009). See text for details of groundwater influence.

Additionally, the increase in δD and $\delta^{18}O$ towards the plateau center could also result from progressive mixing between southerly- and northerly-derived air masses (in the lee of the Taurus and Pontic Mountains, respectively). However, a linear mixing model between the two initial moisture compositions (that is, the most negative δD and $\delta^{18}O$ values) at the leeward flanks in the N and the S (Fig. 2.3C and D) alone does not explain

the observed high δD and $\delta^{18}O$ values in the plateau interior due to the downward-convex shape of the distribution of isotopic values along the N-S transect. To some extent, admixing of westerly-derived moisture – which has not undergone significant orographic rainout – to the plateau interior is likely, based on the decrease in GNIP-derived δD_p and $\delta^{18}O_p$ values between the Aegean Sea coast (İzmir GNIP station) and the plateau interior (Ankara GNIP station) of -22 ‰ and -2.7 ‰, respectively (Tab. 2.1; see also Fig. A.1 in the Appendix). Again, whereas this process may not be insignificant, it cannot be entirely accounted for the magnitude of positive isotopic shift towards the plateau interior due to the clear-cut difference in the Meteoric Water Lines between the mountain ranges and the plateau interior, as will be demonstrated in the following section.

2.3.3 Meteoric water lines

Most of the surface water samples plot above the Global Meteoric Water Line (GMWL – Craig, 1961) (Fig. 2.5) that follows the general expression $\delta D = 8.17 \cdot \delta^{18}O + 10.35$ (Rozanski et al., 1993). A classification of water samples based on similar stable isotopic trends as well as geographical location shows that samples collected at the windward side of the Taurus and Pontic Mountains, where δD and $\delta^{18}O$ patterns result mostly from the altitude effect (Fig. 2.3), plot in an array parallel to the GMWL and follow the equations:

$$\text{Windward Pontic Mountains LMWL: } \delta D = 7.1 \cdot \delta^{18}O + 7.3 \quad (1)$$

$$\text{Windward Taurus Mountains LMWL: } \delta D = 7.2 \cdot \delta^{18}O + 10.8 \quad (2)$$

In contrast, samples from the plateau interior define a markedly different local meteoric water line (LMWL):

$$\text{Plateau Interior LMWL: } \delta D = 4.0 \cdot \delta^{18}O - 29.3 \quad (3)$$

For precipitation originating in the eastern Mediterranean, values of d have been reported as high as +20 ‰ and above (Gat and Carmi, 1970). This translates to an Eastern Mediterranean Water Line (EMWL) of about $\delta D = 8 \cdot \delta^{18}O + 20$. Analysis of available isotopic data of monthly precipitation (δD_p and $\delta^{18}O_p$) obtained through the Turkey GNIP stations in a period from 2001 to 2003 results in a specific Turkish Meteoric Water Line (TMWL) that follows the equation: $\delta D = 7.7 \cdot \delta^{18}O + 13.1$ (Dirican et al., 2005). The TMWL is in good agreement with the LMWLs of both windward mountain flanks presented here (eqs 1 and 2).

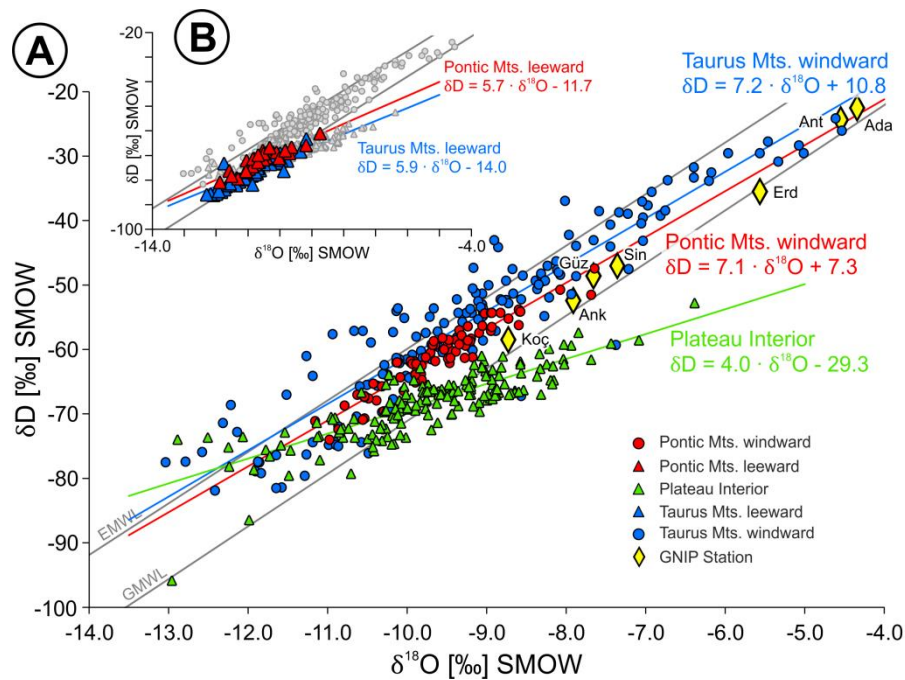


Fig. 2.5 (A) δD versus $\delta^{18}O$ of water samples collected on the plateau margins ($n_{\text{north}} = 73$, $n_{\text{south}} = 154$) and the plateau interior ($n = 172$). The corresponding LMWLs are compared to the long-term values of selected GNIP stations (IAEA/WMO, 2006) as well as to the Global Meteoric Water Line (Rozanski et al., 1993) and the Eastern Mediterranean Water Line (Gat and Carmi, 1970). (B) δD versus $\delta^{18}O$ of water samples collected in the rain shadow areas ($n_{\text{north}} = 36$, $n_{\text{south}} = 47$) with corresponding LMWLs. The remaining part of the dataset – as shown in Fig. 2.5A – is indicated by gray symbols for comparison. Abbreviations of the GNIP stations: Ada – Adana; Ank – Ankara; Ant – Antalya; Erd – Erdemli; Guz – Güzeloluk; Koc – Koçbeyli; Sin – Sinop. See Fig. 2.1 for GNIP station locations, and Tab. 2.1 for GNIP instrumental records.

For precipitation originating in the eastern Mediterranean, values of d have been reported as high as +20 ‰ and above (Gat and Carmi, 1970). This translates to an Eastern Mediterranean Water Line (EMWL) of about $\delta D = 8 \cdot \delta^{18}O + 20$. Analysis of available isotopic data of monthly precipitation (δD_p and $\delta^{18}O_p$) obtained through the Turkey GNIP stations in a period from 2001 to 2003 results in a specific Turkish Meteoric Water Line (TMWL) that follows the equation: $\delta D = 7.7 \cdot \delta^{18}O + 13.1$ (Dirican et al., 2005). The TMWL is in good agreement with the LMWLs of both windward mountain flanks presented here (eqs 1 and 2).

Waters sampled between the windward mountain flanks and the evaporation-dominated plateau interior delineate rain shadow areas that can be described by:

$$\text{Leeward Pontic Mountains LMWL: } \delta D = 5.7 \cdot \delta^{18}O - 11.7 \quad (4)$$

$$\text{Leeward Taurus Mountains LMWL: } \delta D = 5.9 \cdot \delta^{18}O - 14.0 \quad (5)$$

Both regions hence represent slightly more arid environmental conditions as compared to the windward mountain flanks and document that secondary evaporation influences the stable isotopic composition of surface water flows sampled on the lee side of both

mountain ranges. This influence is reflected in the lower slopes of these two LMWLs when compared to the windward side of the mountain ranges (eqs 1 and 2). Evaporation on the leeward sides however plays a minor role relative to the central plateau region. This is manifested by the different slopes of the LMWLs in the plateau interior and the leeward sides (3.9 versus 5.7 and 5.9; eqs 3 to 5).

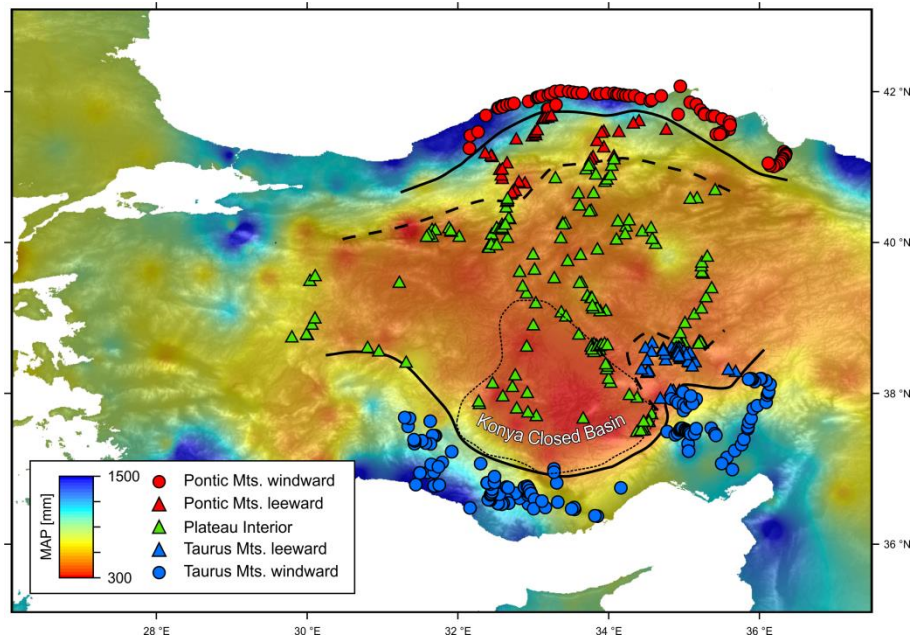


Fig. 2.6 Meteoric water isotopic regimes over Central Anatolia as derived from the analysis of the Meteoric Water Lines, and compared to the distribution of the mean annual precipitation (MAP).

A comparison of the geographical extent of the zones, based on the classification above (Fig. 2.6), shows that while in the north both the windward and the leeward zones are largely parallel to the Pontic Mountain range, in the south only the windward zone runs parallel to the Taurus Mountain range. The leeward zone, based on its LMWL, is developed only in the eastern part of the CAP, immediately leeward of the Taurus Mountain range, whereas in the western part, the Plateau Interior Zone connects directly to the Taurus Mountains. δD and $\delta^{18}O$ values in this area, corresponding to the Konya Closed Basin, define a LMWL of $\delta D = 4.1 \cdot \delta^{18}O - 28.0$, which is in very good agreement with the Plateau Interior LMWL (eq 3). This reflects an evaporative climatic regime for the Konya Closed Basins comparable to the Plateau interior, well in line with its very low MAT and MAP values.

2.3.4 Constraining isotopic lapse rates using Average Catchment Elevations

A cornerstone in paleoaltimetry is a robust characterization of the altitude effect on hydrogen and oxygen isotopes in precipitation (“isotopic lapse rate”). Previous studies

applied various methods to constrain the isotopic lapse rate of orographic precipitation, using thermodynamic approaches (Rowley and Garzione, 2007 with references therein) or empirical estimations based on stable isotopic data of precipitation and surface runoff (e.g., Poage and Chamberlain, 2001; Quade et al., 2007; Hren et al., 2009; Quade et al., 2011). Since stable isotope paleoaltimetry ultimately yields precipitation-weighted hypsometric mean elevations, reflecting the interplay of topography, relief, and rainfall patterns in mountain ranges, we calculate upstream catchment elevations for each sampling point along individual drainages (see Methods section). Calculated average catchment elevations (ACEs) for all 180 surface water samples exceed the sampling elevations by about 510 m on average. The ACEs for the 302 spring waters however are, on average, only 23 m above the corresponding sampling elevations. This is mainly due to the fact that (1) the GIS-based hydrological approach applied here only takes geomorphology into account and that (2) no detailed constraints exist for groundwater flow paths and subsurface hydraulics within the small catchments. Since the δD and $\delta^{18}O$ values of springs are usually lower than those of the nearby surface water flows, the springs likely represent precipitation recharged at elevations higher than suggested by the calculated ACEs (Fig. 2.7). Therefore, the actual catchment areas of the sampled springs should be considerably larger than calculated and, especially in the high-relief areas of the Taurus and Pontic Mountains, their average catchment elevations are also most likely higher than predicted by our model.

Tab. 2.2 Linear correlation coefficients (R^2) between isotopic composition and sampling elevation (SE) as well as average catchment elevation (ACE) for all samples from the windward flanks of the Pontic and Taurus Mountains.

	n		R^2 of δD values				R^2 of $\delta^{18}O$ values			
	springs	surface waters	springs		surface water flows		springs		surface water flows	
			SE	ACE	SE	ACE	SE	ACE	SE	ACE
Pontic Mts., windward	33	40	0.51	0.50	0.03	0.32	0.48	0.47	0.02	0.20
Taurus Mts., windward	61	93	0.58	0.56	0.41	0.74	0.51	0.51	0.36	0.68

In Tab. 2.2 we compare linear correlation coefficients between isotopic compositions and the two different types of elevation information. As expected, the correlation between elevation and isotopic composition of meteoric water significantly increases for streams and creeks if ACEs rather than actual sampling elevations are taken, whereas no improvement is evident for springs. In order to account for the difficulties inherent to integrating spring samples with catchment elevation information, all relevant calculations are based here on ACEs for surface water samples only.

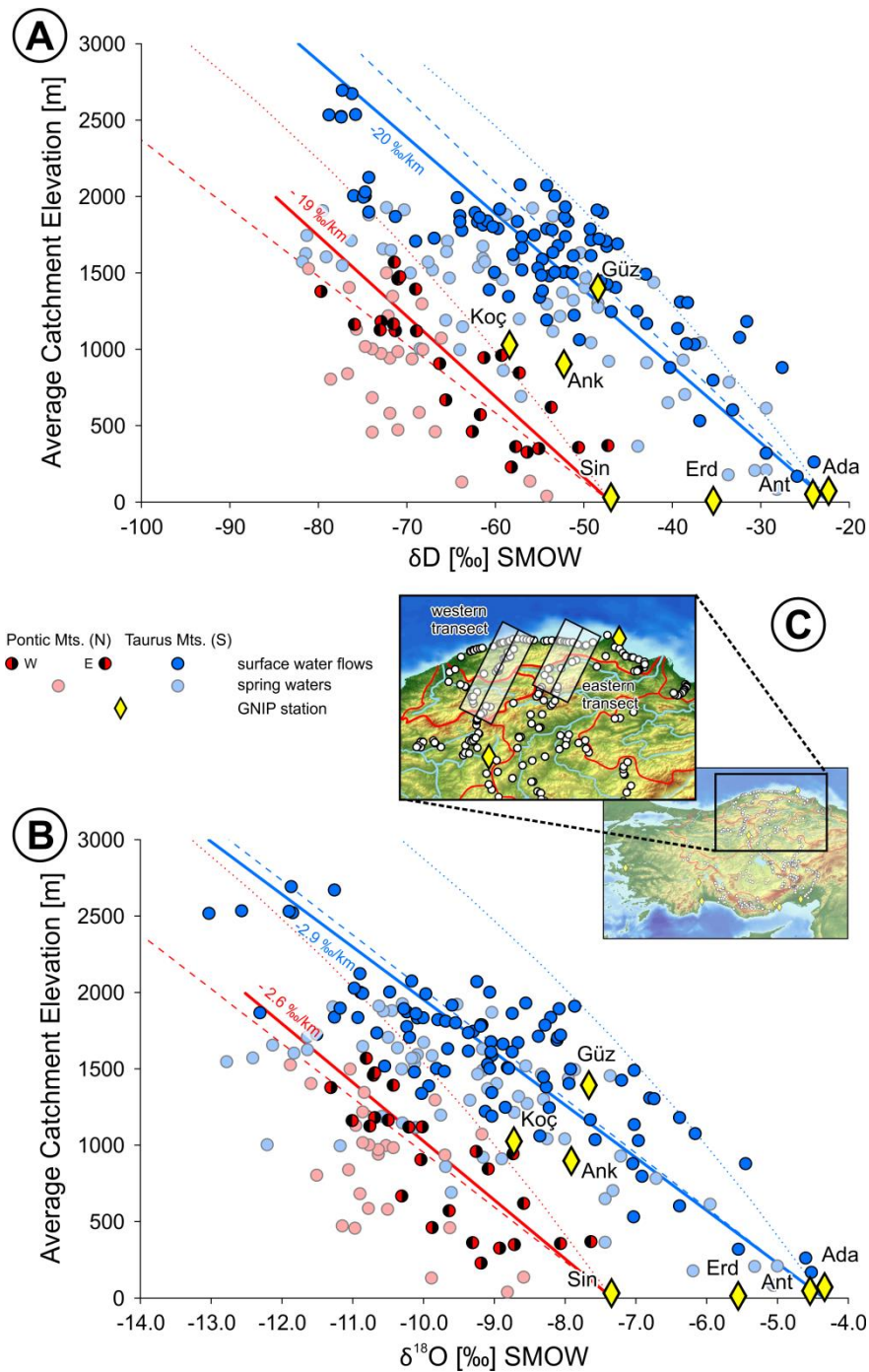


Fig. 2.7 (A) δD and (B) $\delta^{18}O$ versus average catchment elevation of water samples collected on the northern (two individual transects plotted together, $n_{\text{springs}} = 26$, $n_{\text{surface water flows}} = 26$) and southern plateau margins ($n_{\text{springs}} = 61$, $n_{\text{surface water flows}} = 93$). Isotopic lapse rates are based on surface water flows only indicated by solid lines and are compared to the precipitation trends by Poage and Chamberlain (2001 – dashed lines) as well as Currie et al. (2005 – dotted lines). The initial – sea-level – isotopic compositions correspond to long-term average precipitation records from the coastal GNIP stations Sinop (Pontic Mts.) and Adana (Taurus Mts.) (IAEA/WMO, 2006). Abbreviations of the GNIP stations as in Fig. 2.5; see Fig. 2.1 for GNIP station locations, and Tab. 2.1 for GNIP instrumental records.

Figure 2.7 shows the relationship of catchment elevation with isotopic fractionation of hydrogen and oxygen in modern meteoric waters of the Taurus and Pontic Mountains, for an elevation range from sea-level up to approximately 2700 m (Taurus Mountains) and 1400 m (Pontic Mountains). Based on the paucity of samples from surface water

flows in the Pontic Mountains we focused on two transects for the lapse rate calculation (western and eastern transect in Fig. 2.7C; Tab. A2.2 in the Appendix). Isotopic lapse rates of about -20 ‰/km for δD and -2.9 ‰/km for $\delta^{18}O$ in the Taurus Mountains, as well as -19 ‰/km for δD and -2.6 ‰/km for $\delta^{18}O$ in the Pontic Mountains are in good agreement with the global average on the windward side of major mountain belts of -2.8 ‰/km for $\delta^{18}O$ (Poage and Chamberlain, 2001; Lechler and Niemi, 2011). The near-sea level δD and $\delta^{18}O$ values of the Taurus and Pontic precipitation trends are based on the robust, long-term (multi-year to decadal) precipitation record of the GNIP stations at the Black Sea (Sinop) and Mediterranean Sea coasts (Adana) (Tab. 2.1). Forcing a linear regression through these near-sea level values, the elevation-dependent hydrogen and oxygen isotope fractionation is reasonably close to that derived from thermodynamic considerations (Rowley et al. 2001; Currie et al., 2005; Rowley and Garzione 2007) as well as that from empirical datasets in major mountain ranges (Poage and Chamberlain, 2001).

2.4 *Challenges and perspectives for stable isotope paleoaltimetry*

The present-day topography of the CAP is well reflected in the spatial patterns of δD and $\delta^{18}O$ of meteoric waters. Samples collected from the windward flanks of both mountain ranges show the distinct isotopic fingerprint of different air masses and upstream moisture trajectories. First, stable isotope lapse rates calculated from surface runoff are consistent with the present-day global average in larger mountain belts. Second, the spatial distribution of water samples analyzed in this study outlines two regions of isotopic rain shadows in the lee of either mountain range that provide reliable first-order information on upstream depletion in D and ^{18}O due to orographic rainfall (leeward flanks in Fig. 2.6). Both, windward slope isotope-elevation relationships (e.g., Mulch et al., 2006) and temporally transient leeward depletion patterns in D and ^{18}O ("isotopic rain shadow"; e.g., Chamberlain et al., 1999; Poage and Chamberlain, 2002) currently record the impact of present-day topography. Assuming that no major changes in large-scale Northern hemisphere atmospheric circulation patterns have occurred over the (Late) Neogene (at least on tectonic timescales and rates; Micheels et al., 2011) stable isotope paleoaltimetry approaches have a high potential of detecting changing rainout and aridity patterns along the plateau margins and within the rain shadow regions of the plateau interior through time. Under the current climate and hydrologic conditions, however, the strong evaporative enrichment in ^{18}O (and to a lesser degree D) in surface water flows of the central part of the CAP would render stable isotope paleoaltimetry approaches challenging at best.

In addition, the strong evaporative influence on the stable isotopic composition of meteoric waters makes the CAP comparable to other major plateaus on Earth; for example, the Tibetan Plateau (Quade et al., 2011). Both share general topographic (bordered by orographic barriers, relatively uniform plateau elevations) and certain climatological similarities (steep negative precipitation gradient towards the arid plateau interiors, evaporative effect on meteoric water δD and $\delta^{18}O$ values). At present, however, mixing between southeasterly derived summer monsoon air masses and springtime precipitation from westerly marine or continental sources explains some of the observed variation in Tibet (Quade et al., 2011) whereas the influence of air mass mixing on isotopic patterns on the CAP does not appear to play a dominant role. To some degree these differences in meteoric water isotopic patterns on the CAP and Tibet are most likely caused by the difference in the prevailing temperatures and hence, the precipitation-evaporation balance between the two plateau regions, ultimately controlled by plateau elevation. The Tibetan Plateau stands at about 4500 m. whereas the CAP reaches only about 1000 m average elevation, leading to a MAT below 0 °C for the most part of the Tibetan Plateau and to about 9 to 12 °C for the CAP along with a clearly higher difference between MAT and mean summer temperatures. We suggest that the CAP is a prominent example of an initial stage of plateau growth where (semi-)arid conditions prevail that are accompanied by evaporation as the main process shaping the stable isotopic composition of meteoric waters. During later stages of plateau uplift, temperature decrease restricts the influence of evaporative processes on isotopic fractionation, allowing air mass mixing to become increasingly dominant for meteoric δD and $\delta^{18}O$ patterns.

Despite the relatively simple first-order rainfall–topography relationships characteristic for the CAP, in the following we would like to highlight two further observations that have more general implications for stable isotope paleoaltimetry in orogenic plateau regions.

2.4.1 The role of winter recharge for δD and $\delta^{18}O$ of near-surface groundwater

Spring and surface water samples from the central CAP (Ankara) region display a bias towards mean monthly winter precipitation δD and $\delta^{18}O$ values when compared to the rainfall data from the Ankara GNIP station (Fig. 2.8). We interpret this bias to result from the strongly seasonal (winter dominant) rainfall pattern along the CAP margins and within the CAP interior that ultimately results in a positive precipitation-evaporation balance during the cold season and winter-dominated groundwater recharge. A seasonal bias in both rainfall (as well as groundwater recharge) and mineral proxy

formation has implications for oxygen and hydrogen isotope paleoclimate and paleoelevation records.

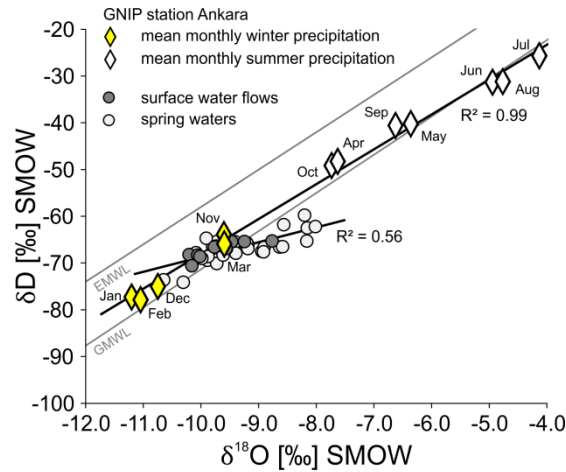


Fig. 2.8 δD versus $\delta^{18}O$ of water samples collected in a 70-km radius around the GNIP station in Ankara (IAEA/WMO, 2006) compared to the mean monthly precipitation recorded at this station. Note that the sample data form an array that best corresponds to the mean winter (December to May) precipitation values.

First, winter dominance of low- δD and low- $\delta^{18}O$ groundwater recharge dampens any potential signal of evaporative conditions in the plateau interior and may mask the onset of continental aridity as typically seen in high-elevation plateau regions. For our present-day CAP, stable isotope record, winter-dominated groundwater recharge (and associated runoff) implies that the observed convex isotope versus distance pattern (between about 300 to 600 km in Figs. 2.3C and D) actually underestimates the amount of evaporative enrichment in D and ^{18}O within the plateau interior. If similar seasonality prevailed during the geologic past, such conditions would bias individual stable isotope paleoaltimetry proxies in different ways: proxies from lacustrine or alluvial environments would record the combined effects of (distal) winter-dominated runoff (negative bias in $\delta^{18}O$) and lake water evaporation (positive bias in $\delta^{18}O$) whereas pedogenic or authigenic minerals that grow in soils actually record local soil water conditions during the time of mineral growth. Pedogenic carbonates as an example are a common stable isotope paleoaltimetry proxy, yet with a strongly seasonal (warm season-dominated) growth pattern (Breecker et al., 2009). We would like to point out that any stable isotope paleoaltimetry reconstruction based solely on records within plateau interiors will be affected by such seasonality effects. For the CAP, we conclude that analysis of $\delta^{18}O$ (and to a lesser degree δD) values of pedogenic proxy minerals within the plateau interior requires consideration of rainfall seasonality including a variably strong bias towards winter precipitation even during warm season growth of the proxy minerals.

2.4.2 Topographically driven subsurface groundwater flow

Topographically driven subsurface groundwater flow characterizes the near surface hydrology in the catchment that feeds the fault-controlled Konya and Tuz Gölü basins (Fig. 2.4 and 2.6; Bayari et al., 2009). Radiocarbon and stable isotope data for modern groundwater indicate that subsurface flow induces “transported” hydrogen and oxygen isotopic signals that blur the real extent of the isotopic rain shadow (Figs. 2.3 and 2.4). The large hydraulic head between the recharge (Taurus Mountains) and discharge (Konya Closed Basin) areas induces a pattern of northward increasing radiocarbon groundwater ages and decreasing $\delta^{18}\text{O}$ values with increasing distance from the high-elevation Taurus range (Bayari et al., 2009). Interestingly, springs near Tuz Gölü that are fed by the deepest aquifers (1) originating at high elevations in the Taurus Mountains and (2) characterized by the oldest radiocarbon ages (and hence the longest subsurface residence and travel times) show d values characteristic for the leeward rain shadow region of the Taurus Mountains and hence a Mediterranean moisture source (Bayari et al., 2009; best seen between about 150 and 400 km in Figs. 2.3C, D and 2.4). We consider it very likely that this subsurface flow pattern has been in place at least since adequate topographic gradients have existed between the southern CAP margin (Taurus Mountains) and the CAP interior (Tuz Gölü) which date back up to about 8 Ma; when deposition of marine sediments onlapping the Taurus basement ceased and surface uplift of the Central Taurus Mountains most likely commenced (Cosentino et al., 2012). Therefore, fault-bounded mineralizations (for example calcite cements, secondary groundwater precipitates and their fluid inclusions) in low-elevation discharge areas of fault-controlled groundwater flow (for example along the NW-trending Tuz Gölü Fault at the E margin of the Tuz Gölü basin) may be potential candidates for paleoclimate (paleo-groundwater composition) and stable isotope paleoaltimetry applications. This may be a general feature of plateau margins where relatively simple topographic and hydraulic gradients characterize range-to-basin groundwater flow in continental plateau interiors and provides additional opportunity for stable isotope paleoclimate/paleoaltimetry reconstructions in places where secondary evaporation of, for example, lake and soil waters renders stable isotope proxy results in lacustrine or pedogenic environments questionable.

2.5 Conclusions

We present the first comprehensive hydrogen (δD) and oxygen ($\delta^{18}\text{O}$) isotope dataset of modern meteoric waters (streams, creeks, and springs in small catchments) from the

Central Anatolian Plateau (CAP) and its orographically accentuated margins with special emphasis on rainfall-topography relationships along the CAP margins. Hydrogen and oxygen isotope analysis of more than 480 stream, creek, and spring water samples allows us to establish a first-order isotopic template for the plateau region which may serve as a reference against which paleoelevation proxy data recovered from, for example, paleosols, fossil teeth, and lipids may be more accurately interpreted and tested. The ability of our data to reliably mirror longer-term, catchment-specific isotopic patterns on an annual to decadal scale, unbiased by sub-annual hydrometeorologically-driven fluctuations, is warranted by a comparison to long-term rainfall data series recorded at the stations of the Global Network of Isotopes in Precipitation (GNIP).

Central Anatolia exhibits a characteristic pattern of orographic rainout, isotopic rain shadow development as well as secondary evaporation, strongly controlled by its modern topographic and climatic setting. We identify "quasi-symmetrical" isotopic lapse rates at the S and N margins of the CAP with -20‰/km (δD) and -2.9‰/km ($\delta^{18}\text{O}$), as well as -19‰/km (δD) and -2.6‰/km ($\delta^{18}\text{O}$), respectively. However, moisture entering the plateau from the S is isotopically distinct from that derived from sources to the N with $\Delta(\delta\text{D}_{\text{N-S}})$ of about 20‰ and $\Delta(\delta^{18}\text{O}_{\text{N-S}})$ of about 3‰ when measured at sea level. The semi-arid plateau interior with a mean precipitation rate as low as 300-500 mm/yr and mean summer temperatures attaining 23°C , undergoes severe sub-cloud and/or surface evaporation as evidenced by systematic enrichment in D and ^{18}O in surface runoff.

The regional δD and $\delta^{18}\text{O}$ patterns of present-day meteoric water as a result of up-slope distillation during orographic rainout and individual low-elevation starting compositions dependent on moisture source and upstream air parcel trajectories can be a powerful tool for reconstructing paleoaltimetry of the CAP despite its moderate size and geographic location relative to dominant air-parcel trajectories. The preservation potential of any paleoprecipitation proxy material on the uplifting margins of the CAP seems moderate, but the windward sides of the plateau margins and the "isotopic rain shadows" on their leeward sides are both prime candidates to retain non-evaporative isotopic signals of past precipitation.

2.6 Acknowledgements

AM acknowledges support through DFG-MU 2845/1-1 and the European Science Foundation Topo Europe initiative. This study was supported through the LOEWE funding program of Hesse's Ministry of Higher Education, Research, and the Arts. The ASTER GDEM data used in this study are a property of the Ministry of Economy, Trade,

and Industry of Japan (METI) and NASA. Details on the implementation of the ACE calculation provided by T. Schildgen (Potsdam) were invaluable. M. Demircan (State Meteorological Service, Ankara) generously provided long-term temperature and precipitation data of Turkey. T. Chavez and S. Terzer (IAEA, Vienna) kindly provided us with the latest GNIP datasets. Thanks are extended to C. Wenske (Hannover) and U. Treffert (Frankfurt) for laboratory support. The paper benefited from thoughtful field discussions with the Topo Europe Vertical Anatolian Movements Project members, as well as from the detailed, very constructive reviews of D. Breecker, A. Lechler, and editorial remarks by C. P. Chamberlain.

2.7 References

- Bayari, C. S., Ozyurt, N. N., and Kilani, S., 2009, Radiocarbon age distribution of groundwater in the Konya Closed Basin, central Anatolia, Turkey: *Hydrogeology Journal*, v. 17, p. 347-365.
- Biryol, B., C., Beck, S. L., Zandt, G., and Özacar, A. A., 2011, Segmented African lithosphere beneath the Anatolian region inferred from teleseismic P-wave tomography: *Geophysical Journal International*, v. 184, p. 1037-1057.
- Blisniuk, P. M., and Stern, L. A., 2005, Stable isotope paleoaltimetry: A critical review: *American Journal of Science*, v. 305, p. 1033-1074.
- Breecker, D. O., Sharp, Z. D., and McFadden, L. D., 2009, Seasonal bias in the formation and stable isotopic composition of pedogenic carbonate in modern soils from central New Mexico, USA: *Geological Society of America Bulletin*, v. 121, p. 630-640.
- Campani, M., Mulch, A., Kempf, O., Schlunegger, F., and Mancktelow, N., 2012, Miocene paleotopography of the Central Alps: *Earth and Planetary Science Letters*, v. 337-338, p. 174-185.
- Cavazza, W., Federici, I., Okay, A. I., and Zattin, M., 2011, Apatite fission-track thermochronology of the Western Pontides (NW Turkey): *International Journal of Earth Sciences* v. 98, p. 1935-1947.
- Chamberlain, C. P., Poage, M. A., Craw, D., and Reynolds, R. C., 1999, Topographic development of the Southern Alps recorded by the isotopic composition of authigenic clay minerals, South Island, New Zealand: *Chemical Geology*, v. 155, p. 297-294.
- Cosentino, D., Schildgen, T. F., Cipollari, P., Faranda, C., Gliozzi, E., Hudáčková, N., Lucifora, S., and Strecker, M. R., 2012, Late Miocene surface uplift of the southern margin of the Central Anatolian Plateau, Central Taurides, Turkey: *Geological Society of America Bulletin*, v. 124, p. 133-145.
- Craig, H., 1961, Isotopic Variations in Meteoric Waters: *Science*, v. 301, p. 1701-1702.
- Craig, H., and Gordon, L. I., 1965, Deuterium and oxygen-18 variations in the ocean and the marine atmosphere, in Tongiorgi, E., editor, *Stable Isotopes in Oceanographic Studies and Paleotemperatures*, Laboratorio de Geologia Nucleare, Pisa, p. 1-122.
- Currie, B. S., Rowley, D. B., and Tabor, N. J., 2005, Middle Miocene paleoaltimetry of southern Tibet – implications for the role of mantle thickening and delamination in the Himalayan orogen: *Geology*, v. 33, p. 181-184.
- Cyr, A., Currie, B. S., and Rowley, D. B., 2005, Geochemical and stable isotope evaluation of Fenghuoshan Group lacustrine carbonates, north-central Tibet – implications for the paleoaltimetry of Late Eocene Tibetan Plateau: *Journal of Geology*, v. 113, p. 517-533.
- Dansgaard, W., 1964, Stable isotopes in precipitation: *Tellus*, v. 16, p. 436-468.
- Dirican, A., Ünal, S., Acar, Y., and Demircan, M., 2005, The temporal and seasonal variation of H-2 and O-18 in atmospheric water vapour and precipitation from Ankara, Turkey in relation to air mass trajectories at Mediterranean Basin, in IAEA-TECDOC-1453, *Isotopic composition of precipitation in the Mediterranean Basin in relation to air circulation patterns and climate*: Vienna, International Atomic Energy Agency, p. 191–215, available online at: <http://www-pub.iaea.org/MTCD/publications/> .
- Ehlers, T. A., and Poulsen, C. J., 2009, Influence of Andean uplift on climate and paleoaltimetry estimates: *Earth and Planetary Science Letters*, v. 281, p. 238-248.

- Galewsky, J., 2009, Orographic precipitation isotopic ratios in stratified atmospheric flows – Implications for paleoelevation studies: *Geology*, v. 37, p. 791-794.
- Gans, C. R., Beck, S. L., Zandt, G., Biryol, C. B., and Özacar, A. A., 2009, Detecting the limit of slab break-off in central Turkey – New high-resolution Pn tomography results: *Geophysical Journal International*, v. 179, p. 1566-1572.
- Garzione, C. N., Dettman, D. L., Quade, J., DeCelles, P. G., and Butler, R.F., 2000a, High times on the Tibetan Plateau: paleoelevation of the Thakkhola graben, Nepal: *Geology*, v. 28, p. 339-342.
- Garzione, C. N., Hoke, G. D., Libarkin, J. C., Withers, S., MacFadden, B. J., Eiler, J., Ghosh, P., and Mulch, A., 2008, Rise of the Andes: *Science*, v. 320, p. 1304-1307.
- Garzione, C. N., Molnar, P., Libarkin, J. C., and MacFadden, B. J., 2006, Rapid late Miocene rise of the Bolivian Altiplano: evidence for removal of mantle lithosphere: *Earth and Planetary Science Letters*, v. 241, p. 543-556.
- Garzione, C. N., Quade, J., DeCelles, P. G., and English, N. B., 2000b, Predicting paleoelevation of Tibet and the Himalaya from $\delta^{18}\text{O}$ vs altitude gradients in meteoric water across the Nepal Himalaya: *Earth and Planetary Science Letters*, v. 183, p. 215-229.
- Gat, J., and Carmi, I., 1970, Evolution of the isotopic composition of atmospheric waters in the Mediterranean Sea area: *Journal of Geophysical Research*, v. 75, p. 3039-3048.
- Gat, J. R., Klein, B., Kushnir, Y., Roether, W., Wernli, H., Yam, R., and Shemesh, A., 2003, Isotope composition of air moisture over the Mediterranean Sea – index of the air–sea interaction pattern: *Tellus*, v. 55B, p. 953-965.
- Görür, N., and Tüysüz, O., 2001, Cretaceous to Miocene palaeogeographic evolution of Turkey: implications for hydrocarbon potential: *Journal of Petroleum Geology*, v. 24, p. 119-146.
- Görür, N., Sakiñç, M., Barka, A., Akkök, R., and Ersoy, Ş., 1995, Miocene to Pliocene palaeogeographic evolution of Turkey and its surroundings: *Journal of Human Evolution*, v. 28, p. 309-324.
- Horton, T. W., Sjostrom, D. J., Abruzzese, M. J., Poage, M. A., Waldbauer, J. R., Hren, M., Wooden, J., and Chamberlain, C. P., 2004, Spatial and temporal variation of Cenozoic surface elevation in the Great Basin and Sierra Nevada: *American Journal of Science*, v. 304, p. 862-888.
- Hren, M. T., Bookhagen, B., Blisniuk, P. M., Booth, A. L., and Chamberlain, C. P., 2009, $\delta^{18}\text{O}$ and δD of streamwaters across the Himalaya and Tibetan Plateau: Implications for moisture sources and paleoelevation reconstructions: *Earth and Planetary Science Letters*, v. 288, p. 20-32.
- IAEA/WMO, 2006, Global Network of Isotopes in Precipitation – The GNIP Database, available online at: <http://www.iaea.org/water>.
- Ingraham, N. L., and Taylor, B. E., 1991, Light stable isotope systematics of large-scale hydrologic regimes in California and Nevada: *Water Resources Research*, v. 27, p. 77-90.
- Insel, N., Poulsen, C., and Ehlers, T., 2009, Influence of the Andes Mountains on South American moisture transport, convection, and precipitation: *Climate Dynamics*, v. 35, p. 1477-1492.
- Lechler, A. R. and N. A. Niemi, 2011, Controls on the spatial variability of modern meteoric $\delta^{18}\text{O}$: empirical constraints from the western US and east Asia and implications for stable isotope studies: *American Journal of Science*, v. 311, p. 664-700.
- Lüttig, G. and Steffens, P., 1975, Paleogeographic Atlas of Turkey from the Oligocene to the Pleistocene: Bundesanstalt für Geowissenschaften und Rohstoffe, Hannover, Germany, 64 p.

- Kendall, C., and Coplen, T., 2001, Distribution of oxygen-18 and deuterium in river waters across the United States: *Hydrological Processes*, v. 15, p. 1363-1393.
- Micheels, A., Bruch, A. A., Eronen, J., Fortelius, M., Harzhauser, M., Utescher, T. and Mosbrugger, V., 2011, Analysis of heat transport mechanisms from a Late Miocene model experiment with a fully-coupled atmosphere-ocean general circulation model: *Palaeogeography, Palaeoclimatology, Palaeoecology*, v. 304, p. 337-350.
- Mix, H. T., Mulch, A., Kent-Corson, M. L., and Chamberlain, C. P., 2011, Cenozoic migration of topography in the North American Cordillera: *Geology*, v. 39, p. 87-90.
- Mulch, A., and Chamberlain, C. P., 2007, Stable isotope paleoaltimetry in orogenic belts – The silicate record in surface and crustal geological archives: *Reviews in Mineralogy and Geochemistry*, v. 66, p. 89-118.
- Mulch, A., Graham, C., and Chamberlain, C. P., 2006, Hydrogen isotopes in Eocene river gravels and paleoelevation of the Sierra Nevada: *Science*, v. 313, p. 87-89.
- Mulch, A., Sarna-Wojcicki, A., Perkins, M., and Chamberlain, C. P., 2008, A Miocene to Pleistocene climate and elevation record of the Sierra Nevada (California): *Proceedings of the National Academy of Sciences of the United States of America*, v. 105, p. 1-6.
- Mulch, A., Uba, C. E., Strecker, M. R., Schoenberg, R., and Chamberlain, C. P., 2010, Late Miocene climate variability and surface elevation in the central Andes: *Earth and Planetary Science Letters*, v. 290, p. 173-182.
- Müller, U. C., Pross, J., Tzedakis, P. C., Gamble, C., Kotthoff, U., Schmiedl, G., Wulf, S., and Christanis, K., 2011, The role of climate in the spread of modern humans into Europe: *Quaternary Science Reviews*, v. 30, p. 273-279.
- Pfahl, S., and Wernli, H., 2008, Air parcel trajectory analysis of stable isotopes in water vapor in the Eastern Mediterranean: *Journal of Geophysical Research*, v. 113, p. 1-6.
- Page, M. A., and Chamberlain, C. P., 2001, Empirical relationships between elevation and the stable isotope composition of precipitation and surface waters – considerations for studies of paleoelevation: *American Journal of Science*, v. 301, p. 1-15.
- Page, M. A., and Chamberlain, C. P., 2002, Stable isotopic evidence for a pre-Middle Miocene rainshadow in the western Basin and Range – implications for the surface uplift of the Sierra Nevada: *Tectonics*, v. 21, p. 1-10.
- Poulsen, C., Ehlers, T., and Insel, N., 2010, Onset of convective rainfall during gradual late Miocene rise of the central Andes: *Science*, v. 328, p. 490-493.
- Quade, J., Breecker, D. O., Daeron, M., and Eiler, J., 2011, The paleoaltimetry of Tibet – an isotopic perspective: *American Journal of Science*, v. 311, p. 77-115.
- Quade, J., Garzzone, C., and Eiler, J., 2007, Paleoelevation reconstruction using pedogenic carbonates: *Reviews in Mineralogy and Geochemistry*, v. 66, p. 53-87.
- Rindsberger, M., Magaritz, M., Carmi, I., and Gilad, D., 1983, The relation between air mass trajectories and the water isotope composition of rain in the Mediterranean Sea area: *Geophysical Research Letters*, v. 10, p. 43-46.
- Rowley, D. B., and Currie, B. S., 2006, Paleo-altimetry of the late Eocene to Miocene Lunpola Basin, central Tibet: *Nature*, v. 439, p. 677-681.

- Rowley, D., and Garzzone, C., 2007, Stable isotope-based paleoaltimetry: *Annual Review of Earth and Planetary Sciences*, v. 35, p. 463-508.
- Rowley, D. B., Pierrehumbert, R. T., and Currie, B. S., 2001, A new approach to stable isotope-based paleoaltimetry: implications for paleoaltimetry and paleohypsometry of the High Himalaya since the Late Miocene: *Earth and Planetary Science Letters*, v. 188, p. 253-268.
- Rozanski, K., Araguás-Araguás, L., and Gonfiantini, R., 1993, Isotopic patterns in modern global precipitation, *in* Swart, P. K., Lohmann, K. C., McKenzie, J., and Savin, S., (Eds.), *Climate Change in Continental Isotopic Records: Geophysical Monograph 78*, p. 1-37.
- Sarış, F., Hannah, D., and Eastwood, W. J., 2010, Spatial variability of precipitation regimes over Turkey: *Hydrological Sciences Journal*, v. 55, p. 234-249.
- Schildgen, T. F., Cosentino, D., Bookhagen, B., Niedermann, S., Yıldırım, C., Echtler, H., Wittmann, H., and Strecker, M. R., 2012a, Multi-phased uplift of the southern margin of the Central Anatolian plateau, Turkey: A record of tectonic and upper mantle processes: *Earth and Planetary Science Letters*, v. 317-318, p. 85-95.
- Schildgen, T. F., Cosentino, D., Caruso, A., Buchwaldt, R., Yıldırım, C., Bowring, S. A., Rojay, B., Echtler, H., and Strecker, M. R., 2012b, Surface expression of eastern Mediterranean slab dynamics: Neogene topographic and structural evolution of the southwest margin of the Central Anatolian Plateau, Turkey: *Tectonics*, v. 31, p. 1-21.
- Şengör, A. M. C., Tüysüz, O., İmren, C., Sakiç, M., Eyidoğan, H., Görür, N., Le Pichon, X. and Rangin, C., 2005, The North Anatolian fault – A new look: *Annual Review of Earth and Planetary Sciences*, v. 33, p. 37-112.
- Sensoy, S., Demircan, M., Ulupinar, Y., and Balta, İ., 2008, *Climate of Turkey: Turkish State Meteorological Service, Ankara*. Retrieved from <http://www.dmi.gov.tr/iklim/iklim.aspx> on April 24, 2009.
- Türkeş, M., 2003, Spatial and temporal variations in precipitation and aridity index series of Turkey *in* Bolle, H.-J., (Ed.), *Mediterranean climate – variability and trends. Regional Climate Studies: Heidelberg, Springer*, p. 181-213.
- Türkeş, M. and Erlat, E., 2005, Climatological responses of winter precipitation in Turkey to variability of the North Atlantic Oscillation during the period 1930-2001: *Theoretical and Applied Climatology*, v. 81, p. 45-69.
- Vachon, R. W., Welker, J. M., White, J. W. C., and Vaughn, B. H., 2010, Moisture source temperatures and precipitation $\delta^{18}\text{O}$ -temperature relationships across the United States: *Water Resources Research*, v. 46, W07523.
- Yıldırım, C., Schildgen, T. F., Echtler, H., Melnick, D., and Strecker, M., 2011, Late Neogene and active orogenic uplift in the Central Pontides associated with the North Anatolian Fault; implications for the northern margin of the Central Anatolian Plateau, Turkey: *Tectonics*, v. 30, p. TC5005.

Chapter 3

Paleohydrological changes in the Eastern Mediterranean region during the early Holocene recorded in plant wax *n*-alkane distributions and $\delta^{13}\text{C}_{\text{TOC}}$ - new data from Tenaghi Philippon, NE Greece

Fabian Schemmel¹, Eva M. Niedermeyer¹, Andreas Koutsodendris², Jörg Pross^{1,2}, Jens Fiebig³, Andreas Mulch^{1,3}

¹ Senckenberg Biodiversity and Climate Research Centre (BiK-F), Frankfurt am Main, Germany

² Paleoenvironmental Dynamics Group, Institute of Earth Sciences, Heidelberg University, Heidelberg, Germany

³ Institute of Geosciences, Goethe University Frankfurt, Frankfurt am Main, Germany

Submitted for publication in Organic Geochemistry

Abstract Holocene climate dynamics have strongly influenced precipitation patterns in the Eastern Mediterranean region. This holds particularly true for the '8.2 kyr B.P. climatic event', arguably the strongest perturbation of early Holocene climate. Here we present a biomarker record of leaf wax-derived *n*-alkane distributions and stable isotopic composition of total organic carbon ($\delta^{13}\text{C}_{\text{TOC}}$) along with palynological data from the fen peat archive of Tenaghi Philippon (TP), NE Greece, for the early Holocene (ca. 8.7 to 7.5 kyr B.P.). Our record documents the response of the local vegetation to changing hydrological conditions in the peatland at Tenaghi Philippon. The long-chain *n*-alkanes *n*-C₂₇, *n*-C₂₉ and *n*-C₃₁, typical for vascular terrestrial plants, dominate the peat sequence. A period of relatively dry surface conditions, indicated by low values of the 'aquatic index' (P_{aq}) and by elevated Average Chain Length (ACL) values, in concert with elevated $\delta^{13}\text{C}_{\text{TOC}}$ values, precedes the 8.2 kyr B.P. climatic event from ca. 8.7 to 8.2 kyr B.P.. Slightly wetter, more humid conditions, as suggested by an increase in P_{aq} values as well as reduced ACL and $\delta^{13}\text{C}_{\text{TOC}}$ values, characterize the interval of the 8.2 kyr B.P. climatic event. Notably, the increase in surface wetness coincides with the reorganization of atmospheric circulation patterns and a shift in precipitation seasonality as documented in previously published stable isotopic and palynological reconstructions from TP. Following the 8.2 kyr B.P. climatic event, a distinct change in paleohydrology at TP becomes apparent from ca. 7.9 kyr B.P. onward. An increase in the abundance of the mid-chain length *n*-alkanes *n*-C₂₃ and *n*-C₂₅, indicative of an increased contribution of aquatic plants to the sediment, together with a steep increase in P_{aq} and a decrease in ACL values as well as variations in $\delta^{13}\text{C}_{\text{TOC}}$, imply considerably elevated surface moisture levels, likely caused by the increased activity of the karstic system of the

surrounding mountains. Collectively, the biomarker proxies presented here reveal a concise picture of changing moisture conditions at TP over the investigated time interval that is consistent with both new and previously published palynological data.

3.1 Introduction

Multiproxy studies of high-resolution terrestrial climate archives are important for understanding past environmental conditions on the continents. Peat accumulations, as one example of such environmental archives, form from (partially) preserved plant remains and provide a comprehensive record of changes in regional climate, biome composition and biomass accumulation through time (e.g., Dise, 2009). A variety of proxies from peatland records such as pollen, plant macrofossils, peat humification and testate amoebae have been studied to infer past climatic change, mainly temperature and precipitation (Chambers et al., 2012 and references therein). Additionally, the investigation of plant-derived leaf wax *n*-alkanes from peat archives is especially promising for paleoclimatic characterizations. Originally formed as part of the plant cuticle, leaf wax *n*-alkanes contribute to the protective properties of the epicuticular wax layer that isolates the leaf tissue from the atmosphere, protecting the leaf from evaporative water loss (Riederer and Schreiber, 2001; Koch and Ensikat, 2008). Lacking functional groups, leaf wax *n*-alkanes can persist in sedimentary archives and are routinely used as biomarkers in paleoenvironmental reconstructions (Eglinton and Eglinton, 2008; Castañeda and Schouten, 2011; Sachse et al., 2012). Typically, terrestrial plants synthesize a characteristic range of long-chain *n*-alkanes with high abundances of *n*-C₂₇, *n*-C₂₉ and *n*-C₃₁ and with a strong predominance of odd-numbered chain lengths over even-numbered chain lengths (Eglinton and Hamilton, 1967). Leaf wax *n*-alkanes accumulate rapidly during leaf flush and distributions and abundances remain largely constant throughout the growing season (Tipple et al., 2013). The distribution of *n*-alkanes in sedimentary archives is strongly controlled by the prevailing vegetation and environmental factors as well as post-depositional alteration during the early stages of diagenesis. While sedimentary *n*-alkane distributions mostly do not discriminate between individual plant species, broad ecosystem changes are well reflected in the *n*-alkane record (Bush and McInerney, 2013). While mid-chain length *n*-alkanes *n*-C₂₃ and *n*-C₂₅ usually maximize in aquatic plants (Ficken et al., 2000), long-chain length compounds *n*-C₂₇, *n*-C₂₉ and *n*-C₃₁ are often characteristic for terrestrial plants (Eglinton and Hamilton, 1967). Thus, the P_{aq} index, the ratio of mid- to long-chain length homologues reflects the relative contribution of aquatic to terrestrial plants to the sediment (Ficken et al., 2000). Further, the distribution of sedimentary *n*-alkanes allows

an estimation of the physiological adaptation of the in-situ vegetation to the prevailing environmental conditions. Variations in the Average Chain Length (ACL) of sedimentary *n*-alkanes have been linked to changes in the evaporative regime with warmer and/or drier environments causing the biosynthesis of longer *n*-alkane chain length and thus higher ACL values (Gagosian et al., 1987; Rommerskirchen et al., 2003; Sachse et al., 2006; Vogts et al., 2012). However, post-depositional alteration may strongly influence *n*-alkane distribution patterns in the geological record, thus potentially obfuscating trends in past vegetation and environmental conditions. The Carbon Preference Index (CPI) is the numerical representation of the odd-over-even predominance of leaf wax *n*-alkanes (Bray and Evans, 1961). While CPI values from modern terrestrial plants show huge fluctuations across different plant groups, sedimentary CPI values approach unity with increasing maturity and thus provide a measure for the degree of alteration of sedimentary *n*-alkanes and their fidelity to the source material (e.g., Bush and McInerney, 2013).

Changes in predominant vegetation as well as evaporative regime at a given site are also reflected in the stable isotopic composition of total organic carbon ($\delta^{13}\text{C}_{\text{TOC}}$). While ultimately being controlled by the $\delta^{13}\text{CO}_2$ value of the ambient atmosphere, the main photosynthetic pathways utilized by the in-situ vegetation strongly affect $\delta^{13}\text{C}_{\text{TOC}}$ (O'Leary, 1988). Differences in the isotopic discrimination between the C_3 and the C_4 photosynthetic pathways lead to characteristic isotopic values of C_3 and C_4 plants, with C_3 plants showing significantly lower $\delta^{13}\text{C}$ values than C_4 plants. Additionally, vascular terrestrial plants can adapt to increasing aridity by closing the leaf stomata to counteract water loss (e.g., Marshall et al., 2008), which results in ^{13}C enrichment of photosynthetic products (Farquhar et al., 1989).

The high abundance of organic material in peat facilitates the analysis of plant-derived, leaf wax *n*-alkane distribution as well as stable isotopic records of total organic carbon and thus provides important information on changes in past peat bog environments (Zhou et al., 2005, 2010; Nichols et al., 2006; Zheng et al., 2007; Li et al., 2013).

The Philippi peatland in NE Greece is the thickest known peat deposit in the world (Christanis, 1983; Pross et al., 2015). Its intermediate location in the Eastern Mediterranean region between the climate systems of the high and low latitudes makes the area particularly sensitive to rapid climate change (e.g., Lionello et al., 2012). Arguably the strongest perturbation of Holocene climate occurred during the 8.2 kyr B.P. climatic event (see reviews by Alley and Ágústsdóttir, 2005; Rohling and Pälike, 2005). Generally linked to the drainage of ice-dammed Laurentide meltwater lakes and the subsequent reduction of Atlantic Meridional Overturning Circulation (Barber et al., 1999;

Renssen et al., 2001), this event strongly affected climate dynamics in the Eastern Mediterranean region (e.g., Bar-Matthews et al., 1997; Kotthoff et al., 2008a; Pross et al., 2009), causing major paleoceanographic variations in the Aegean Sea (Rohling et al., 2002). The dominating influence of the lower-latitude, monsoonally-controlled climate systems was disrupted by a period of pronounced impact of the Siberian High on the region, eventually leading to the interruption of the formation of Sapropel S1 in the Aegean Sea (Kotthoff et al., 2008a; Rohling et al., 2015). Stable isotope geochemical and palynological reconstructions from the Philippi peatland indicate changes in air mass trajectories as well as a decline in winter temperature and a shift in precipitation seasonality in relation with the 8.2 kyr B.P. climatic event (Pross et al., 2009; Peyron et al., 2011; Schemmel et al., 2016).

Here, we present an organic multiproxy record from a core from Tenaghi Philippon (TP). Our aim is to reconstruct the impact of rapid climate change during the 8.2 kyr. B.P. climatic event on the paleohydrological conditions at TP. We document changes in leaf wax *n*-alkane distributions (P_{aq} , ACL, CPI) as well as in the stable carbon isotopic composition of total organic carbon from the peat deposit and interpret these proxy records in relation to environmental and ecological changes during the 8.2 kyr B.P. climatic event. We show that changes in *n*-alkane distribution and $\delta^{13}C_{TOC}$ over time strongly reflect variations in peat surface moisture conditions, ultimately controlled by the prevailing precipitation regime.

3.2 *Material and methods*

3.2.1 Study site

The TP site is located in the Philippi peatland in the Drama Basin, NE Greece (Fig. 3.1, e.g., Pross et al., 2015). The low-elevation, intramontane Drama Basin formed by Neogene extensional tectonics, with basin subsidence leading to the formation of a topogenic fen, supplied by surface and groundwater. The aquifer is mainly fed by mineral-rich waters derived from the karstic system of the Pangeon and Lekanis mountains on the SW and E edge of the basin as well as by surface runoff from the Phalakron mountain range to the N of the basin (Christanis, 1983; Kalaitzidis and Christanis, 2002). The Philippi peatland has been characterized by telmatic and limnic conditions since the mid-Pleistocene until being drained artificially in the 1930s and 1940s (Christanis, 1983; Pross et al., 2015). The sediments of the Philippi peatland mainly consist of fen peat and lignite along with marls and calcareous clays (Christanis, 1983; Pross et al., 2015 and references therein). The analyzed core (TP-2005, 40°

58.40' N, 24° 13.42' E, 40 m.a.s.l.) spans ca. 312 kyr (Fletcher et al., 2013) and comprises the upper 60 m of the TP archive (Pross et al., 2007). Sediments of the interval presented here (472–536 cm core depth) are composed almost entirely of peat with very little contribution of fine-grained, clastic material.

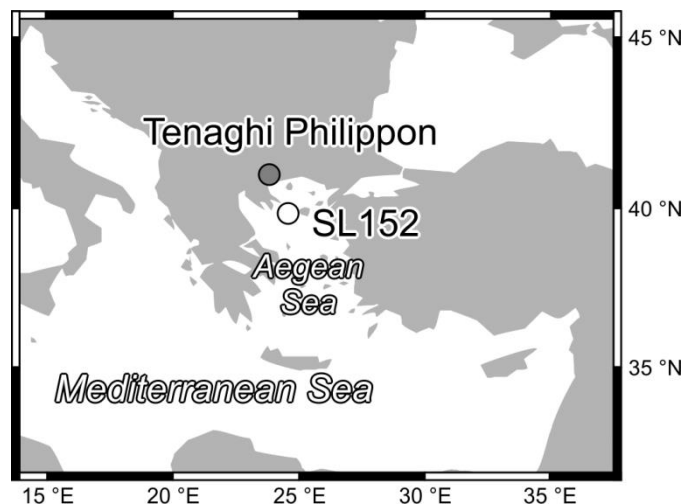


Fig. 3.1 Locations of Tenaghi Philippon and marine core SL152 in the northeastern Mediterranean region.

Palynological correlation with the well-dated marine core SL152 from the northern Aegean Sea (Fig. 3.1; Kotthoff et al., 2008a, b; Kotthoff et al., 2011) serves as primary age control for the Holocene section of the TP-2005 core and has further been confirmed by radiocarbon dates and palynostratigraphical information (Pross et al., 2009). The application of the age model of Pross et al. (2009) for the present study allows direct correlation between our new geochemical data with previously published palynological (Pross et al., 2009; Peyron et al., 2011) and stable isotopic data (Schemmel et al., 2016) from the same core interval. We analyzed 35 peat samples from the core interval between 472 cm and 536 cm, corresponding to the time interval from ca. 8.7 to 7.5 kyr B.P., thus attaining a temporal resolution of ca. 15 to ca. 50 years (Tab. 3.1).

The present-day climate of the Aegean region is characterized by strong precipitation seasonality (Lionello et al., 2012). During the typically mild winters, but also well into spring and fall, eastward-moving cyclones produce high amounts of rainfall in western Greece and over the eastern Aegean Sea, with associated rain shadows over eastern Greece and the central Aegean Sea (Dotsika et al., 2010). Pronounced anticyclonic activity over the entire Eastern Mediterranean region strongly limits summer rainfall, causing widespread dry conditions during the generally hot summers. Local convective storms can cause pronounced individual precipitation events during the summer months

either through thermal instability or by North African depressions reaching the Aegean region from the southwest (Argiriou and Lykoudis, 2006; Dotsika et al., 2010).

3.2.2 Lipid extraction, purification, and quantification

Lipids were extracted from freeze-dried and finely ground sediment samples (ca. 1 g dry weight) with a Büchi Speed Extractor at 100 °C and 100 bar using 20 ml of a mixture of dichloromethane/methanol (9:1) for 10 min, which was repeated 3 times. Total lipid extracts (TLE) were dried under a stream of N₂ at 36 °C and saponified with 1M NaOH at 80 °C for 3 h. Neutral lipids were extracted with hexane and separated by silica-gel column chromatography to neutral (hexane), semi-polar (dichloromethane/hexane 2:1) and polar fractions (methanol). The neutral fraction was subsequently separated by AgNO₃-coated silica using hexane as eluent to obtain saturated hydrocarbons containing the *n*-alkanes.

3.2.3 *n*-alkane concentration

n-alkanes were analyzed by gas chromatography/mass spectrometry (GC/MS) using a Thermo Finnigan Trace GC equipped with a HP-5MS column (30 m x 0.25 mm x 0.25 µm) connected to a Thermo Finnigan DSQ II mass spectrometer at the Institute of Geosciences, Goethe University Frankfurt. The GC oven was held at 70 °C for 1 min, ramped at 10 °C/min to a final temperature of 320 °C, which was held for 15 min. *n*-alkanes were identified by comparison of their mass spectra and retention time to an external standard containing C₇ to C₄₀ *n*-alkanes (Supelco) at a concentration of 25 ng/µl, and were quantified using TIC peak areas calibrated against the external standard. Precision of the quantification is 96% as inferred from the standard deviation of repeated standard runs (n = 5).

3.2.4 Stable carbon isotope ($\delta^{13}\text{C}_{\text{TOC}}$) measurements

Carbon isotope analyses on bulk organics were performed at the Goethe University/BiK-F Joint Stable Isotope Facility Frankfurt. To ensure the removal of inorganic carbon, samples were washed with 10 % HCl at 40 °C for 24 hours before being centrifuged four times at 2800 to 3000 rpm for 4 to 8 minutes and dried for 24 hours at 40 °C. Typically, pre-treatment resulted in <1 % mass loss. The residual bulk organic carbon in the peat fraction was then oxidized to CO₂ using a Flash EA 1112 (Thermo Finnigan) (e.g., van

de Schootbrugge et al., 2008). The isotopic composition of the evolved CO₂ was analyzed using a MAT 253 gas source mass spectrometer (Thermo Finnigan). USGS 24 and IAEA-CH-7 were analyzed along with the samples to check for accuracy. Replicate analyses of reference materials and samples revealed that analytical precision was better than ± 0.2 ‰.

3.2.5 Palynology

The preparation for palynological analysis followed standard procedures, including sediment freeze-drying, weighting, treatment with HCl (10 %), NaOH (10 %), HF (40 %), heavy-liquid separation with Na₂WO₄ × 2 H₂O, acetolysis and slide preparation with glycerin jelly. Palynological slides were analyzed at 400x magnification. Pollen percentages for arboreal and non-arboreal taxa were calculated excluding Poaceae, Cyperaceae and aquatic pollen as well as fern spores and algae. Percentages of Cyperaceae, Poaceae, aquatics, spores and algae were calculated relative to the sum of arboreal and non-arboreal pollen.

3.3 Results and discussion

3.3.1 *n*-alkane distribution and CPI

Chain lengths of sedimentary *n*-alkanes from TP range from *n*-C₁₆ to *n*-C₃₃ with a distinct odd-over-even predominance (Tab. 3.1; Fig. 3.2a). Most samples are dominated by the long-chain compounds *n*-C₂₇, *n*-C₂₉ and *n*-C₃₁, with minor contributions from mid-chain compounds *n*-C₂₃ and *n*-C₂₅. Shorter chain lengths (<23) are virtually absent in most samples (Tab. 3.1; Fig. 3.2a). The distribution of *n*-alkanes with maxima in the long-chain compounds is typical for contributions from the epicuticular waxes of vascular terrestrial plants to the sediment (Fig. 3.2a; Eglinton and Hamilton, 1967; Eglinton and Eglinton, 2008). The upper part of the sampled core section is marked by increasing concentrations of mid-chain compounds, usually ascribed to the contribution of aquatic plants (Ficken et al., 2000; Mügler et al., 2008). These characteristic *n*-alkane distribution patterns suggest that the prevalent vegetation cover at TP during the investigated time interval from ca. 8.7 to 7.5 kyr B.P. mainly consisted of vascular terrestrial plants. This interpretation is in agreement with previously published palynological investigations, concluding the *in-situ* vegetation consisted mainly of

Tab. 3.1 *n*-alkane concentration, *n*-alkane distributions and $\delta^{13}\text{C}_{\text{TOC}}$ values of the studied interval of core TP-2005.

Core depth [cm]	Age [kyr B.P.]	<i>n</i> -alkane concentrations [$\mu\text{g/g}$ dry sample]																												$\delta^{13}\text{C}_{\text{TOC}}$ [% PDB]
		C ₁₆	C ₁₇	C ₁₈	C ₁₉	C ₂₀	C ₂₁	C ₂₂	C ₂₃	C ₂₄	C ₂₅	C ₂₆	C ₂₇	C ₂₈	C ₂₉	C ₃₀	C ₃₁	C ₃₂	C ₃₃	ACL	CPI	P _{aq}								
472	7.54	0.2	0.7	1.0	2.1	1.4	1.9	1.5	17.0	4.0	21.9	2.6	28.8	1.7	26.6	1.1	14.7	0.0	2.7	27.0	10.3	0.48								
475	7.60	0.3	0.9	1.2	2.6	1.7	2.1	1.4	17.0	2.6	17.9	1.4	20.2	0.9	15.6	1.2	8.0	0.0	1.5	26.5	10.9	0.60								
478	7.67	0.4	1.1	1.3	3.8	1.9	2.5	1.8	19.7	4.3	22.2	3.5	30.1	3.2	32.6	2.1	20.4	0.0	4.1	27.2	8.7	0.44								
481	7.73	0.4	1.1	1.4	4.3	2.3	3.6	2.7	16.6	4.2	18.5	2.6	26.5	2.0	30.0	1.4	18.0	0.0	3.3	27.3	8.9	0.42								
484	7.78	0.5	1.2	1.6	4.0	2.2	2.5	1.7	10.6	4.6	14.8	3.4	26.9	2.8	34.7	1.7	21.9	0.0	4.7	27.8	8.2	0.31								
487	7.85	0.3	0.6	0.8	1.6	1.4	1.7	1.6	5.5	3.5	7.7	2.0	16.1	1.4	23.4	0.7	13.6	0.0	1.9	28.0	7.4	0.26								
490	7.90	0.4	0.9	1.1	1.6	1.5	1.4	1.2	5.5	3.0	7.1	1.7	12.0	1.1	16.6	0.6	10.2	0.0	1.6	27.7	7.0	0.32								
491	7.92	0.3	0.8	1.2	1.6	1.6	1.5	1.3	4.4	2.7	6.2	1.6	12.6	1.1	18.4	0.6	10.3	0.0	1.5	27.9	7.4	0.27								
492	7.94	0.3	0.8	1.0	1.3	1.3	1.3	1.1	3.1	2.3	4.9	1.4	11.7	1.1	17.6	0.6	10.6	0.0	1.7	28.2	7.7	0.22								
493	7.95	0.3	0.6	0.8	1.1	1.1	0.9	0.8	1.5	1.2	2.8	0.8	7.6	0.9	12.7	0.6	7.6	0.0	1.4	28.4	7.8	0.17								
494	7.97	0.4	1.1	1.4	1.5	1.5	1.1	1.2	2.1	3.2	6.1	2.0	17.1	1.4	26.2	0.8	13.5	0.0	2.2	28.3	7.9	0.17								
495	7.99	0.3	0.7	1.0	1.5	1.3	1.5	2.0	2.7	5.9	7.2	3.0	15.2	1.4	21.2	0.7	11.1	0.0	2.3	28.1	4.6	0.23								
496	8.00	0.3	0.7	0.9	1.3	1.1	1.1	1.4	2.7	4.4	5.1	2.5	10.3	1.8	15.4	1.1	10.0	0.0	2.7	28.1	4.2	0.23								
497	8.02	0.4	1.0	1.5	2.6	1.6	1.5	1.4	2.0	4.4	3.0	1.5	4.3	0.4	5.3	0.3	5.1	0.0	1.4	27.9	2.7	0.32								
498	8.04	0.4	1.1	1.4	2.5	1.4	1.4	1.1	2.1	3.8	3.4	1.1	3.9	0.4	4.3	0.4	3.3	0.0	1.3	27.4	2.8	0.42								
499	8.06	0.3	0.9	1.0	1.9	1.1	0.9	1.1	2.6	3.6	3.5	1.5	6.1	1.1	8.0	0.8	6.1	0.0	2.0	27.9	3.6	0.30								
500	8.07	0.3	0.9	0.9	1.6	1.0	1.0	1.1	3.0	3.4	3.9	1.8	6.5	1.4	8.8	1.3	7.0	0.0	2.2	27.9	3.5	0.30								
501	8.09	0.4	0.8	1.0	1.6	1.1	1.1	0.9	5.4	2.8	8.5	2.3	17.1	2.1	23.2	1.3	15.1	0.0	2.5	28.0	7.6	0.27								
502	8.11	0.4	0.9	1.1	2.1	1.7	1.6	1.2	7.8	3.0	11.7	2.7	19.1	2.2	23.1	1.4	13.4	0.0	2.9	27.6	7.5	0.35								
503	8.12	0.5	1.0	1.3	2.0	1.5	1.4	1.1	5.8	2.8	9.1	2.3	16.7	1.9	21.8	1.2	13.0	0.0	2.2	27.8	7.5	0.30								
504	8.14	0.4	0.8	0.9	1.7	1.2	1.3	1.1	5.5	3.2	9.3	2.6	16.8	2.3	23.0	1.3	15.3	0.0	2.8	28.0	7.0	0.28								
505	8.16	0.4	0.7	1.0	1.5	1.2	1.1	1.0	3.8	3.2	7.1	2.5	15.3	2.0	21.7	1.2	14.3	0.0	3.1	28.1	6.7	0.23								
506	8.17	0.3	0.6	0.8	1.5	1.2	1.5	1.2	5.0	3.2	8.6	2.8	17.6	2.3	24.0	1.2	15.6	0.0	2.8	28.0	7.0	0.26								
507	8.19	0.4	0.7	0.9	1.6	1.1	1.1	0.8	5.0	3.0	8.9	2.7	17.3	2.3	24.0	1.4	14.3	0.0	2.5	28.0	7.1	0.27								
508	8.20	0.5	1.0	1.1	1.8	1.9	2.3	1.8	4.5	3.2	7.6	2.5	15.4	2.0	21.6	1.4	12.2	0.0	2.2	28.0	5.9	0.26								
509	8.22	0.3	0.6	0.8	1.2	1.1	1.0	0.9	3.3	2.9	6.5	2.3	13.7	1.7	20.2	1.1	12.5	0.0	2.2	28.1	6.6	0.23								
512	8.27	0.3	0.6	0.8	1.2	1.0	1.0	0.8	3.0	2.4	5.4	1.8	11.9	1.3	18.3	0.9	10.9	0.0	2.3	28.2	7.3	0.22								
515	8.32	0.1	0.4	0.7	1.1	1.0	0.9	0.9	2.7	2.5	4.8	1.7	11.1	1.3	17.0	0.7	10.3	0.0	1.9	28.2	6.9	0.21								
518	8.37	0.3	0.6	0.8	1.2	1.4	1.1	0.9	2.4	2.2	4.4	1.4	10.6	1.2	16.8	0.6	9.9	0.0	1.5	28.2	7.4	0.20								
521	8.42	0.1	0.2	0.5	0.9	0.7	0.7	0.7	1.6	1.5	2.9	0.8	7.2	0.6	12.2	0.6	7.3	0.0	1.5	28.3	7.8	0.19								
524	8.46	0.1	0.5	0.8	1.2	0.9	0.7	0.5	2.0	1.1	2.5	0.7	6.1	0.6	9.8	0.4	5.9	0.0	1.3	28.1	8.4	0.22								
527	8.51	0.1	0.3	0.6	0.9	0.9	0.8	0.9	2.3	1.9	3.8	1.1	8.4	1.0	13.4	0.5	8.2	0.0	1.2	28.2	7.1	0.22								
530	8.56	0.3	0.5	0.7	0.9	0.7	0.7	0.6	1.7	1.0	2.5	0.7	6.2	0.8	9.9	0.5	6.5	0.0	1.3	28.3	7.8	0.20								
533	8.61	0.1	0.4	0.7	1.1	0.9	0.7	0.7	2.1	2.0	3.8	1.2	9.6	1.1	14.9	0.7	9.2	0.0	1.8	28.3	7.4	0.20								
536	8.66	0.1	0.4	0.8	1.0	0.9	0.7	0.9	2.0	2.0	4.0	1.4	9.7	1.6	13.8	1.2	8.1	0.0	1.9	28.2	5.6	0.22								

Cyperaceae and Poaceae (Christanis, 1983). However, the increase in n -C₂₃ and n -C₂₅ after ca. 7.8 kyr B.P. (487 cm core depth) may indicate the expansion of aquatic plants at the site. A notable exception from the characteristic n -alkane distribution pattern of TP occurs between ca. 8.1 and 8.0 kyr B.P. (500 to 495 cm core depth). A drop in absolute n -alkane concentrations coincides with a decrease in abundances of the long-chain compounds n -C₂₇, n -C₂₉ and n -C₃₁ (Tab. 3.1; Fig. 3.2a: 498 cm core depth). This interval of changing n -alkane patterns is also evident in a notable decrease in CPI values (Fig. 3.2b; Schemmel et al., 2016). CPI values represent the relative proportions of odd-numbered and even-numbered n -alkane chain lengths, with

$$\text{CPI} = [\sum_{\text{odd}}(n\text{-C}_{21-33}) + \sum_{\text{odd}}(n\text{-C}_{23-35})] / 2\sum_{\text{even}}(n\text{-C}_{22-34})$$

thus providing an estimate of the influence of diagenesis and other postdepositional alteration (e.g., Bush and McInerney, 2013). In biological and geological samples, CPI values >1 reflect predominance of odd over even chain lengths (Bray and Evans, 1961). High CPI values (CPI >> 1) generally indicate epicuticular leaf waxes of vascular terrestrial plants as sources (Bray and Evans, 1961; Eglinton and Hamilton, 1967). CPI values for most TP samples range between 5.6 and 10.9 and generally increase with decreasing depth.

CPI values between ca. 8.1 and 8.0 kyr B.P. (500 to 495 cm) reach a mean value of 3.6 (Fig. 3.2b). The pronounced decrease in odd-over-even predominance between ca. 8.1 and 8.0 kyr B.P. is likely a reflection of changes in the in-situ vegetation at TP. Modern vascular plants display a wide range of CPI values (Bush and McInerney, 2013). Changes in environmental conditions during the 8.2 kyr B.P. climatic event may have triggered a decrease in vegetation cover respectively a change in in-situ vegetation towards species synthesizing lower amounts of odd-numbered n -alkanes deposited in the sediment. Alternatively, decreasing CPI values in peat environments have previously been linked to changes in microbial degradation of organic material, related to the depth of the water table (Kuder and Kunge, 1998; Xie et al., 2004; Zhou et al., 2005, 2010). However, the decrease in CPI between ca. 8.1 and 8.0 kyr B.P. is not caused by an increase in the contribution of even numbered n -alkanes to the sediment (Fig. 3.2a; Tab. 3.1). It is rather the result of a decrease in the abundances of the long-chain n -alkanes n -C₂₇, n -C₂₉ and n -C₃₁, suggesting changes in primary production. Thus, we interpret the CPI record of TP to primarily reflect changes in vegetation at the site in relation to variations in environmental conditions during the 8.2 kyr B.P. climatic event and to have only secondarily resulted from degradation during the early stages of diagenesis.

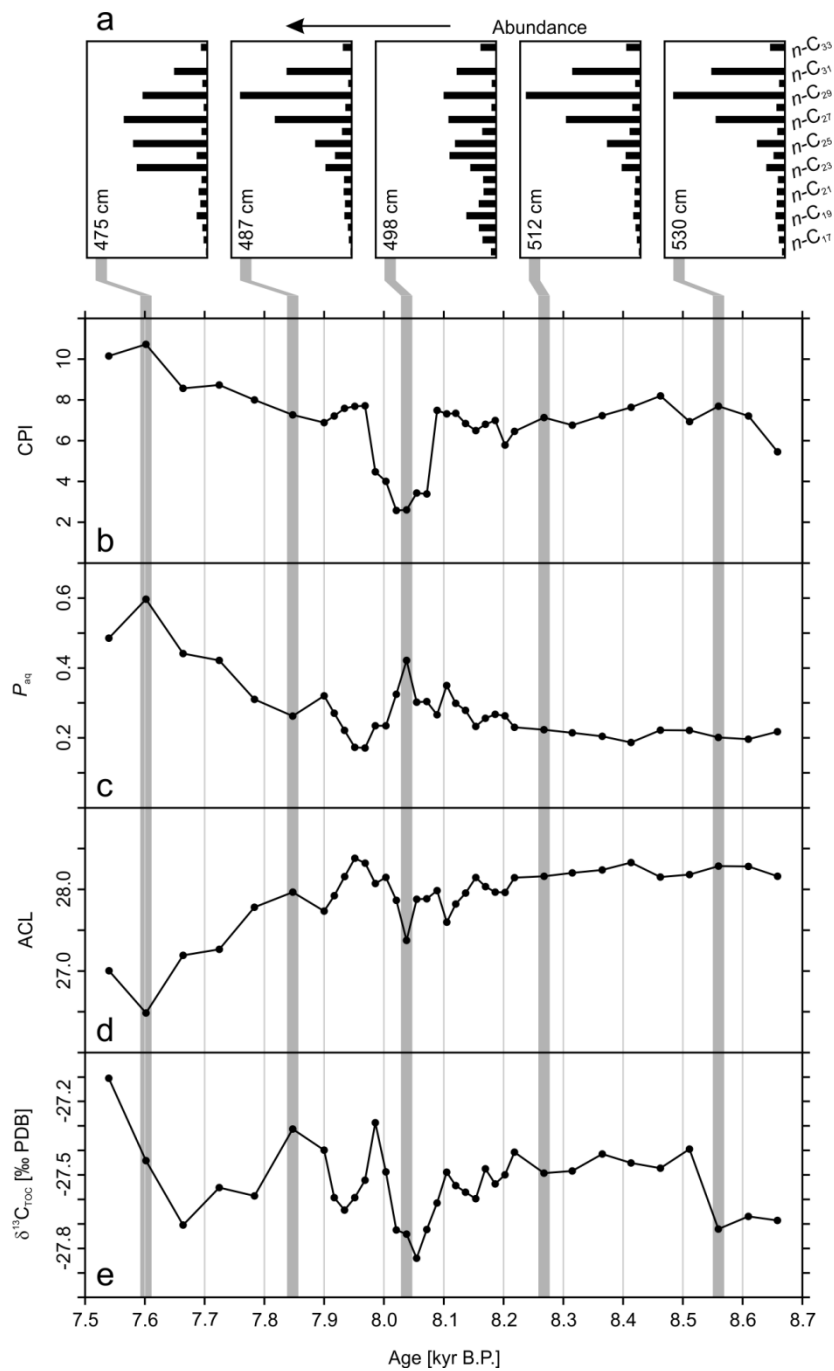


Fig. 3.2 *n*-alkane distributions and stable carbon isotopic composition of total organic carbon of the studied section of core TP-2005. a. *n*-alkane relative abundance from five selected sediment samples. Gray bars indicate the corresponding ages in the peat sequence. b. CPI values. c. *P*_{aq} values. d. ACL values. e. $\delta^{13}\text{C}_{\text{TOC}}$ values.

3.3.2 P_{aq} index

The P_{aq} index is a relative measure of *n*-alkanes deriving from submerged and floating aquatic macrophytes versus emergent and terrestrial plants in lacustrine sediments (Ficken et al., 2000) and is defined as

$$P_{aq} = (n-C_{23} + n-C_{25}) / (n-C_{23} + n-C_{25} + n-C_{29} + n-C_{31}).$$

For the telmatic peat deposits from TP, we apply the P_{aq} index accordingly as a proxy for the contribution of vascular terrestrial plants versus aquatic plants, utilizing the characteristic differences in *n*-alkane distribution between the two plant types. Thus, we gain a measure for changes in surface moisture conditions at TP, specifically the depth of the water table (Nichols et al., 2006; Zheng et al., 2007; Yamamoto et al., 2010; Zhou et al., 2010). The P_{aq} values of TP show a broad increase during the investigated time interval from ca. 0.2 in the lower section to ca. 0.6 near 7.6 kyr B.P. (Fig. 3.2c; 475 cm core depth). The lower section of the core before ca. 8.2 kyr B.P. (505 cm core depth) is characterized by relatively stable P_{aq} values of around 0.2 to 0.3, suggesting a relatively low water table and the prevalence of vascular terrestrial plants at TP. The interval between ca. 8.2 and 8.0 kyr B.P. (505 to 493 cm core depth) shows an increase to the relative maximum of ca. 0.4 at ca. 8.05 kyr B.P. (498 cm core depth) that may be indicative of wetter conditions at the site. P_{aq} values increase almost uniformly in the upper core section until the maximum of ca. 0.6 around ca. 7.6 kyr B.P. (475 cm core depth). This strong increase in P_{aq} implies an expansion of aquatic plants at TP, suggesting a pronounced shift in surface moisture conditions.

3.3.3 ACL values

The ACL value is the weighted average chain length of the odd-numbered 23 to 31 *n*-alkanes in sedimentary samples, where

$$ACL = [(23 \cdot n-C_{23}) + (25 \cdot n-C_{25}) + (27 \cdot n-C_{27}) + (29 \cdot n-C_{29}) + (31 \cdot n-C_{31})] / \sum_{\text{odd}}(n-C_{23-31}).$$

ACL values in sedimentary sequences hold paleoclimatic significance because vascular terrestrial plants may develop longer chain wax lipids in warmer climates to avoid water loss due to increased evaporation (Gagosian et al., 1987). In peat sequences, ACL values have been linked to prevailing moisture conditions, with higher ACL values occurring under warmer and drier, more evaporative conditions and vice versa (Zhou et al., 2005, 2010; Yamamoto et al., 2010, Huang et al., 2014). The ACL values from TP range between 26.5 and 28.4 and show a decreasing trend with decreasing core depth

(Fig. 3.2d). The lower part of the core until ca. 8.2 kyr B.P. (505 cm core depth) shows high and stable ACL values around ca. 28.1. ACL values are somewhat lower during the interval between ca. 8.2 and 8.0 kyr B.P. (505 to 493 cm core depth), culminating in a relative minimum of 27.4 at ca. 8.05 kyr B.P. (498 cm core depth). The upper section of the core from ca. 8.0 kyr B.P. (493 cm core depth) is characterized by successively decreasing values, reaching the minimum of 26.5 at ca. 7.6 kyr B.P. (475 cm core depth). A tripartition comparable to that apparent in the P_{aq} index is evident, albeit of the opposite sign. Similar to the low P_{aq} values, high ACL values in the lower part of the core imply prevailing dry conditions at the site. The fluctuations between ca. 8.2 and 8.0 kyr B.P. suggest a minor increase in available moisture before moisture levels increase significantly in the upper part of the core after ca. 7.8 kyr B.P.

3.3.4 $\delta^{13}C_{TOC}$ values

The $\delta^{13}C$ values of plant material are influenced by multiple ecological and environmental factors including but not limited to photosynthetic pathway, stomatal conductance and atmospheric $\delta^{13}CO_2$ (O'Leary, 1988; Farquhar et al., 1989; Marshall et al., 2008). With $\delta^{13}C_{TOC}$ values from TP ranging from ca. -27.1 to -27.8 ‰ (average of -27.5 ‰), the vegetation at the site predominantly uses the C_3 photosynthetic pathway over the investigated time interval (O'Leary, 1988). However minor fluctuations in the $\delta^{13}C_{TOC}$ record of 0.7 ‰ become apparent (Fig. 3.2e). Given the full range of $\delta^{13}C$ variability between different plant functional types (O'Leary, 1988), together with an analytical error of 0.2 ‰ an overall variation of 0.7 ‰ is at the level of significance. Yet, as the temporal pattern of $\delta^{13}C_{TOC}$ variability resembles that of changes in P_{aq} , ACL and CPI, it requires further attention. The lower part of the core (527 to 509 cm core depth) is characterized by relatively high and stable $\delta^{13}C_{TOC}$ values around ca. -27.4 ‰ up until ca. 8.2 kyr B.P. (509 cm core depth). Between ca. 8.2 and 8.0 kyr B.P. (509 to 495 cm core depth), $\delta^{13}C_{TOC}$ values successively decrease, attaining the minimum of -27.8 ‰ at ca. 8.05 kyr B.P. (499 cm core depth). The upper part of the core from ca. 8.0 kyr B.P. (495 cm core depth) onward shows fluctuating $\delta^{13}C_{TOC}$ values around -27.5 ‰ with an interval of ^{13}C depletion around ca. 7.65 kyr B.P. (478 cm core depth), followed by pronounced enrichment towards the top of the core interval (475 cm core depth). Lacking large shifts in $\delta^{13}C_{TOC}$ indicative of a pronounced vegetation change between C_3 and C_4 vegetation and with no indication of changes in atmospheric $\delta^{13}CO_2$ values (Indermöhle et al., 1999; Elsig et al., 2009; Schmitt et al., 2012), the minor fluctuations in the $\delta^{13}C_{TOC}$ record from TP are likely caused by plant physiological responses to environmental stress over the majority of the investigated time interval. The $\delta^{13}C$ isotopic

composition of vascular terrestrial plants may reflect adaptation to climatic variations over time. Vascular plants respond to the increase in atmospheric CO₂ concentration or humidity by reducing stomatal conductance, resulting in the enrichment of ¹³C of CO₂ in the leaf and eventually all photosynthetic products (Cowan and Farquhar, 1977; Farquhar et al., 1989; Marshall et al., 2008). Since there is no conceivable correlation between δ¹³C_{TOC} from TP and reconstructions of atmospheric CO₂ concentration over the same time interval (Wagner et al., 2002), we suggest changes in humidity to be the primary control over stomatal conductance and thus fluctuations in the δ¹³C_{TOC} record of TP (e.g., Diefendorf et al., 2010). However, in wetland environments where strong changes in surface moisture regime may occur, the presence of aquatic plants and possibly algae also needs to be taken into account. Carbon isotope fractionation in aquatic plants is often small, especially in sluggish water environments, due to the limitations of diffusion of CO₂ dissolved in water (O'Leary, 1988; Farquhar et al., 1989). On the other hand, δ¹³C values of freshwater algae are influenced by a variety of ecological factors, like rate of diffusion of CO₂, δ¹³C of dissolved organic carbon, the physiological state of the algae among others, but are usually depleted in ¹³C relative to C₃ plants (Hamilton and Lewis, 1992). Thus, the presence of aquatic plants and algae may significantly alter the sedimentary δ¹³C_{TOC} record. Therefore, depending on the relative contribution of vascular terrestrial and aquatic plants and algae to the sediment, interpretation of δ¹³C_{TOC} from TP in terms of humidity change is challenging and will be discussed in more detail below.

3.3.5 Palynological reconstruction

Individual pollen taxa have been grouped according to their respective plant types into the following groups: Arboreal taxa, non-arboreal taxa, aquatic taxa and fern spores. Arboreal taxa largely dominate the palynological record of TP from 8.7 to 7.5 kyr B.P. with relatively minor contributions from non-arboreal taxa, grass (Poaceae) and sedges (Cyperaceae) and aquatic taxa (Fig. 3.3). Due to the lack of tree fossils in the Philippi peatland (Christanis, 1983), it is unlikely that trees were growing within the peat bog but rather on the margins and mountain slopes surrounding the TP basin. As such, the contribution of arboreal taxa to the sediment is considered allochthonous and therefore omitted from further discussion. The palynological record reveals two periods of ecological changes on the peat bog over the studied interval as suggested by the aquatic taxa and the fern spores percentages, as well as changes in the presence of

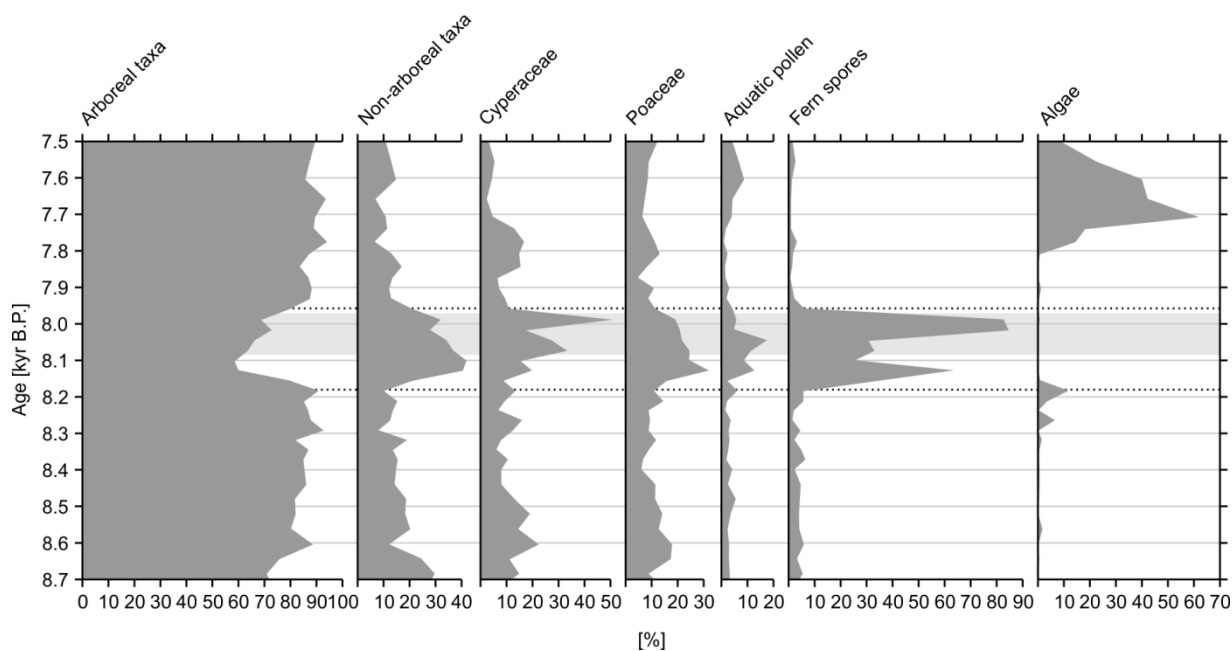


Fig. 3.3 Pollen record of the studied section of core TP-2005. Pollen and spores percentages of major plant groups and algae calculated relative to the sum of arboreal and non-arboreal pollen count per sample. Dashed lines mark the winter cooling during the 8.2 kyr B.P. climatic event at Tenaghi Philippon (Pross et al. 2009). Gray bar marks the interval of pronounced change in precipitation seasonality related to the 8.2 kyr B.P. climatic event (compare Fig. 3.4).

algae in the sediments. The first period, i.e., between ca. 8.2 and 8.0 kyr B.P. (505 to 495 cm core depth) is marked by two distinct maxima in fern spores percentages, along with increasing amounts of pollen from aquatic taxa, and also transiently of Poaceae and Cyperaceae (Fig. 3.3). These results point to rising of the water table at TP affecting the aquatic plants but also the grasses and sedges that primarily grow at the peat bog as well as allowing the expansion of fern plants. The second phase, between ca. 7.8 and 7.5 kyr B.P. (484 to 475 cm core depth), is associated with increasing presence of algae (predominantly *Pediastrum*) in the TP sediments (Fig. 3.3). This indicates a higher water table and also point to presence of subaerial freshwater pools.

3.3.6 Multiproxy reconstructions of early to mid-Holocene paleohydrology

Combining the various paleoclimate proxy records from TP allows the reconstruction of the predominant humidity and surface moisture conditions at the site between 7.5 and 8.7 kyr B.P., with a special focus on the regional response to the 8.2 kyr B.P. cooling between ca. 8.2 and 8.0 kyr B.P. (Fig. 3.4a; compare Pross et al., 2009). The *n*-alkane distributions and $\delta^{13}\text{C}_{\text{TOC}}$ record of TP together with new and previously published palynological studies (Pross et al., 2009; Peyron et al., 2011) and stable hydrogen isotopes of leaf wax *n*-alkanes ($\delta\text{D}_{\text{wax}}$; Schemmel et al. 2016) from the same core section reveal three distinct periods with differing hydrological conditions at TP across

the investigated interval (Fig. 3.4). Preceding the 8.2 kyr B.P. climatic event, the pre-event interval (ca. 8.7 to 8.2 kyr B.P.) is characterized by a good preservation of *n*-alkanes in the sediment as indicated by relatively high CPI values (Fig. 3.4d). Low P_{aq} and high ACL values respectively, imply relatively dry surface conditions and the predominance of vascular terrestrial plants during this interval (Fig. 3.4e, f). As the *n*-alkane distributions of vascular terrestrial plants reflect the time of leaf formation in spring and early summer (Tipple et al., 2013), dry conditions at the site are likely influenced by low summer rainfall amounts, also evident in the precipitation reconstruction based on palynological data (Fig. 3.4b, Peyron et al., 2011). This assumption is supported by previous works linking surface moisture conditions in peatlands to water table changes strongly influenced by summer climatic conditions (Charman et al., 2004; Charman, 2007). The notion of comparably dry surface conditions is further corroborated by elevated $\delta^{13}C_{TOC}$ values during the pre-event interval, suggesting low humidity conditions (Fig. 3.4g), as well as by the relatively low amount of aquatic plant pollen, fern spores, and algae (Fig. 3.3). The regional response to the 8.2 kyr B.P. climatic event is evident in a pronounced decline in winter temperatures between ca. 8.2 and 7.95 kyr B.P. as well as changes in atmospheric circulation, manifesting in a shift in precipitation seasonality and in precipitation-based δD_{wax} values (Fig. 3.4a, b, c; Pross et al., 2009; Peyron et al., 2011; Schemmel et al., 2016). Notably, the changes in palynological temperature reconstructions predate the signals of the precipitation proxies by roughly 100 years (Fig. 3.4; gray bar). The biomarker records of TP uniformly show variations during the period of the 8.2 kyr B.P. climatic event (ca. 8.2 to 7.95 kyr B.P.), culminating at ca. 8.05 kyr B.P., coeval with the shifts in precipitation seasonality and δD_{wax} . As discussed above, the pronounced drop in CPI values between ca. 8.1 and 8.0 kyr B.P. likely reflects changes in vegetation at TP rather than microbial degradation during the early stages of diagenesis (Fig. 3.4d). The palynological record reveals a shift in local vegetation between ca. 8.2 and 8.0 kyr B.P. towards an increased amount of fern plants at the site (Fig. 3.4l). Several fern species have been reported to produce only low amounts of *n*-alkanes with a minor odd-over-even predominance (Lytle et al., 1976). Hence, the observed shift in local vegetation may be responsible for the decrease in CPI between ca. 8.1 and 8.0 kyr B.P.. Also, the expansion of fern plants between ca. 8.2 and 8.0 kyr B.P., along with the increase in pollen from grasses and sedges as well as the slight increase in aquatic plant pollen (Fig. 3.4h, i, k), is indicative of an increase in soil moisture, likely related to the increase in summer precipitation (Fig. 3.4b). The sensitivity to changes in precipitation is further highlighted by successively increasing P_{aq} values and a simultaneous decrease in ACL

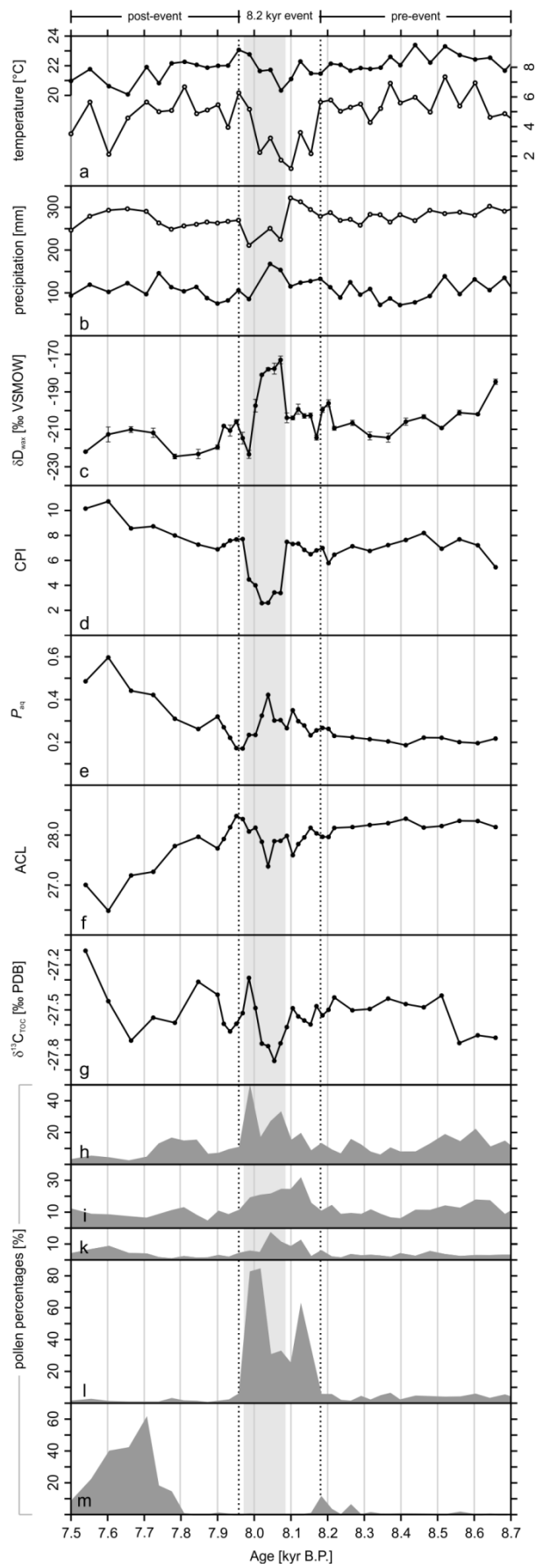


Fig. 3.4 (see opposite page) Comparison of *n*-alkane distribution, stable carbon isotopic composition of total organic carbon and selected pollen taxa with plant wax-derived stable hydrogen isotopic composition (δD_{wax}) and palynological reconstructions of seasonal temperature and precipitation of the studied section of core TP-2005. a. Seasonal temperature (Pross et al., 2009). b. Seasonal precipitation (Peyron et al., 2011). Dots indicate summer reconstructions. Circles indicate winter reconstructions. c. δD_{wax} values (Schemmel et al., 2016). d. P_{aq} values. e. ACL values. f. $\delta^{13}C_{TOC}$ values. g. CPI values. h. Cyperaceae. i. Poaceae. k. Aquatic taxa. l. Fern spores. m. Algae. Dashed lines mark the duration of the 8.2 kyr B.P. climatic event winter cooling (Pross et al., 2009). Gray bar marks the duration of the change in precipitation seasonality related to the 8.2 kyr B.P. climatic event (Peyron et al., 2011).

during the 8.2 kyr B.P. climatic event, implying wetter surface conditions (Fig. 3.4e, f). The maximum increase in summer rainfall coincides with the increase in P_{aq} and the decrease in ACL. Further, successively decreasing $\delta^{13}C_{TOC}$ values, indicative of increasingly humid conditions during the 8.2 kyr B.P. climatic event, occur at the same time as the changes in both P_{aq} and ACL (Fig. 3.4g: gray bar). Together, biomarker and pollen records imply increases in surface wetness coeval with the increase in summer precipitation between ca. 8.1 and 8.0 kyr B.P., suggesting the increase in summer precipitation to be the main control for the observed variations (Fig. 3.4: gray bar). The post-event interval (ca. 7.95 to 7.5 kyr B.P.) marks the rise of CPI values back to pre-event levels (Fig. 3.4d), associated with a return of local vegetation at TP to pre-event conditions (Fig. 3.4h, i, k, l), possibly reflecting a return of the precipitation regime to pre-event levels (Fig. 3.4b). Yet, a strong increase of P_{aq} and a similar decrease of ACL values imply a pronounced change towards significantly wetter surface conditions (Fig. 3.4e, f). With no conceivable correspondence of increasingly wetter surface conditions to the palynological precipitation reconstructions (Fig. 3.4b: Peyron et al., 2011), we suggest a change in basin hydrology to be the cause for the observed changes in the biomarker proxy records. The basin hydrology that controls the depth of the water table of the Philippi peatland has varied during the transition from the Late Glacial into the Holocene. The inflow of surface waters from the northern margins of the Drama Basin that dominated groundwater influx during Late Glacial times gradually declined and was eventually replaced by inflow from a karstic groundwater system bringing about telmatic conditions in the basin (Christanis, 1983). Fluctuations of the water table during the mid-Holocene occasionally caused limnotelmatic conditions to expand in the Philippi peatland (Kalaitzidis and Christanis, 2002). We propose that increased activity of the karstic system surrounding the Drama Basin may have raised the water table during the post-event interval, waterlogging the site at least temporarily. Consequently, increasing P_{aq} and decreasing ACL values after ca. 7.8 kyr B.P. would result from the increased contribution of aquatic plant material to the sediment. This assumption is supported by the appearance of the freshwater green algae *Pediastrum* as well as an increase in the percentages of aquatic plant pollen between ca. 7.8 and 7.5 kyr B.P. (Fig. 3.4k, m). The interpretation of $\delta^{13}C_{TOC}$ as a humidity proxy in the upper part of the core after ca. 8.0 kyr B.P. becomes ambiguous. Even though the general trend in $\delta^{13}C_{TOC}$ largely agrees with

the trends of the P_{aq} and ACL records, indicating an increasingly humid environment, several variations become apparent, most notably around ca. 7.65 kyr B.P. (Fig. 3.4e, f, g). We suggest that these variations in $\delta^{13}C_{TOC}$ at TP are caused by the (partial) submergence of the peat surface and the subsequent appearance of algae at TP (Fig. 3.4m). Thus, the increased contribution of algae, generally depleted in ^{13}C compared to terrestrial C_3 plants, to the peat deposit could have altered $\delta^{13}C_{TOC}$ values.

3.4 Conclusions

Our multiproxy study of paleohydrological conditions in the Philippi peatland reveals the effects of changing surface moisture conditions between ca. 8.7 and 7.5 kyr B.P. on the local vegetation at TP. Relatively dry conditions with an abundance of vascular terrestrial plants are evident from ca. 8.7 to 8.0 kyr B.P. from low P_{aq} and high ACL values, respectively. Slightly elevated $\delta^{13}C_{TOC}$ values during this interval might reflect a physiological response of vascular plants to low humidity at the site, or a change in vegetation composition in general. High CPI values indicate good preservation of organic material. Changing atmospheric circulation patterns during the 8.2 kyr B.P. climatic event between ca. 8.1 and 8.0 kyr B.P. are accompanied by an increase in precipitation that is evident in an increasingly wet peat surface and more humid conditions at the site, highlighting a possible control of summer climatic conditions on the prevalent vegetation in the Philippi peatland. The upper part of the section between ca. 8.0 and 7.5 kyr B.P. is marked by a general increase in surface wetness. A strongly elevated water table, likely caused by the increased activity of the karstic system surrounding the Drama Basin, may have led to the submergence of the peat surface, increased preservation of organic material by anoxic conditions in the upper peat layer as well as favoring the expansion of algae and aquatic plants, as supported by deviations in $\delta^{13}C_{TOC}$ and the palynological record.

3.5 Acknowledgements

FS, EMN, AK, JP, JF and AM acknowledge support through the LOEWE funding program (Landes-Offensive zur Entwicklung wissenschaftlich-ökonomischer Exzellenz) of Hesse's Ministry of Higher Education, Research, and the Arts. We thank U. Treffert (Senckenberg BiK-F, Frankfurt), T. Potouridis, W. Püttmann and S. Hofmann (Goethe University Frankfurt) and U. Müller, for valuable technical assistance and advise.

3.6 References

- Alley, R. B., and Ágústssdóttir, A. M., 2005, The 8k event: cause and consequences of a major Holocene abrupt climate change: *Quaternary Science Reviews*, v. 24, no. 10-11, p. 1123–1149, doi: 10.1016/j.quascirev.2004.12.004.
- Argiriou, A. A., and Lykoudis, S., 2006, Isotopic composition of precipitation in Greece: *Journal of Hydrology*, v. 327, no. 3-4, p. 486–495, doi: 10.1016/j.jhydrol.2005.11.053.
- Bar-Matthews, M., Ayalon, A., and Kaufman, A., 1997, Late Quaternary Paleoclimate in the Eastern Mediterranean Region from Stable Isotope Analysis of Speleothems at Soreq Cave, Israel: *Quaternary Research*, v. 47, no. 2, p. 155–168, doi: 10.1006/qres.1997.1883.
- Barber, D.C., Dyke, A., Hillaire-Marcel, C., Jennings, A.E., Andrews, J.T., Kerwin, M.W., Bilodeau, G., McNeely, R., Southon, J., Morehead, M.D., and Gagnon, J.-M., 1999, Forcing of the cold event of 8,200 years ago by catastrophic drainage of Laurentide lakes: *Nature*, v. 400, no. July, p. 344–348.
- Bray, E., and Evans, E., 1961, Distribution of *n*-paraffins as a clue to recognition of source beds: *Geochimica et Cosmochimica Acta*, v. 22, no. 1, p. 2–15, doi: 10.1016/0016-7037(61)90069-2.
- Bush, R. T., and McInerney, F. A., 2013, Leaf wax *n*-alkane distributions in and across modern plants: Implications for paleoecology and chemotaxonomy: *Geochimica et Cosmochimica Acta*, v. 117, p. 161–179, doi: 10.1016/j.gca.2013.04.016.
- Chambers, F. M., Booth, R. K., De Vleeschouwer, F., Lamentowicz, M., Le Roux, G., Mauquoy, D., Nichols, J. E., and van Geel, B., 2012, Development and refinement of proxy-climate indicators from peats: *Quaternary International*, v. 268, p. 21–33, doi: 10.1016/j.quaint.2011.04.039.
- Castañeda, I. S., and Schouten, S., 2011, A review of molecular organic proxies for examining modern and ancient lacustrine environments: *Quaternary Science Reviews*, v. 30, no. 21-22, p. 2851–2891, doi: 10.1016/j.quascirev.2011.07.009.
- Charman, D. J., 2007, Summer water deficit variability controls on peatland water-table changes: implications for Holocene palaeoclimate reconstructions: *The Holocene*, v. 17, no. 2, p. 217–227, doi: 10.1177/0959683607075836.
- Charman, D., Brown, A., Hendon, D., and Karofeld, E., 2004, Testing the relationship between Holocene peatland palaeoclimate reconstructions and instrumental data at two European sites: *Quaternary Science Reviews*, v. 23, no. 1-2, p. 137–143, doi: 10.1016/j.quascirev.2003.10.006.
- Christanis, K., 1983, Genese und Fazies der Torf-Lagerstätte von Philippi (Griechisch-Mazedonien) als Beispiel der Entstehung einer Braunkohle-Lagerstätte vom stark telmatischen Typ: *Technische Universität Carolo-Wilhelmina zu Braunschweig*, 1-180 p.
- Cowan, I., and Farquhar, G., 1977, Stomatal function in relation to leaf metabolism and environment. *in* Jennings DH, (Ed), *Integration of Activity in the Higher Plants*. Cambridge, UK: Cambridge Univ Press; 1977. pp. 471–505.
- Diefendorf, A. F., Mueller, K. E., Wing, S. L., Koch, P. L., and Freeman, K. H., 2010, Global patterns in leaf ¹³C discrimination and implications for studies of past and future climate.: *Proceedings of the National Academy of Sciences of the United States of America*, v. 107, no. 13, p. 5738–43, doi: 10.1073/pnas.0910513107.
- Dise, N. B., 2009, Peatland response to global change: *Science*, v. 326, no. 5954, p. 810–1, doi: 10.1126/science.1174268.

- Dotsika, E., Lykoudis, S., and Poutoukis, D., 2010, Spatial distribution of the isotopic composition of precipitation and spring water in Greece: *Global and Planetary Change*, v. 71, no. 3-4, p. 141–149, doi: 10.1016/j.gloplacha.2009.10.007.
- Eglinton, T. I., and Eglinton, G., 2008, Molecular proxies for paleoclimatology: *Earth and Planetary Science Letters*, v. 275, no. 1-2, p. 1–16, doi: 10.1016/j.epsl.2008.07.012.
- Eglinton, G., and Hamilton, R. J., 1967, Leaf Epicuticular Waxes: *Science*, v. 156, no. 780, p. 1322–35.
- Elsig, J., Schmitt, J., Leuenberger, D., Schneider, R., Eyer, M., Leuenberger, M., Joos, F., Fischer, H., and Stocker, T. F., 2009, Stable isotope constraints on Holocene carbon cycle changes from an Antarctic ice core: *Nature*, v. 461, no. 7263, p. 507–510, doi: 10.1038/nature08393.
- Farquhar, G. D., Ehleringer, J. R., and Hubick, K. T., 1989, Carbon Isotope Discrimination and Photosynthesis: *Annual Review of Plant Physiology and Plant Molecular Biology*, v. 40, p. 503–537.
- Ficken, K. J., Li, B., Swain, D. L., and Eglinton, G., 2000, An *n*-alkane proxy for the sedimentary input of submerged/floating freshwater aquatic macrophytes: *Organic Geochemistry*, v. 31.
- Fletcher, W.J., Müller, U.C., Koutsodendris, A., Christanis, K., and Pross, J., 2013, A centennial-scale record of vegetation and climate variability from 312 to 240 ka (Marine Isotope Stages 9c-a, 8 and 7a) from Tenaghi Philippon, NE Greece: *Quaternary Science Reviews*, v. 78, p. 108-125, doi: 10.1016/j.quascirev.2013.08.005.
- Gagosian, R. B., Peltzer, E. T., and Merrill, J. T., 1987, Long-range transport of terrestrially derived lipids in aerosols from the south Pacific: *Nature*, v. 325, no. 26, p. 800–803.
- Hamilton, S.K., and Lewis, W.M., 1992, Stable carbon and nitrogen isotopes in algae and detritus from the Orinoco River floodplain, Venezuela: *Geochimica et Cosmochimica Acta*, v. 56, no. 12, p. 4237–4246, doi: 10.1016/0016-7037(92)90264-J.
- Huang, X., Xue, J., Meyers, P. A., Gong, L., Wang, X., Liu, Q., Qin, Y., and Wang, H., 2014, Hydrologic influence on the $\delta^{13}\text{C}$ variation in long chain *n*-alkanes in the Dajihu peatland, central China: *Organic Geochemistry*, v. 69, p. 114–119, doi: 10.1016/j.orggeochem.2014.01.016.
- Indermühle, A., Stocker, T. F., Joos, F., Fischer, H., Smith, H. J., Wahlen, M., Deck, B., Mastroianni, D., Tschumi, J., Blunier, T., Meyer, R., and Stauffer, B., 1999, Holocene carbon-cycle dynamics based on CO₂ trapped in ice at Taylor Dome, Antarctica: *Nature*, v. 398, p. 121–126.
- Kalaitzidis, S., and Christanis, K., 2002, Mineral Matter in the Philippi Peat in Relation to Peat/Lignite-Forming Conditions in Greece: *Energy Sources*, v. 24, p. 69–81.
- Koch, K., and Ensikat, H. J., 2008, The hydrophobic coatings of plant surfaces: Epicuticular wax crystals and their morphologies, crystallinity and molecular self-assembly: *Micron*, v. 39, no. 7, p. 759–772, doi: 10.1016/j.micron.2007.11.010.
- Kotthoff, U., Pross, J., Müller, U. C., Peyron, O., Schmiedl, G., Schulz, H., and Bordon, A., 2008a, Climate dynamics in the borderlands of the Aegean Sea during formation of sapropel S1 deduced from a marine pollen record: *Quaternary Science Reviews*, v. 27, no. 7-8, p. 832–845, doi: 10.1016/j.quascirev.2007.12.001.
- Kotthoff, U., Müller, U. C., Pross, J., Schmiedl, G., Lawson, I. T., Van De Schootbrugge, B., and Schulz, H., 2008b, Lateglacial and Holocene vegetation dynamics in the Aegean region: an integrated view based on pollen data from marine and terrestrial archives: *The Holocene*, v. 18, no. 7, p. 1019–1032, doi: 10.1177/0959683608095573.

- Kotthoff, U., Koutsodendris, A., Pross, J., Schmiedl, G., Bornemann, A., Marino, G., Peyron, O., Schiebel, R., 2011. Impact of Lateglacial cold events on the northern Aegean region reconstructed from marine and terrestrial proxy data. *Journal of Quaternary Science* 26, 86-96.
- Kuder, T., and Kruge, M. A., 1998, Preservation of biomolecules in sub-fossil plants from raised peat bogs - A potential paleoenvironmental proxy: *Organic Geochemistry*, v. 29, no. 5-7 -7 pt 2, p. 1355–1368, doi: 10.1016/S0146-6380(98)00092-8.
- Li, H.-C., Liew, P.-M., Seki, O., Kuo, T.-S., Kawamura, K., Wang, L.-C., and Lee, T.-Q., 2013, Paleoclimate variability in central Taiwan during the past 30KyrS reflected by pollen, $\delta^{13}\text{C}_{\text{TOC}}$, and *n*-alkane- δD records in a peat sequence from Toushe Basin: *Journal of Asian Earth Sciences*, v. 69, p. 166–176, doi: 10.1016/j.jseaes.2012.12.005.
- Lionello, P., Abrantes, F., Congedi, L., Dulac, F., Gacic, M., Gomis, D., Clare, G., Hoff, H., Kutiel, H., Luterbacher, J., Planton, S., Reale, M., Schröder, K., Struglia, M. V., Toreti, A., Tsimplis, M., Ulbrich, U., and Xoplaki, E., 2012, Mediterranean Climate - Background Information, in Lionello, P. (Ed), *The Climate of the Mediterranean Region*, Elsevier B. V., Amsterdam, p. 1-56.
- Lytle, T.F., Lytle, J.S., and Caruso, A., 1976, Hydrocarbons and Fatty Acids of Ferns: *Phytochemistry*, v. 15, no. 6, p. 965–970.
- Marshall, J. D., Brooks, J. R., and Lajtha, K., 2008, Sources of variation in the stable isotopic composition of plants, in Michener, R. and Lajtha, K. (Eds.), *Stable Isotopes in Ecology and Environmental Science*, Wiley-Blackwell, p. 22–60.
- Mügler, I., Sachse, D., Werner, M., Xu, B., Wu, G., Yao, T., and Gleixner, G., 2008, Effect of lake evaporation on δD values of lacustrine *n*-alkanes: A comparison of Nam Co (Tibetan Plateau) and Holzmaar (Germany): *Organic Geochemistry*, v. 39, no. 6, p. 711–729, doi: 10.1016/j.orggeochem.2008.02.008.
- Nichols, J. E., Booth, R. K., Jackson, S. T., Pendall, E. G., and Huang, Y., 2006, Paleohydrologic reconstruction based on *n*-alkane distributions in ombrotrophic peat: *Organic Geochemistry*, v. 37, no. 11, p. 1505–1513, doi: 10.1016/j.orggeochem.2006.06.020.
- O'Leary, M. H., 1988, Carbon Isotopes Photosynthesis - Fractionation techniques may reveal new aspects of carbon dynamics in plants: *BioScience*, v. 38, no. 5, p. 328–336.
- Peyron, O., Goring, S., Dormoy, I., Kotthoff, U., Pross, J., de Beaulieu, J.-L., Drescher-Schneider, R., Vanniere, B., and Magny, M., 2011, Holocene seasonality changes in the central Mediterranean region reconstructed from the pollen sequences of Lake Accesa (Italy) and Tenaghi Philippon (Greece): *The Holocene*, v. 21, no. 1, p. 131–146, doi: 10.1177/0959683610384162.
- Pross, J., Tzedakis, P., Schmiedl, G., Christanis, K., Hooghiemstra, H., Müller, U.C., Kotthoff, U., Kalaitzidis, S., and Milner, A., 2007, Tenaghi Philippon (Greece) Revisited: Drilling a Continuous Lower-Latitude Terrestrial Climate archive of the Last 250,000 Years: *Scientific Drilling*, v. 5, p. 44–46, doi: 10.2204/iodp.sd.5.06.2007.
- Pross, J., Kotthoff, U., Müller, U. C., Peyron, O., Dormoy, I., Schmiedl, G., Kalaitzidis, S., and Smith, A. M., 2009, Massive perturbation in terrestrial ecosystems of the Eastern Mediterranean region associated with the 8.2 kyr B.P. climatic event: *Geology*, v. 37, no. 10, p. 887–890, doi: 10.1130/G25739A.1.
- Pross, J., Koutsodendris, A., Christanis, K., Fischer, T., Fletcher, W. J., Hardiman, M., Kalaitzidis, S., Knipping, M., Kotthoff, U., Milner, A. M., Müller, U. C., Schmiedl, G., Siavalas, G., Tzedakis, P. C., Wulf, S., 2015, The 1.35-Ma-long terrestrial climate archive of Tenaghi Philippon, northeastern Greece: Evolution, exploration and perspectives for future research. *Newsletters on Stratigraphy* 48, 253-276.

- Renssen, H., Goosse, H., Fichet, T., and Campin, J.-M., 2001, The 8.2 kyr BP event simulated by a global atmosphere-sea-ice-ocean model: *Geophysical Research Letters*, v. 28, no. 8, p. 1567–1570.
- Riederer, M., and Schreiber, L., 2001, Protecting against water loss: analysis of the barrier properties of plant cuticles.: *Journal of experimental botany*, v. 52, no. 363, p. 2023–2032, doi: 10.1093/jexbot/52.363.2023.
- Rohling, E.J., and Pälike, H., 2005, Centennial-scale climate cooling with a sudden cold event around 8,200 years ago: *Nature*, v. 434, no. 7036, p. 975–979.
- Rohling, E. J., Mayewski, P. A., Abu-Zied, R. H., Casford, J. S. L., and Hayes, A., 2002, Holocene atmosphere-ocean interactions: records from Greenland and the Aegean Sea: *Climate Dynamics*, v. 18, no. 7, p. 587–593, doi: 10.1007/s00382-001-0194-8.
- Rohling, E.J., Marino, G., and Grant, K.M., 2015, Mediterranean climate and oceanography, and the periodic development of anoxic events (sapropels): *Earth-Science Reviews*, v. 143, p. 62–97, doi: 10.1016/j.earscirev.2015.01.008.
- Rommerskirchen, F., Eglinton, G., Dupont, L., Güntner, U., Wenzel, C., and Rullkötter, J., 2003, A north to south transect of Holocene southeast Atlantic continental margin sediments: Relationship between aerosol transport and compound-specific $\delta^{13}\text{C}$ land plant biomarker and pollen records: *Geochemistry Geophysics Geosystems*, v. 4, no. 12, p. 1–29.
- Sachse, D., Radke, J., and Gleixner, G., 2006, δD values of individual *n*-alkanes from terrestrial plants along a climatic gradient - Implications for the sedimentary biomarker record: *Organic Geochemistry*, v. 37, no. 4, p. 469–483, doi: 10.1016/j.orggeochem.2005.12.003.
- Sachse, D., Billault, I., Bowen, G.J., Chikaraishi, Y., Dawson, T. E., Feakins, S. J., Freeman, K. H., Magill, C. R., McInerney, F. A., van der Meer, M. T. J., Polissar, P., Robins, R. J., Sachs, J. P., Schmidt, H.-L., et al., 2012, Molecular Paleohydrology: Interpreting the Hydrogen-Isotopic Composition of Lipid Biomarkers from Photosynthesizing Organisms: *Annual Review of Earth and Planetary Sciences*, v. 40, no. 1, p. 221–249, doi: 10.1146/annurev-earth-042711-105535.
- Schemmel, F., Niedermeyer, E. M., Schwab, V. F., Gleixner, G., Pross, J., and Mulch, A., 2016, Plant wax δD values record changing Eastern Mediterranean atmospheric circulation patterns during the 8.2 kyr B.P. climatic event: *Quaternary Science Reviews*, v. 133, p. 96–107, doi: 10.1016/j.quascirev.2015.12.019.
- Schmitt, J., Schneider, R., Elsig, J., Leuenberger, D., Laurantou, A., Chappellaz, J., Köhler, P., Joos, F., Stocker, T.F., Leuenberger, M., and Fischer, H., 2012, Carbon Isotope Constraints on the Deglacial CO_2 Rise from Ice Cores: *Science*, v. 711, doi: 10.1126/science.1217161.
- Tipple, B. J., Berke, M. A., Doman, C. E., Khachatryan, S., and Ehleringer, J. R., 2013, Leaf-wax *n*-alkanes record the plant-water environment at leaf flush: *Proceedings of the National Academy of Sciences of the United States of America*, v. 110, no. 7, p. 2659–64, doi: 10.1073/pnas.1213875110.
- van de Schootbrugge, B., Payne, J. L., Tomasovych, A., Pross, J., Fiebig, J., Benbrahim, M., Föllmi, K. B., and Quan, T. M., 2008, Carbon cycle perturbation and stabilization in the wake of the Triassic-Jurassic boundary mass-extinction event: *Geochemistry, Geophysics, Geosystems*, v. 9, no. 4, doi: 10.1029/2007GC001914.
- Vogts, A., Schefuß, E., Badewien, T., and Rullkötter, J., 2012, *n*-Alkane parameters from a deep sea sediment transect off southwest Africa reflect continental vegetation and climate conditions: *Organic Geochemistry*, v. 47, p. 109–119, doi: 10.1016/j.orggeochem.2012.03.011.

- Wagner, F., Aaby, B., and Visscher, H., 2002, Rapid atmospheric CO₂ changes associated with the 8,200-years-B.P. cooling event.: Proceedings of the National Academy of Sciences of the United States of America, v. 99, no. 19, p. 12011–4, doi: 10.1073/pnas.182420699.
- Xie, S., Nott, C. J., Avsejs, L. A., Maddy, D., Chambers, F. M., and Evershed, R. P., 2004, Molecular and isotopic stratigraphy in an ombrotrophic mire for paleoclimate reconstruction: *Geochimica et Cosmochimica Acta*, v. 68, no. 13, p. 2849–2862, doi: 10.1016/j.gca.2003.08.025.
- Yamamoto, S., Kawamura, K., Seki, O., Meyers, P. A., Zheng, Y., and Zhou, W., 2010, Environmental influences over the last 16ka on compound-specific $\delta^{13}\text{C}$ variations of leaf wax *n*-alkanes in the Hani peat deposit from northeast China: *Chemical Geology*, v. 277, no. 3-4, p. 261–268, doi: 10.1016/j.chemgeo.2010.08.009.
- Zheng, Y., Zhou, W., Meyers, P. A., and Xie, S., 2007, Lipid biomarkers in the Zoigê-Hongyuan peat deposit: Indicators of Holocene climate changes in West China: *Organic Geochemistry*, v. 38, no. 11, p. 1927–1940, doi: 10.1016/j.orggeochem.2007.06.012.
- Zhou, W., Xie, S., Meyers, P. A., and Zheng, Y., 2005, Reconstruction of late glacial and Holocene climate evolution in southern China from geolipids and pollen in the Dingnan peat sequence: *Organic Geochemistry*, v. 36, no. 9, p. 1272–1284, doi: 10.1016/j.orggeochem.2005.04.005.
- Zhou, W., Zheng, Y., Meyers, P. A., Jull, A. J. T., and Xie, S., 2010, Postglacial climate-change record in biomarker lipid compositions of the Hani peat sequence, Northeastern China: *Earth & Planetary Science Letters*, v. 294, no. 1-2, p. 37–46, doi: 10.1016/j.epsl.2010.02.035.

Chapter 4

Plant wax δD values record changing Eastern Mediterranean atmospheric circulation patterns during the 8.2 kyr B.P. climatic event

Fabian Schemmel¹, Eva M. Niedermeyer¹, Valérie F. Schwab², Gerd Gleixner³, Jörg Pross^{1,4}, Andreas Mulch^{1,5}

¹ Senckenberg Biodiversity and Climate Research Centre (BiK-F), Frankfurt am Main, Germany

² Institute for Inorganic and Analytic Chemistry, University Jena, Jena, Germany

³ Max Planck Institute for Biogeochemistry, Jena, Germany

⁴ Paleoenvironmental Dynamics Group, Institute of Earth Sciences, University Heidelberg, Heidelberg, Germany

⁵ Institute of Geosciences, Goethe University Frankfurt, Frankfurt am Main, Germany

Published in *Quaternary Science Reviews* (2016), 133, p. 96–107,
doi: 10.1016/j.quascirev.2015.12.019

Abstract Throughout the Holocene, the climate of the Mediterranean region has been strongly influenced by variability in the atmospheric circulation of the high and low latitudes. A prominent example for such Holocene climate perturbations is the '8.2 kyr B.P. climatic event'. Reorganization of Northern Hemisphere atmospheric circulation patterns resulted in variations of temperature and precipitation distribution across the Mediterranean. The effects of changing high- and low-latitude atmospheric circulation on Mediterranean climate in relation to the 8.2 kyr B.P. climatic event are, however, not well understood. Here we present a high-resolution record of stable hydrogen isotope composition of plant-wax *n*-alkanes (δD_{wax}) across the 8.2 kyr B.P. climatic event from the Tenaghi Philippon peat deposit (NE Greece) in order to characterize patterns of precipitation and changes in atmospheric circulation in the Eastern Mediterranean region. Our record reveals pronounced changes in δD_{wax} that correlate closely with previously published palynological data. A long-term decline in δD_{wax} values characterizes the lower part of the section. The 8.2 kyr B.P. climatic event itself is connected to two distinct positive δD_{wax} excursions: a minor shift in δD_{wax} around 8.2 kyr B.P. and a major shift in δD_{wax} between ca. 8.1 and 8.0 kyr B.P.. The upper part of the section shows a progressive trend towards higher δD_{wax} values. We link shifts in δD_{wax} to changes in Mediterranean air mass trajectories supplying precipitation to NE Greece caused by variations in the relative contributions of northerly-derived, D-depleted moisture and southerly-derived, D-enriched moisture. Possible control mechanisms for alternating air mass trajectories include changes in the influence of the Siberian High and differences in the influence of the African and Asian monsoon circulation on

anticyclonic conditions in the Mediterranean region as well as regional inflow of moist air masses from the Aegean Sea.

4.1 Introduction

Perturbations of northern hemisphere high- and low-latitude climate systems strongly affect temperature and precipitation patterns in the Mediterranean region (e.g., Lionello et al., 2006). Over the course of the Holocene, Mediterranean climate has been influenced repeatedly by abrupt climate change (Mayewski et al., 2004; Wanner et al., 2011). Arguably the most prominent example of Holocene climate variations is the so-called '8.2 kyr B.P. climatic event' (Alley et al., 1997). Triggered by a meltwater outburst of ice-dammed Laurentide lakes into the North Atlantic, this event led to climate deterioration in the North Atlantic region during a period of reduced solar activity (Alley and Ágústsdóttir, 2005; Rohling and Pälike, 2005). As a result, shifts in northern hemisphere climatological and oceanographic conditions occurred that also affected moisture transport and rainfall patterns in the Mediterranean region (Berger and Guilaine, 2009; Morrill et al., 2013). However, despite a broad spectrum of paleoclimatic data, the effects of changing atmospheric and oceanic circulation on Eastern Mediterranean precipitation patterns have still largely remained elusive.

Coinciding with the interruption of the formation of sapropel S1 in the Eastern Mediterranean, the 8.2 kyr B.P. climatic event has been characterized by large-scale atmospheric circulation changes with increased influence of the Siberian High and a concurrent weakening of the impact of low-latitude monsoonal circulation (Kotthoff et al., 2008a). Various marine and terrestrial proxy records from the Aegean region show signs of temperature and/or precipitation changes during that time (Rohling et al., 2002; Dormoy et al., 2009; Marino et al., 2009; Triantaphyllou et al., 2009; Geraga et al., 2010; Kouli et al., 2012). Further, high-resolution pollen records from the paleoclimate archive of Tenaghi Philippon (TP), northeastern Greece, indicate that strengthening of the Siberian High during the 8.2 kyr B.P. climatic event led to a decline in winter temperatures and precipitation seasonality, resulting in a major vegetation setback, mainly at the expense of evergreen tree taxa (Pross et al., 2009; Peyron et al., 2011). It has been hypothesized that precipitation in the Eastern Mediterranean region during formation of Sapropel S1 originated from regional sources (Kallel et al., 1997). The impact of supraregional atmospheric circulation changes in relation to the 8.2 kyr B.P. climatic event, however, is still poorly understood.

As disparate air mass trajectories carry moisture with different oxygen ($\delta^{18}\text{O}$) and hydrogen (δD) isotopic compositions, stable isotopes in precipitation provide the opportunity to track large-scale atmospheric circulation changes (e.g., Roberts et al., 2010; Spötl et al., 2010; Göktürk et al., 2011). Here we present a high-resolution δD record of plant wax *n*-alkanes ($\delta\text{D}_{\text{wax}}$) from TP. We show that changes in $\delta\text{D}_{\text{wax}}$ values from the TP site are linked to changes in precipitation source area, and document that the 8.2 kyr B.P. climatic event was accompanied by pronounced atmospheric reorganization in the Eastern Mediterranean region.

4.1.1 The 8.2 kyr B.P. climatic event

Characterized by the largest deviation in the Holocene $\delta^{18}\text{O}$ record, the 8.2 kyr B.P. climatic event represents a period marked by distinct cooling in Greenland ice cores (e.g., Alley et al., 1997; Kobashi et al., 2007). The initial abrupt cooling culminated in a period of persistently lower temperatures before returning to pre-event conditions. The decline in $\delta^{18}\text{O}$ values started at 8.247 kyr B.P. and lasted 160.5 ± 5.5 yrs, with maximum cooling over 69 ± 2 yrs (Thomas et al., 2007). Proxy and model evidence suggest that central Greenland cooling was triggered by a massive addition of freshwater into the North Atlantic, resulting in a reduction of the Atlantic Meridional Overturning Circulation (AMOC) and subsequent sea-ice increase in the northern high latitudes (Renssen et al., 2001; Bauer et al., 2004). Rapid drainage of the Laurentide meltwater lakes into the Labrador Sea occurred at 8.47 ± 0.3 kyr B.P. (Barber et al., 1999), weakening the deep, southward flowing branch of the AMOC from ca. 8.38 to 8.27 kyr B.P. (Kleiven et al., 2008). However, the climatic response to a weakened AMOC state is not limited to Greenland and the North Atlantic region (Alley et al., 1997; Alley and Ágústsdóttir, 2005). Model and proxy records suggest that changes in atmospheric conditions related to the 8.2 kyr B.P. climatic event occurred simultaneously in Greenland and on a hemispheric scale (LeGrande et al., 2006; Kobashi et al., 2007). The quasi-hemispheric nature of the 8.2 kyr B.P. climatic event is evident in a temperature decline and hydrological changes in many locations of the northern hemisphere, especially in Europe, as opposed to broad regions of the southern hemisphere, the Pacific or the tropics (Alley and Ágústsdóttir, 2005; Morrill and Jacobsen, 2005; Rohling and Pälike, 2005; Wiersma et al., 2011). Northern hemisphere 8.2 kyr cooling has been further shown to strongly affect low-latitude climate patterns such as the monsoonal systems (Wang et al., 2005; Cheng et al., 2009; Liu et al., 2013) and to coincide with a southward shift of the Intertropical Convergence Zone (ITCZ) (Haug et al., 2001). Complications in identifying regional and global responses to the 8.2

kyr B.P. climatic event, however, arise from the fact that this rapid and distinct cooling event is embedded in a weak millennial-scale cooling oscillation from ca. 8.5 to 8.0 kyr B.P., which has been linked to solar forcing (Rohling and Pälike, 2005).

4.1.2 Present-day Mediterranean climate

Mediterranean climate is characterized by a strong seasonality in precipitation. Cyclogenetic activity over most of the Mediterranean basin causes rainfall maxima during the typically mild winters. Summer aridity, in turn, is favored by a northward shift of the North African anticyclones and strengthening of the Azores High, thus blocking the eastward movement of air into the Mediterranean region (Fig. 4.1; e.g., Lionello et al., 2012). Its intermediate location between the climate systems of the high and low latitudes leads to a distinct sensitivity of Mediterranean atmospheric circulation to the variability of supraregional circulation patterns, such as the Siberian High, the North Atlantic Oscillation (NAO) and the monsoonal systems (Fig. 4.1). These influences vary depending on the season and location in the basin. The Eastern Mediterranean region is exposed to the Asian Monsoon systems in summer and the Siberian High in winter, whereas the northern and western parts are primarily under the influence of the NAO. Additionally, the southern and eastern parts of the Mediterranean region are strongly influenced by the seasonal migration of the ITCZ through the descending branch of the Hadley cell (e.g., Lionello et al., 2012).

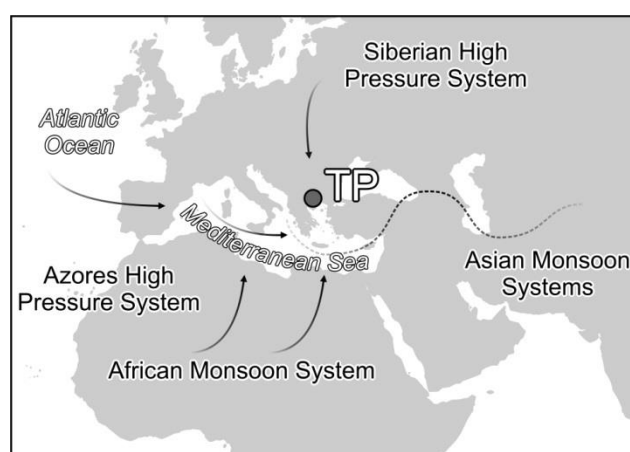


Fig. 4.1 Major atmospheric circulation patterns affecting Mediterranean climate dynamics (after Lionello et al., 2006; Staubwasser and Weiss, 2006). Dashed line represents influence of the Asian Monsoon Systems through Rossby wave propagation.

These atmospheric circulation mechanisms control precipitation seasonality in the Aegean region. During winter and well into fall and spring, cyclones with an eastward trajectory, originating over the Atlantic Ocean and/or the western Mediterranean Sea

dominate, resulting in high amounts of rainfall in western Greece and the eastern Aegean Sea, and associated rain shadows over eastern Greece and the central Aegean Sea. Summer rainfall is typically sparse. Atmospheric stability by means of strong anticyclonic activity and the deflection of eastward moving depressions into the Mediterranean region caused by the northward extension of the strengthened Azores High induce summer aridity. Individual precipitation events are caused by local convective storms that are favored either by thermal instability or by North African depressions approaching the Aegean region from the southwest (Fig. 4.1; Argiriou and Lykoudis, 2006; Dotsika et al., 2010).

4.1.3 Stable isotopes in modern Mediterranean precipitation

The isotopic composition of precipitation in the Eastern Mediterranean region varies significantly depending on moisture source, air mass trajectory and potential air mass mixing (Argiriou and Lykoudis, 2006; Dotsika et al., 2010, Schemmel et al., 2013). Both atmospheric moisture transport from the North Atlantic and vapor recycling over the Mediterranean basin itself contribute to the stable isotopic composition of precipitation, especially in the eastern part of the Mediterranean region (Roberts et al., 2010). Because of its semi-enclosed setting and high evaporation rates, evaporative enrichment in ^{18}O of seawater occurs particularly in the eastern part of the basin and contrasts $\delta^{18}\text{O}$ of atmospheric moisture delivered to the region by the Westerlies (Mariotti et al., 2002; Roberts et al., 2010). Additionally, temperature seasonality in the Mediterranean region exerts considerable control on the stable hydrogen ($\delta\text{D}_{\text{precip}}$) and oxygen ($\delta^{18}\text{O}_{\text{precip}}$) isotopic composition of precipitation. $\delta\text{D}_{\text{precip}}$ values in northwestern Greece are generally lower in winter and higher in summer, with a mean seasonal difference of ca. 30 ‰ (Argiriou and Lykoudis, 2006). Lower summer $\delta\text{D}_{\text{precip}}$ values during intervals of increased precipitation (“amount effect”) are subordinate (Argiriou and Lykoudis, 2006). The complex topography of Greece exerts additional control on the spatial distribution of $\delta\text{D}_{\text{precip}}$ through orographic effects. $\delta\text{D}_{\text{precip}}$ values are typically lower in eastern Greece, likely caused by orographic rain out along high topography in western Greece (Pindos Mountains) as well as by the effect of continentality on air masses originating over Central Europe (Dotsika et al., 2010).

4.2 Material and methods

4.2.1 Study site

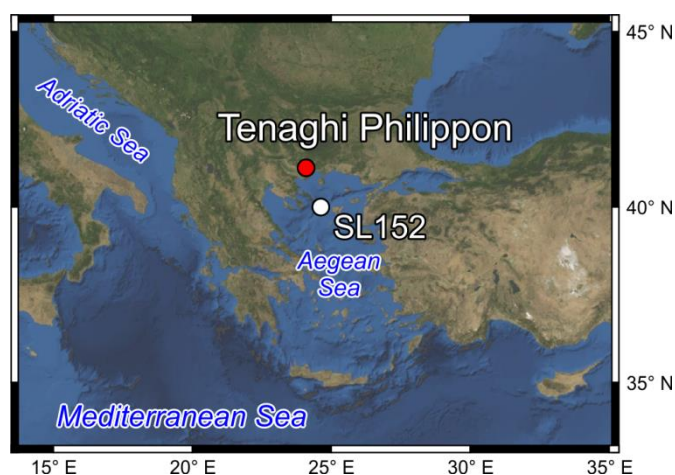


Fig. 4.2 Map of the northeastern Mediterranean region with the locations of Tenaghi Philippon and marine core SL152.

The sample material originates from a new core drilled at the classical locality of Tenaghi Philippon, located within the Philippi peatland of the Drama Basin, northeastern Greece (Fig. 4.2; Wijmstra, 1969; Pross et al., 2015). The core (TP-2005, 40°58.40'N, 24°13.42'E, 40 m.a.s.l.) comprises the upper 60 m of the TP archive (Pross et al., 2007); its base has an age of ca. 312 kyr B.P. (Fletcher et al., 2013). Surrounded by the Phalakron Range (2232 m.a.s.l.) to the north, the Menikion (1266 m.a.s.l.) and Pangaion (1956 m.a.s.l.) ranges to the west and south, the Lekanis Mountains (1150 m.a.s.l.) to the east and separated from the Aegean Sea by the Symvolon Range (477 m.a.s.l.) to the southeast, the Drama Basin is a low-elevation basin characteristic for the region. Neogene extensional tectonics led to basin subsidence and the formation of a topogenic fen. Since the mid-Pleistocene, and until the onset of man-made drainage in the 1930s and 1940s, the Philippi peatland was characterized by telmatic and limnic conditions. The sediment accumulated during that time mainly consists of fen peat and lignite along with marls and calcareous clays (Christanis, 1983; compare also review of Pross et al., 2015, and references therein). Sedimentologically, the interval presented here is composed of peat with little contribution of fine-grained clastic material. Sedimentation rates are rather constant between ca. 0.5 and 0.6 mm/yr (Tab. A.3 in the Appendix). For the present study, we applied the age model of Pross et al. (2009), which has been developed for the early to middle Holocene section of the TP-2005 core based on palynological correlation with the well-dated marine core SL152 from the northern Aegean Sea (Kotthoff et al., 2008a, b), radiocarbon dates and additional palynostratigraphical information (Pross et al., 2009). This procedure allows direct correlation of our new geochemical data for the TP-2005 core with the decadal-scale-

resolution palynological data of Pross et al. (2009) from the same core interval. We analyzed 35 peat samples from the depth interval 472–536 cm, which corresponds to the time interval from ca. 8.7 kyr B.P. to ca. 7.5 kyr B.P.; this yields a temporal resolution of our dataset between ca. 15 and ca. 50 years (Tab. 4.1).

4.2.2 Lipid extraction, purification, and quantification

Lipids were extracted from freeze-dried and finely ground sediment samples (ca. 1 g dry weight) with a Büchi Speed Extractor at 100 °C and 100 bar using 20 ml of a mixture of dichloromethane/methanol (9:1) for 10 min, which was repeated 3 times. Total lipid extracts (TLE) were dried under a stream of N₂ at 36 °C and saponified with 1M NaOH at 80 °C for 3 h. Neutral lipids were extracted with hexane and separated by silica-gel column chromatography to neutral (hexane), semi-polar (dichloromethane/hexane 2:1) and polar fractions (methanol). The neutral fraction was subsequently separated by AgNO₃-coated silica using hexane as eluent to obtain saturated hydrocarbons containing the *n*-alkanes.

4.2.3 *n*-alkane concentration

n-alkanes were analyzed by gas chromatography/mass spectrometry (GC/MS) using a Thermo Finnigan Trace GC equipped with a HP-5MS column (30 m x 0.25 mm x 0.25 µm) connected to a Thermo Finnigan DSQ II mass spectrometer at Goethe University Frankfurt. The GC oven was held at 70 °C for 1 min, ramped at 10 °C/min to a final temperature of 320 °C, which was held for 15 min. *n*-alkanes were identified by comparison of their mass spectra and retention time to an external standard containing C₇ to C₄₀ *n*-alkanes (Supelco) at a concentration of 25 ng/µl, and were quantified using TIC peak areas calibrated against the external standard. Precision of the quantification is 96% as inferred from the standard deviation of repeated standard runs (n = 5).

4.2.4 δD measurements

δD values of individual *n*-alkanes were measured at least in triplicate using an Agilent 7890A gas chromatograph (GC) coupled to a Thermo Delta V plus isotope-ratio mass spectrometer (IRMS) via a pyrolysis furnace, operated at 1430 °C. The GC was equipped with a DB-5ms column (30 m x 0.25 mm, 0.25 µm film thickness) and the injector was operated in splitless mode at 320 °C. The GC oven was held at 110 °C for

1 min, ramped at 5 °C/min to 320 °C held for 8 min, and ramped at 30 °C/min to a final temperature of 350 °C. Data processing and the daily H^{3+} correction were accomplished using Isodat v3.0 software as described by Sessions et al. (2001). An external standard containing 19 *n*-alkanes (*n*-C₁₅ to *n*-C₃₃) with known δD values was analyzed periodically to monitor analytical performance, and a drift correction was applied to sample δD values. In addition, an internal standard (*n*-C₃₄) was added to all samples prior to isotope analysis and yielded a standard deviation (1σ) of 3.4 ‰ after offset correction. All measurements were made at MPI-BGC Jena. Values are reported in permil [‰] relative to VSMOW.

4.3 Results

Chain length distributions of TP *n*-alkanes show a strong odd-over-even predominance with long chain *n*-alkane abundances (*n*-C₂₇, *n*-C₂₉ and *n*-C₃₁) typically two to four times higher than those of the mid chain length (*n*-C₂₃ and *n*-C₂₅) compounds (Tab. 4.1). *n*-alkanes of shorter chain lengths (<23) are virtually absent in all investigated samples. δD patterns of all three long chain *n*-alkanes (*n*-C₂₇, *n*-C₂₉ and *n*-C₃₁) are broadly similar and show identical trends (Tab. 4.1, Fig. 4.3). δD values of the most abundant *n*-alkane (*n*-C₂₉) range between -170 ‰ and -225 ‰. δD values of the *n*-C₂₇ and *n*-C₂₉ alkanes attain similar values with offsets of usually <10 ‰ (δD *n*-C₂₇ = -184 ‰ to -223 ‰) whereas δD *n*-C₃₁ values are usually up to 20 ‰ higher compared to δD *n*-C₂₇ and *n*-C₂₉ (δD *n*-C₃₁ = -177 ‰ to -214 ‰). δD *n*-C₂₉ values show an overall decrease with decreasing sampling depth from -185 ‰ in the lowest sample (536 cm) to -222 ‰ at the top of the section (472 cm). From ca. 8.7 to 8.4 kyr B.P. (536 to 515 cm), δD *n*-C₂₉ values continually decrease by about 30 ‰ with δD *n*-C₂₉ = -185 ‰ (536 cm) and δD *n*-C₂₉ = -214 ‰ (515 cm). Most notable is a rapid increase (ca. 30 ‰) in δD *n*-C₂₉ values from -204 ‰ to -173 ‰ (500 to 501 cm) followed by a large magnitude (ca. 45 ‰) negative excursion with δD *n*-C₂₉ = -178 ‰ (498 cm) to δD *n*-C₂₉ = -223 ‰ (495 cm) between ca. 8.1 and 8.0 kyr B.P. (Fig. 4.3: Isotope event 'B'). This pronounced δD event is embedded in a period of generally higher δD *n*-C₂₉ values from ca. 8.15 to 8.0 kyr B.P. (504 to 490 cm). A second, less distinct δD *n*-C₂₉ excursion including a negative shift of ca. 15 ‰ predates isotope event 'B' and occurs around 8.2 kyr B.P. (508 - 505 cm) (Fig. 4.3: Isotope event 'A'). The upper part of the core from ca. 7.9 to 7.5 kyr B.P. (490 to 472 cm) generally has the lowest δD values in all investigated samples, though a marked positive shift of ca. 15 ‰ in δD *n*-C₂₉ characterizes the uppermost part of the section.

Tab. 4.1 δD and CPI values of the long chain *n*-alkanes *n*-C₂₇, *n*-C₂₉ and *n*-C₃₁ from the early to mid-Holocene of core TP-2005 (Carbon Preference Index; $CPI = [\sum_{odd}(C_{21-33}) + \sum_{odd}(C_{23-35})]/[2\sum_{even}(C_{22-34})]$).

Sampling depth [cm]	CPI	δD <i>n</i> -C ₂₇ [‰ VSMOW]	SD	δD <i>n</i> -C ₂₉ [‰ VSMOW]	SD	δD <i>n</i> -C ₃₁ [‰ VSMOW]	SD
472	10.3	-215	3.2	-222	0.3	-213	2.3
475	10.9	-210	1.0	-213	4.0	-200	8.6
478	8.7	-204	3.9	-210	1.6	-203	4.6
481	8.9	-202	0.1	-212	2.5	-202	0.6
484	8.2	-223	1.1	-225	1.3	-211	6.6
487	7.4	-223	1.1	-223	2.5	-214	1.7
490	7.0	-214	2.4	-219	1.1	-202	3.7
491	7.4	-204	3.6	-208	0.4	-200	4.5
492	7.7	-207	5.2	-211	2.9	-198	1.8
493	7.8	-220	2.6	-206	1.1	-200	4.2
494	7.9	-209	3.0	-215	3.1	-198	3.5
495	4.6	-223	3.1	-223	2.2	-203	4.0
496	4.2	-204	0.6	-197	3.4	-187	5.9
497	2.7	-200	0.9	-181	0.4	-182	0.3
498	2.8	-200	4.4	-178	0.8	-181	1.2
499	3.6	-189	4.3	-178	2.9	-183	3.5
500	3.5	-184	3.5	-173	2.1	-189	2.5
501	7.6	-202	2.2	-204	2.6	-193	2.2
502	7.5	-206	2.3	-204	1.0	-191	3.1
503	7.5	-196	3.9	-199	2.7	-187	5.7
504	7.0	-201	4.4	-203	1.2	-190	4.4
505	6.7	-206	3.4	-203	1.3	-193	2.6
506	7.0	-212	3.1	-214	1.3	-199	2.1
507	7.1	-203	2.7	-199	1.5	-188	2.7
508	5.9	-199	4.1	-196	1.9	-181	1.5
509	6.6	-210	3.2	-209	1.0	-202	2.0
512	7.3	-215	4.8	-207	1.4	-196	3.9
515	6.9	-213	3.4	-214	2.1	-202	1.9
518	7.4	-221	3.2	-214	2.4	-202	5.0
521	7.8	-203	3.4	-206	1.9	-196	6.0
524	8.4	-200	8.2	-203	1.1	-196	3.5
527	7.1	-203	3.5	-209	0.4	-197	1.2
530	7.8	-209	6.6	-201	1.3	-195	3.3
533	7.4	-197	5.6	-202	0.2	-193	0.9
536	5.6	-184	3.9	-185	1.4	-177	1.6

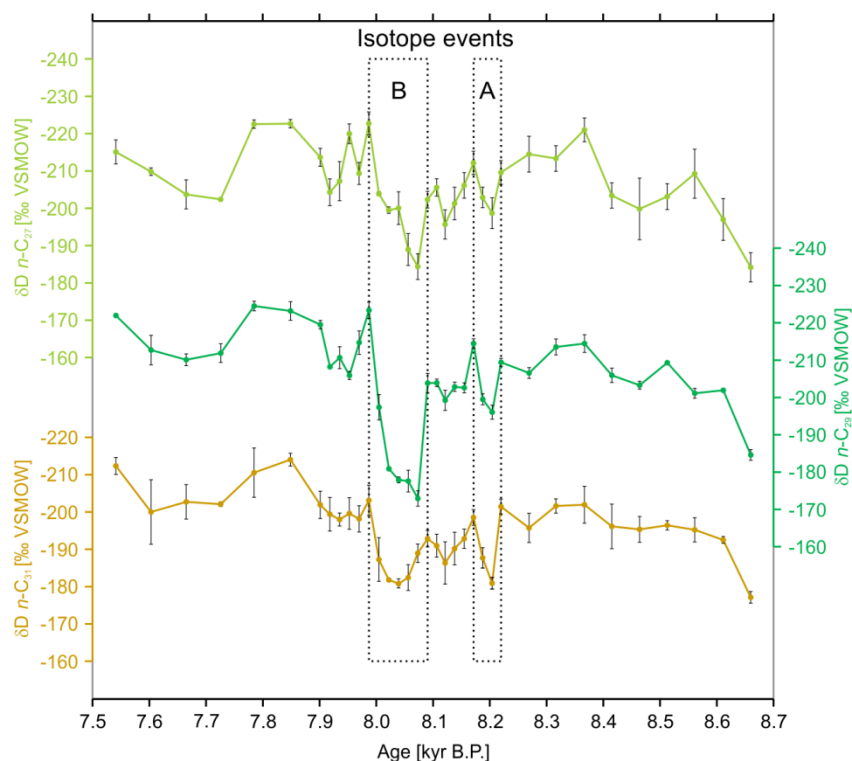


Fig. 4.3 δD isotopic composition of the long chain n -alkanes n -C₂₇, n -C₂₉ and n -C₃₁ of core TP-2005. Dotted boxes indicate isotope events 'A' and 'B' (see text for details).

4.4 Discussion

Long-chain n -alkanes (n -C₂₇, n -C₂₉ and n -C₃₁) are integral parts of epicuticular waxes of vascular terrestrial plants (Eglinton and Eglinton, 2008; Sachse et al., 2012), whereas mid chain length n -alkanes typically represent the contribution of wetland plant species in peat ecosystems (e.g., Baas et al., 2000; Pancost et al., 2002). For the interpretation of our δD_{wax} time series, we focus on the most abundant n -alkane, n -C₂₉. δD_{wax} values are governed by δD of the source water available during plant growth (Sachse et al., 2010; Tipple et al., 2013). The vegetation of the Philippi peatland was dominated by graminoids (mostly Cyperaceae and to a minor extent Poaceae) with the virtual absence of woody plants (Christanis, 1983). Growth of short-rooted plants (e.g., graminoids) mainly occurs in spring and early summer when soil water availability increases (Schwab et al., 2015). Over the time interval presented here, surface conditions in the Philippi peatland were likely dry (in summer) before the onset of full telmatic conditions during the mid-Holocene (Christanis, 1994; Kalaitzidis and Christanis, 2002). Hence, the δD values of soil water during plant growth at TP largely reflect δD_{precip} , enabling the use of δD n -alkane data for precipitation reconstructions (Liu and Huang, 2005; Schefuß et al., 2005; Polissar et al., 2009; Sachse et al., 2012).

Biosynthesis of plant waxes usually results in D-depletion of δD_{wax} compared to source water δD values. However, net fractionation factors are assumed to be rather constant

for a given plant type but need to be considered in paleoenvironments where large vegetation shifts have occurred (Chikaraishi and Naraoka, 2003; Smith and Freeman, 2006; Pedentchouk et al., 2008; Sachse et al., 2012). The vegetation of the Philippi peatland was stable at least over the last 30 kyr (Christanis, 1983). Climatic changes over that interval mainly led to shifts in the vegetation surrounding the Drama Basin. Pollen data document a massive reduction in total tree and *Quercus* pollen on the mountain slopes bordering the Drama Basin (Pross et al., 2009). A comparison between the decline in tree pollen and δD_{wax} values reveals that the most pronounced δD_{wax} excursion (Isotope event 'B') occurs during the recovery of the tree population in the region back to pre-8.2 kyr climatic event levels, whereas isotope event 'A' develops shortly before the massive tree-pollen decline (Fig. 4.4a, b). We expect the plant wax contribution from the surrounding vegetation to be minor compared to plant waxes derived from *in situ* production within the peatland. Therefore, a bias of δD_{wax} in response to vegetation shifts over the interval of the 8.2 kyr B.P. climatic event appears unlikely.

4.4.1 Environmental influences on δD_{wax}

Three key variables need to be considered to interpret changes in δD_{wax} at TP during the early to mid-Holocene transition: 1) Effects of changes in atmospheric circulation patterns and moisture transport on δD_{precip} , 2) influence of regional paleoclimatic change on δD_{wax} variability and 3) changes in SST and δD in the moisture source area(s).

4.4.1.1 Effects of changes in atmospheric circulation patterns and moisture transport on δD_{precip}

Changes in atmospheric circulation over the Mediterranean basin affect δD_{precip} values by modifying the relative contribution of water vapor from different source regions. Analysis of present day wind fields over Greece and the Aegean Sea provides insight into the potential magnitude of such changes: Throughout most of the year precipitation over the Aegean region is controlled by continental, northerly-derived air masses, related to the strength of the Siberian High (Poulos et al, 1997). These air masses typically carry D-depleted moisture due to generally lower ambient air temperatures and longer (continental) air mass trajectories. During spring and fall, in turn, warmer, marine southerly winds with a strong evaporative component of the proximal Mediterranean Sea are common and result in D-enriched precipitation (Poulos et al., 1997; Argiriou and Lykoudis, 2006; Dotsika et al., 2010, Schemmel et al., 2013). Hence, varying relative

contributions of northerly- and southerly-derived air masses to local precipitation in northeastern Greece will strongly affect δD_{precip} . Based on the effect of present-day atmospheric circulation on δD_{precip} , we propose that changes of δD_{wax} values at TP reflect shifts in the predominant air mass trajectories. The strong positive excursions in δD_{wax} between ca. 8.1 and 8.0 kyr B.P. and around 8.2 kyr B.P. (Isotope events 'A' and 'B', Fig. 4.4a) indicate abrupt atmospheric circulation changes, likely related to atmospheric reorganization during the 8.2 kyr B.P. climatic event. Increasing relative contribution of high- δD , southerly-derived water vapor with a strong Mediterranean component and decreasing contribution of low- δD , northerly-derived water vapor from a distal water source leads to a pronounced increase in δD in local precipitation. Likewise, increasingly lower δD_{wax} values between ca. 8.7 and 8.2 kyr B.P. suggest a long-term increase of northerly-derived moisture to local precipitation prior to the 8.2 kyr B.P. climatic event. The pattern in δD_{wax} between ca. 7.9 and 7.5 kyr B.P. reveals a more complex pattern with varying contributions of southerly (higher δD_{wax} values) and northerly sources (lower δD_{wax} values).

4.4.1.2 Influence of regional paleoclimatic change on δD_{wax} variability

Decadal- to centennial-scale resolution palynological analyses from TP have provided detailed insight into paleoclimatic changes in northeastern Greece during the early and middle Holocene (Wijmstra, 1969; Pross et al., 2009; Müller et al, 2011). Pollen-based climate reconstructions suggest a strong change in precipitation amount and seasonality at TP associated with the 8.2 kyr B.P. climatic event (Peyron et al., 2011). Collectively, the pollen data point to a gradual increase of both summer and winter precipitation around 8.3 kyr B.P. that abruptly turned into a significant decrease in precipitation seasonality between ca. 8.1 and 8.0 kyr B.P., with a corresponding increase (decrease) in summer (winter) rainfall amount (Fig. 4.4d). When compared to the δD_{wax} record, the decrease in seasonality coincides with the marked positive shift in δD_{wax} ($\Delta\delta D_{\text{wax}} \approx 30 \text{ ‰}$) during isotope event 'B' (Fig. 4.4a, d: dark gray area). The close temporal correlation between changes in rainfall seasonality and the increase in δD_{wax} values collectively support the interpretation that δD_{wax} reflects changes in air mass trajectories. Accordingly, we suggest an increase of southerly-derived, D-enriched moisture between ca. 8.1 and 8.0 kyr B.P. with a strong Mediterranean component during plant growth. In addition to precipitation source and seasonality, TP δD_{wax} values may be influenced by changes in ambient air temperature. Today, rainfall seasonality, temperature and δD_{precip} in Greece are closely correlated, resulting in lower δD_{precip} values in winter and higher

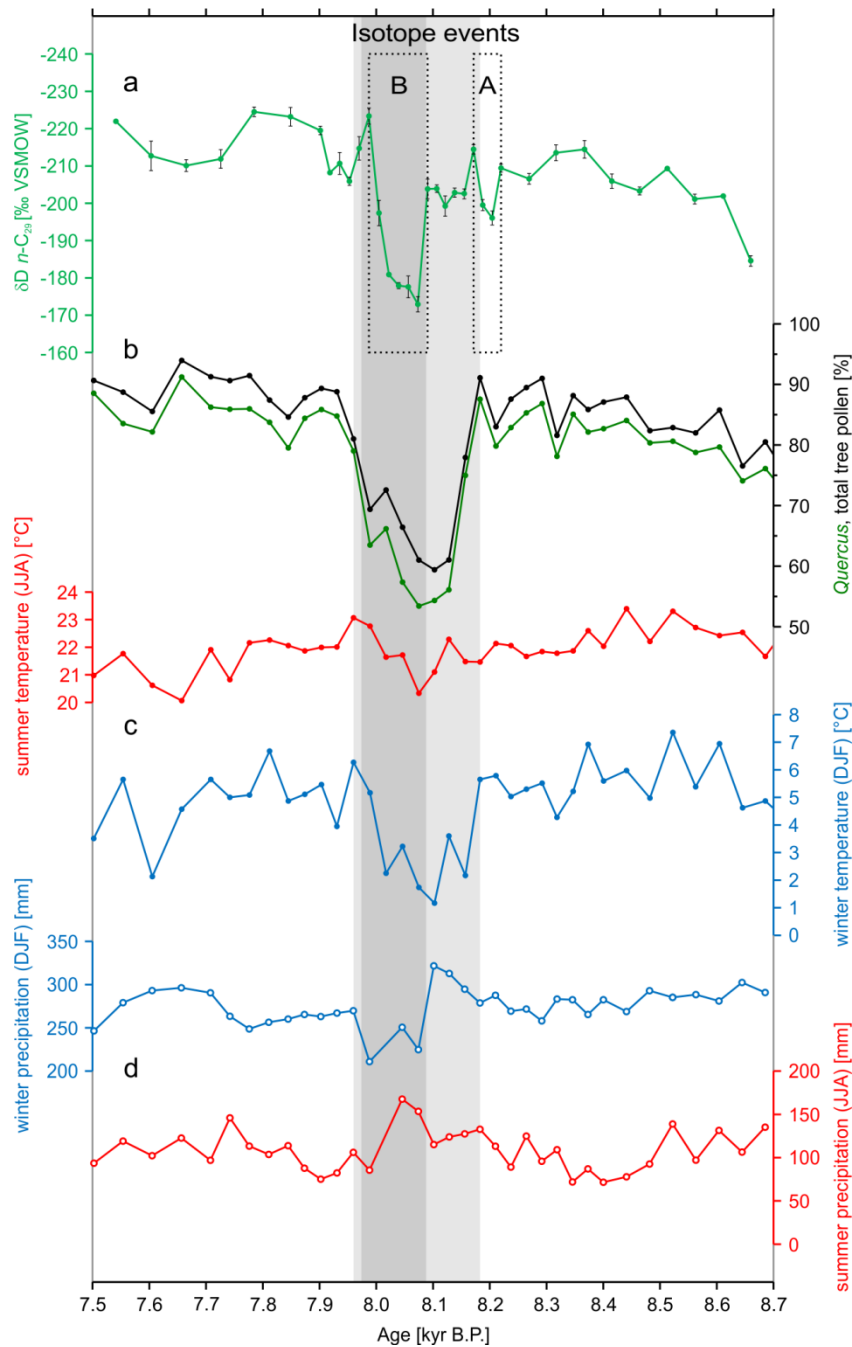


Fig. 4.4 Comparison of δD_{wax} of core TP-2005 to local paleoclimatic parameters. a. $\delta D n-C_{29}$ (this study). b. Tree pollen percentages (Pross et al., 2009). c. Seasonal summer and winter temperatures (Pross et al., 2009). d. Seasonal summer and winter precipitation (Peyron et al., 2011). Light gray area indicates duration of winter cooling at TP in response to the 8.2 kyr B.P. climatic event (Fig. 4.4c). Dark gray area indicates period of decreased precipitation seasonality (Fig. 4.4d). Dotted boxes indicate isotope events 'A' and 'B' (see text for details).

values in summer (Argiriou and Lykoudis, 2006). Therefore, changes in air temperature and their potential effect on δD_{precip} over the course of the Holocene need to be considered, especially in relation to 8.2 kyr cooling. If temperature had been the major driver of δD_{precip} during the 8.2 kyr B.P. climatic event, we would expect δD_{wax} to be D-depleted in response to cooling (Dansgaard, 1964). However, the δD_{wax} record displays a D-enrichment of up to 30 ‰ during that interval. Although we cannot fully

exclude the influence of temperature change on δD_{wax} (which would have “dampened” the magnitude of the observed D-enrichment), it is unlikely that temperature had a significant effect on δD_{precip} . This conclusion is supported by pollen-derived summer and winter temperature reconstructions from TP, showing a strong response to 8.2 kyr cooling, mainly expressed by lower winter temperatures (Pross et al., 2009). The decline in winter temperature in the Philippi peatland, related to strengthening of the influence of the Siberian High on northeastern Greece, set in at around 8.2 kyr B.P., whereas the strong positive δD_{wax} excursion is delayed by about 100 years (Fig. 4.4a, c: light gray areas). The pattern of isotope event 'B' displays no resemblance with the duration of pronounced winter cooling, making (winter) temperature change an unlikely cause for the observed δD_{wax} variations. However, the generally increased δD_{wax} values between ca. 8.15 and 8.0 kyr B.P. may be related to changes in the moisture source areas in the North Atlantic in response to the 8.2 kyr B.P. climatic event (LeGrande and Schmidt, 2008; see Section 4.4.1.3). Additionally, evaporation of soil water as well as transpiration from plant leaves can lead to D-enrichment in plant lipids, especially in summer, which may amplify or diminish changes in δD_{precip} and δD_{wax} (Sachse et al., 2012; Kahmen et al., 2013a, b). Considering the climatic changes in northeastern Greece during the 8.2 kyr B.P. climatic event we only expect little changes in evaporative enrichment. With minor fluctuations in temperature together with increase in summer precipitation between ca. 8.1 and 8.0 kyr B.P. (Fig. 4.4c, d), neither evaporation from soil water nor transpiration of leaf water are likely to have exerted dominant control on δD_{wax} values compared to pre- and post-8.2 kyr B.P. climatic event Holocene conditions.

4.4.1.3 Changes in SST and δD in the moisture source area(s)

During the 8.2 kyr B.P. climatic event, variations in sea-surface temperature (SST) and isotopic composition in the North Atlantic source area may have contributed to shifts in δD_{precip} at TP. With the Northern Atlantic Ocean and the Mediterranean Sea as ultimate sources for precipitation (Flocas and Giles, 1991), changes in δD of source water can directly influence δD_{precip} , whereas SST changes affect evaporation of source water and the isotopic fractionation between source water and water vapor. For the early and middle Holocene, SST reconstructions reveal a complex pattern in the North Atlantic and Mediterranean Sea including increased SST in response to orbital forcing and relative cooling in relation to the 8.2 kyr B.P. climatic event (Marchal et al., 2002; Rohling et al., 2002; Gogou et al., 2007; Marino et al., 2009; Siani et al., 2010). However, a lack of response to rapid northern hemisphere cooling or even responses of the opposite sign have also been reported (Kallel et al., 1997; Emeis et al., 2000; Sangiorgi et al., 2003;

Mayewski et al., 2004). The absence of clear trends in source water conditions during the studied interval is corroborated by marine $\delta^{18}\text{O}$ values showing both higher (Emeis et al., 2000; Rohling et al., 2002; Sangiorgi et al., 2003; Risebrobakken et al., 2003; Geraga et al., 2010) and lower $\delta^{18}\text{O}$ values (Kallel et al., 1997; Marino et al., 2009; Siani et al., 2010) during the 8.2 kyr B.P. climatic event. Collectively, the observed patterns of changing SST and marine stable oxygen isotopic composition are insufficient to explain the pattern and magnitude of changes in $\delta\text{D}_{\text{wax}}$ at TP during isotope events 'A' and 'B' (Fig. 4.4a). Still, 8.2 kyr freshwater forcing in the North Atlantic Ocean has been suggested to affect $\delta^{18}\text{O}_{\text{precip}}$ over the Eastern Mediterranean and Aegean region (LeGrande and Schmidt, 2008). The projected increase of less than 0.3 ‰ in $\delta^{18}\text{O}_{\text{precip}}$, however, would only translate into an increase of ca. 2-3 ‰ in $\delta\text{D}_{\text{precip}}$ (Rozanski et al., 1993). Hence, freshwater forcing alone does not suffice to produce the large changes in $\delta\text{D}_{\text{wax}}$ of isotope events 'A' and 'B', but may contribute to the generally increased $\delta\text{D}_{\text{wax}}$ values during the 8.2 kyr B.P. climatic event (winter) cooling between ca. 8.15 and 8.0 kyr B.P. (Fig. 4.4a, c: light gray area).

4.5 Mechanisms

As a result of the above considerations, we suggest changes in atmospheric circulation to be the dominant control on $\delta\text{D}_{\text{wax}}$ values at TP during the 8.2 kyr B.P. climatic event. Varying contributions of D-depleted, northerly-derived as opposed to D-enriched, southerly-derived moisture transported to the Philippi peatland strongly affected the isotopic composition of local precipitation during the early and middle Holocene. However, increasing contributions from a proximal source together with the strong change in precipitation seasonality implies a major reorganization in large-scale atmospheric circulations over the Aegean region during the 8.2 kyr B.P. climatic event that is strong enough to overcome typical Mediterranean climate patterns.

4.5.1 The 8.2 kyr B.P. climatic event

Strong anticyclonic activity over the Mediterranean basin in summer inhibits lifting of air masses, providing a limiting factor for cloud formation and in turn contributing to the prevailing dry conditions characteristic for the Mediterranean region (e.g., Lionello et al., 2006). The close temporal correlation between isotope events 'A' and 'B' and increasing summer precipitation (Fig. 4.4a, d) implies weakening of the predominant anticyclonic

activity in the Aegean region, leading to a relative increase in moist air from proximal, Mediterranean sources.

4.5.1.1 Influence of the Asian summer monsoon

Climate proxy records suggest teleconnections between northern hemisphere 8.2 kyr cooling and the monsoonal circulation systems (Wang et al., 2005; Cheng et al., 2009; Liu et al., 2013). High-resolution $\delta^{18}O$ stalagmite records from China and Oman reveal a

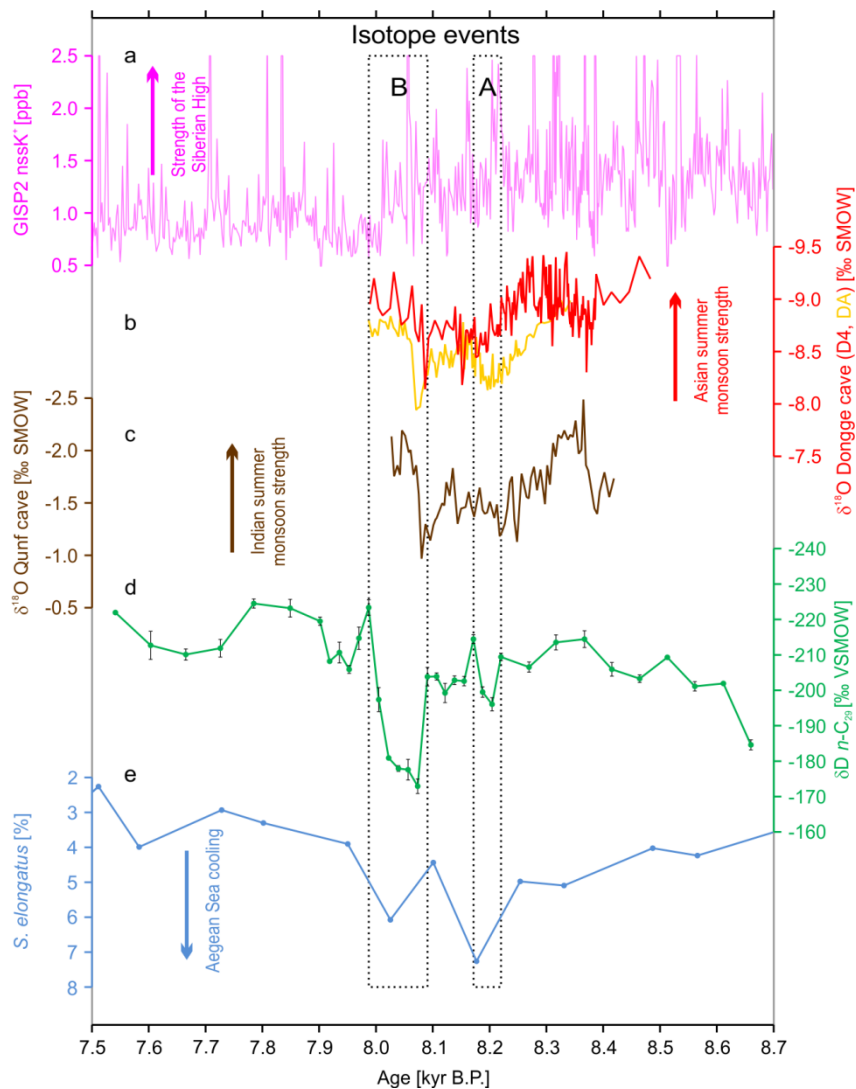


Fig. 4.5 Comparison of δD_{wax} of core TP-2005 to regional and supraregional paleoclimatic parameters. a. Non sea-salt potassium record from GISP2 ice core, Greenland (Mayewski et al., 1997). b. Speleothem $\delta^{18}O$ records from Dongge cave, China (Cheng et al., 2009). c. Speleothem $\delta^{18}O$ records from Qunf cave, southern Oman (Cheng et al., 2009). d. $\delta D n-C_{29}$ (this study). e. Relative amount of cold water dinocyst species *Spiniferites elongatus* from the Central Aegean Sea (Marino et al., 2009). Dotted boxes indicate isotope events 'A' and 'B' (see text for details). All previously published records have been plotted using their original age models.

distinct 'double-plunging' structure of Asian summer monsoon weakening at ca. 8.21 ± 0.02 kyr B.P. and 8.08 ± 0.03 kyr B.P., both convincingly correlated to climatic changes associated with the 8.2 kyr B.P. climatic event (Fig. 4.5b, c; Cheng et al., 2009). The Asian summer monsoon system influences the upper troposphere Rossby wave pattern (Rodwell and Hoskins 1996), a major forcing factor for anticyclonic centers over the Eastern Mediterranean region in summer. Changes in the strength of the Asian summer monsoon systems have the potential to alter the Rossby wave pattern, influencing the strength and/or positioning of the Eastern Mediterranean anticyclones, and inhibiting (or favoring) the formation of summer rainfall derived from the Eastern Mediterranean Sea through stabilizing or destabilizing atmospheric conditions (Staubwasser and Weiss, 2006). The weakening of the Asian summer monsoon systems during the 8.2 kyr B.P. climatic event (Cheng et al., 2009) may have reduced subsidence over the Eastern Mediterranean region by reducing the strength and/or shifting the centers of anticyclonic activity through Rossby wave propagation. The reduction in subsidence, in turn, would have favored decreased atmospheric stability that allowed an increase in ascending air masses from the Mediterranean basin and a potential increase in (summer) rainfall sourced from the Eastern Mediterranean region (Fig. 4.6).

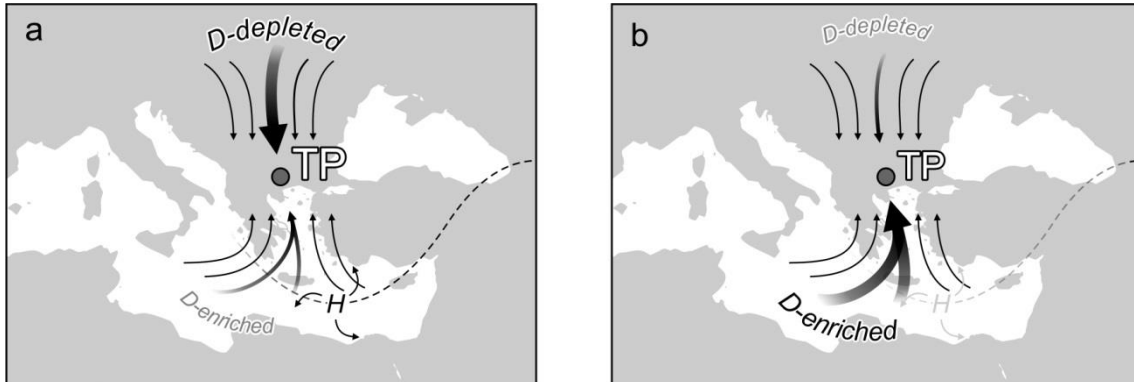


Fig. 4.6 Schematic figures of principal air mass trajectories affecting the Drama Basin before and after (a) and during (b) the isotope events occurring in relation to the 8.2 kyr B.P. climatic event. Bold arrows indicate increased contribution of D-depleted (a) and D-enriched (b) moisture to local precipitation. Dashed line represents the influence of the Asian Monsoon Systems on Eastern Mediterranean anticyclones through Rossby wave propagation.

The close temporal correlation (within dating uncertainties) between the strong D-enrichment in δD_{wax} during isotope event 'B', increase in summer precipitation and renewed weakening of the Asian summer monsoon systems at 8.08 ± 0.03 kyr B.P. (Fig. 4.5b, c, d) suggests a decreasing influence of anticyclonic activity over the Aegean Sea. Decreased subsidence favors an increase in ascending air masses over this proximal source, eventually producing increased amounts of D-enriched precipitation at TP. Interestingly, the reduction in Asian summer monsoon strength at 8.21 ± 0.02 kyr

B.P. only correlates with a weak positive D-excursion and a minor increase in summer precipitation during isotope event 'A' (Fig. 4.5b, c, d). However, the strength of the Siberian High increased prior to ca. 8.1 kyr B.P. (Fig. 4.5a; Mayewski et al., 1997; Meeker and Mayewski, 2002). This may indicate a stronger northerly component in precipitation over the Drama Basin and the Philippi peatland during that time. The influence exerted by the strong Siberian High before ca. 8.1 kyr B.P. likely limited the inflow of southerly winds and reduced the amounts of Mediterranean-sourced, D-enriched precipitation in favor of D-depleted moisture derived from a distal source. The weakening of the Siberian High after ca. 8.1 kyr B.P. could have translated into a decreasing influence of northerly winds on the Drama Basin and the Philippi peatland accordingly, highlighting the responsiveness of the region to high- and low-latitude climate forcing.

4.5.1.2 Hadley circulation

Present-day Mediterranean summer aridity is reinforced by seasonal latitudinal shifts of the descending branch of the Hadley cell and associated anticyclonic activity (e.g., Lionello et al., 2012). In response to peak summer insolation, the early Holocene ITCZ and the associated climate systems of the Indian and African monsoons extended further north than at present (Haug et al., 2001; Fleitmann et al., 2003; Tzedakis, 2007). Accordingly, dry summer conditions in the northern Mediterranean borderlands may have been enhanced (Jones et al., 2006; Tinner et al., 2009). Both model studies and proxy data show a southward shift of the ITCZ and corresponding weakening of monsoonal circulation in response to northern hemisphere cooling and reduction of the AMOC (Haug et al., 2001; Fleitmann et al., 2003; Chiang and Bitz, 2005; Broccoli et al., 2006). A southward shift at ca. 8 kyr B.P., possibly related to tropical Atlantic Ocean cooling (deMenocal et al., 2000; Chiang and Bitz, 2005), may have weakened the influence of the prevailing Hadley circulation over the Mediterranean region, thus reducing the strength of the Azores High, allowing the penetration of westerly winds into the Mediterranean basin and leading to increased cyclogenesis (Gaetani et al., 2007; Lionello et al., 2012). The resulting increase in the contribution of D-enriched, Mediterranean-derived moisture to local precipitation would explain both the increased variability in δD_{wax} between ca. 8.2 and 8.0 kyr B.P. as well as generally higher summer precipitation during that time (Fig. 4.5a, d: light gray area). Hence, the intensification of eastward-moving cyclones over the Mediterranean Sea in summer is likely to have transport D-enriched moisture to northeastern Greece (Hatzianastassiou et al., 2007).

4.5.1.3 'Mediterranean Monsoon'

A third option for increasing amounts of D-enriched precipitation during isotope events 'A' and 'B' is a regional 'Mediterranean Monsoon' (Arz et al., 2003). Increased land-sea temperature differences during the 8.2 kyr B.P. climatic event could have allowed inflow of moist air masses from the Aegean Sea, hence increasing D-enriched regional precipitation at TP. Even though the 'Mediterranean Monsoon' was originally proposed as a driving mechanism for higher precipitation in the Southeastern Mediterranean region during summer insolation maxima, several lines of evidence suggest that a similar mechanism may have contributed to increased summer precipitation over the Philippi peatland and to the positive shifts in precipitation derived δD_{wax} values. A high-resolution record of central Aegean SST shows two concise temperature minima at ca. 8.2 kyr B.P. and ca. 8.05 kyr B.P. (Fig. 4.5e; Marino et al., 2009). Terrestrial summer temperatures at TP over the same time interval are uniformly high with very little variation (Fig. 4.4c; Pross et al., 2009). High terrestrial summer temperatures may have induced regional thermal lows strong enough to overcome the prevailing anticyclonic activity, drawing in moist air masses from the Aegean Sea. Episodes of Aegean Sea cooling have generally been explained by stronger influence of the Siberian High in winter and spring (Rohling et al., 2002; Kotthoff et al., 2008a) and may have persisted into the summer months due to higher thermal inertia of sea water. Elevated land-sea temperature differences at ca. 8.2 kyr B.P. and ca. 8.05 kyr B.P. may have promoted inflow of proximal, D-enriched moisture into the Drama Basin and the Philippi peatland, thus contributing to increasing summer precipitation amounts with higher δD values during isotope events 'A' and 'B'.

4.5.2 Stable isotopes in precipitation prior and after the 8.2 kyr B.P. climatic event

In addition to the characterization of changing air mass trajectories during the 8.2 kyr B.P. climatic event, the δD_{wax} record allows the investigation of the influence of atmospheric circulation changes on precipitation patterns during the early and middle Holocene. Pollen-based reconstructions show relatively stable temperature and precipitation conditions before ca. 8.2 kyr B.P. and after ca. 8.0 kyr B.P. (Fig. 4.4c, d). δD_{wax} values over the same periods show remarkable similarities and suggest common climate forcing in the Drama Basin prior to and after the northern hemisphere cooling event. By applying a similar pattern of varying contributions of southerly-derived, D-enriched and northerly-derived, D-depleted vapor to local precipitation, changes in δD_{wax} values can be linked to atmospheric circulation changes between ca. 8.7 and 7.5 kyr B.P.. The time interval presented here broadly coincides with the formation of

sapropel S1 in the Aegean Sea between ca. 9 and 7 kyr B.P.. The prevailing strong influence of the low-latitude climate systems on the Aegean region was punctuated by the increased strength of the Siberian High in winter and spring between ca. 8.4 and 8.0 kyr B.P., which caused an interruption in the formation of Sapropel S1 and thereby a subdivision of Sapropel S1 into an older S1a and a younger S1b interval (e.g., Rohling et al., 2002; Kotthoff et al., 2008a). The steep decrease in δD_{wax} prior to ca. 8.4 kyr B.P. could be the reflection of long-term changes in the relative contributions of different air masses to local precipitation with a gradual increase in D-depleted, northerly-derived moisture (strengthening of the Siberian High) and a corresponding decrease in D-enriched, southerly-derived moisture (weakening of the lower-latitude monsoonal circulation) on the Aegean region including the Philippi peatland.

Regional climate of the Northern and Eastern Mediterranean region during S1b has been characterized as increasingly humid (Kallel et al., 1997; Kotthoff et al., 2008a). Taking into account dating uncertainties and climatic differences based on the general heterogeneity of Mediterranean climate, a general picture of relatively high precipitation amounts with the distinct possibility of heavy rainstorms across all seasons emerges for the time period from ca. 8 kyr B.P. well into the mid-Holocene (Bar-Matthews et al., 1999, 2000; Zanchetta et al., 2007; Göktürk et al., 2011; Zhornyak et al., 2011). Increasing annual and seasonal precipitation amounts at TP (Pross et al., 2009; Peyron et al., 2011) as well as D-enrichment of δD_{wax} starting around 7.8 kyr B.P. mirror this trend (Fig. 4.4a, c, d). It has been hypothesized that increased advection from the Mediterranean Sea as opposed to the otherwise dominant westerly flow of Atlantic-derived precipitation caused higher rainfall during S1b (Kallel et al., 1997; Spötl et al., 2010). Higher relative proportions of proximally sourced, D-enriched precipitation during plant growth after ca. 7.8 kyr B.P. could explain the observed stable isotopic shift towards higher δD values.

4.6 Conclusions

δD values of long chain plant wax *n*-alkanes *n*-C₂₇, *n*-C₂₉ and *n*-C₃₁ from Tenaghi Philippon reflect changes in δD of precipitation. We identify two intervals of pronounced increase in δD_{wax} during the 8.2 kyr B.P. climatic event. The strongest δD_{wax} excursion (Isotope event 'B') between ca. 8.1 and 8.0 kyr B.P. coincides with the recovery of regional vegetation to pre-8.2 kyr climatic event levels. A second interval of increased δD_{wax} values around 8.2 kyr B.P. (Isotope event 'A') precedes the major vegetation turnover. The temporal discrepancy between the (winter) temperature driven responses

in terrestrial vegetation and δD_{wax} values implies strong variations in Eastern Mediterranean atmospheric circulation affecting δD_{precip} during the 8.2 kyr B.P. climatic event.

We propose that the observed changes in δD_{wax} , especially during isotope events 'A' and 'B', are primarily caused by changes in the relative contributions of different air masses (with different δD values) to local precipitation. The ensuing δD_{precip} changes are driven by decreasing amounts of predominantly northerly winds (D-depleted precipitation) due to a distal water source and complex air mass trajectories, and an increase in southerly winds (D-enriched moisture) with a strong Mediterranean component. Our interpretation of atmospheric circulation changes causing higher amounts of precipitation originating in the Mediterranean and/or Aegean Sea is supported by pollen-derived precipitation reconstructions from TP. Possible atmospheric mechanisms favoring the ascension of air masses and subsequent increase in Mediterranean-sourced precipitation during plant growth include hemispheric teleconnections between the African and Asian monsoon systems and the influence of the Siberian High as well as a regional mechanism of increased land-sea-temperature difference. The influence of high and low latitude climate systems on terrestrial climate patterns at TP is further supported by trends in δD_{wax} during the pre- and post-8.2 kyr climatic event time intervals. This study highlights the sensitivity of Mediterranean climate dynamics to variations in high and low latitude climate circulations in relation to rapid climate change and may provide insight into future challenges for the Mediterranean region under the looming threat of anthropogenic global warming.

4.7 Acknowledgements

FS, EMN, AM and JP acknowledge support through the LOEWE funding program (Landes-Offensive zur Entwicklung wissenschaftlich-ökonomischer Exzellenz) of Hesse's Ministry of Higher Education, Research, and the Arts. JP acknowledges funding by the German Research Foundation (DFG; grant PR 651/3). We thank U. Treffert (Senckenberg BiK-F, Frankfurt), U. Müller, T. Potouridis, W. Püttmann (Goethe University Frankfurt), A. Koutsodendris (University of Heidelberg), and F. Günther, S. Rühlow and A. Thiele (all MPI Jena) for valuable technical assistance. We thank two anonymous reviewers for their suggestions that significantly improved the manuscript.

4.8 References

- Alley, R. B., and Ágústssdóttir, A. M., 2005, The 8k event: cause and consequences of a major Holocene abrupt climate change: *Quaternary Science Reviews*, v. 24, no. 10-11, p. 1123–1149, doi: 10.1016/j.quascirev.2004.12.004.
- Alley, R. B., Mayewski, P. A., Sowers, T., Stuiver, M., Taylor, K. C., and Clark, P. U., 1997, Holocene climatic instability: A prominent, widespread event 8200 yr ago: *Geology*, v. 25, no. 6, p. 483–486, doi: 10.1130/0091-7613(1997)025<0483.
- Argiriou, A. A., and Lykoudis, S., 2006, Isotopic composition of precipitation in Greece: *Journal of Hydrology*, v. 327, no. 3-4, p. 486–495, doi: 10.1016/j.jhydrol.2005.11.053.
- Arz, H. W., Lamy, F., Pätzold, J., Muller, P. J., and Prins, M., 2003, Mediterranean moisture source for an early-Holocene humid period in the northern Red Sea.: *Science*, v. 300, no. 5616, p. 118–21, doi: 10.1126/science.1080325.
- Baas, M., Pancost, R., Van Geel, B., and Damste, J.S.S., 2000, A comparative study of lipids in Sphagnum species: *Organic Geochemistry*, v. 31, p. 535–541, doi:10.1016/S0146-6380(00)00037-1.
- Barber, D. C., Dyke, A., Hillaire-Marcel, C., Jennings, A. E., Andrews, J. T., Kerwin, M. W., Bilodeau, G., McNeely, R., Southon, J., Morehead, M. D., and Gagnon, J.-M., 1999, Forcing of the cold event of 8,200 years ago by catastrophic drainage of Laurentide lakes: *Nature*, v. 400, no. July, p. 344–348, doi: 10.1038/22504.
- Bar-Matthews, M., Ayalon, A., Kaufman, A., and Wasserburg, G. J., 1999, The Eastern Mediterranean paleoclimate as a reflection of regional events: Soreq cave, Israel: *Earth and Planetary Science Letters*, v. 166, no. 1-2, p. 85–95, doi: 10.1016/S0012-821X(98)00275-1.
- Bar-Matthews, M., Ayalon, A., and Kaufman, A., 2000, Timing and hydrological conditions of Sapropel events in the Eastern Mediterranean, as evident from speleothems, Soreq cave, Israel: *Chemical Geology*, v. 169, no. 1-2, p. 145–156, doi: 10.1016/S0009-2541(99)00232-6.
- Bauer, E., Ganopolski, A., and Montoya, M., 2004, Simulation of the cold climate event 8200 years ago by meltwater outburst from Lake Agassiz: *Paleoceanography*, v. 19, no. 3, p. 1–13, doi: 10.1029/2004PA001030.
- Berger, J.-F., and Guilaine, J., 2009, The 8200calBP abrupt environmental change and the Neolithic transition: A Mediterranean perspective: *Quaternary International*, v. 200, no. 1-2, p. 31–49, doi: 10.1016/j.quaint.2008.05.013.
- Broccoli, A. J., Dahl, K. A., and Stouffer, R. J., 2006, Response of the ITCZ to Northern Hemisphere cooling: *Geophysical Research Letters*, v. 33, no. 1, p. n/a–n/a, doi: 10.1029/2005GL024546.
- Cheng, H., Fleitmann, D., Edwards, R. L., Wang, X., Cruz, F. W., Auler, A. S., Mangini, A., Wang, Y., Kong, X., Burns, S. J., and Matter, A., 2009, Timing and structure of the 8.2 kyr B.P. event inferred from ^{18}O records of stalagmites from China, Oman, and Brazil: *Geology*, v. 37, no. 11, p. 1007–1010, doi: 10.1130/G30126A.1.
- Chiang, J. C. H., and Bitz, C. M., 2005, Influence of high latitude ice cover on the marine Intertropical Convergence Zone: *Climate Dynamics*, v. 25, no. 5, p. 477–496, doi: 10.1007/s00382-005-0040-5.
- Chikaraishi, Y., and Naraoka, H., 2003, Compound-specific δD – $\delta^{13}\text{C}$ analyses of *n*-alkanes extracted from terrestrial and aquatic plants: *Phytochemistry*, v. 63, no. 3, p. 361–371, doi: 10.1016/S0031-9422(02)00749-5.

- Christanis, K., 1983, Genese und Fazies der Torf-Lagerstätte von Philippi (Griechisch-Mazedonien) als Beispiel der Entstehung einer Braunkohle-Lagerstätte vom stark telmatischen Typ: Technische Universität Carolo-Wilhelmina zu Braunschweig.
- Christanis, K., 1994, The genesis of the Nissi peatland (northwestern Greece) as an example of peat and lignite deposit formation in Greece: *International Journal of Coal Geology*, v. 26, p. 63–77, doi: 10.1016/0166-5162(94)90032-9.
- Dansgaard, W., 1964, Stable isotopes in precipitation: *Tellus*, v. 16, n. 4, p. 436–468, <http://dx.doi.org/10.1111/j.2153-3490.1964.tb00181.x>
- deMenocal, P., Ortiz, J., Guilderson, T., and Sarnthein, M., 2000, Coherent High- and Low-Latitude Climate Variability During the Holocene Warm Period: *Science*, v. 288, no. 5474, p. 2198–2202, doi: 10.1126/science.288.5474.2198.
- Dormoy, I., Peyron, O., Combourieu Nebout, N., Goring, S., Kotthoff, U., Magny, M., and Pross, J., 2009, Terrestrial climate variability and seasonality changes in the Mediterranean region between 15 000 and 4000 years BP deduced from marine pollen records: *Climate of the Past*, v. 5, no. 4, p. 615–632, doi: 10.5194/cp-5-615-2009.
- Dotsika, E., Lykoudis, S., and Poutoukis, D., 2010, Spatial distribution of the isotopic composition of precipitation and spring water in Greece: *Global and Planetary Change*, v. 71, no. 3-4, p. 141–149, doi: 10.1016/j.gloplacha.2009.10.007.
- Eglinton, T. I., and Eglinton, G., 2008, Molecular proxies for paleoclimatology: *Earth and Planetary Science Letters*, v. 275, no. 1-2, p. 1–16, doi: 10.1016/j.epsl.2008.07.012.
- Emeis, K.-C., Struck, U., Schulz, H.-M., Rosenberg, R., Bernasconi, S., Erlenkeuser, H., Sakamoto, T., and Martinez-Ruiz, F., 2000, Temperature and salinity variations of Mediterranean Sea surface waters over the last 16,000 years from records of planktonic stable oxygen isotopes and alkenone unsaturation ratios: *Palaeogeography, Palaeoclimatology, Palaeoecology*, v. 158, p. 259–280, doi: 10.1016/S0031-0182(00)00053-5.
- Fleitmann, D., Burns, S. J., Mudelsee, M., Neff, U., Kramers, J., Mangini, A., and Matter, A., 2003, Holocene forcing of the Indian monsoon recorded in a stalagmite from southern Oman.: *Science*, v. 300, no. 5626, p. 1737–9, doi: 10.1126/science.1083130.
- Fletcher, W. J., Müller, U. C., Koutsodendris, A., Christanis, K., and Pross, J., 2013, A centennial-scale record of vegetation and climate variability from 312 to 240 ka (Marine Isotope Stages 9c-a, 8 and 7a) from Tenaghi Philippon, NE Greece: *Quaternary Science Reviews*, v. 78, p. 108-125, doi: 10.1016/j.quascirev.2013.08.005.
- Flocas, A. A. and Giles, B. D., 1991, Distribution and intensity of frontal rainfall over Greece: *International Journal of Climatology*, v. 11, no. 4, p. 429-442, doi: 10.1002/joc.3370110407
- Gaetani, M., Baldi, M., Dalu, G. A., and Maracchi, G., 2007, Connessioni tra il clima della regione Mediterranea e l’Africa Occidentale attraverso la circolazione meridiana di Hadley, *in* *Clima e cambiamenti climatici*, Consiglio Nazionale delle Ricerche, Roma, p. 23–26.
- Geraga, M., Ioakim, C., Lykousis, V., Tsaila-Monopolis, S., and Mylona, G., 2010, The high-resolution palaeoclimatic and palaeoceanographic history of the last 24,000 years in the central Aegean Sea, Greece: *Palaeogeography, Palaeoclimatology, Palaeoecology*, v. 287, no. 1-4, p. 101–115, doi: 10.1016/j.palaeo.2010.01.023.

- Gogou, A., Bouloubassi, I., Lykousis, V., Arnaboldi, M., Gaitani, P., and Meyers, P. A., 2007, Organic geochemical evidence of Late Glacial–Holocene climate instability in the North Aegean Sea: Palaeogeography, Palaeoclimatology, Palaeoecology, v. 256, no. 1-2, p. 1–20, doi: 10.1016/j.palaeo.2007.08.002.
- Göktürk, O. M., Fleitmann, D., Badertscher, S., Cheng, H., Edwards, R. L., Leuenberger, M., Fankhauser, A., Tüysüz, O., and Kramers, J., 2011, Climate on the southern Black Sea coast during the Holocene: implications from the Sofular Cave record: Quaternary Science Reviews, v. 30, no. 19-20, p. 2433–2445, doi: 10.1016/j.quascirev.2011.05.007.
- Hatzianastassiou, N., Katsoulis, B., Pnevmatikos, J., and Antakis, V., 2008, Spatial and Temporal Variation of Precipitation in Greece and Surrounding Regions Based on Global Precipitation Climatology Project Data: Journal of Climate, v. 21, no. 6, p. 1349–1370, doi: 10.1175/2007JCLI1682.1.
- Haug, G. H., Hughen, K. A., Sigman, D. M., Peterson, L. C., and Röhl, U., 2001, Southward migration of the intertropical convergence zone through the Holocene.: Science, v. 293, no. 5533, p. 1304–8, doi: 10.1126/science.1059725.
- Jones, M. D., Roberts, C. N., Leng, M. J., and Türkeş, M., 2006, A high-resolution late Holocene lake isotope record from Turkey and links to North Atlantic and monsoon climate: Geology, v. 34, no. 5, p. 361, doi: 10.1130/G22407.1.
- Kahmen, A., Schefuß, E., and Sachse, D., 2013a, Leaf water deuterium enrichment shapes leaf wax *n*-alkane δD values of angiosperm plants I: Experimental evidence and mechanistic insights: Geochimica et Cosmochimica Acta, v. 111, p. 39–49, doi: 10.1016/j.gca.2012.09.003.
- Kahmen, A., Hoffmann, B., Schefuß, E., Arndt, S. K., Cernusak, L. A., West, J. B., and Sachse, D., 2013b, Leaf water deuterium enrichment shapes leaf wax *n*-alkane δD values of angiosperm plants II: Observational evidence and global implications: Geochimica et Cosmochimica Acta, v. 111, p. 50–63, doi: 10.1016/j.gca.2012.09.004.
- Kalaitzidis, S., and Christanis, K., 2002, Mineral Matter in the Philippi Peat in Relation to Peat/Lignite-Forming Conditions in Greece: Energy Sources, v. 24, p. 69–81, doi: 10.1080/00908310252712316.
- Kallel, N., Paterne, M., Duplessy, J.-C., Vergnaud-Grazzini, C., Pujol, C., Labeyrie, L., Arnold, M., Fontugne, M., and Pierre, C., 1997, Enhanced rainfall in the mediterranean region during the last sapropel event: Oceanologica Acta, v. 20, no. 5, p. 697–712, doi: 10.1016/j.quascirev.2006.12.003.
- Kleiven, H. F., Kissel, C., Laj, C., Ninnemann, U. S., Richter, T. O., and Cortijo, E., 2008, Reduced North Atlantic deep water coeval with the glacial Lake Agassiz freshwater outburst.: Science, v. 319, no. 5859, p. 60–4, doi: 10.1126/science.1148924.
- Kobashi, T., Severinghaus, J. P., Brook, E. J., Barnola, J.-M., and Grachev, A. M., 2007, Precise timing and characterization of abrupt climate change 8200 years ago from air trapped in polar ice: Quaternary Science Reviews, v. 26, no. 9-10, p. 1212–1222, doi: 10.1016/j.quascirev.2007.01.009.
- Kotthoff, U., Pross, J., Müller, U. C., Peyron, O., Schmiedl, G., Schulz, H., and Bordon, A., 2008a, Climate dynamics in the borderlands of the Aegean Sea during formation of sapropel S1 deduced from a marine pollen record: Quaternary Science Reviews, v. 27, no. 7-8, p. 832–845, doi: 10.1016/j.quascirev.2007.12.001.
- Kotthoff, U., Müller, U. C., Pross, J., Schmiedl, G., Lawson, I. T., van de Schootbrugge, B., and Schulz, H., 2008b, Lateglacial and Holocene vegetation dynamics in the Aegean region: An integrated view based on pollen data from marine and terrestrial archives: The Holocene, v. 18, p. 1019–1032, doi: 10.1177/0959683608095573.

- Kouli, K., Gogou, A., Bouloubassi, I., Triantaphyllou, M. V., Ioakim, C., Katsouras, G., Roussakis, G., and Lykousis, V., 2012, Late postglacial paleoenvironmental change in the northeastern Mediterranean region: Combined palynological and molecular biomarker evidence: *Quaternary International*, v. 261, p. 118–127, doi: 10.1016/j.quaint.2011.10.036.
- LeGrande, A. N., and Schmidt, G. A., 2008, Ensemble, water isotope-enabled, coupled general circulation modeling insights into the 8.2 ka event: *Paleoceanography*, v. 23, no. 3, p. 1–19, doi: 10.1029/2008PA001610.
- LeGrande, A. N., Schmidt, G. A., Shindell, D. T., Field, C. V., Miller, R. L., Koch, D. M., Faluvegi, G., and Hoffmann, G., 2006, Consistent simulations of multiple proxy responses to an abrupt climate change event: *Proceedings of the National Academy of Sciences*, v. 103, no. 27, p. 837–842, doi: 10.1073/pnas.0510095103.
- Lionello, P., Boscolo, R., Alpert, P., Artale, V., Li, L., Luterbacher, J., May, W., Trigo, R., Tsimplis, M., Ulbrich, U., and Xoplaki, E., 2006, The Mediterranean Climate : An Overview of the Main Characteristics and Issues, in Lionello, P., Malanotte-Rizzoli, P., and Boscolo, R. (Eds.), *Mediterranean Climate Variability*, Elsevier B.V., Amsterdam, p. 1–26.
- Lionello, P., Abrantes, F., Congedi, L., Dulac, F., Gacic, M., Gomis, D., Clare, G., Hoff, H., Kutiel, H., Luterbacher, J., Planton, S., Reale, M., Schröder, K., Struglia, M. V., Toreti, A., Tsimplis, M., Ulbrich, U., and Xoplaki, E., 2012, Mediterranean Climate - Background Information, in Lionello, P. (Ed.), *The Climate of the Mediterranean Region*, Elsevier B. V., Amsterdam, p. 1-56.
- Liu, Y.-H., Henderson, G. M., Hu, C.-Y., Mason, A. J., Charnley, N., Johnson, K. R., and Xie, S.-C., 2013, Links between the East Asian monsoon and North Atlantic climate during the 8,200 year event: *Nature Geoscience*, v. 6, no. 2, p. 117–120, doi: 10.1038/ngeo1708.
- Liu, W., and Huang, Y., 2005, Compound specific D/H ratios and molecular distributions of higher plant leaf waxes as novel paleoenvironmental indicators in the Chinese Loess Plateau: *Organic Geochemistry*, v. 36, no. 6, p. 851–860, doi: 10.1016/j.orggeochem.2005.01.006.
- Marchal, O., Cacho, I., Stocker, T. F., Grimalt, J. O., Calvo, E., Martrat, B., Shackleton, N., Vautravers, M., Cortijo, E., Kreveld, S. Van, Andersson, C., Koc, N., Chapman, M., Saffi, L., et al., 2002, Apparent long-term cooling of the sea surface in the northeast Atlantic and Mediterranean during the Holocene: *Quaternary Science Reviews*, v. 21, p. 455–483, doi:10.1016/S0277-3791(01)00105-6.
- Marino, G., Rohling, E. J., Sangiorgi, F., Hayes, A., Casford, J. L., Lotter, A. F., Kucera, M., and Brinkhuis, H., 2009, Early and middle Holocene in the Aegean Sea: interplay between high and low latitude climate variability: *Quaternary Science Reviews*, v. 28, no. 27-28, p. 3246–3262, doi: 10.1016/j.quascirev.2009.08.011.
- Mariotti, A., Struglia, M. V., Zeng, N., and Lau, K.-M., 2002, The Hydrological Cycle in the Mediterranean Region and Implications for the Water Budget of the Mediterranean Sea: *Journal of Climate*, v. 15, p. 1674–1690, doi: 10.1175/1520-0442(2002)015<1674:THCITM>2.0.CO;2.
- Mayewski, P. A., Meeker, L. D., Twickler, M. S., Lyons, W. B., and Prentice, M., 1997, Major features and forcing of high-latitude northern hemisphere atmospheric circulation using a 110,000-year-long glaciochemical series: *Journal of Geophysical Research*, v. 102, p. 345–366.
- Mayewski, P. A., Rohling, E. E., Curt Stager, J., Karlén, W., Maasch, K. A., David Meeker, L., Meyerson, E. A., Gasse, F., van Kreveld, S., Holmgren, K., Lee-Thorp, J., Rosqvist, G., Rack, F., Staubwasser, M., et al., 2004, Holocene climate variability: *Quaternary Research*, v. 62, no. 3, p. 243–255, doi: 10.1016/j.yqres.2004.07.001.
- Meeker, L. D., and Mayewski, P. A., 2002, A 1400-year high-resolution record of atmospheric circulation over the North Atlantic and Asia: *The Holocene*, v. 12, no. 3, p. 257–266, doi: 10.1191/0959683602h1542ft.

- Morrill, C., and Jacobsen, Robert, M., 2005, How widespread were climate anomalies 8200 years ago? *Geophysical Research Letters*, v. 32, no. 19, p. 1–4, doi: 10.1029/2005GL023536.
- Morrill, C., Anderson, D. M., Bauer, B. A., Buckner, R., Gille, E. P., Gross, W. S., Hartman, M., and Shah, A., 2013, Proxy benchmarks for intercomparison of 8.2 ka simulations: *Climate of the Past*, v. 9, no. 1, p. 423–432, doi: 10.5194/cp-9-423-2013.
- Müller, U. C., Pross, J., Tzedakis, P. C., Gamble, C., Kotthoff, U., Schiedl, G., Wulf, S., Christanis, K., 2011. The role of climate in the spread of modern humans into Europe. *Quaternary Science Reviews* 30, 273-279.
- Pancost, R. D., Baas, M., van Geel, B., and Sinninghe Damsté, J. S., 2002, Biomarkers as proxies for plant inputs to peats: an example from a sub-boreal ombrotrophic bog: *Organic Geochemistry*, v. 33, no. 7, p. 675–690, doi: 10.1016/S0146-6380(02)00048-7.
- Pedentchouk, N., Sumner, W., Tipple, B., and Pagani, M., 2008, $\delta^{13}C$ and δD compositions of *n*-alkanes from modern angiosperms and conifers: An experimental set up in central Washington State, USA: *Organic Geochemistry*, v. 39, no. 8, p. 1066–1071, doi: 10.1016/j.orggeochem.2008.02.005.
- Peyron, O., Goring, S., Dormoy, I., Kotthoff, U., Pross, J., de Beaulieu, J.-L., Drescher-Schneider, R., Vanniere, B., and Magny, M., 2011, Holocene seasonality changes in the central Mediterranean region reconstructed from the pollen sequences of Lake Accesa (Italy) and Tenaghi Philippon (Greece): *The Holocene*, v. 21, no. 1, p. 131–146, doi: 10.1177/0959683610384162.
- Polissar, P. J., Freeman, K. H., Rowley, D. B., McInerney, F. A., and Currie, B.S., 2009, Paleoaltimetry of the Tibetan Plateau from D/H ratios of lipid biomarkers: *Earth & Planetary Science Letters*, v. 287, no. 1-2, p. 64–76, doi: 10.1016/j.epsl.2009.07.037.
- Poulos, S. E., Drakopoulos, P. G., and Collins, M. B., 1997, Seasonal variability in sea surface oceanographic conditions in the Aegean Sea (Eastern Mediterranean): an overview: *Journal of Marine Systems*, v. 13, no. 1-4, p. 225–244, doi: 10.1016/S0924-7963(96)00113-3.
- Pross, J., Tzedakis, P.C., Christanis, K., Schiedl, G., Hooghiemstra, H., Müller, U. C., Kotthoff, U., and Milner, A., 2007. Tenaghi Philippon re-visited: Drilling a continuous lower-latitude terrestrial climate archive of the last 250,000 years: *Scientific Drilling*, v. 5, p. 30-32, doi: 10.2204/iodp.sd.5.06.2007.
- Pross, J., Kotthoff, U., Müller, U. C., Peyron, O., Dormoy, I., Schiedl, G., Kalaitzidis, S., and Smith, A. M., 2009, Massive perturbation in terrestrial ecosystems of the Eastern Mediterranean region associated with the 8.2 kyr B.P. climatic event: *Geology*, v. 37, no. 10, p. 887–890, doi: 10.1130/G25739A.1.
- Pross, J., Koutsodendris, A., Christanis, K., Fischer, T., Fletcher, W. J., Hardiman, M., Kalaitzidis, S., Knipping, M., Kotthoff, U., Milner, A. M., Müller, U. C., Schiedl, G., Siavalas, G., Tzedakis, P. C., and Wulf, S., 2015, The 1.35-Ma-long terrestrial climate archive of Tenaghi Philippon, northeastern Greece: Evolution, exploration and perspectives for future research: *Newsletters on Stratigraphy*, v. 48, p. 253-276, doi: 10.1127/nos/2015/0063.
- Renssen, H., Goosse, H., Fichefet, T., and Campin, J.-M., 2001, The 8.2 kyr BP event simulated by a global atmosphere-sea-ice-ocean model: *Geophysical Research Letters*, v. 28, no. 8, p. 1567–1570, doi: 10.1029/2000GL012602.
- Risebrobakken, B., Jansen, E., Andersson, C., Mjelde, E., and Hevrøy, K., 2003, A high-resolution study of Holocene paleoclimatic and paleoceanographic changes in the Nordic Seas: *Paleoceanography*, v. 18, no. 1, p. n/a–n/a, doi: 10.1029/2002PA000764.
- Roberts, C. N., Zanchetta, G., and Jones, M. D., 2010, Oxygen isotopes as tracers of Mediterranean climate variability: An introduction: *Global and Planetary Change*, v. 71, no. 3-4, p. 135–140, doi: 10.1016/j.gloplacha.2010.01.024.

- Rodwell, M. J., and Hoskins, B. J., 1996, Monsoons and the dynamics of deserts: *Quarterly Journal of the Royal Meteorological Society*, no. 122, p. 1385–1404, doi: 10.1002/qj.49712253408.
- Rohling, E. J., and Pälike, H., 2005, Centennial-scale climate cooling with a sudden cold event around 8,200 years ago: *Nature*, v. 434, no. 7036, p. 975–979, doi: 10.1038/nature03421.
- Rohling, E. J., Cane, T. R., Cooke, S., Sprovieri, M., Bouloubassi, I., Emeis, K. C., Schiebel, R., Kroon, D., Jorissen, F. J., Lorre, A., and Kemp, A. E. S., 2002, African monsoon variability during the previous interglacial maximum: *Earth and Planetary Science Letters*, v. 202, no. 1, p. 61–75, doi: 10.1016/S0012-821X(02)00775-6.
- Rozanski, K., Araguás-Araguás, L., and Gonfiantini, R., 1993, Isotopic Patterns in Modern Global Precipitation, *in* Swart, P.K., Lohmann, K.C., McKenzie, J., and Savin, S. (Eds.), *Climate Change in Continental Isotopic Records*, American Geophysical Union, p. 1–36.
- Sachse, D., Gleixner, G., Wilkes, H., and Kahmen, A., 2010, Leaf wax *n*-alkane δD values of field-grown barley reflect leaf water δD values at the time of leaf formation: *Geochimica et Cosmochimica Acta*, v. 74, no. 23, p. 6741–6750, doi: 10.1016/j.gca.2010.08.033.
- Sachse, D., Billault, I., Bowen, G. J., Chikaraishi, Y., Dawson, T. E., Feakins, S. J., Freeman, K. H., Magill, C. R., McInerney, F. A., van der Meer, M. T. J., Polissar, P., Robins, R. J., Sachs, J. P., Schmidt, H.-L., et al., 2012, Molecular Paleohydrology: Interpreting the Hydrogen-Isotopic Composition of Lipid Biomarkers from Photosynthesizing Organisms: *Annual Review of Earth and Planetary Sciences*, v. 40, no. 1, p. 221–249, doi: 10.1146/annurev-earth-042711-105535.
- Sangiorgi, F., Capotondi, L., Combourieu Nebout, N., Vigliotti, L., Brinkhuis, H., Giunta, S., Lotter, A. F., Morigi, C., Negri, A., and Reichert, G.-J., 2003, Holocene seasonal sea-surface temperature variations in the southern Adriatic Sea inferred from a multiproxy approach: *Journal of Quaternary Science*, v. 18, no. 8, p. 723–732, doi: 10.1002/jqs.782.
- Schefuss, E., Schouten, S., and Schneider, R. R., 2005, Climatic controls on central African hydrology during the past 20,000 years: *Nature*, v. 437, no. 7061, p. 1003–6, doi: 10.1038/nature03945.
- Schemmel, F., Mikes, T., Rojay, B., and Mulch, A., 2013, The impact of topography on isotopes in precipitation across the Central Anatolian Plateau (Turkey): *American Journal of Science*, v. 313, no. 2, p. 61–80, doi: 10.2475/02.2013.01.
- Schwab, V. F., Garcin, Y., Sachse, D., Todou, G., Séné, O., Onana, J., Achoundong, G., and Gleixner, G., 2015, Organic Geochemistry Effect of aridity on $\delta^{13}C$ and δD values of C_3 plant- and C_4 graminoid-derived leaf wax lipids from soils along an environmental gradient in Cameroon (Western Central Africa): *Organic Geochemistry*, v. 78, p. 99–109, doi: 10.1016/j.orggeochem.2014.09.007.
- Sessions, A. L., Burgoyne, T. W., and Hayes, J. M., 2001, Determination of the H^3 factor in hydrogen isotope ratio monitoring mass spectrometry: *Analytical Chemistry*, v. 73, no. 2, p. 200–207, doi: 10.1021/ac000488m.
- Siani, G., Paterne, M., and Colin, C., 2010, Late glacial to Holocene planktic foraminifera bioevents and climatic record in the South Adriatic Sea: *Journal of Quaternary Science*, v. 25, no. 5, p. 808–821, doi: 10.1002/jqs.1360.
- Smith, F. A., and Freeman, K. H., 2006, Influence of physiology and climate on δD of leaf wax *n*-alkanes from C_3 and C_4 grasses: *Geochimica et Cosmochimica Acta*, v. 70, no. 5, p. 1172–1187, doi: 10.1016/j.gca.2005.11.006.
- Spötl, C., Nicolussi, K., Patzelt, G., and Boch, R., 2010, Humid climate during deposition of sapropel 1 in the Mediterranean Sea: Assessing the influence on the Alps: *Global and Planetary Change*, v. 71, no. 3-4, p. 242–248, doi: 10.1016/j.gloplacha.2009.10.003.

- Staubwasser, M., and Weiss, H., 2006, Holocene climate and cultural evolution in late prehistoric–early historic West Asia: *Quaternary Research*, v. 66, no. 3, p. 372–387, doi: 10.1016/j.yqres.2006.09.001.
- Thomas, E. R., Wolff, E. W., Mulvaney, R., Steffensen, J. P., Johnsen, S. J., Arrowsmith, C., White, J. W. C., Vaughn, B., and Popp, T., 2007, The 8.2ka event from Greenland ice cores: *Quaternary Science Reviews*, v. 26, no. 1-2, p. 70–81, doi: 10.1016/j.quascirev.2006.07.017.
- Tinner, W., van Leeuwen, J. F. N., Colombaroli, D., Vescovi, E., van der Knaap, W. O., Henne, P. D., Pasta, S., D'Angelo, S., and La Mantia, T., 2009, Holocene environmental and climatic changes at Gorgo Basso, a coastal lake in southern Sicily, Italy: *Quaternary Science Reviews*, v. 28, no. 15-16, p. 1498–1510, doi: 10.1016/j.quascirev.2009.02.001.
- Tipple, B. J., Berke, M. A., Doman, C. E., Khachatryan, S., and Ehleringer, J. R., 2013, Leaf-wax *n*-alkanes record the plant-water environment at leaf flush: *Proceedings of the National Academy of Sciences of the United States of America*, v. 110, no. 7, p. 2659–64, doi: 10.1073/pnas.1213875110.
- Triantaphyllou, M. V., Ziveri, P., Gogou, A., Marino, G., Lykousis, V., Bouloubassi, I., Emeis, K.-C., Kouli, K., Dimiza, M., Rosell-Melé, A., Papanikolaou, M., Katsouras, G., and Nunez, N., 2009, Late Glacial–Holocene climate variability at the south-eastern margin of the Aegean Sea: *Marine Geology*, v. 266, no. 1-4, p. 182–197, doi: 10.1016/j.margeo.2009.08.005.
- Tzedakis, P. C., 2007, Seven ambiguities in the Mediterranean palaeoenvironmental narrative: *Quaternary Science Reviews*, v. 26, no. 17-18, p. 2042–2066, doi: 10.1016/j.quascirev.2007.03.014.
- Wang, Y., Cheng, H., Edwards, R. L., He, Y., Kong, X., An, Z., Wu, J., Kelly, M. J., Dykoski, C. A., and Li, X., 2005, The Holocene Asian monsoon: links to solar changes and North Atlantic climate.: *Science*, v. 308, no. 5723, p. 854–7, doi: 10.1126/science.1106296.
- Wanner, H., Solomina, O., Grosjean, M., Ritz, S. P., and Jetel, M., 2011, Structure and origin of Holocene cold events: *Quaternary Science Reviews*, v. 30, no. 21-22, p. 3109–3123, doi: 10.1016/j.quascirev.2011.07.010.
- Wiersma, A. P., Roche, D. M., and Renssen, H., 2011, Fingerprinting the 8.2 ka event climate response in a coupled climate model: *Journal of Quaternary Science*, v. 26, no. 1, p. 118–127, doi: 10.1002/jqs.1439.
- Wijmstra, T. A., 1969, Palynology of the first 30 meters of a 120 m deep section in northern Greece: *Acta Botanica Neerlandica*, v. 18, p. 511-528, doi: 10.1111/j.1438-8677.1969.tb00591.x
- Zanchetta, G., Drysdale, R. N., Hellstrom, J. C., Fallick, A. E., Isola, I., Gagan, M. K., and Pareschi, M. T., 2007, Enhanced rainfall in the Western Mediterranean during deposition of sapropel S1: stalagmite evidence from Corchia cave (Central Italy): *Quaternary Science Reviews*, v. 26, no. 3-4, p. 279–286, doi: 10.1016/j.quascirev.2006.12.003.
- Zhornyak, L. V., Zanchetta, G., Drysdale, R. N., Hellstrom, J. C., Isola, I., Regattieri, E., Piccini, L., Baneschi, I., and Couchoud, I., 2011, Stratigraphic evidence for a “pluvial phase” between ca 8200–7100 ka from Renella cave (Central Italy): *Quaternary Science Reviews*, v. 30, no. 3-4, p. 409–417, doi: 10.1016/j.quascirev.2010.12.003.

Chapter 5

Conclusions and outlook

5.1 *Conclusions*

The biomarker record of Tenaghi Philippon (TP) yields new insights into the dynamics of rapid climate change during the northern hemisphere cooling of the 8.2 kyr B.P. climatic event in the Eastern Mediterranean region as well as into paleoenvironmental and paleoecological responses across the early Holocene. Investigating present-day influences on the net isotopic budgets of meteoric waters from the Central Anatolian Plateau (CAP) in Turkey allows the interpretation of precipitation-derived stable hydrogen isotopic compositions of leaf wax *n*-alkanes from vascular terrestrial plants (δD_{wax}) in the context of atmospheric circulation changes in the Aegean region across the early Holocene.

The transect of meteoric waters from the CAP highlights several characteristic features essential for the interpretation of stable hydrogen (δD) and oxygen ($\delta^{18}\text{O}$) isotopes in precipitation in the Eastern Mediterranean region. δD and $\delta^{18}\text{O}$ values from the CAP evolve as a result of air mass trajectories, topography, climatic conditions and seasonality. Despite being bordered by large, proximal bodies of water to the north and the south, the Black Sea and the Mediterranean Sea respectively, meteoric waters from the CAP display fundamental isotopic differences related to their origin, with northerly derived air masses producing precipitation considerably depleted in D and ^{18}O compared to southerly derived air. The influence of orographic rainout along the plateau margins leads to successively lower δD and $\delta^{18}\text{O}$ values as air masses adiabatically accent the slopes of the Pontide and Taurus Mountains. However, prevailing evaporitic conditions exert substantial isotopic enrichment on meteoric waters across the plateau interior, to a degree obfuscating the influence of air mass trajectory and topography. Additionally, this study highlights the importance of seasonality of rainfall for δD and $\delta^{18}\text{O}$ in precipitation, with summer precipitation being considerably more enriched in heavy isotopes than winter rainfall due to the temperature dependence of fractionation processes in the hydrological cycle. Accordingly, the detailed investigation of δD and $\delta^{18}\text{O}$ values from the CAP provides a template of relevant present-day influences on stable isotopes in meteoric waters in the Eastern Mediterranean region, thus allowing the comparison of present-day mechanisms with Holocene changes in the region.

δD_{wax} from geological archives provide an excellent tool to trace changes in δD in precipitation through time. The δD_{wax} values from TP show large variations across the early Holocene, indicating substantial variations in paleoprecipitation in the region.

Especially during the interval of northern hemisphere cooling during the 8.2 kyr B.P. climatic event, two events of pronounced isotopic enrichment are evident at TP. A minor shift, labeled isotope event 'A', occurs around ca. 8.2 kyr B.P. followed by a major shift, labeled isotope event 'B', between ca. 8.1 and 8.0 kyr B.P.. Notably, both isotopic enrichment events lack temporal correspondence with the regional expression of the pronounced winter cooling related to the 8.2 kyr B.P. climatic event (Pross et al., 2009). Isotope event 'A' precedes the interval of winter cooling while Isotope event 'B' occurs during the recovery of regional winter temperature back to Holocene levels. However, palynological reconstructions of seasonal precipitation distributions from TP imply a decrease in precipitation seasonality during the 8.2 kyr B.P. climatic event, most strongly expressed during the interval between ca. 8.1 and 8.0 kyr B.P. (Peyron et al., 2011). The general seasonal bias of δD_{wax} towards spring and summer precipitation (Sachse et al., 2010; Tipple et al., 2013) together with the close temporal correspondence between changing precipitation seasonality towards increased summer precipitation amounts and the excursions in δD_{wax} imply strong control of summer precipitation on the δD_{wax} record from TP. This notion is strengthened by indications of wetter surface conditions at TP during the interval of changing precipitation seasonality from *n*-alkane distribution patterns, stable carbon isotopic composition of total organic carbon ($\delta^{13}C_{TOC}$) and palynological data, highlighting the role of summer precipitation for vegetation dynamics in peatlands (Charman et al., 2004; Charman, 2007). Additionally, the observed increase in surface wetness at TP during the 8.2 kyr B.P. climatic event negates the possibility of evotranspiration as main driver for the isotopic enrichment during isotope events 'A' and 'B', as evident from the investigation of meteoric waters from the CAP.

As demonstrated on the plateau margins on the CAP, differing trajectories of air masses affecting the Eastern Mediterranean region can produce precipitation with distinct stable isotopic compositions. Hence, varying contributions of D-depleted, northerly-derived moisture from a distal source and D-enriched, southerly-derived moisture with a strong Mediterranean component may have affected precipitation dynamics at TP during the early Holocene and the 8.2 kyr B.P. climatic event. However, inflow of southerly-derived moisture towards TP requires the destabilization of atmospheric conditions by weakening the strong anticyclonic activity of the early Holocene, limiting advection of moisture from the Mediterranean Sea (Tzedakis et al., 2009; Lionello et al., 2012). Weakening of the Asian summer monsoon circulation at ca. 8.21 kyr B.P. and ca. 8.08 kyr B.P., related to northern hemisphere cooling during the 8.2 kyr B.P. climatic event (Wang et al., 2005; Cheng et al., 2009; Liu et al., 2013) may have destabilized Eastern Mediterranean anticyclones through propagating atmospheric Rossby waves, permitting the formation of Mediterranean-sourced precipitation (Rodwell and Hoskins, 1996;

Staubwasser and Weiss, 2006). Additionally, a southward shift of the Intertropical Convergence Zone (ITCZ) and the associated Hadley circulation around 8.2 kyr B.P. (Haug et al., 2001; Fleitmann et al., 2003) may have weakened the Azores High in summer, allowing the penetration of westerly winds into the Mediterranean basin, leading to increased cyclogenesis (Gaetani et al., 2007; Lionello et al., 2012). Further, lowered Aegean sea surface temperature (SST), linked to winter outbreaks of the strengthened Siberian High (Rohling et al., 2002; Kotthoff et al., 2008) may have increased the difference in land-sea temperature in summer due to the thermal inertia of water. High resolution SST reconstructions from the Aegean Sea show two distinct temperature minima at ca. 8.2 kyr B.P. and ca. 8.05 kyr B.P. (Marino et al., 2009) while uniformly high terrestrial summer temperatures (Pross et al., 2009) may have induced terrestrial thermal lows strong enough to destabilize local atmospheric conditions, drawing in moist air masses from the Aegean Sea, a circulation similar to the 'Mediterranean monsoon' (Arz et al., 2003). To conclude, this thesis reveals pronounced changes in atmospheric circulations in response to northern hemisphere cooling during the 8.2 kyr B.P. climatic event in the Aegean region and presents possible regional mechanisms as well as hemispheric-scale teleconnections between the climate systems of the high and low latitudes and the Eastern Mediterranean climate dynamics. Thus, with the 8.2 kyr B.P. climatic event as a possible analogue for future climate change (Alley and Ágústsdóttir, 2005), the insights gained in this thesis may contribute to the improvement of further projections and -hopefully- the successful mitigation of the challenges humanity will face in the coming decades.

5.2 *Outlook*

The classical site of Tenaghi Philippon provides excellent conditions for organic geochemical investigations of climate and ecosystem dynamics. With a new coring campaign initiated 2009, the new climate archive now attains a minimum age of ca. 1.1 Ma (Pross et al., 2015). Thus, the climate archive of TP covers the full range of the obliquity dominated '41 kyr world', with the great advantage of permitting paleoenvironmental reconstructions from the same location, circumventing the uncertainties of stacking shorter-term records. Also, the sensitivity of the Eastern Mediterranean region to perturbations in high and low latitude climate systems allows insights into the impacts of glacial-interglacial as well as rapid climate changes on regional climate dynamics to be obtained from TP and may yield valuable information on hemispheric to global-scale teleconnections. The organic geochemical approach is facilitated by the abundance and preservation of molecular fossils from plants and

bacteria at the site and strongly benefits from the extensive palynological research conducted at TP.

5.2.1 Tenaghi Philippon: The 8.2 kyr B.P. climatic event...

Considering the abundance of molecular fossils in the climate archive of TP, additional organic geochemical investigations would help to constrain the regional responses to northern hemisphere cooling during the 8.2 kyr B.P. climatic event as well as to further compare palynological data with the biomarker record. This thesis is based on numerous studies investigating various environmental influences on multiple plant-based proxies. Despite the enormous effort, our understanding of many underlying biochemical mechanisms remains poor while variability between species and individual plants in the present databases can be great (e.g., Sachse et al., 2012; Bush and McInerney, 2013). However, extensive palynological data and the proposition of Nissi Fen in northwestern Greece as a modern analogue to the 'original' Philippi peatland, prior to anthropogenic influences (Christanis, 1994), allows the investigation of relevant biochemical mechanisms of peatland vegetation. Sampling of present-day vegetation from Nissi Fen and consequent growth experiments under controlled conditions may yield much needed information on *n*-alkane concentrations and distribution patterns as well as stable isotopic compositions in different plants, thus enhancing the interpretation of the biomarker record from TP. Additionally, the investigation of compound-specific $\delta^{13}\text{C}$ of leaf-wax *n*-alkanes and of cellulose may provide more detailed information about changes in humidity conditions prevalent at the site (Hong et al., 2001; Seki et al., 2009; Yamamoto et al., 2010). Also, over the past decade, the investigation of glycerol dialkyl glycerol tetraether (GDGT) as a proxy of soil temperature received widespread attention (Sinninghe Damsté et al., 2000; Weijers et al., 2007a; Peterse et al., 2011; Huguet et al., 2014). Assumed to originate from a group of anaerobic soil bacteria, GDGTs are present in many globally distributed soils (Weijers et al., 2007b; Schouten et al., 2013). Preliminary results suggest the presents and applicability of GDGTs as proxy for soil temperature at TP (E. Niedermeyer, unpublished results). The establishment of an independent proxy for temperature may yield additional information about the regional responses to northern hemisphere cooling during the 8.2 kyr B.P. climatic event as well as allow the comparison of pollen-derived temperature and biomarker-derived temperature reconstructions. Further, organic geochemical investigation of TP may provide crucial information about the feasibility of the Carbon Preference Index (CPI) of long chain *n*-alkanes as a paleoclimate proxy. While being commonly used to estimate the fidelity of molecular plant fossils to the original source material (e.g., Bush and

McInerney, 2013), several studies propose *n*-alkane CPI values as a proxy for paleoclimatic conditions in peatland due to the climatic dependence of microbial activity in the upper peat horizon (Kuder and Krüge, 1998; Xie et al., 2004; Zhou et al., 2005, 2010; Zheng et al., 2007). Thus, exploring the relationship between *n*-alkane CPI values, paleoclimatic conditions and other proxies for microbial activity in peatlands, like sedimentary methyl ketone concentrations (Lehtonen and Ketola, 1990) or the ration between methyl ketones and *n*-alkanoic acid (Zheng et al., 2007) may establish *n*-alkane CPI as a proxy for paleoclimate at TP.

5.2.2 ...and beyond

While the aforementioned organic geochemical investigations would greatly benefit the understanding of the local responses to northern hemisphere cooling during the 8.2 kyr B.P. climatic event, the climate archive of TP provides the excellent opportunity to compare the knowledge about Holocene rapid climate change with different periods of pronounced climatic changes, both abrupt and orbitally-influenced. For example, the millennial-scale cooling of the Younger Dryas has been linked to a slowdown of the Atlantic Meridional Overturning Circulation (AMOC) (e.g., Carlson, 2010) and has consequently been compared to the 8.2 kyr B.P. climatic event (Alley et al., 1997). Regarding the changes in atmospheric circulation in the Aegean region around 8.2 kyr B.P. through hemispheric teleconnections proposed in this thesis, an integrated pollen-biomarker approach from TP may provide additional insight into the similarities and differences between the 8.2 kyr B.P. climatic event and the Younger Dryas. Also, a similar approach across glacial-interglacial transitions, like the Pleistocene-Holocene transition, or a comparison between Holocene climate and the climatic conditions of Marine Isotope Stages (MIS) 5 and 11 may yield important information about Eastern Mediterranean climate dynamics and would benefit greatly from extensive palynological data from the respective periods (Koutsodendris et al., 2012; Milner et al., 2012).

5.2.3 Mediterranean climatic dynamics across the 8.2 kyr B.P. climatic event

The atmospheric circulation changes during the 8.2 kyr B.P. climatic event proposed in this thesis are based on numerous studies of present-day atmospheric conditions and proxy-based reconstructions of Holocene climate. However, atmospheric general circulation models (GCM) of the 8.2 kyr B.P. climatic event are often limited to the hemispheric to global climatic responses (Renssen et al., 2002; LeGrande et al., 2006;

LeGrande and Schmitt, 2008; Renssen et al., 2010; Wiersma et al., 2011; Morill et al., 2013). Despite the difficulty in establishing GCMs in the Eastern Mediterranean region due to complex topographic features (Hahmann et al., 2007; Lionello et al., 2012), this thesis would benefit greatly from the validation from a GCM with high spatial resolution. Also, the establishment of a GCM of Eastern Mediterranean atmospheric conditions along with the integration of indications of atmospheric circulation changes from other prominent climate archives like Sufolar cave in Turkey (Fleitmann et al., 2009) and Soreq cave in Israel (Bar-Matthews et al., 1999) would help to constrain the regional extent of the atmospheric circulation changes proposed in this thesis. Further, a similar organic geochemical approach as presented here, conducted in peatlands in Spain (Ortiz et al., 2010, López-Días et al., 2010) may provide crucial insight into early Holocene atmospheric variability (e.g., Magny et al., 2013). Collectively, the study of molecular plant fossils from the Holocene and beyond in the Mediterranean region has the potential to contribute strongly to the understanding of atmospheric circulation dynamics in the past and may thus be able to correctly predict and - hopefully - mitigate the effects of future climate change. As Eglinton and Eglinton (2008) put it: 'The utility and applications of biomarkers may only be limited by our imagination'.

5.3 References

- Alley, R. B., and Ágústssdóttir, A. M., 2005, The 8k event: cause and consequences of a major Holocene abrupt climate change: *Quaternary Science Reviews*, v. 24, no. 10–11, p. 1123–1149, doi: 10.1016/j.quascirev.2004.12.004.
- Alley, R. B., Mayewski, P. A., Sowers, T., Stuiver, M., Taylor, K. C., and Clark, P. U., 1997, Holocene climatic instability: A prominent, widespread event 8200 yr ago: *Geology*, v. 25, no. 6, p. 483–486, doi: 10.1130/0091-7613(1997)025<0483.
- Arz, H. W., Lamy, F., Pätzold, J., Muller, P. J., and Prins, M., 2003, Mediterranean moisture source for an early-Holocene humid period in the northern Red Sea.: *Science*, v. 300, no. 5616, p. 118–21, doi: 10.1126/science.1080325.
- Bar-Matthews, M., Ayalon, A., Kaufman, A., and Wasserburg, G.J., 1999, The Eastern Mediterranean paleoclimate as a reflection of regional events: Soreq cave, Israel: *Earth and Planetary Science Letters*, v. 166, no. 1–2, p. 85–95, doi: 10.1016/S0012-821X(98)00275-1.
- Bush, R. T., and McInerney, F. A., 2013, Leaf wax *n*-alkane distributions in and across modern plants: Implications for paleoecology and chemotaxonomy: *Geochimica et Cosmochimica Acta*, v. 117, p. 161–179, doi: 10.1016/j.gca.2013.04.016.
- Carlson, A. E., 2010, What Caused the Younger Dryas Cold Event? *Geology*, v. 38, no. 4, p. 383–384, doi: 10.1130/focus042010.1.
- Charman, D., Brown, A., Hendon, D., and Karofeld, E., 2004, Testing the relationship between Holocene peatland palaeoclimate reconstructions and instrumental data at two European sites: *Quaternary Science Reviews*, v. 23, no. 1–2, p. 137–143, doi: 10.1016/j.quascirev.2003.10.006.
- Charman, D. J., 2007, Summer water deficit variability controls on peatland water-table changes: implications for Holocene palaeoclimate reconstructions: *The Holocene*, v. 17, no. 2, p. 217–227, doi: 10.1177/0959683607075836.
- Cheng, H., Fleitmann, D., Edwards, R. L., Wang, X., Cruz, F. W., Auler, A. S., Mangini, A., Wang, Y., Kong, X., Burns, S. J., and Matter, A., 2009, Timing and structure of the 8.2 kyr B.P. event inferred from ¹⁸O records of stalagmites from China, Oman, and Brazil: *Geology*, v. 37, no. 11, p. 1007–1010, doi: 10.1130/G30126A.1.
- Christanis, K., 1994, The genesis of the Nissi peatland (northwestern Greece) as an example of peat and lignite deposit formation in Greece: *International Journal of Coal Geology*, v. 26, p. 63–77.
- Eglinton, T. I., and Eglinton, G., 2008, Molecular proxies for paleoclimatology: *Earth and Planetary Science Letters*, v. 275, no. 1–2, p. 1–16, doi: 10.1016/j.epsl.2008.07.012.
- Fleitmann, D., Burns, S. J., Mudelsee, M., Neff, U., Kramers, J., Mangini, A., and Matter, A., 2003, Holocene forcing of the Indian monsoon recorded in a stalagmite from southern Oman.: *Science*, v. 300, no. 5626, p. 1737–9, doi: 10.1126/science.1083130.
- Fleitmann, D., Cheng, H., Badertscher, S., Edwards, R. L., Mudelsee, M., Göktürk, O. M., Fankhauser, A., Pickering, R., Raible, C. C., Matter, A., Kramers, J., and Tüysüz, O., 2009, Timing and climatic impact of Greenland interstadials recorded in stalagmites from northern Turkey: *Geophysical Research Letters*, v. 36, no. 19, p. L19707, doi: 10.1029/2009GL040050.
- Gaetani, M., Baldi, M., Dalu, G. A., and Maracchi, G., 2007, Connessioni tra il clima della regione Mediterranea e l’Africa Occidentale attraverso la circolazione meridiana di Hadley, in *Clima e cambiamenti climatici*, Consiglio Nazionale delle Ricerche, Roma, p. 23–26.

- Hahmann, A. N., Rostkier-Edelstein, D., Warner, T. T., Liu, Y., Vandenberghe, F., and Swerdlin, S. P., 2007, Toward a climate downscaling for the Eastern mediterranean at high-resolution: *Advances in Geosciences*, v. 12, no. January, p. 159–164, doi: 10.5194/adgeo-12-159-2008.
- Haug, G. H., Hughen, K. A., Sigman, D. M., Peterson, L. C., and Röhl, U., 2001, Southward migration of the intertropical convergence zone through the Holocene.: *Science*, v. 293, no. 5533, p. 1304–8, doi: 10.1126/science.1059725.
- Hong, Y. T., Wang, Z. G., Jiang, H. B., Lin, Q. H., Hong, B., Zhu, Y. X., Wang, Y., Xu, L. S., Leng, X. T., and Li, H. D., 2001, A 6000-year record of changes in drought and precipitation in northeastern China based on a $\delta^{13}\text{C}$ time series from peat cellulose: *Earth and Planetary Science Letters*, v. 185, no. 1–2, p. 111–119, doi: 10.1016/S0012-821X(00)00367-8.
- Huguet, A., Francez, A.-J., Jusselme, M. D., Fosse, C., and Derenne, S., 2014, A climatic chamber experiment to test the short term effect of increasing temperature on branched GDGT distribution in Sphagnum peat: *Organic Geochemistry*, v. 73, p. 109–112, doi: 10.1016/j.orggeochem.2014.05.010.
- Kotthoff, U., Pross, J., Müller, U. C., Peyron, O., Schmiedl, G., Schulz, H., and Bordon, A., 2008, Climate dynamics in the borderlands of the Aegean Sea during formation of sapropel S1 deduced from a marine pollen record: *Quaternary Science Reviews*, v. 27, no. 7–8, p. 832–845, doi: 10.1016/j.quascirev.2007.12.001.
- Koutsodendris, A., Pross, J., Müller, U. C., Brauer, A., Fletcher, W. J., Köhl, N., Kirilova, E., Verhagen, F. T. M., Lücke, A., and Lotter, A. F., 2012, A short-term climate oscillation during the Holsteinian interglacial (MIS 11c): An analogy to the 8.2ka climatic event? *Global and Planetary Change*, v. 92–93, p. 224–235, doi: 10.1016/j.gloplacha.2012.05.011.
- Kuder, T., and Krüger, M. A., 1998, Preservation of biomolecules in sub-fossil plants from raised peat bogs - A potential paleoenvironmental proxy: *Organic Geochemistry*, v. 29, no. 5–7–7 pt 2, p. 1355–1368, doi: 10.1016/S0146-6380(98)00092-8.
- LeGrande, A. N., and Schmidt, G. A., 2008, Ensemble, water isotope-enabled, coupled general circulation modeling insights into the 8.2 ka event: *Paleoceanography*, v. 23, no. 3, p. 1–19, doi: 10.1029/2008PA001610.
- LeGrande, A. N., Schmidt, G. A., Shindell, D. T., Field, C. V., Miller, R. L., Koch, D. M., Faluvegi, G., and Hoffmann, G., 2006, Consistent simulations of multiple proxy responses to an abrupt climate change event: *Proceedings of the National Academy of Sciences*, v. 103, no. 27, p. 837–842.
- Lehtonen, K., and Ketola, M., 1990, Occurrence of long-chain acyclic methyl ketones in Sphagnum and Carex peats of various degrees of humification: *Organic Geochemistry*, v. 15, no. 3, p. 275–280.
- Lionello, P., Abrantes, F., Congedi, L., Dulac, F., Gacic, M., Gomis, D., Clare, G., Hoff, H., Kutiel, H., Luterbacher, J., Planton, S., Reale, M., Schröder, K., Struglia, M. V., Toreti, A., Tsimplis, M., Ulbrich, U., and Xoplaki, E., 2012, Mediterranean Climate - Background Information, *in* Lionello, P. (Ed.), *The Climate of the Mediterranean Region*, Elsevier B. V., Amsterdam, p. 1-56.
- Liu, Y.-H., Henderson, G. M., Hu, C.-Y., Mason, A. J., Charnley, N., Johnson, K. R., and Xie, S.-C., 2013, Links between the East Asian monsoon and North Atlantic climate during the 8,200 year event: *Nature Geoscience*, v. 6, no. 2, p. 117–120, doi: 10.1038/ngeo1708.
- López-Días, V., Borrego, Á. G., Blanco, C. G., Arboleya, M., López-Sáez, J. A., and López-Merino, L., 2010, Biomarkers in a peat deposit in Northern Spain (Huelga de Bayas, Asturias) as proxy for climate variation: *Journal of Chromatography*, v. 1217, no. 21, p. 3538–46, doi: 10.1016/j.chroma.2010.03.038.

- Magny, M., Combourieu-Nebout, N., de Beaulieu, J. L., Bout-Roumazelles, V., Colombaroli, D., Desprat, S., Francke, A., Joannin, S., Ortu, E., Peyron, O., Revel, M., Sadori, L., Siani, G., Sicre, M. A., et al., 2013, North–south palaeohydrological contrasts in the central Mediterranean during the Holocene: tentative synthesis and working hypotheses: *Climate of the Past*, v. 9, no. 5, p. 2043–2071, doi: 10.5194/cp-9-2043-2013.
- Marino, G., Rohling, E. J., Sangiorgi, F., Hayes, A., Casford, J. L., Lotter, A. F., Kucera, M., and Brinkhuis, H., 2009, Early and middle Holocene in the Aegean Sea: interplay between high and low latitude climate variability: *Quaternary Science Reviews*, v. 28, no. 27–28, p. 3246–3262, doi: 10.1016/j.quascirev.2009.08.011.
- Milner, A. M., Collier, R. E. L., Roucoux, K. H., Muller, U. C., Pross, J., Kalaitzidis, S., Christanis, K., and Tzedakis, P.C., 2012, Enhanced seasonality of precipitation in the Mediterranean during the early part of the Last Interglacial: *Geology*, v. 40, no. 10, p. 919–922, doi: 10.1130/G33204.1.
- Morrill, C., Anderson, D. M., Bauer, B. A., Buckner, R., Gille, E. P., Gross, W. S., Hartman, M., and Shah, A., 2013, Proxy benchmarks for intercomparison of 8.2 ka simulations: *Climate of the Past*, v. 9, no. 1, p. 423–432, doi: 10.5194/cp-9-423-2013.
- Ortiz, J. E., Gallego, J. L. R., Torres, T., Diaz-Bautista, A., and Sierra, C., 2010, Palaeoenvironmental reconstruction of Northern Spain during the last 8000 cal yr BP based on the biomarker content of the Ronanzas peat bog (Asturias): *Organic Geochemistry*, v. 41, no. 5, p. 454–466.
- Peterse, F., Prins, M. A., Beets, C. J., Troelstra, S. R., Zheng, H., Gu, Z., Schouten, S., and Sinninghe Damsté, J. S., 2011, Decoupled warming and monsoon precipitation in East Asia over the last deglaciation: *Earth and Planetary Science Letters*, v. 301, no. 1–2, p. 256–264, doi: 10.1016/j.epsl.2010.11.010.
- Peyron, O., Goring, S., Dormoy, I., Kotthoff, U., Pross, J., de Beaulieu, J.-L., Drescher-Schneider, R., Vanniere, B., and Magny, M., 2011, Holocene seasonality changes in the central Mediterranean region reconstructed from the pollen sequences of Lake Accesa (Italy) and Tenaghi Philippon (Greece): *The Holocene*, v. 21, no. 1, p. 131–146, doi: 10.1177/0959683610384162.
- Pross, J., Kotthoff, U., Müller, U. C., Peyron, O., Dormoy, I., Schmiedl, G., Kalaitzidis, S., and Smith, A. M., 2009, Massive perturbation in terrestrial ecosystems of the Eastern Mediterranean region associated with the 8.2 kyr B.P. climatic event: *Geology*, v. 37, no. 10, p. 887–890, doi: 10.1130/G25739A.1.
- Pross, J., Koutsodendris, A., Christanis, K., Fischer, T., Fletcher, W. J., Hardiman, M., Kalaitzidis, S., Knipping, M., Kotthoff, U., Milner, A. M., Müller, U. C., Schmiedl, G., Siavalas, G., Tzedakis, P.C., et al., 2015, The 1.35-Ma-long terrestrial climate archive of Tenaghi Philippon, northeastern Greece: Evolution, exploration, and perspectives for future research: *Newsletters on Stratigraphy*, v. 48, no. 3, p. 253–276, doi: 10.1127/nos/2015/0063.
- Renssen, H., Goosse, H., and Fichefet, T., 2002, Modeling the effect of freshwater pulses on the early Holocene climate: The influence of high-frequency climate variability: *Paleoceanography*, v. 17, no. 2, p. 1–16.
- Renssen, H., Goosse, H., Crosta, X., and Roche, D. M., 2010, Early holocene laurentide ice sheet deglaciation causes cooling in the high-latitude southern hemisphere through oceanic teleconnection: *Paleoceanography*, v. 25, no. 3, p. 1–15, doi: 10.1029/2009PA001854.
- Rodwell, M. J., and Hoskins, B. J., 1996, Monsoons and the dynamics of deserts: *Quarterly Journal of the Royal Meteorological Society*, no. 122, p. 1385–1404.
- Rohling, E. J., Mayewski, P. A., Abu-Zied, R. H., Casford, J. S. L., and Hayes, A., 2002, Holocene atmosphere-ocean interactions: records from Greenland and the Aegean Sea: *Climate Dynamics*, v. 18, no. 7, p. 587–593, doi: 10.1007/s00382-001-0194-8.

- Sachse, D., Gleixner, G., Wilkes, H., and Kahmen, A., 2010, Leaf wax *n*-alkane δD values of field-grown barley reflect leaf water δD values at the time of leaf formation: *Geochimica et Cosmochimica Acta*, v. 74, no. 23, p. 6741–6750, doi: 10.1016/j.gca.2010.08.033.
- Sachse, D., Billault, I., Bowen, G. J., Chikaraishi, Y., Dawson, T. E., Feakins, S. J., Freeman, K. H., Magill, C. R., McInerney, F. A., van der Meer, M. T. J., Polissar, P., Robins, R. J., Sachs, J. P., Schmidt, H.-L., et al., 2012, Molecular Paleohydrology: Interpreting the Hydrogen-Isotopic Composition of Lipid Biomarkers from Photosynthesizing Organisms: *Annual Review of Earth and Planetary Sciences*, v. 40, no. 1, p. 221–249, doi: 10.1146/annurev-earth-042711-105535.
- Schouten, S., Hopmans, E. C., and Sinninghe Damsté, J. S., 2013, The organic geochemistry of glycerol dialkyl glycerol tetraether lipids: A review: *Organic Geochemistry*, v. 54, p. 19–61, doi: 10.1016/j.orggeochem.2012.09.006.
- Seki, O., Meyers, P. A., Kawamura, K., Zheng, Y., and Zhou, W., 2009, Hydrogen isotopic ratios of plant wax *n*-alkanes in a peat bog deposited in northeast China during the last 16kyr: *Organic Geochemistry*, v. 40, no. 6, p. 671–677, doi: 10.1016/j.orggeochem.2009.03.007.
- Sinninghe Damsté, J. S., Hopmans, E. C., Pancost, R. D., Schouten, S., and Geenevasen, J. A. J., 2000, Newly discovered non-isoprenoid glycerol dialkyl glycerol tetraether lipids in sediments: *Chemical Communications*, no. 17, p. 1683–1684, doi: 10.1039/b004517i.
- Staubwasser, M., and Weiss, H., 2006, Holocene climate and cultural evolution in late prehistoric–early historic West Asia: *Quaternary Research*, v. 66, no. 3, p. 372–387, doi: 10.1016/j.yqres.2006.09.001.
- Tipple, B. J., Berke, M. A., Doman, C. E., Khachatryan, S., and Ehleringer, J. R., 2013, Leaf-wax *n*-alkanes record the plant-water environment at leaf flush: *Proceedings of the National Academy of Sciences of the United States of America*, v. 110, no. 7, p. 2659–64, doi: 10.1073/pnas.1213875110.
- Tzedakis, P. C., Pälike, H., Roucoux, K. H., and de Abreu, L., 2009, Atmospheric methane, southern European vegetation and low-mid latitude links on orbital and millennial timescales: *Earth and Planetary Science Letters*, v. 277, no. 3–4, p. 307–317, doi: 10.1016/j.epsl.2008.10.027.
- Wang, Y., Cheng, H., Edwards, R. L., He, Y., Kong, X., An, Z., Wu, J., Kelly, M. J., Dykoski, C. A., Li, X., 2005. The Holocene Asian monsoon: links to solar changes and North Atlantic climate: *Science* 308 (no. 5723), 854e857. <http://dx.doi.org/10.1126/science.1106296>.
- Weijers, J. W. H., Schefuss, E., Schouten, S., and Sinninghe Damsté, J. S., 2007a, Coupled thermal and hydrological evolution of tropical Africa over the last deglaciation: *Science*, v. 315, no. 5819, p. 1701–4, doi: 10.1126/science.1138131.
- Weijers, J. W. H., Schouten, S., Van Den Donker, J. C., Hopmans, E. C., and Sinninghe Damsté, J. S., 2007b, Environmental controls on bacterial tetraether membrane lipid distribution in soils: *Geochimica et Cosmochimica Acta*, v. 71, no. 3, p. 703–713, doi: 10.1016/j.gca.2006.10.003.
- Wiersma, A. P., Roche, D. M., and Renssen, H., 2011, Fingerprinting the 8.2 ka event climate response in a coupled climate model: *Journal of Quaternary Science*, v. 26, no. 1, p. 118–127, doi: 10.1002/jqs.1439.
- Xie, S., Nott, C. J., Avsejs, L. A., Maddy, D., Chambers, F. M., and Evershed, R. P., 2004, Molecular and isotopic stratigraphy in an ombrotrophic mire for paleoclimate reconstruction: *Geochimica et Cosmochimica Acta*, v. 68, no. 13, p. 2849–2862, doi: 10.1016/j.gca.2003.08.025.
- Yamamoto, S., Kawamura, K., Seki, O., Meyers, P. A., Zheng, Y., and Zhou, W., 2010, Environmental influences over the last 16ka on compound-specific $\delta^{13}C$ variations of leaf wax *n*-alkanes in the Hani peat deposit from northeast China: *Chemical Geology*, v. 277, no. 3–4, p. 261–268, doi: 10.1016/j.chemgeo.2010.08.009.

Zheng, Y., Zhou, W., Meyers, P. A., and Xie, S., 2007, Lipid biomarkers in the Zoigê-Hongyuan peat deposit: Indicators of Holocene climate changes in West China: *Organic Geochemistry*, v. 38, no. 11, p. 1927–1940, doi: 10.1016/j.orggeochem.2007.06.012.

Zhou, W., Xie, S., Meyers, P. A., and Zheng, Y., 2005, Reconstruction of late glacial and Holocene climate evolution in southern China from geolipids and pollen in the Dingnan peat sequence: *Organic Geochemistry*, v. 36, no. 9, p. 1272–1284, doi: 10.1016/j.orggeochem.2005.04.005.

Zhou, W., Zheng, Y., Meyers, P. A., Jull, A. J. T., and Xie, S., 2010, Postglacial climate-change record in biomarker lipid compositions of the Hani peat sequence, Northeastern China: *Earth & Planetary Science Letters*, v. 294, no. 1–2, p. 37–46, doi: 10.1016/j.epsl.2010.02.035.

Zusammenfassung

Geologische Untersuchungen von Perioden abrupten Klimawandels sind ein wichtiger Aspekt für das Verständnis der gegenwärtigen und zukünftigen Klimaentwicklung der Erde. Doch wenngleich während der jüngeren Erdgeschichte vor allem orbitale Prozesse große Klimaveränderungen, wie zum Beispiel Glazial/Interglazial-Übergänge, ausgelöst haben, reichen externe Einflüsse meist nicht aus, um die gesamte Klimavariabilität der Erde zu erklären. Besonders deutlich wird dies während des Holozäns. Der globale Abkühlungstrend, der, bedingt durch die Abnahme der Insolation seit dem letzten glazialen Maximum, das gesamte Holozän dominiert, wurde mehrfach von abrupten Klimaveränderungen unterbrochen, die weitgehend ohne Entsprechung in externen Einflüssen sind. So hatten, vor allem während des frühen Holozän, die Präsenz sowie das sukzessive Abschmelzen der großen Eisschilde deutliche Auswirkungen auf globale und regionale Klimamuster. Dabei nimmt der Laurentidische Eisschild auf dem nordamerikanischen Kontinent und die Präsenz der beiden gewaltigen Schmelzwasserseen Agassiz und Ojibway am südlichen Gletscherrand eine besondere Rolle ein. Der, im Zuge des endgültigen Zusammenbruchs des Laurentidischen Eisschildes ausgelöster Schmelzwasserpuls setzte um 8.47 kyr B.P. eine erhebliche Menge Wasser durch die Hudson Bay in die Labradorsee frei und führte zu einer massiven Verlangsamung der thermohalinen Zirkulation in nordatlantischen Ozean. Die daraus resultierende Abnahme des Wärmetransports des Golfstroms in Richtung Europa gilt als Auslöser für die beträchtlichen Klimaschwankungen in weiten Teilen der nördlichen Hemisphäre während des sogenannten '*8.2 kyr B.P. climatic events*'. Trotz der relativ kurzen Dauer von nur etwa zwei Jahrhunderten gehört das *8.2 kyr B.P. climatic event* zu den größten abrupten Klimaschwankungen des Holozäns, vor allem im Nordatlantikraum und in Europa. Dort zeigen Klimarekonstruktionen oft Hinweise auf starke Temperaturabnahmen (meist im Winter) sowie auf deutliche Veränderungen in atmosphärischen Zirkulationsmustern, die die räumliche und saisonale Verteilung von Niederschlägen oft signifikant beeinflussten. Der Einfluss des *8.2 kyr B.P. climatic events* ist in einer Vielzahl geologischer Ablagerungen im Mittelmeerraum besonders ausgeprägt. Bedingt durch die besondere geographische Lage, im Einflussgebiet zwischen den Klimasystemen der höheren und niederen Breiten, wird das Klima im Mittelmeerraum als besonders empfindlich gegenüber den Auswirkungen abrupter Klimaschwankungen beschrieben. So weisen neben geologischen Untersuchungen auch archäologische Funde aus der östlichen Mittelmeerregion auf die massiven Auswirkungen des *8.2 kyr B.P. climatic events* auf die Entwicklung frühmenschlicher Gesellschaften hin. Dennoch beschränkt sich die Bedeutung des *8.2 kyr B.P. climatic events* nicht nur auf paläoklimatische Zusammenhänge während des frühen Holozäns. In den vergangenen Jahrzehnten bestätigte eine wachsende Anzahl von wissenschaftlichen Untersuchungen den anthropogenen Einfluss auf die Klimaentwicklung

der Erde. Dabei wird als sehr wahrscheinlich angenommen, dass der Golfstrom im 21. Jahrhundert durch steigende CO₂-Konzentrationen in der Atmosphäre sowie den Zustrom von Schmelzwasser der Grönlandgletscher deutlich abgeschwächt wird, was dementsprechend den Wärmetransport Richtung Europa nachhaltig beeinflussen wird. Wiederum wird der Mittelmeerraum als besonders empfindlich gegenüber damit einhergehenden Klimaschwankungen identifiziert. Bedingt durch die starke Niederschlagssaisonalität in weiten Teilen der Region, können vor allem Veränderungen der atmosphärischen Zirkulation, die für den Mittelmeerraum charakteristischen mesoskaligen Klimamuster nachhaltig beeinflussen und signifikante Veränderungen in regionalen Niederschlagsverteilungsmustern bewirken. In diesem Zusammenhang gilt das *8.2 kyr B.P. climatic event* mit seiner vergleichsweise klaren Beziehung vom Ursache und Wirkung als mögliche Entsprechung für das Szenario einer zukünftigen Verlangsamung des Golfstroms und den damit einhergehenden klimatischen Veränderungen. Die vorliegende Arbeit geht dementsprechend der Frage nach, wie sich die atmosphärischen Zirkulationsmuster während des *8.2 kyr B.P. climatic events* im östlichen Mittelmeerraum verändert haben.

Die Untersuchung der stabilen Isotope von Wasserstoff (δD) und Sauerstoff ($\delta^{18}\text{O}$) im Niederschlag ist ein ausgezeichnetes Mittel, Veränderungen in atmosphärischen Zirkulationsmustern über die Zeit zu identifizieren. Dieser Ansatz beruht auf thermodynamischen Fraktionierungsprozessen, die während des hydrologischen Kreislaufs auf feuchte Luftmassen wirken und in charakteristischen Verteilungen von leichten und schweren Isotopen in Wasserdampf und Niederschlag resultieren. Neben der Analyse rezenter Wasserproben, ermöglicht die Anwendung an geeigneten Proxymaterialien dabei ebenso die Rekonstruktion der stabilen Isotopie des Niederschlags über geologische Zeiträume. Allerdings, obwohl charakteristisch und vorhersehbar, verlaufen Fraktionierungsprozesse von stabilen Isotopen im Niederschlag nicht gradlinig, da eine Vielzahl physiologischer, meteorologischer und klimatischer Faktoren die Abläufe des hydrologischen Kreislaufs beeinflussen können. Da es weiterhin durch physikalische, biologische und geologische Einflüsse häufig auch zu Fraktionierung beim Übergang in geologische Ablagerungen kommt, ist es unabdingbar, die wesentlichen Fraktionierungsprozesse zu identifizieren, um fundierte Aussagen über die Entwicklung von δD und $\delta^{18}\text{O}$ im Paläoniederschlag zu treffen. Dementsprechend umfasst die vorliegende Arbeit drei Studien mit dem Ziel (1) Einflüsse auf δD und $\delta^{18}\text{O}$ in Niederschlag aus der östlichen Mittelmeerregion zu charakterisieren, (2) eine Beschreibung paläoklimatischer und paläoökologischer Parameter zu liefern, um (3) die atmosphärischen Zirkulationsmuster während des *8.2 kyr B.P. climatic events* fundiert zu rekonstruieren. Zu diesem Zweck analysieren wir δ und $\delta^{18}\text{O}$ in rezenten meteorischen Oberflächenwässern vom Zentralanatolischen Plateau (*Central Anatolian Plateau; CAP*), Türkei, um die wesentlichen

physiologischen, meteorologischen und klimatischen Einflüsse auf Fraktionierung während des hydrologischen Kreislaufs grundlegend zu beschreiben. Darüber hinaus rekonstruieren wir mit Hilfe eines Multiproxy-Ansatzes die paläoklimatische Entwicklung der Region während des *8.2 kyr B.P. climatic events* anhand von molekularen Pflanzenfossilien, stabilen Kohlenstoffisotopen ($\delta^{13}\text{C}_{\text{TOC}}$) und palynologischen Untersuchungen an einem Torfbohrkern aus dem geologischen Archiv von Tenaghi Philippon (TP) im Drama Becken, Griechenland. Abschließend identifizieren wir Veränderungen in δD in sedimentären *n*-Alkanen epicuticularer Blattwaxe von vaskulären Landpflanzen ($\delta\text{D}_{\text{wax}}$) von TP, um so Rückschlüsse auf Variationen in der stabilen Isotopie des Niederschlags während des *8.2 kyr B.P. climatic events* zu ziehen und diese in einen atmosphärischen Kontext zu setzen.

Die Analyse von mehr als 480 Proben meteorischer Oberflächenwässer aus einem Profil von der Schwarzmeerküste und das Pontische Gebirge im Norden über das gesamte CAP bis über das Taurusgebirge und zur Mittelmeerküste im Süden zeigt die maßgeblichen Einflüsse unterschiedlicher Luftmassen, ihren Ursprungsgebieten und Flugbahnen ebenso wie die Auswirkungen von Topographie und Klima auf die Zusammensetzung der stabilen Isotope im Niederschlag im östlichen Mittelmeerraum. Die initialen δD und $\delta^{18}\text{O}$ Werte in Küstennähe können, bedingt durch unterschiedliche Ursprungsgebiete und Flugbahnen der Luftmassen, zwischen dem nördlichen und dem südlichen Plateaurand deutlich unterschieden werden, wobei die absoluten Werte in Süden in δD etwa 20 ‰ und in $\delta^{18}\text{O}$ etwa 3 ‰ schwerer sind als im Norden des Plateaus. Der orographische Niederschlag, der durch den adiabatischen Aufstieg der Luftmassen an den Flanken der beiden Gebirgszüge entsteht, hat außerdem einen signifikanten Einfluss auf δD und $\delta^{18}\text{O}$ in den meteorischen Wässern. Die deutliche Abnahme von -20 ‰/km in δD und -2.9 ‰/km in $\delta^{18}\text{O}$ am Taurusgebirge bzw. -19 ‰/km in δD und -2.6 ‰/km in $\delta^{18}\text{O}$ am Pontischen Gebirge bezeichnet einen ausgeprägten isotopischen Regenschatteneffekt in den äußeren Randgebieten des Plateauinneren. Die stark evaporativen Bedingungen auf dem Plateau führen zu einer signifikanten Anreicherung der schweren Isotope D und ^{18}O in den Oberflächenwässern, da die leichten Isotope bevorzugt verdampfen. Die daraus resultierende Zunahme in δD und $\delta^{18}\text{O}$ auf dem Plateauinneren ist so ausgeprägt, dass die Effekte der unterschiedlichen Initialzusammensetzungen und der Topographie zum Teil vollständig überdeckt werden.

Um vergleichbare Umwelteinflüsse während des *8.2 kyr B.P. climatic events* in TP einschätzen zu können, muss die Klimaentwicklungen zu dieser Zeit, vor allem mögliche evaporative Effekte, charakterisiert werden. Torfablagerungen, wie die von TP, eignen sich hervorragend dazu, Klimaveränderungen anhand der Vegetationsdynamik nachzuverfolgen. Zu diesem Zweck verfolgen wir einen Multiproxy-Ansatz, um die Entwicklung und Klimaabhängigkeit der Oberflächenfeuchtigkeit des Torfmoors im Drama Becken mit Hilfe

von Biomarkern und Pollen während des frühen Holozäns (ca. 8.7 - 7.5 kyr B.P.) zu rekonstruieren. Da die gesamte Vegetation ebenso wie individuelle Pflanzen im Becken auf Klimaänderungen reagieren, vergleichen wir palynologische Informationen mit den charakteristischen Mengen- und Verteilungsmustern von sedimentären *n*-Alkanen epicuticularer Blattwachse und $\delta^{13}\text{C}_{\text{TOC}}$ Werten. Das untersuchte Profil zeigt Hinweise auf vergleichsweise weniger feuchte Oberflächenbedingungen während des Intervalls von ca. 8.7 bis 8.2 kyr B.P.. Der aquatische Index (P_{aq}), der auf typischen *n*-Alkanverteilungsmustern in Wasser- und Landpflanzen basiert, deutet in diesem Intervall eine klare Prävalenz von Landpflanzen gegenüber Wasserpflanzen an. Die Annahme von weniger feuchten Oberflächenbedingungen wird außerdem durch hohe durchschnittliche *n*-Alkankettenlängenwerte (*Average Chain Length; ACL*) und niedrige $\delta^{13}\text{C}_{\text{TOC}}$ Werte bestärkt. Hohe ACL Werte deuten dabei auf trockene und/oder warme Ökosysteme hin, da Landpflanzen unter diesen Bedingungen oft verstärkt länger-kettige *n*-Alkane synthetisieren. Eine Abnahme der $\delta^{13}\text{C}_{\text{TOC}}$ Werte in vaskulären Landpflanzen wird als Reaktion auf niedrigere, umgebende Luftfeuchtigkeit gewertet, da unter trockenen Bedingungen vaskuläre Landpflanzen in der Lage sind, ihre Stomata zu schließen und sich so vor dem Austrocknen zu schützen. Da dabei gleichzeitig der Gasaustausch zwischen Blatt und Atmosphäre behindert wird, kommt es im Inneren des Blattes, und dementsprechend auch in den Photosyntheseprodukten, zu einer Anreicherung von ^{13}C . Pollendaten aus diesem Intervall belegen eine fast völlige Abwesenheit von aquatischen Taxa und unterstützen so die Interpretation der Biomarkerinformationen. Während des 8.2 kyr B.P. *climatic events* (ca. 8.2 - 7.9 kyr B.P.) deuten Biomarker und Pollendaten auf eine Zunahme der Feuchtigkeit in TP hin. Steigende P_{aq} und $\delta^{13}\text{C}_{\text{TOC}}$ Werte, zusammen mit sinkenden ACL Werten und einer Zunahme der aquatischen Taxa stimmen dabei zeitlich mit früheren Pollenstudien von TP überein, die vor allem während der zweiten Hälfte des Events eine Abnahme der Niederschlagsseasonalität mit sinkenden Winter- und steigenden Sommerniederschlagsmengen zeigen. Die deutlichste Änderung der Oberflächenfeuchtigkeit in TP zeigt sich erst nach dem 8.2 kyr B.P. *climatic event*. Maxima in P_{aq} zusammen mit ACL Minima und stark schwankenden $\delta^{13}\text{C}_{\text{TOC}}$ Werten werden von einer weiteren Zunahme der aquatischen Taxa und dem Auftreten von Süßwassergrünalgen begleitet, was eine signifikante Veränderung der Hydrologie des Gebietes nahelegt. Frühere sedimentologische und geochemische Untersuchungen im Drama Becken belegen zu dieser Zeit eine Zunahme der Aktivität der Karstsysteme der umliegenden Gebirge, was möglicherweise zu einem starken Anstieg des Grundwasserspiegels geführt hat.

Um mögliche Variationen in der atmosphärischen Zirkulation während des 8.2 kyr B.P. *climatic events* zu rekonstruieren, untersuchen wir δD von langkettigen *n*-Alkanen, typisch für vaskuläre Landpflanzen. Diese werden als Teil der epicuticularen Wachsschicht während

des Blattwachstums im Frühjahr und Frühsommer synthetisiert und stehen dabei im isotopischen Gleichgewicht mit δD des für Photosynthese zur Verfügung stehenden Wassers. Da in der Regel Niederschlag die Wasserquelle von Landpflanzen ist, zeichnen δD_{wax} Werte aus sedimentären Archiven Veränderungen in δD des Niederschlags über die Zeit nach. Die Untersuchung von δD_{wax} in TP von ca. 8.7 - 7.5 kyr B.P. zeigt relative niedrige, stabile Werte während des Zeitraums vor dem *8.2 kyr B.P. climatic events*. Während des Events jedoch werden zwei Intervalle mit stark positiven δD_{wax} Werten deutlich. Ein schneller Anstieg um etwa 30 ‰ um 8.2 kyr B.P. geht dabei einem ausgeprägterem Ereignis voraus, das zwischen ca. 8.1 und 8.0 kyr B.P. eine Zunahme in δD_{wax} von etwa 45 ‰ zeigt, bevor die δD_{wax} Werte im jüngeren Teil der untersuchten Sektion bis 7.5 kyr B.P. wieder deutlich zurückgehen. Da eine Zunahme von evaporativen Bedingungen, wie auf dem CAP, bzw. Transpiration der Pflanzen während des *8.2 kyr B.P. climatic events* unwahrscheinlich ist, wie Pollen und Biomarker zeigen, deuten die beiden starken Anreicherungsereignisse auf Änderungen in atmosphärischen Zirkulationen hin. Die isotopischen Unterschiede zwischen den Initialzusammensetzungen in den rezenten Oberflächenwässern vom Nord- und vom Südrand des CAP legen dabei nahe, dass verstärkt südliche, in D angereicherte Luftmassen das Drama Becken und TP während des *8.2 kyr B.P. climatic events* erreicht haben, was zu deutlich höheren δD Werten im Niederschlag geführt hat. Diese Annahme wird von früheren palynologischen Beobachtungen abnehmender Niederschlagsseasonalität zu dieser Zeit bestärkt. Eine solche Zunahme im Zustrom von südlichen Luftmassen jedoch deutet dabei auf weitreichende atmosphärische Einflüsse auf den östlichen Mittelmeerraum hin, da hierfür die im Frühjahr und Sommer über dem Mittelmeer dominierenden Hochdruckbedingungen abgeschwächt werden müssen, die die Niederschlagsbildung in der Region behindern. Mögliche Mechanismen hierfür sind unter anderem der Einfluss hemisphärischer Prozesse, wie der Monsun- und der Hadley-Zirkulation auf den östlichen Mittelmeerraum, ebenso wie regionale Unterschiede in Land-Ozean-Temperatur im Ägäisraum. Zusammenfassend legt die vorliegende Arbeit massive Veränderungen in der atmosphärischen Zirkulation während des *8.2 kyr B.P. climatic events* nahe, die die Empfindlichkeit der Region gegenüber Variationen hemisphärischer Klimasysteme unterstreicht und damit ein mögliches Zukunftsszenario für den östlichen Mittelmeerraum für die kommenden Jahrzehnte präsentiert.

Acknowledgements

When I began my thesis, someone told me that the next few years would be an amazing experience. Not only would I expand my scientific knowledge but I would also improve on a personal level, get to know myself better. They told me that I would learn how I will cope under the pressure of the everyday scientific life, how I would deal with colleagues, coauthors, other scientists. How I would learn to be precise, focused, sophisticated. How to gain scientific insight and how to defend it before others, logical and reasonable.

I thought none of it. Being in my late twenties, I thought I knew how I and (mostly) everything around me worked. How wrong I was...

The past few year have been everything I was promised. Amazing, terrifying, awesome, heartbreaking, cruel, wonderful, challenging, easy, difficult... they have been fantastic. And what they told me was right. Now as this chapter of my life is ending, it is not the humble scientific contributions I am proud of but the simple fact that now I know a lot better who I am.

However, none of this I could have achieved on my own. I met so many great, funny, terrible, interesting people who -willingly or not- helped me, supported me, fought me, taught me, motivated me. From all these people, I have tried to learn and to all these people I will be forever grateful.

First and foremost, though, I have to thank Andreas Mulch who took my interest (back than I didn't really know what stable isotopes were), nurtured it and gave me an opportunity. At times overwhelming me and at time almost abandoning me, he taught me to be levelheaded, to keep the bigger picture in mind and not to lose myself in details.

While at the same time, Jörg Pross assumed the role of *advocatus diaboli*. Listening to me, to my reasoning, he took it upon himself to deliberately point out holes, encouraging me, reminding me to be precise and accurate in everything I do. To me, he was the voice of reason and logic, always listening, always prudent, always criticizing, and always honest.

Eva Niedermeyer challenged me. Constantly. She challenged my understanding of scientific basics as well as my conclusions. With patience, she listened to me, let me take my own time and follow my own approaches while defending her own ideas, her own interpretations. Sometimes even in heated arguments. Which I truly enjoyed.

But I would also like to thank so many people for their amazing support in so many different areas, be it field work, work in the lab or managing the varying tasks of everyday scientific life.

In the field, Bora Rojay was invaluable. With his unsurpassed knowledge of the geology of Turkey and his impressive belly dancing skills, he easily lets complex tectonic processes come to life.

I am also deeply grateful to Valérie Schwab, Gerd Gleixner and everyone at MPI-BGC Jena. Not only did you give me the opportunity to work in your lab and stay in your institute, you have been present, patient and supportive of me. Whatever the question, whatever the time, you have been most helpful.

I am indebted to Andreas Koutsodendris who always took the time to answer my questions. From the depth of the water table in a certain greek basin in summer to complex reconstructions of pollen data, I truly enjoyed working with you.

I would also like to extend my gratitude to the hands-on support everyone gave me in our labs in Hannover and in Frankfurt. Christiane Wenske, Uli Treffert, Jens Fiebig, Sven Hoffmann, Theo Potouridis, from the bottom of my heart, thank you for your help, your patience, your expertise, everything.

And thank you Iryna for guiding me through all administrative obstacles.

Also, thank you Tina, Katha, Matt, Liam, Vanessa, Marion, Emilia, Tamas, Aude (and everyone I may have forgotten) for making me laugh, cry, think, angry, for passing time, for listening to me, for trusting me, for providing balance.

I am also grateful to my family, for supporting me, always.

With you, I have been through good times and I have been through bad times. Thank you from the bottom of my heart for believing in me. I would be nothing without you.

And finally, now that I find myself head over heels in my next adventure, I would like to dedicate these lines to my new family. Anna, Liv and Luke, you will never know just how much you mean to me.

"Allons-y"

Appendix

Tab. A.1 Geographic coordinates of sample locations (WGS84), elevations, calculated average catchment elevations and stable hydrogen and oxygen isotopic ratios of meteoric water samples in Central Anatolia.

sample #	sample type	latitude [°N]	longitude [°E]	sampling elevation [m]	average catchment elevation [m]	catchment area [km ²]	sampling date	δD SMOW [‰]	δ ¹⁸ O SMOW [‰]	d [‰]
08-Erm-001	stream	36.5603	32.9549	524	1612	2476.95	26. Sep 08	-51.2	-9.1	21.2
08-Erm-002	creek	36.5570	32.9404	520	1223	115.26	26. Sep 08	-51.1	-9.1	21.9
08-Erm-005	creek	36.6327	32.8255	605	1389	411.52	27. Sep 08	-60.7	-9.9	18.7
08-Erm-009	creek	36.6966	32.7675	785	1503	224.12	27. Sep 08	-60.1	-9.8	18.5
08-Erm-010	creek	36.6541	32.6184	1326	1789	196.48	27. Sep 08	-54.2	-9.2	19.2
08-Erm-011	creek	36.6148	32.6562	1061	1747	230.34	27. Sep 08	-55.6	-9.3	18.8
08-Erm-012	creek	36.5682	32.6806	730	1191	3.75	27. Sep 08	-54.2	-9.0	18.1
08-Erm-013	stream	36.5681	32.6809	705	1690	1064.18	27. Sep 08	-46.2	-8.1	18.8
08-Erm-014	stream	36.5628	32.6092	782	1707	997.16	27. Sep 08	-47.5	-8.1	17.4
08-Erm-015	creek	36.5511	32.5880	877	1509	10.02	27. Sep 08	-52.1	-8.8	18.5
08-Erm-016	creek	36.5605	32.5414	925	1136	0.03	27. Sep 08	-39.4	-7.0	16.8
08-Erm-017	creek	36.5663	32.5393	900	1714	50.26	27. Sep 08	-49.2	-8.4	17.8
08-Erm-018	stream	36.5663	32.5393	900	1723	891.89	27. Sep 08	-48.3	-8.1	16.3
08-Erm-019	creek	36.6083	32.4413	1058	1310	0.20	27. Sep 08	-39.1	-6.8	15.4
08-Erm-020	stream	36.6116	32.4217	1050	1787	650.29	27. Sep 08	-49.3	-8.3	17.0
08-Erm-021	creek	36.6130	32.4099	1085	1305	0.32	27. Sep 08	-38.3	-6.8	15.7
08-Erm-022	stream	36.6772	32.4402	1152	1865	387.10	27. Sep 08	-52.2	-8.8	17.8
08-Erm-023	creek	36.6852	32.5572	1416	1589	2.19	27. Sep 08	-54.7	-9.0	17.6
08-Erm-024	spring	36.6769	32.9342	1650	1674	0.01	28. Sep 08	-61.4	-10.0	18.6
08-Erm-025	spring	36.7011	32.9518	1568	1595	0.00	28. Sep 08	-61.4	-10.1	19.3
08-Erm-026	spring	36.7188	32.9315	1493	1537	0.01	28. Sep 08	-61.9	-10.1	19.1
08-Erm-027	creek	36.7188	32.9315	1485	1834	152.54	28. Sep 08	-62.0	-10.1	18.7
08-Erm-030	spring	36.7556	32.9072	1609	1708	0.01	28. Sep 08	-65.4	-10.5	18.6
08-Erm-031	spring	36.7764	32.8883	1631	1638	0.00	28. Sep 08	-65.5	-10.4	17.5
08-Erm-032	creek	36.7805	32.8918	1675	1778	2.88	28. Sep 08	-63.8	-10.2	18.1
08-Erm-033	creek	36.7917	32.9244	1710	1918	19.13	28. Sep 08	-59.5	-9.6	17.3
08-Erm-034	creek	36.7708	32.9372	1665	1874	33.35	28. Sep 08	-64.0	-10.2	17.9
08-Erm-035	creek	36.7339	32.9565	1542	1835	51.25	28. Sep 08	-64.0	-10.0	16.1
08-Erm-036	creek	36.6943	32.9764	1460	1823	71.43	28. Sep 08	-61.2	-9.8	17.2
08-Erm-037	creek	36.6933	32.9730	1425	1814	239.86	28. Sep 08	-61.4	-9.7	16.1
08-Erm-038	creek	36.6193	33.0236	1020	1790	371.18	28. Sep 08	-59.7	-9.2	13.8
08-Erm-039	stream	36.5803	33.3270	128	1500	4662.55	28. Sep 08	-51.3	-7.9	12.1
08-Erm-040	stream	36.4861	33.5521	85	1382	12128.34	29. Sep 08	-54.7	-8.3	11.5
08-Erm-041	spring	36.3965	33.8511	106	177	0.02	29. Sep 08	-33.7	-6.2	15.9
08-Erm-042	stream	36.4008	33.8193	25	1345	12870.01	29. Sep 08	-58.5	-9.0	13.8
08-Erm-043	creek	36.5085	33.5437	96	1531	1462.87	29. Sep 08	-55.2	-9.1	17.6
08-Erm-044	spring	36.6934	32.4496	1208	1301	0.03	30. Sep 08	-48.4	-8.3	18.1
08-Erm-045	creek	36.7169	32.4609	1230	1894	345.18	30. Sep 08	-47.9	-8.1	16.8
08-Erm-046	stream	36.7536	32.4605	1282	1932	290.48	30. Sep 08	-52.1	-8.6	16.4
08-Erm-047	creek	36.7536	32.4605	1282	1678	7.14	30. Sep 08	-52.9	-9.1	19.5
08-Erm-048	stream	36.8186	32.4374	1410	2003	207.61	30. Sep 08	-53.3	-9.1	19.3
08-Erm-049	stream	36.8355	32.3939	1470	2072	147.67	30. Sep 08	-54.2	-9.3	19.8
08-Erm-050	creek	36.8365	32.4006	1450	1838	6.39	30. Sep 08	-51.8	-8.2	13.9

sample #	sample type	latitude [°N]	longitude [°E]	sampling elevation [m]	average catchment elevation [m]	catchment area [km ²]	sampling date	δD SMOW [‰]	δ ¹⁸ O SMOW [‰]	<i>d</i> [‰]
08-Erm-051	creek	36.8403	32.4931	1816	1911	9.77	30. Sep 08	-48.5	-7.9	14.5
08-Erm-052	creek	36.9179	32.4919	1508	1894	63.35	30. Sep 08	-62.3	-10.3	19.9
08-Erm-053	stream	37.0912	32.3113	1274	1863	436.34	30. Sep 08	-61.8	-10.1	19.1
VP-01-01	creek	36.4948	33.0089	1264	1480	6.24	13. May 09	-53.9	-10.1	27.1
VP-01-02	creek	36.5097	33.1649	518	1340	0.99	13. May 09	-55.0	-10.0	25.2
VP-01-05	spring	36.7789	32.6511	1896	1924	0.01	18. May 09	-55.8	-9.5	20.4
VP-01-06	spring	36.7723	32.6746	1855	1871	0.00	18. May 09	-53.5	-9.0	18.8
VP-01-07	spring	36.5946	33.1177	698	861	0.02	19. May 09	-59.1	-9.7	18.4
VP-01-08	creek	36.8368	33.3160	1377	1491	0.01	21. May 09	-43.0	-7.0	13.2
VP-01-09	creek	37.3491	35.0496	627	1061	5.23	22. May 09	-50.5	-8.4	16.4
VP-01-10	spring	37.2552	35.0545	251	365	0.02	22. May 09	-43.9	-7.4	15.6
VP-01-11	creek	36.7681	34.1613	1076	1405	5.47	23. May 09	-46.4	-8.0	17.2
VP-01-12	creek	37.0181	33.2788	1427	1426	0.00	24. May 09	-47.4	-7.2	10.3
VP-01-13	spring	36.9764	33.2787	1468	1491	0.02	24. May 09	-60.0	-9.2	13.4
VP-01-14	stream	36.4908	33.5117	118	880	315.72	26. May 09	-40.3	-7.1	16.1
VP-01-15	creek	36.5035	32.1692	612	880	0.08	27. May 09	-27.6	-5.5	16.1
VP-01-16	creek	36.7927	31.7054	175	261	0.22	29. May 09	-24.0	-4.6	12.9
VP-01-17	stream	36.7963	31.6977	87	1077	257.40	29. May 09	-32.4	-6.2	17.0
VP-01-18	spring	36.8071	31.7640	585	614	0.01	29. May 09	-29.4	-6.0	18.3
VP-01-19	creek	36.9735	31.6145	291	1032	45.14	29. May 09	-37.5	-7.0	18.3
VP-01-20	spring	36.9772	31.6962	872	929	0.01	29. May 09	-38.8	-7.2	19.0
VP-01-21	spring	37.1071	31.8032	1422	1495	0.01	29. May 09	-43.8	-7.9	19.2
VP-01-22	stream	37.0806	31.6568	430	1447	788.59	30. May 09	-48.1	-8.3	18.4
VP-01-23	stream	36.9696	31.5085	763	1182	8.89	30. May 09	-31.6	-6.4	19.5
VP-01-24	spring	36.9665	31.5109	762	784	0.00	30. May 09	-33.6	-6.7	20.2
VP-01-25	stream	36.8132	31.4543	19	1246	2438.06	30. May 09	-46.9	-8.2	18.9
VP-01-26	spring	37.0468	31.7537	997	1042	0.03	31. May 09	-36.8	-8.0	27.3
VP-01-28	creek	37.2477	31.9283	1465	1737	0.31	31. May 09	-52.1	-9.4	22.9
VP-01-29	spring	37.2477	31.9283	1465	1632	0.08	31. May 09	-50.4	-9.2	23.0
VP-01-30	creek	37.2477	31.9283	1465	1673	0.18	31. May 09	-47.4	-8.7	22.0
VP-01-32	creek	37.4576	31.7138	1683	2076	0.20	01. Jun 09	-57.2	-10.2	24.2
VP-01-33	spring	37.4551	31.7014	1836	1882	0.01	01. Jun 09	-58.8	-10.5	24.8
VP-01-34	spring	37.4601	31.6768	1582	1588	0.01	01. Jun 09	-57.9	-9.9	21.1
VP-01-35	spring	37.3510	31.6469	1366	1405	0.05	01. Jun 09	-49.9	-9.0	21.9
VP-01-36	stream	37.3615	31.5847	1381	1612	239.71	01. Jun 09	-49.2	-8.8	20.8
VP-01-37	spring	37.3921	31.5339	1345	1371	0.04	01. Jun 09	-52.4	-9.1	20.4
VP-01-38	stream	37.3536	31.4374	1212	1633	162.33	01. Jun 09	-53.5	-9.7	23.8
VP-01-40	spring	37.3908	31.4393	1255	1273	0.00	01. Jun 09	-48.4	-8.5	19.9
VP-01-41	spring	37.4057	31.4309	1272	1295	0.02	01. Jun 09	-54.2	-9.4	20.6
VP-01-42	spring	37.6484	31.6459	1137	1147	0.17	01. Jun 09	-63.7	-10.3	18.7
VP-01-46	spring	37.5806	31.3519	1424	1438	0.00	02. Jun 09	-42.1	-8.0	21.6
VP-01-47	stream	37.6874	31.3717	1205	1781	88.35	02. Jun 09	-53.6	-9.2	20.0
VP-01-48	spring	37.6961	31.3089	1503	1572	0.01	02. Jun 09	-61.2	-10.1	19.8
VP-01-49	creek	39.8701	33.0033	1052	1473	39.92	04. Jun 09	-68.2	-10.2	13.5
VP-01-50	spring	39.8706	33.0031	1054	1150	0.01	04. Jun 09	-66.2	-9.5	9.6
VP-01-51	creek	40.2830	33.3927	963	1015	0.79	06. Jun 09	-65.3	-8.8	4.9
VP-01-52	spring	40.2792	33.4249	965	965	0.00	06. Jun 09	-74.1	-10.3	8.4
VP-01-53	spring	40.0915	32.6634	1023	1042	0.02	08. Jun 09	-61.8	-8.6	6.8

sample #	sample type	latitude [°N]	longitude [°E]	sampling elevation [m]	average catchment elevation [m]	catchment area [km ²]	sampling date	δD SMOW [‰]	δ ¹⁸ O SMOW [‰]	<i>d</i> [‰]
VP-01-54	spring	40.0328	32.4598	962	977	0.01	08. Jun 09	-65.5	-9.4	9.8
VP-02-01	spring	39.9686	32.4148	1074	1084	0.00	18. Jun 09	-65.4	-9.7	12.4
VP-02-02	stream	39.8664	33.6281	779	1042	690.08	24. Jun 09	-68.6	-10.0	11.6
VP-02-03	stream	40.0679	34.1021	616	1136	19807.58	24. Jun 09	-62.2	-8.6	6.4
VP-02-04	creek	40.1756	34.4416	767	1109	977.38	24. Jun 09	-65.1	-9.2	8.4
VP-02-05	spring	40.2398	34.2305	665	672	0.03	25. Jun 09	-67.0	-9.5	8.8
VP-02-08	stream	40.3215	34.2687	714	1088	180.38	26. Jun 09	-64.8	-9.2	8.6
VP-02-09	spring	40.0113	34.6201	1183	1236	0.04	26. Jun 09	-70.2	-10.2	11.2
VP-02-10	stream	40.0744	34.5744	902	1239	284.72	26. Jun 09	-66.5	-9.4	8.9
VP-02-11	stream	40.3079	34.1199	565	1111	22705.00	27. Jun 09	-61.4	-8.0	2.8
VP-02-13	spring	40.4484	33.7685	604	632	0.02	27. Jun 09	-66.9	-8.3	-0.4
VP-02-14	stream	40.4379	33.7433	605	1101	1897.41	27. Jun 09	-64.7	-8.2	0.5
VP-02-15	stream	40.6794	33.8007	856	1305	327.17	27. Jun 09	-66.3	-8.9	4.8
VP-02-18	creek	40.8306	33.9518	1469	1562	0.09	01. Jul 09	-71.1	-10.4	12.1
VP-02-19	spring	40.8591	33.9771	1746	1781	0.11	01. Jul 09	-70.5	-10.9	16.7
VP-02-20	spring	40.9194	34.0221	1029	1036	0.00	01. Jul 09	-65.0	-9.2	8.8
VP-02-21	stream	41.0430	34.0405	837	1478	75.15	01. Jul 09	-72.1	-10.8	14.3
VP-02-22	spring	41.1274	34.0717	1641	1657	0.01	01. Jul 09	-75.6	-11.5	16.1
VP-02-23	stream	41.1669	34.0688	1248	1570	44.14	01. Jul 09	-71.4	-10.8	15.1
VP-02-24	stream	41.2848	33.9340	911	1459	280.19	01. Jul 09	-71.0	-10.7	14.7
VP-02-25	stream	41.3691	33.8441	800	1474	297.30	01. Jul 09	-70.8	-10.7	14.7
VP-02-27	stream	41.6315	34.3988	488	1126	78.58	03. Jul 09	-73.0	-10.8	13.1
VP-02-28	stream	41.5985	34.3248	513	1165	180.82	05. Jul 09	-71.5	-10.5	12.5
VP-02-29	stream	41.4878	34.1331	595	1162	346.27	05. Jul 09	-75.9	-11.0	12.2
VP-02-30	stream	41.4929	33.9350	643	1120	2047.77	05. Jul 09	-68.9	-10.2	12.8
VP-02-31	stream	41.4769	33.9056	665	1394	336.80	05. Jul 09	-69.0	-10.4	14.4
VP-02-32	stream	41.5184	34.7590	285	1093	6224.98	06. Jul 09	-68.9	-10.1	11.9
VP-02-33	stream	41.7001	34.9151	691	1134	33.60	06. Jul 09	-67.8	-10.4	15.2
VP-02-34	stream	41.8602	35.0760	54	735	276.75	06. Jul 09	-62.4	-9.8	16.1
VP-02-35	creek	42.0705	34.9461	9	64	1.47	07. Jul 09	-54.3	-9.0	17.9
VP-02-37	spring	41.1578	33.7925	1118	1218	0.01	10. Jul 09	-72.1	-10.9	14.8
VP-02-38	spring	41.0659	33.7500	1830	1865	0.00	10. Jul 09	-74.8	-11.6	17.8
VP-02-39	stream	40.9958	33.7020	1095	1704	116.09	10. Jul 09	-72.8	-10.9	14.0
VP-02-40	stream	40.6769	33.5991	823	1283	172.66	10. Jul 09	-69.3	-10.1	11.3
VP-02-42	stream	40.5186	33.6145	688	1168	1980.92	11. Jul 09	-63.1	-8.9	8.3
VP-03-01	spring	37.9438	34.8249	1905	1907	0.00	21. Sep 09	-79.5	-11.3	10.7
VP-03-02	spring	37.9140	34.8902	1911	1928	0.00	21. Sep 09	-72.3	-10.3	10.1
VP-03-03	stream	37.8896	34.9184	1820	2124	6.24	21. Sep 09	-74.3	-10.9	12.9
VP-03-04	stream	37.8895	34.9181	1819	2029	55.25	21. Sep 09	-74.7	-11.0	13.1
VP-03-05	spring	37.7900	34.9881	1446	1456	0.01	21. Sep 09	-59.2	-7.4	-0.2
VP-03-06	spring	37.8665	34.9909	1861	1879	0.00	23. Sep 09	-74.3	-10.6	10.3
VP-03-07	spring	37.8386	35.0239	1511	1520	0.01	23. Sep 09	-67.1	-8.6	1.4
VP-03-08	creek	37.9098	35.1165	1646	2002	6.89	23. Sep 09	-74.7	-10.9	12.4
VP-03-09	creek	37.9092	35.1175	1637	2005	6.93	23. Sep 09	-76.0	-10.5	7.8
VP-03-10	stream	37.9086	35.1187	1630	2673	67.47	23. Sep 09	-76.2	-11.3	13.9
VP-03-11	spring	39.1252	33.9609	1053	1054	0.00	25. Sep 09	-62.2	-8.2	3.7
VP-03-12	spring	39.1210	33.8883	1013	1013	0.00	25. Sep 09	-72.2	-10.3	10.4
VP-03-13	spring	39.1605	33.8466	1181	1194	0.09	25. Sep 09	-64.0	-8.8	6.7

sample #	sample type	latitude [°N]	longitude [°E]	sampling elevation [m]	average catchment elevation [m]	catchment area [km ²]	sampling date	δD SMOW [‰]	δ ¹⁸ O SMOW [‰]	<i>d</i> [‰]
VP-03-14	spring	39.1570	33.7955	1182	1183	0.01	25. Sep 09	-67.4	-9.9	12.1
VP-03-16	spring	39.3246	33.7172	1209	1240	0.01	25. Sep 09	-73.3	-11.1	15.5
VP-03-17	spring	39.2953	33.7654	1132	1136	0.00	25. Sep 09	-65.6	-9.8	12.8
VP-03-18	spring	39.2946	33.7799	1132	1159	0.02	25. Sep 09	-66.5	-9.7	11.1
VP-03-19	spring	39.1892	33.7852	1295	1312	0.01	25. Sep 09	-69.5	-10.1	11.2
TW-10-01	creek	40.2049	32.5794	1040	1196	10.69	13. May 10	-65.4	-9.5	10.4
TW-10-02	spring	40.2049	32.5794	1045	1098	0.02	13. May 10	-66.5	-9.8	11.9
TW-10-03	spring	40.2637	32.5916	1254	1326	0.00	13. May 10	-69.0	-10.1	11.7
TW-10-04	creek	40.1334	32.4567	1068	1209	3.89	14. May 10	-70.6	-10.2	10.7
TW-10-05	spring	40.1334	32.4564	1067	1095	0.03	14. May 10	-66.1	-9.2	7.4
TW-10-06	spring	39.9582	32.4197	1040	1068	0.02	16. May 10	-67.9	-9.4	7.3
TW-10-07	spring	40.0032	32.4481	944	953	0.01	17. May 10	-59.8	-8.2	5.9
TW-10-08	spring	39.9935	32.5230	804	932	0.30	17. May 10	-62.5	-8.2	2.8
TW-10-09	creek	40.1998	32.5937	1022	1178	13.21	18. May 10	-66.1	-9.6	10.4
TW-10-10	spring	40.1997	32.5936	1019	1025	0.00	18. May 10	-66.4	-9.6	10.4
TW-10-11	spring	40.1995	32.5939	1013	1028	0.00	18. May 10	-66.9	-9.6	9.6
TW-10-12	spring	40.2030	32.5898	999	1041	0.00	18. May 10	-66.9	-9.6	9.9
TW-10-13	creek	40.2029	32.5898	997	1186	12.17	18. May 10	-65.4	-9.3	8.6
TW-10-14	spring	40.2137	32.5249	1200	1218	0.02	19. May 10	-67.8	-10.1	12.9
TW-10-15	creek	40.2166	32.5220	1181	1247	1.75	19. May 10	-66.6	-9.8	11.6
TW-10-16	spring	40.2171	32.5221	1183	1217	0.02	19. May 10	-69.4	-9.9	9.7
TW-10-17	creek	40.2183	32.5204	1164	1243	1.94	19. May 10	-66.9	-9.6	9.7
TW-10-18	spring	40.2056	32.5598	1166	1196	0.01	19. May 10	-65.7	-9.2	8.0
TW-10-19	spring	39.1068	33.3722	917	990	0.42	20. May 10	-79.2	-10.7	6.4
TW-10-20	spring	38.6092	33.8831	1306	1334	0.00	21. May 10	-78.1	-12.2	19.7
TW-10-21	spring	38.5963	33.8523	1093	1113	0.01	21. May 10	-66.3	-8.6	2.8
TW-10-22	spring	38.5955	33.8327	1039	1057	0.00	21. May 10	-63.3	-9.0	8.8
TW-10-23	spring	38.5823	33.8049	966	1036	0.04	21. May 10	-65.4	-8.9	6.0
TW-10-24	spring	38.6185	33.7849	988	991	0.00	21. May 10	-65.4	-10.3	16.7
TW-10-25	spring	38.6715	33.8344	1205	1236	0.01	21. May 10	-66.6	-10.6	18.0
TW-10-26	spring	38.6889	33.8015	1110	1119	0.01	21. May 10	-64.7	-10.2	16.6
TW-10-27	spring	38.6766	33.7756	1051	1073	0.02	21. May 10	-65.7	-10.0	14.5
TW-10-28	stream	38.6542	33.7670	988	1158	56.55	21. May 10	-62.9	-8.3	3.7
TW-10-29	spring	38.6160	33.7793	964	991	0.03	21. May 10	-72.2	-10.3	9.9
TW-10-30	spring	38.6581	33.8443	1244	1244	0.00	21. May 10	-57.3	-7.8	5.4
TW-10-31	spring	38.6618	33.8835	1214	1218	0.00	21. May 10	-63.6	-8.6	4.9
TW-10-32	spring	38.6708	33.8953	1214	1231	0.12	21. May 10	-67.9	-9.8	10.2
TW-10-33	spring	38.6756	33.8998	1216	1220	0.02	21. May 10	-64.6	-8.9	6.8
TW-10-34	spring	38.6928	33.9463	1317	1317	0.00	21. May 10	-73.5	-12.1	23.0
TW-10-35	spring	38.6720	33.9825	1371	1396	0.01	21. May 10	-75.1	-12.2	22.8
TW-10-36	spring	37.9664	34.6789	1264	1264	0.00	22. May 10	-71.3	-10.6	13.3
TW-10-37	spring	38.0721	34.8161	1363	1363	0.00	22. May 10	-73.4	-11.8	20.6
TW-10-38	spring	38.0710	34.8526	1375	1375	0.03	22. May 10	-70.5	-10.3	11.6
TW-10-39	spring	38.0685	34.9310	1460	1460	0.00	22. May 10	-75.4	-10.7	10.1
TW-10-40	spring	38.0348	34.9814	1540	1548	0.02	22. May 10	-77.3	-12.8	24.9
TW-10-41	spring	37.9839	35.0834	1656	1656	0.02	22. May 10	-72.7	-12.1	24.3
TW-10-42	spring	37.9573	35.0875	1741	1745	0.00	22. May 10	-81.3	-11.6	11.3
TW-10-43	spring	37.9426	35.0818	1620	1626	0.00	22. May 10	-81.4	-11.6	11.7

sample #	sample type	latitude [°N]	longitude [°E]	sampling elevation [m]	average catchment elevation [m]	catchment area [km ²]	sampling date	δD SMOW [‰]	δ ¹⁸ O SMOW [‰]	<i>d</i> [‰]
TW-10-44	spring	37.9125	35.0742	1573	1573	0.00	22. May 10	-81.8	-12.4	17.5
TW-10-45	stream	37.8935	35.1007	1589	2524	85.69	22. May 10	-77.4	-11.9	17.4
TW-10-46	stream	37.8983	35.1061	1611	2534	84.83	22. May 10	-78.8	-11.9	16.4
TW-10-47	stream	37.8878	35.1000	1533	2520	86.08	22. May 10	-77.4	-13.0	26.8
TW-10-48	spring	37.9181	35.1341	1680	1711	0.00	22. May 10	-76.3	-11.6	16.8
TW-10-49	stream	37.9181	35.1341	1680	2695	65.96	22. May 10	-77.3	-11.9	17.7
TW-10-50	creek	37.9410	35.1540	1637	2536	0.00	22. May 10	-75.8	-12.6	24.8
TW-10-51	spring	37.8825	35.1077	1604	1604	0.01	22. May 10	-79.1	-11.8	15.5
TW-10-52	spring	37.7601	34.5673	1115	1115	0.00	23. May 10	-68.1	-9.8	10.5
TW-10-53	spring	37.6675	34.5324	1384	1386	0.00	23. May 10	-71.4	-10.1	9.2
TW-10-54	spring	37.6579	34.5290	1460	1467	0.00	23. May 10	-73.6	-10.0	6.5
TW-10-55	spring	37.5502	34.4734	1437	1489	0.21	23. May 10	-73.5	-10.2	8.4
TW-10-56	spring	37.5473	34.4465	1465	1465	0.00	23. May 10	-75.5	-11.8	18.7
TW-10-57	spring	37.5287	34.3706	1512	1518	0.02	23. May 10	-73.2	-10.1	7.4
TW-10-58	creek	37.5434	34.4222	1520	1642	12.18	23. May 10	-72.8	-11.5	19.4
TW-10-59	spring	37.6630	34.4604	1212	1212	0.01	23. May 10	-71.3	-11.1	17.7
TW-10-60	spring	37.5105	34.7705	947	997	0.05	24. May 10	-64.0	-11.2	25.4
TW-10-61	creek	37.5104	34.7736	940	1726	634.37	24. May 10	-66.9	-11.5	25.2
TW-10-62	spring	37.4695	34.8793	1004	1004	0.00	24. May 10	-68.5	-12.2	29.2
TW-10-63	spring	37.4916	34.9118	1190	1198	0.02	24. May 10	-57.3	-9.8	20.8
TW-10-64	creek	37.5304	34.9373	1169	1519	17.80	24. May 10	-57.0	-10.6	27.4
TW-10-65	spring	37.5473	34.9452	1189	1190	0.00	24. May 10	-65.6	-10.6	19.1
TW-10-66	stream	37.5563	34.9548	1106	1899	1280.32	24. May 10	-74.3	-11.2	15.1
TW-10-67	creek	37.5579	34.9756	1294	1839	6.92	24. May 10	-60.9	-11.3	29.2
TW-10-68	creek	37.5396	35.0113	1219	1736	4.88	24. May 10	-57.0	-10.7	28.3
TW-10-69	spring	37.5329	35.0139	1175	1216	0.01	24. May 10	-52.7	-8.7	17.1
TW-10-70	spring	37.5248	35.0325	1019	1117	0.04	24. May 10	-53.5	-10.1	27.4
TW-10-71	creek	37.5111	35.0331	935	1484	3.63	24. May 10	-54.8	-9.7	22.9
TW-10-72	stream	37.5104	35.0545	890	1869	1363.76	24. May 10	-71.3	-12.3	27.2
TW-10-73	creek	37.4987	35.0683	864	1249	0.55	24. May 10	-44.0	-8.9	26.8
TW-10-74	spring	37.4800	35.0829	881	911	0.01	24. May 10	-42.9	-8.9	28.3
TW-10-75	spring	37.4845	35.1322	901	921	0.01	24. May 10	-47.2	-9.2	26.1
TW-10-76	stream	37.5522	35.1545	913	1837	136.17	24. May 10	-57.5	-10.9	29.9
TW-10-77	stream	37.5579	35.3527	675	1037	77.41	24. May 10	-38.4	-7.6	22.2
TW-10-78	creek	37.4854	35.4010	875	1167	11.17	24. May 10	-42.9	-7.7	18.3
TW-10-79	spring	37.4625	35.4148	691	691	0.00	24. May 10	-57.1	-9.6	19.8
TW-10-80	spring	37.1701	35.5608	206	209	0.00	24. May 10	-29.4	-5.0	10.7
TW-10-81	spring	37.9818	34.3750	1174	1181	0.01	25. May 10	-76.5	-11.7	17.3
TW-10-82	spring	38.0156	34.2709	1242	1242	0.05	25. May 10	-73.6	-12.5	26.4
TW-10-83	spring	38.1764	34.0262	1052	1069	0.02	25. May 10	-73.9	-12.9	29.1
TW-10-84	spring	38.2290	33.9997	998	998	0.19	25. May 10	-66.2	-8.5	2.0
TW-10-85	spring	38.3555	33.9719	955	990	0.27	25. May 10	-69.2	-9.9	9.9
TW-10-86	spring	38.3902	33.9904	964	1007	0.17	25. May 10	-69.1	-9.8	9.0
TW-10-87	spring	38.4215	33.9597	980	990	0.05	25. May 10	-67.7	-9.8	10.3
TW-10-88	spring	38.8146	33.6056	921	990	0.60	25. May 10	-62.8	-9.8	15.8
TW-10-89	spring	39.0518	33.4353	906	990	2.94	25. May 10	-86.4	-12.0	9.4
TW-10-90	spring	39.2270	33.0369	1001	1012	0.06	25. May 10	-70.0	-9.4	5.5
TW-10-91	spring	39.3572	32.9142	1073	1087	0.01	25. May 10	-70.1	-9.7	7.7

sample #	sample type	latitude [°N]	longitude [°E]	sampling elevation [m]	average catchment elevation [m]	catchment area [km ²]	sampling date	δD SMOW [‰]	δ ¹⁸ O SMOW [‰]	d [‰]
TW-10-92	spring	39.6408	32.8258	1058	1060	0.00	25. May 10	-66.6	-8.6	2.5
TW-10-93	stream	40.1044	32.0277	502	1216	4629.62	26. May 10	-61.0	-8.8	9.3
TW-10-94	spring	40.1707	31.9258	649	684	0.01	26. May 10	-70.4	-11.0	17.2
TW-10-96	spring	40.2177	31.8916	810	858	0.02	26. May 10	-70.8	-10.9	16.6
TW-10-97	spring	40.1853	31.9153	718	821	0.01	26. May 10	-59.3	-7.9	4.1
TW-10-98	stream	40.1936	31.6674	504	1284	2476.48	26. May 10	-66.1	-9.7	11.2
TW-10-99	spring	40.1918	31.7120	656	678	0.03	26. May 10	-62.7	-8.8	7.8
TW-10-100	spring	40.1006	31.6723	485	498	0.00	26. May 10	-64.7	-9.3	9.4
TW-10-101	spring	40.1331	31.6238	551	615	0.00	26. May 10	-66.9	-10.0	13.2
TW-10-102	spring	40.1050	31.5969	489	490	0.00	26. May 10	-52.7	-6.4	-1.7
VP-06-01	spring	38.6303	34.9101	1057	1080	0.00	15. Jun 10	-81.5	-11.4	9.5
VP-06-02	spring	38.4894	34.9471	1330	1352	0.00	15. Jun 10	-78.5	-10.9	8.5
VP-06-03	spring	38.4925	34.9507	1324	1324	0.00	15. Jun 10	-78.5	-10.9	9.0
VP-06-04	spring	38.5124	34.9459	1276	1288	0.01	15. Jun 10	-83.8	-11.8	10.4
VP-06-05	spring	38.5243	34.9331	1301	1306	0.00	15. Jun 10	-80.9	-11.3	9.2
VP-06-06	spring	38.3332	34.5302	1333	1359	0.00	16. Jun 10	-78.5	-11.0	9.7
VP-06-07	spring	38.3079	34.5080	1500	1510	0.01	16. Jun 10	-79.8	-11.2	10.1
VP-06-08	creek	38.3077	34.5093	1473	1668	3.82	16. Jun 10	-78.3	-11.0	9.8
VP-06-09	spring	38.3154	34.5075	1466	1466	0.00	16. Jun 10	-78.7	-11.0	9.4
VP-06-10	spring	38.3267	34.5201	1404	1404	0.00	16. Jun 10	-78.7	-11.0	9.3
VP-06-11	spring	38.3524	34.4325	1355	1359	0.03	16. Jun 10	-73.8	-10.3	8.5
VP-06-12	creek	38.6235	34.8339	1145	1313	2.57	17. Jun 10	-77.5	-10.7	8.2
VP-06-13	spring	38.6417	34.8291	1115	1126	0.03	17. Jun 10	-85.1	-11.8	9.5
VP-06-14	spring	38.6356	34.8894	1179	1179	0.00	17. Jun 10	-72.4	-9.8	5.7
VP-06-15	spring	38.7013	34.9724	1131	1131	0.00	18. Jun 10	-68.2	-9.1	4.5
VP-06-16	spring	38.7072	34.9858	1115	1117	0.00	18. Jun 10	-64.7	-8.2	0.8
VP-06-17	spring	38.7110	34.9907	1077	1082	0.00	18. Jun 10	-66.6	-8.8	4.1
VP-06-18	spring	38.6408	34.9217	1058	1058	0.00	18. Jun 10	-86.4	-12.1	10.2
VP-06-19	spring	38.6325	34.9168	1061	1061	0.01	18. Jun 10	-85.8	-12.0	10.0
VP-06-20	spring	38.6272	34.7203	1152	1190	0.00	19. Jun 10	-82.4	-11.4	8.5
VP-06-21	spring	38.7333	34.9305	938	939	0.01	19. Jun 10	-67.8	-9.0	4.1
VP-06-22	spring	38.6963	35.2367	1077	1077	0.00	19. Jun 10	-72.4	-9.7	5.1
VP-06-23	spring	38.7223	35.1943	1345	1369	0.01	19. Jun 10	-69.9	-9.4	5.5
VP-06-24	spring	38.7150	35.2169	1223	1223	0.00	19. Jun 10	-75.7	-10.4	7.6
VP-06-25	spring	38.6912	35.1865	1227	1227	0.01	19. Jun 10	-73.1	-10.4	10.3
VP-06-26	spring	38.4465	35.1404	1101	1105	0.77	19. Jun 10	-79.3	-11.4	11.5
VP-06-27	spring	38.4443	35.0733	1313	1332	0.01	19. Jun 10	-82.1	-11.8	12.6
VP-06-28	spring	38.4480	35.0655	1435	1435	0.03	19. Jun 10	-82.9	-11.9	12.5
VP-06-29	spring	38.4551	35.0483	1473	1497	0.02	19. Jun 10	-83.6	-11.9	11.3
VP-06-30	spring	38.3924	35.1025	1122	1122	0.33	19. Jun 10	-71.9	-10.0	8.2
VP-06-31	spring	38.5505	35.0837	1489	1491	0.01	19. Jun 10	-76.5	-10.8	10.1
VP-06-32	spring	38.5715	35.0690	1390	1391	0.00	19. Jun 10	-72.2	-10.0	7.4
VP-06-33	spring	38.6326	34.9388	1117	1117	0.00	20. Jun 10	-85.9	-12.2	11.5
VP-06-34	spring	38.5920	34.9910	1210	1210	0.00	20. Jun 10	-76.3	-10.6	8.6
VP-06-35	spring	38.5426	35.0226	1494	1514	0.01	20. Jun 10	-77.2	-11.0	10.7
VP-06-36	spring	38.6175	34.9098	1091	1091	0.01	20. Jun 10	-82.0	-11.6	10.5
VP-06-37	spring	38.5485	34.8702	1299	1317	0.02	20. Jun 10	-78.0	-10.8	8.2
VP-06-38	spring	38.4738	34.7524	1432	1433	0.00	20. Jun 10	-82.8	-11.7	10.6

sample #	sample type	latitude [°N]	longitude [°E]	sampling elevation [m]	average catchment elevation [m]	catchment area [km ²]	sampling date	δD SMOW [‰]	δ ¹⁸ O SMOW [‰]	<i>d</i> [‰]
VP-06-39	spring	38.5497	34.7495	1347	1353	0.28	20. Jun 10	-84.1	-11.7	9.7
VP-06-40	spring	38.5999	34.7191	1262	1266	0.04	20. Jun 10	-84.8	-11.9	10.5
VP-06-41	spring	38.6993	34.5748	1044	1044	0.00	21. Jun 10	-80.0	-11.1	8.6
VP-06-42	spring	38.6358	34.4830	1101	1134	0.00	21. Jun 10	-76.6	-9.9	2.4
VP-06-43	spring	38.5842	34.5668	1328	1362	0.01	21. Jun 10	-82.4	-11.6	10.4
VP-06-44	spring	38.4739	34.5078	1316	1320	0.00	21. Jun 10	-78.8	-11.1	10.0
VP-06-45	spring	38.6235	34.9142	1100	1100	0.01	22. Jun 10	-86.2	-12.3	12.1
VP-06-46	spring	38.5840	34.8990	1160	1161	0.00	22. Jun 10	-79.7	-11.1	9.1
VP-06-47	spring	38.5719	34.9173	1169	1169	0.01	22. Jun 10	-82.2	-10.9	4.7
VP-06-48	spring	38.5243	34.9331	1297	1297	0.00	22. Jun 10	-81.6	-11.6	10.9
VP-07-01	spring	40.0853	33.3671	1072	1094	0.00	6. Oct 10	-68.3	-9.6	8.7
VP-07-03	spring	40.3390	32.6956	970	1033	0.05	10. Oct 10	-66.4	-9.7	11.5
VP-07-04	spring	40.3494	32.6825	993	1012	0.00	10. Oct 10	-68.6	-9.9	10.4
VP-07-05	creek	40.3494	32.6825	993	1289	158.62	10. Oct 10	-68.3	-10.1	12.2
VP-07-06	spring	40.4910	32.6466	966	993	0.00	10. Oct 10	-64.7	-9.9	14.6
VP-07-07	spring	40.5663	32.6529	1084	1113	0.01	10. Oct 10	-72.2	-10.7	13.6
VP-07-08	creek	40.5714	32.6610	1043	1268	0.18	10. Oct 10	-69.1	-10.1	12.0
VP-07-09	spring	40.5850	32.6623	1061	1111	0.03	10. Oct 10	-72.3	-10.8	14.3
VP-07-10	creek	40.6061	32.6648	1097	1288	0.18	10. Oct 10	-69.4	-10.3	12.7
VP-07-11	spring	40.6613	32.7075	1392	1404	0.00	10. Oct 10	-76.5	-11.6	16.2
VP-07-12	spring	40.7038	32.7392	1483	1499	0.01	10. Oct 10	-72.3	-11.0	16.0
VP-07-13	spring	40.8103	32.8938	1122	1131	0.00	10. Oct 10	-75.7	-11.0	12.0
VP-07-14	stream	40.8257	32.8142	1100	1378	4.27	10. Oct 10	-79.7	-11.3	10.8
VP-07-15	spring	40.8682	32.5957	1013	1073	0.02	10. Oct 10	-66.1	-9.2	7.3
VP-07-16	spring	40.9141	32.5826	937	937	0.01	10. Oct 10	-69.4	-9.7	8.2
VP-07-17	spring	40.9869	32.5632	662	683	0.07	10. Oct 10	-73.9	-10.9	13.3
VP-07-18	spring	41.0744	32.6578	434	460	0.01	10. Oct 10	-66.8	-9.6	10.2
VP-07-19	spring	41.3892	32.7786	988	998	0.00	10. Oct 10	-68.2	-10.5	16.0
VP-07-20	spring	41.4297	32.9921	924	942	0.01	10. Oct 10	-71.9	-10.6	13.2
VP-07-21	spring	41.4469	33.0373	974	984	0.00	10. Oct 10	-71.0	-10.4	12.4
VP-07-22	spring	41.4703	33.0246	958	972	0.02	10. Oct 10	-72.9	-10.6	12.2
VP-07-23	spring	41.4826	33.0273	984	1002	0.01	10. Oct 10	-73.9	-10.8	12.3
VP-07-24	spring	41.5117	33.0565	998	1017	0.00	10. Oct 10	-74.7	-10.9	12.2
VP-07-26	spring	41.6588	33.1272	457	581	0.02	10. Oct 10	-71.9	-10.5	12.2
VP-07-27	stream	41.6706	33.1576	413	1121	1702.88	10. Oct 10	-71.3	-10.0	8.9
VP-07-29	spring	41.6772	33.1983	794	804	0.00	10. Oct 10	-78.6	-11.5	13.5
VP-07-30	spring	41.6961	33.2417	813	840	0.00	10. Oct 10	-76.7	-11.1	11.8
VP-07-31	creek	41.7010	33.2433	848	945	0.26	10. Oct 10	-61.3	-8.7	8.6
VP-07-32	spring	41.7728	33.1943	451	457	0.00	10. Oct 10	-73.9	-11.0	13.9
VP-07-33	spring	41.7751	33.2068	570	586	0.00	10. Oct 10	-68.6	-10.8	17.6
VP-07-34	spring	41.8275	33.3051	463	473	0.01	10. Oct 10	-71.0	-11.2	18.2
VP-07-35	spring	41.1232	33.7629	1224	1347	0.01	11. Oct 10	-71.6	-10.8	15.1
VP-07-36	spring	41.0415	33.7359	1501	1601	0.01	11. Oct 10	-78.6	-11.9	16.8
VP-07-37	spring	40.8779	33.2973	1327	1344	0.00	12. Oct 10	-79.5	-11.5	12.3
VP-07-38	spring	40.9259	33.8303	765	780	0.01	14. Oct 10	-73.5	-11.1	15.5
VP-07-39	spring	40.7119	32.7681	1297	1297	0.00	14. Oct 10	-68.3	-9.8	10.4
VP-07-40	spring	40.6814	32.7207	1505	1527	0.01	14. Oct 10	-81.1	-11.9	13.9
VP-07-41	spring	40.2227	32.5939	1032	1059	0.00	15. Oct 10	-66.9	-9.2	6.6

sample #	sample type	latitude [°N]	longitude [°E]	sampling elevation [m]	average catchment elevation [m]	catchment area [km ²]	sampling date	δD SMOW [‰]	δ ¹⁸ O SMOW [‰]	<i>d</i> [‰]
VP-07-42	spring	40.2677	32.6300	1256	1277	0.00	15. Oct 10	-73.6	-10.7	11.6
VP-07-43	spring	40.2650	32.6351	1215	1248	0.01	15. Oct 10	-69.0	-10.0	10.9
VP-08-001	spring	38.0427	32.9239	988	1045	0.08	24. May 11	-95.8	-13.0	7.8
VP-08-002	creek	37.0106	35.6322	83	168	21.97	27. May 11	-25.9	-4.5	10.3
VP-08-003	spring	37.0893	35.4907	230	206	0.00	29. May 11	-30.7	-5.3	11.9
VP-08-004	spring	37.2591	35.6635	82	82	0.00	29. May 11	-28.2	-5.1	12.4
VP-08-005	stream	37.3405	35.7541	70	319	212.63	29. May 11	-29.4	-5.6	15.1
VP-08-006	stream	37.4118	35.7841	99	603	356.12	29. May 11	-33.2	-6.4	17.9
VP-08-007	creek	37.5502	35.8353	293	532	7.16	29. May 11	-36.9	-7.0	19.4
VP-08-008	stream	37.5733	35.8375	360	797	27.05	29. May 11	-35.4	-6.9	20.0
VP-08-009	spring	37.6367	35.8489	658	704	0.01	29. May 11	-38.6	-7.3	20.0
VP-08-010	spring	37.6864	35.8772	649	650	0.00	29. May 11	-40.5	-7.4	19.0
VP-08-011	stream	37.8158	35.9085	556	1504	735.42	29. May 11	-53.3	-9.1	19.3
VP-08-012	stream	37.8532	35.9597	595	1618	3281.78	29. May 11	-58.0	-9.4	17.0
VP-08-013	creek	37.8989	36.0760	737	1503	221.32	29. May 11	-52.3	-8.8	18.1
VP-08-014	spring	37.9934	36.0927	971	1042	0.02	29. May 11	-49.2	-8.3	16.9
VP-08-015	spring	38.0221	36.1055	1221	1320	0.01	29. May 11	-51.2	-8.7	18.1
VP-08-016	spring	38.0403	36.1125	1451	1467	0.01	29. May 11	-49.8	-8.3	16.9
VP-08-017	stream	38.1336	36.1315	1382	1663	38.84	29. May 11	-57.0	-8.9	14.0
VP-08-018	spring	38.1847	36.0758	1570	1571	0.00	29. May 11	-67.6	-10.2	13.8
VP-08-019	creek	38.2119	36.0133	1710	1992	5.84	29. May 11	-64.3	-10.0	15.5
VP-08-020	spring	38.2082	36.0006	1872	1912	0.00	29. May 11	-70.3	-10.6	14.7
VP-08-021	spring	38.1721	35.9272	1648	1648	0.00	29. May 11	-71.8	-10.9	15.1
VP-08-022	spring	38.2025	35.8943	1474	1499	0.01	29. May 11	-69.6	-10.3	12.9
VP-08-023	spring	38.2084	35.8886	1436	1467	0.01	29. May 11	-65.2	-9.2	8.7
VP-08-024	stream	38.2107	35.8692	1341	1708	7113.39	29. May 11	-69.0	-10.2	12.6
VP-08-025	stream	38.2026	35.8479	1330	1803	152.53	29. May 11	-60.3	-9.6	16.1
VP-08-026	spring	38.3214	35.6740	1314	1330	0.03	29. May 11	-75.1	-10.7	10.7
VP-08-027	spring	38.3457	35.5801	1392	1392	0.00	29. May 11	-76.5	-11.0	11.5
VP-08-028	spring	38.0762	34.8191	1360	1360	0.03	30. May 11	-76.9	-10.8	9.2
VP-08-029	creek	37.9839	35.0833	1659	1995	22.58	30. May 11	-74.9	-10.9	12.0
VP-08-030	spring	37.7064	33.6618	1052	1052	0.01	30. May 11	-71.6	-10.3	10.9
VP-08-031	spring	37.7381	33.0439	1008	1045	0.00	30. May 11	-63.5	-9.2	9.9
VP-08-032	spring	37.7836	32.9323	1007	1045	0.95	30. May 11	-77.1	-11.1	11.6
VP-08-033	spring	37.8381	32.7835	1007	1045	0.84	30. May 11	-70.3	-10.1	10.8
VP-08-034	spring	37.9959	32.6012	1002	1045	1.05	30. May 11	-69.2	-10.0	10.7
VP-08-035	spring	38.1216	32.7295	1060	1060	0.01	30. May 11	-73.6	-10.8	12.8
VP-08-036	spring	38.2761	32.7650	981	990	0.23	30. May 11	-69.6	-10.3	12.6
VP-08-037	spring	38.6555	32.9185	954	990	0.84	30. May 11	-71.3	-9.6	5.6
VP-08-038	spring	38.9359	33.0035	975	990	0.20	30. May 11	-64.1	-8.4	2.8
VP-08-039	spring	39.4497	32.8649	1102	1108	0.01	30. May 11	-67.5	-9.0	4.1
VP-08-040	spring	39.6408	32.8258	1059	1060	0.00	30. May 11	-66.5	-8.6	2.2
VP-08-041	spring	39.6705	33.0207	1010	1029	0.01	04. Jun 11	-66.7	-8.9	4.6
VP-08-042	spring	39.5575	33.2798	944	951	0.01	04. Jun 11	-65.3	-8.2	0.1
VP-08-043	spring	39.7835	33.4590	680	678	0.00	04. Jun 11	-62.2	-8.0	2.0
VP-08-044	spring	40.2695	33.3962	919	929	0.01	04. Jun 11	-67.6	-8.9	3.8
VP-08-045	creek	39.4982	33.6405	896	1051	234.60	06. Jun 11	-59.0	-7.4	0.4
VP-08-046	spring	39.4945	33.6134	938	940	0.01	06. Jun 11	-61.5	-7.7	-0.1

sample #	sample type	latitude [°N]	longitude [°E]	sampling elevation [m]	average catchment elevation [m]	catchment area [km ²]	sampling date	δD SMOW [‰]	δ ¹⁸ O SMOW [‰]	<i>d</i> [‰]
VP-08-048	spring	38.1684	32.4667	1214	1214	0.00	07. Jun 11	-68.7	-9.4	6.1
VP-08-049	spring	37.8971	32.2953	1270	1276	0.01	07. Jun 11	-60.6	-8.3	6.0
VP-08-050	spring	37.9285	32.2831	1319	1337	0.00	07. Jun 11	-73.8	-10.5	10.1
VP-08-051	stream	40.9929	32.5932	590	1182	474.48	09. Jun 11	-72.9	-10.7	12.6
VP-08-052	creek	41.1577	32.4652	231	1264	0.56	09. Jun 11	-69.5	-10.5	14.6
VP-08-053	creek	41.1728	32.4469	184	831	1.33	09. Jun 11	-67.0	-10.3	15.6
VP-08-054	stream	41.2042	32.3680	144	1097	155.40	09. Jun 11	-70.1	-10.7	15.3
VP-08-055	creek	41.2530	32.1616	90	605	37.00	09. Jun 11	-63.7	-9.8	14.9
VP-08-056	spring	41.4218	32.1759	30	39	0.00	09. Jun 11	-51.4	-7.7	10.0
VP-08-057	spring	41.4686	32.2751	71	85	0.01	09. Jun 11	-61.1	-9.2	12.3
VP-08-058	spring	41.6872	32.3789	60	84	0.00	09. Jun 11	-61.9	-10.1	19.1
VP-08-059	spring	41.7854	32.5370	6	35	0.00	10. Jun 11	-59.2	-9.6	17.9
VP-08-060	spring	41.7850	32.5407	9	14	0.02	10. Jun 11	-60.4	-9.7	17.2
VP-08-061	spring	41.7890	32.5515	43	62	0.00	10. Jun 11	-61.9	-10.0	17.7
VP-08-062	spring	41.8118	32.5921	224	277	0.01	10. Jun 11	-59.2	-9.7	18.2
VP-08-063	creek	41.8064	32.5970	185	354	0.05	10. Jun 11	-58.6	-9.7	18.7
VP-08-064	creek	41.7999	32.6066	116	413	15.47	10. Jun 11	-61.7	-9.9	17.6
VP-08-065	spring	41.8280	32.6577	128	148	0.00	10. Jun 11	-59.9	-9.5	15.8
VP-08-066	creek	41.8357	32.7091	51	420	2.73	10. Jun 11	-63.7	-9.9	15.4
VP-08-067	spring	41.8454	32.7493	73	90	0.01	10. Jun 11	-57.0	-8.9	14.5
VP-08-068	stream	41.8716	32.9429	-1	1005	2847.10	10. Jun 11	-66.3	-9.7	11.1
VP-08-069	creek	41.9226	33.0509	120	350	2.51	10. Jun 11	-55.1	-8.7	14.7
VP-08-070	spring	41.9311	33.0723	114	136	0.02	10. Jun 11	-56.1	-8.6	12.6
VP-08-071	stream	41.9318	33.0864	5	906	741.68	10. Jun 11	-66.3	-10.0	14.0
VP-08-072	creek	41.9441	33.1222	166	326	0.14	10. Jun 11	-56.4	-8.9	15.0
VP-08-073	creek	41.9606	33.2040	35	229	0.78	10. Jun 11	-58.2	-9.2	15.3
VP-08-074	creek	41.9735	33.2337	6	461	31.42	10. Jun 11	-62.6	-9.9	16.4
VP-08-075	spring	42.0038	33.2945	34	38	0.00	10. Jun 11	-54.2	-8.8	16.4
VP-08-076	stream	42.0102	33.3652	2	668	192.04	10. Jun 11	-65.6	-10.3	16.9
VP-08-077	creek	42.0037	33.4704	62	284	0.94	10. Jun 11	-56.3	-9.2	17.5
VP-08-078	creek	41.9916	33.5298	4	682	131.35	10. Jun 11	-67.1	-10.5	17.1
VP-08-079	spring	41.9845	33.5852	97	132	0.00	10. Jun 11	-58.4	-9.4	16.6
VP-08-080	creek	41.9838	33.6530	35	537	1.36	10. Jun 11	-56.9	-9.3	17.8
VP-08-081	creek	41.9689	33.8403	45	648	22.98	11. Jun 11	-59.0	-9.5	16.8
VP-08-082	stream	41.9739	33.8852	5	917	113.04	11. Jun 11	-64.6	-9.8	13.9
VP-08-083	stream	41.9797	33.9728	1	921	99.03	11. Jun 11	-65.0	-9.9	14.1
VP-08-084	creek	41.9777	34.0726	49	293	0.21	11. Jun 11	-54.0	-8.6	14.6
VP-08-085	creek	41.9625	34.1073	112	449	17.44	11. Jun 11	-58.6	-9.2	15.0
VP-08-086	spring	41.9658	34.1313	217	239	0.00	11. Jun 11	-58.4	-9.5	17.4
VP-08-087	stream	41.9570	34.1920	8	571	54.42	11. Jun 11	-61.7	-9.6	15.4
VP-08-088	stream	41.9501	34.2277	9	960	470.83	11. Jun 11	-59.3	-9.3	14.8
VP-08-089	creek	41.9466	34.2714	5	356	3.17	11. Jun 11	-50.6	-8.1	14.0
VP-08-090	stream	41.9479	34.3407	7	620	133.82	11. Jun 11	-53.7	-8.6	15.0
VP-08-091	stream	41.9104	34.4232	60	369	76.12	11. Jun 11	-47.3	-7.6	13.8
VP-08-092	spring	41.8773	34.5487	126	131	0.00	11. Jun 11	-63.8	-9.9	15.3
VP-08-093	stream	41.8943	34.5724	104	845	221.20	11. Jun 11	-57.3	-9.1	15.4
VP-08-094	creek	41.9452	34.6936	16	362	46.70	11. Jun 11	-57.7	-9.3	16.8
VP-08-095	stream	41.8340	35.1571	-7	826	301.73	11. Jun 11	-62.0	-9.5	13.7

sample #	sample type	latitude [°N]	longitude [°E]	sampling elevation [m]	average catchment elevation [m]	catchment area [km ²]	sampling date	δD SMOW [‰]	δ ¹⁸ O SMOW [‰]	<i>d</i> [‰]
VP-08-096	spring	41.7578	35.2135	90	127	0.01	11. Jun 11	-54.0	-8.6	14.6
VP-08-097	spring	41.7104	35.2614	248	302	0.01	11. Jun 11	-54.2	-8.9	17.3
VP-08-098	creek	41.7016	35.2672	236	550	1.18	11. Jun 11	-54.2	-8.9	17.2
VP-08-099	stream	41.6798	35.3657	41	861	673.70	11. Jun 11	-60.2	-9.4	14.8
VP-08-100	stream	41.6757	35.3995	16	832	753.25	11. Jun 11	-59.9	-9.5	16.3
VP-08-101	stream	41.6393	35.4956	0	770	132.23	11. Jun 11	-58.5	-9.2	15.3
VP-08-102	stream	41.6031	35.5955	29	601	156.92	11. Jun 11	-56.2	-9.1	16.2
VP-08-103	spring	41.5050	35.5907	813	816	0.01	11. Jun 11	-65.2	-10.4	18.2
VP-08-104	creek	41.4628	35.5067	1058	1108	0.01	11. Jun 11	-59.1	-9.3	15.6
VP-08-105	creek	41.4626	35.5043	1061	1330	1.91	11. Jun 11	-64.2	-10.1	16.4
VP-08-106	spring	41.4599	35.4803	1226	1237	0.00	11. Jun 11	-67.5	-10.5	16.3
VP-08-107	spring	41.4366	35.4206	1210	1218	0.00	11. Jun 11	-72.3	-10.9	14.6
VP-08-108	creek	41.4391	35.4677	1421	1425	0.01	11. Jun 11	-61.3	-9.5	14.5
VP-08-109	spring	41.5595	35.6015	533	533	0.00	11. Jun 11	-58.1	-9.6	18.3
VP-08-110	spring	41.2065	36.3139	317	346	0.00	12. Jun 11	-61.1	-9.8	17.0
VP-08-111	spring	41.1847	36.3380	562	583	0.00	12. Jun 11	-61.7	-10.0	17.9
VP-08-112	spring	41.1740	36.3353	689	732	0.00	12. Jun 11	-62.1	-9.9	17.3
VP-08-113	spring	41.1527	36.3303	760	784	0.00	12. Jun 11	-62.1	-9.9	16.9
VP-08-114	spring	41.1175	36.2991	752	752	0.00	12. Jun 11	-66.9	-10.6	18.1
VP-08-115	spring	41.1105	36.2864	832	840	0.00	12. Jun 11	-67.3	-10.5	16.9
VP-08-116	spring	41.0836	36.2751	843	876	0.01	12. Jun 11	-67.2	-10.5	17.0
VP-08-117	spring	41.0575	36.2568	761	773	0.01	12. Jun 11	-69.5	-10.3	12.8
VP-08-118	spring	41.0304	36.2084	801	816	0.00	12. Jun 11	-70.6	-10.5	13.6
VP-08-119	spring	41.0142	36.1778	743	754	0.00	12. Jun 11	-70.8	-10.6	13.6
VP-08-120	creek	41.0267	36.1275	562	789	29.47	12. Jun 11	-61.2	-9.5	14.4
VP-08-121	creek	41.0563	36.1057	485	765	298.73	12. Jun 11	-61.2	-9.3	13.0
VP-08-122	spring	40.7198	35.4040	639	648	0.01	12. Jun 11	-67.0	-8.9	4.0
VP-08-123	spring	40.6135	35.1647	999	1005	0.01	12. Jun 11	-65.7	-9.2	7.8
VP-08-124	spring	40.6058	35.0760	1141	1179	0.03	12. Jun 11	-70.1	-10.1	10.8
VP-08-125	spring	40.2200	34.5594	927	935	0.00	12. Jun 11	-66.9	-9.0	4.9
VP-08-126	spring	40.1391	34.2175	663	670	0.57	12. Jun 11	-58.5	-7.1	-1.9
VP-08-127	spring	39.9378	33.8502	933	942	0.07	12. Jun 11	-66.7	-8.7	2.8
VP-09-01	spring	38.7591	34.9007	1079	1096	0.02	18. Sep 11	-66.2	-8.9	4.8
VP-09-02	spring	38.8316	34.9435	1059	1059	0.00	18. Sep 11	-74.0	-10.4	9.1
VP-09-03	spring	38.9634	35.0055	1164	1164	0.01	18. Sep 11	-74.6	-10.2	6.7
VP-09-04	spring	39.0776	35.1291	1086	1087	0.01	18. Sep 11	-69.6	-9.1	3.1
VP-09-05	spring	39.1588	35.2236	1074	1074	0.00	18. Sep 11	-74.7	-10.2	6.8
VP-09-06	spring	39.3055	35.2849	1102	1103	0.00	18. Sep 11	-67.1	-9.0	5.1
VP-09-07	spring	39.4271	35.3578	1231	1237	0.02	18. Sep 11	-75.1	-10.4	8.3
VP-09-08	spring	39.6168	35.2476	1122	1122	0.01	18. Sep 11	-67.2	-9.5	8.7
VP-09-09	spring	39.6350	35.2302	1082	1082	0.00	18. Sep 11	-68.8	-9.2	4.5
VP-09-10	spring	39.7140	35.2236	1050	1076	0.14	18. Sep 11	-67.1	-8.9	4.0
VP-09-11	spring	39.7629	35.2296	1042	1044	0.02	18. Sep 11	-66.9	-8.7	2.8
VP-09-12	spring	39.8408	35.3000	1124	1133	0.00	18. Sep 11	-67.0	-9.2	6.7
VP-09-13	spring	38.4424	31.3261	966	1028	0.03	24. Sep 11	-63.8	-10.2	18.0
VP-09-14	spring	38.5894	30.9665	973	1041	0.05	24. Sep 11	-70.7	-10.7	14.6
VP-09-15	spring	38.6384	30.8182	985	1028	1.06	24. Sep 11	-65.7	-9.2	8.0
VP-09-16	spring	38.8052	30.0256	1198	1227	0.01	24. Sep 11	-61.7	-9.0	10.5

sample #	sample type	latitude [°N]	longitude [°E]	sampling elevation [m]	average catchment elevation [m]	catchment area [km ²]	sampling date	δD SMOW [‰]	δ ¹⁸ O SMOW [‰]	<i>d</i> [‰]
VP-09-17	spring	38.8143	30.0127	1227	1260	0.02	24. Sep 11	-60.9	-9.1	11.5
VP-09-19	spring	38.7771	29.8173	943	972	0.00	24. Sep 11	-62.3	-9.2	10.9
VP-09-20	spring	38.9425	30.0838	1086	1117	0.00	24. Sep 11	-62.7	-9.1	9.8
VP-09-21	spring	39.0242	30.1241	1015	1036	0.00	24. Sep 11	-59.1	-8.0	5.0
VP-09-22	spring	39.5217	30.0564	884	923	0.01	24. Sep 11	-64.0	-9.0	8.0
VP-09-23	spring	39.5840	30.1249	882	939	0.01	24. Sep 11	-66.4	-9.4	8.4
VP-09-24	spring	39.4976	31.2354	1001	1027	0.01	24. Sep 11	-66.1	-8.9	4.8

Tab. A.2 Isotopic lapse rates in the Pontic and Taurus Mountains based on surface water flows. The Pontic lapse rates are based on a sample subset from two transects; individual lapse rates are shown separately. All lapse rates were forced through the assumed near-sea level δD and δ¹⁸O values of the GNIP station Sinop (Pontic Mts.) and Adana (Taurus Mts.), hence the very low R² value of δ¹⁸O lapse rate of the eastern transect through the Pontic Mountains. R² without forcing would be 0.49.

	lapse rates				n
	δD [‰/km]	R ²	δ ¹⁸ O [‰/km]	R ²	
Pontic Mts.	-19	0.68	-2.6	0.50	26
<i>western transect</i>	-18	0.74	-2.4	0.74	15
<i>eastern transect</i>	-22	0.74	-2.8	0.01*	11
Taurus Mts.	-20	0.71	-2.9	0.68	93

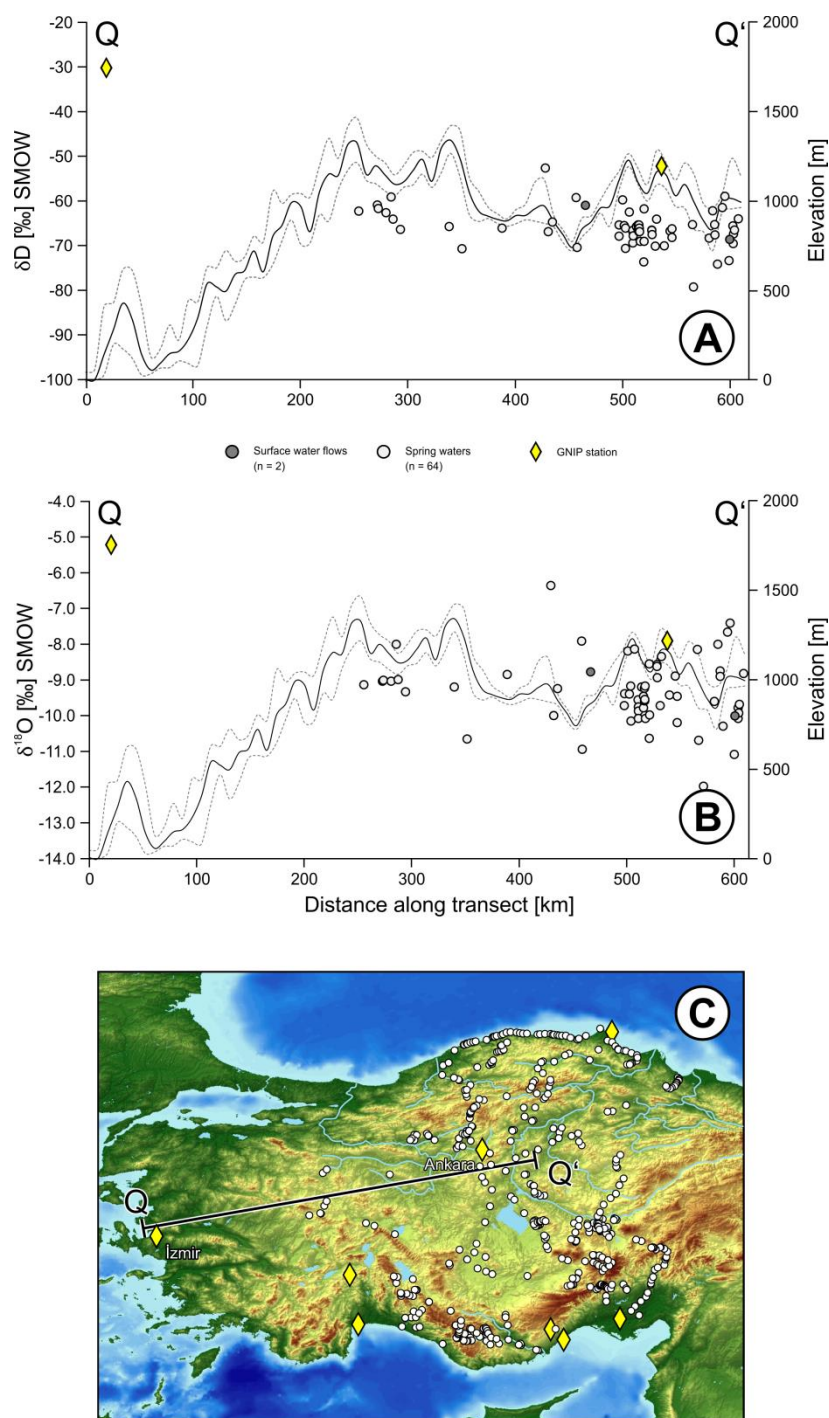


Fig. A.1 Spatial distribution of (A) δD and (B) $\delta^{18}O$ from the Aegean coast towards the plateau interior (C). Included in the transect are samples within a 50-km-swath along the profile as well as the long-term δD_p and $\delta^{18}O_p$ values of the GNIP stations at Izmir and Ankara (IAEA/WMO, 2006). Elevations (dotted and solid lines) correspond to the $Q_{.25}$, $Q_{.50}$ and $Q_{.75}$ quantiles of the elevation distribution at any point along the swath profile.

Tab. A.3 Age-depth correlation and sedimentation rates of core TP-2005 for the early to middle Holocene interval studied.

Sample name	Core depth [cm]	Age [kyr B.P.]	Sedimentation rate [mm/yr]
Phi2-472	472	7.54	0.48
Phi2-475	475	7.60	0.48
Phi2-478	478	7.67	0.49
Phi2-481	481	7.73	0.51
Phi2-484	484	7.78	0.47
Phi2-487	487	7.85	0.57
Phi2-490	490	7.90	0.58
Phi2-491	491	7.92	0.58
Phi2-492	492	7.94	0.58
Phi2-493	493	7.95	0.58
Phi2-494	494	7.97	0.58
Phi2-495	495	7.99	0.57
Phi2-496	496	8.00	0.57
Phi2-497	497	8.02	0.58
Phi2-498	498	8.04	0.59
Phi2-499	499	8.06	0.59
Phi2-500	500	8.07	0.58
Phi2-501	501	8.09	0.61
Phi2-502	502	8.11	0.67
Phi2-503	503	8.12	0.61
Phi2-504	504	8.14	0.58
Phi2-505	505	8.16	0.62
Phi2-506	506	8.17	0.61

Sample name	Core depth [cm]	Age [kyr B.P.]	Sedimentation rate [mm/yr]
Phi2-507	507	8.19	0.61
Phi2-508	508	8.20	0.63
Phi2-509	509	8.22	0.61
Phi2-512	512	8.27	0.63
Phi2-515	515	8.32	0.60
Phi2-518	518	8.37	0.62
Phi2-521	521	8.42	0.61
Phi2-524	524	8.46	0.62
Phi2-527	527	8.51	0.62
Phi2-530	530	8.56	0.60
Phi2-533	533	8.61	0.62
Phi2-536	536	8.66	

Curriculum vitae

Dipl. Geow.

FABIAN SCHEMME

born March 26th, 1980 in Essen
Germany

Lönsstraße 9
31787 Hameln
Germany

fabianschemmel@gmx.de

Education

- 10 / 2010 - 09 / 2016* **PhD student**
Institute of Geosciences, Goethe University Frankfurt am Main,
Germany
PhD Advisors: Prof Dr. Andreas Mulch
Prof. Dr. Jörg Pross
- 10 / 2002 - 10 / 2008* **Academic studies *Earth Sciences***
Leibniz University Hannover, Germany
Degree: Dipl. Geow.
Advisors: Prof. Dr. Friedhelm von Blanckenburg
Dr. Andreas Lückge
- 09 / 2001 - 08 / 2002* **Academic studies *Technology of Renewable Resources***
University of Applied Sciences, Hannover, Germany
- 06 / 2000* **Abitur**
Hölty Gymnasium Wunstorf, Germany

Work experience*since 08 / 2016***Scientific Associate**

DHD-Consulting GmbH

Hildesheim, Germany

*10 / 2010 - 12 / 2014***Research Assistant**Senckenberg Biodiversity and Climate Research Centre
(BiK-F), Frankfurt am Main, Germany*12 / 2008 - 10 / 2010***Research Assistant**

Institute for Geology, Leibniz University Hannover, Germany

Teaching experience*2010*

Introduction to Geology (Civil Engineering/Geodesy)

Petrology (Geography)

Introduction to field work

Introductory mapping course

Publication and conference abstracts

Publications

Schemmel et al. (in rev.): Paleohydrological changes in the Eastern Mediterranean region during the early Holocene recorded in plant wax *n*-alkane distributions and $\delta^{13}\text{C}_{\text{TOC}}$ - new data from Tenaghi Philippon, NE Greece, *Organic Geochemistry*.

Schemmel et al. (2016): Plant wax δD values record changing Eastern Mediterranean atmospheric circulation patterns during the 8.2 kyr B.P. climatic event, *Quaternary Science Reviews*.

Schemmel et al. (2013): The impact of topography on isotopes in precipitation across the Central Anatolian Plateau (Turkey), *American Journal of Science*.

Conference talks

Schemmel et al. (2014): How to recover from a cold event - A high resolution, compound-specific *n*-alkane δD study of the 8.2 ka event (Tenaghi Philippon, Greece), *GeoFrankfurt*, Frankfurt/Main, Germany.

Schemmel et al. (2013): A stable isotope record of orographic precipitation and continental evaporation across the Central Anatolian Plateau, *EGU General Assembly*, Vienna, Austria.

Schemmel et al. (2011): From Rainout to Rainshadow - A stable isotopic perspective of the Central Anatolian Plateau, *Fragile Earth*, Munich, Germany.

Poster presentations

Schemmel et al. (2013): Insights into rapid climate change: A high resolution, compound-specific *n*-alkane δD study of the 8.2 ka event (Tenaghi Philippon, Greece), *AGU Fall Meeting*, San Francisco, USA.

Mikes et al. (2012): Late Miocene Central Anatolian surface uplift and orographic rainout from stable hydrogen and oxygen isotope records, *Goldschmidt Conference*, Montreal, Canada.

Schemmel et al. (2011): A stable isotopic perspective on orographic precipitation and continental evaporation in Turkey, *AGU Fall Meeting*, San Francisco, USA.

Mulch et al. (2010): Neogene topography and precipitation patterns of the Central Anatolian Plateau, *AGU Fall Meeting*, San Fransisco, USA.

Schemmel et al. (2010): A river based stable isotope record of orographic precipitation: Taurus Mountains, south central Turkey, *EGU General Assembly*, Vienna, Austria.

